

# **Photoemission from solids**

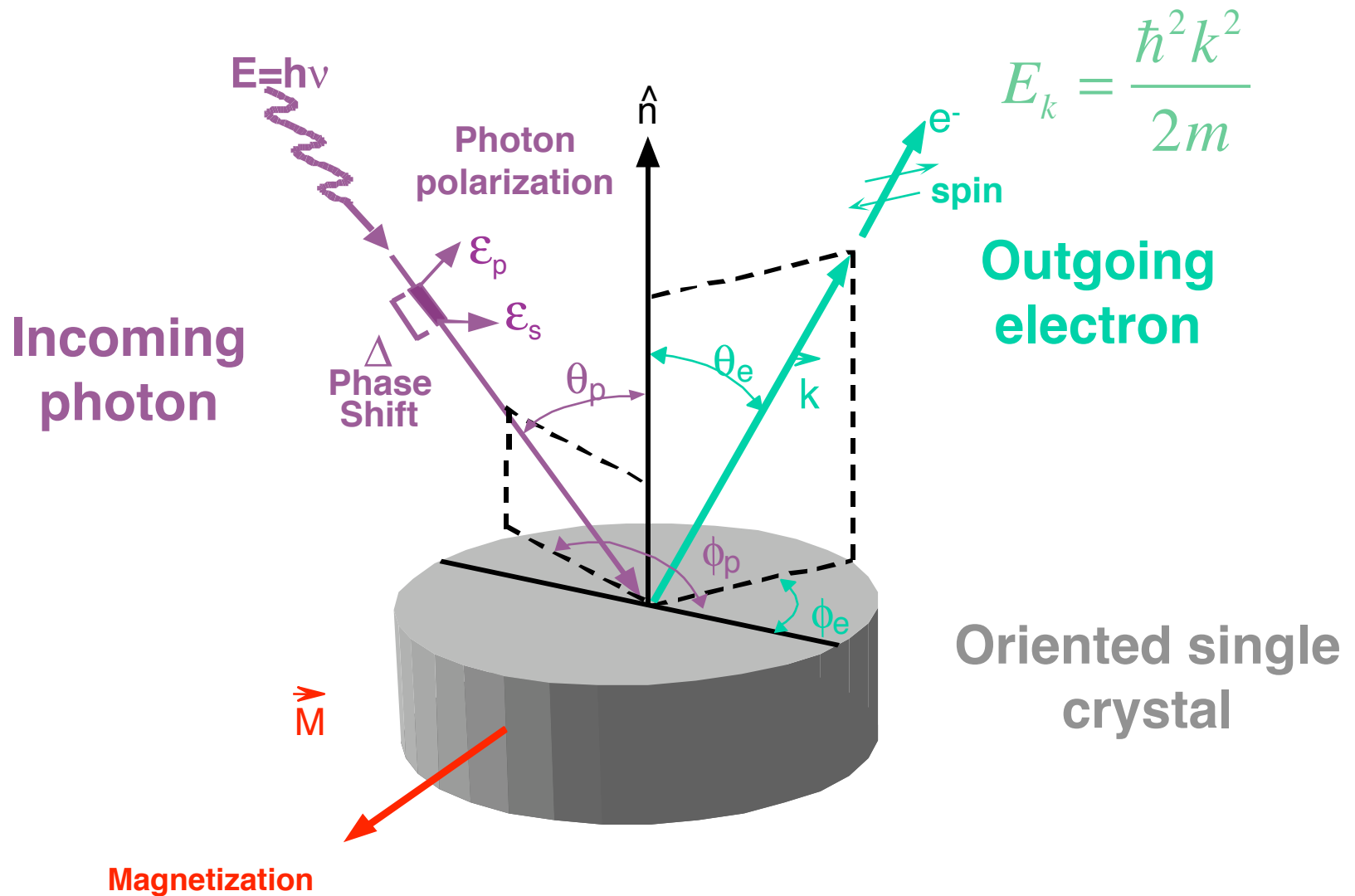
**G. Paolucci**  
**Elettra - Sincrotrone Trieste**

# Outline

# Outline

- **Basics**
  - Photoelectric effect
  - Sources and electron analyzers
  - A bit of quantum mechanics
  - Photoemission cross section & Cooper minimum
- **Valence band angle resolved photoemission**
  - momentum conservation
  - band mapping
  - dipole selection rules
- **Core level photoemission**
  - Element specificity
  - Sensitivity to chemical environment
  - Photoelectron diffraction
  - Time evolution
  - Microscopy

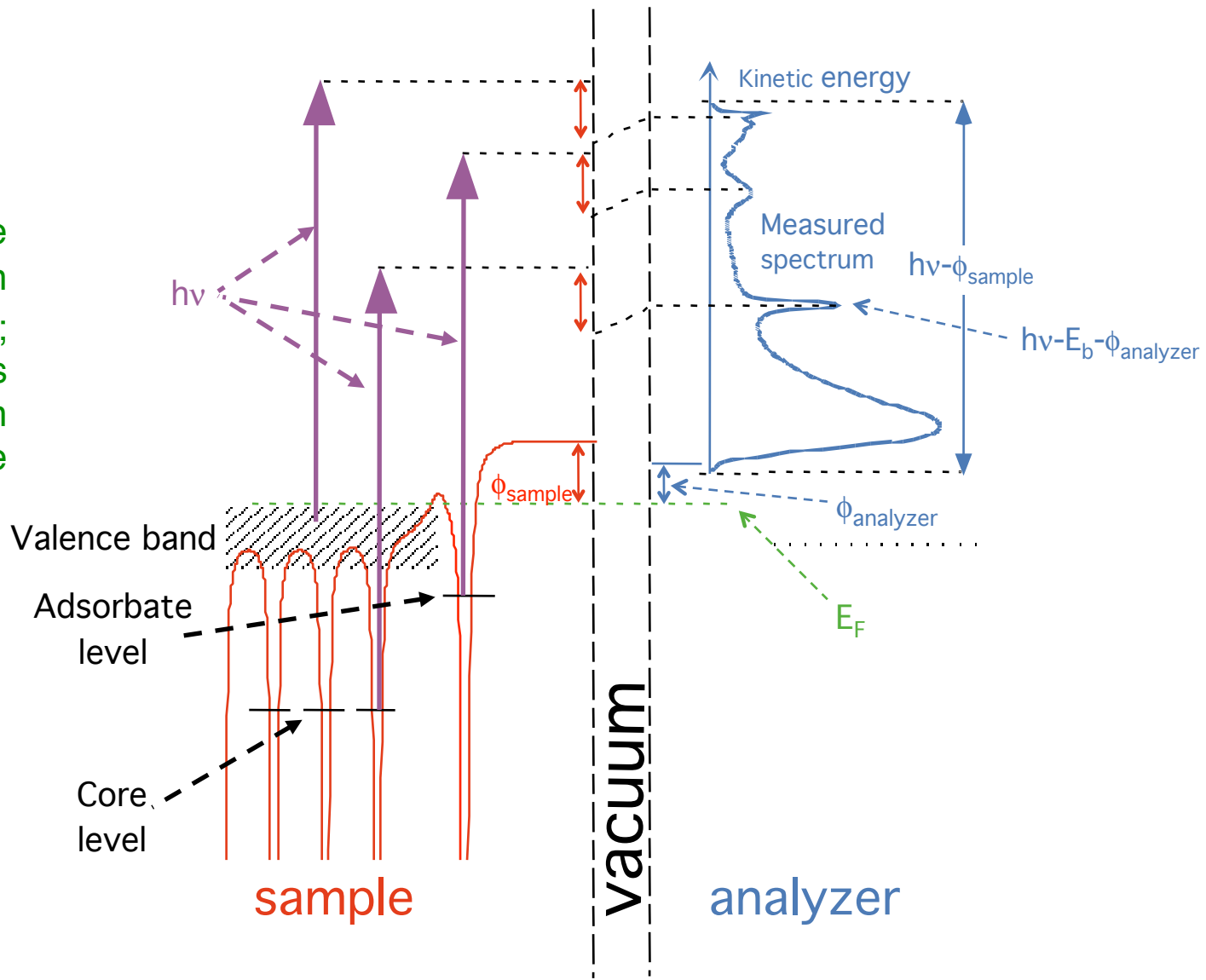
# The photoemission experiment





The electron must overcome the sample work function  $\phi_{\text{sample}}$  in order to reach the vacuum; afterwards its energy is changed by the difference in work function between the analyzer and the sample. So:

$$E_k^{\text{meas}} = h\nu - E_b - \phi_{\text{analyzer}}$$



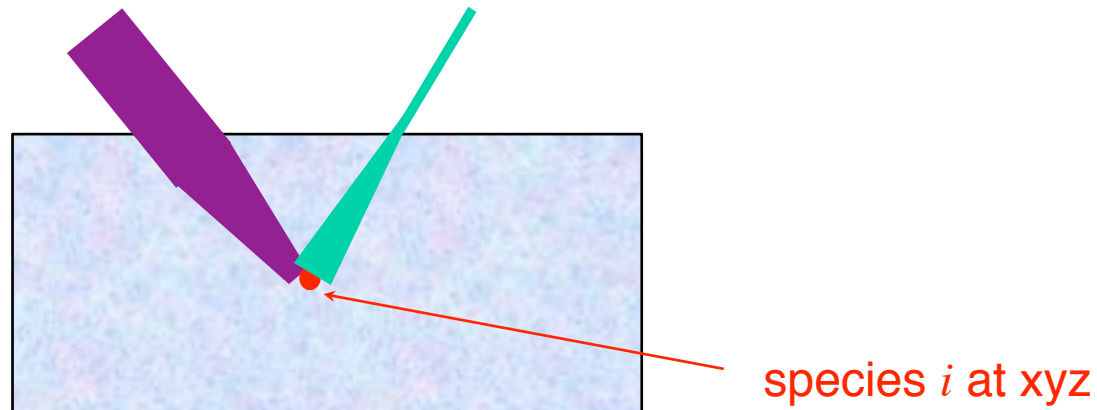
The total photoemission intensity from species  $i$  is obtained by integrating:

relevant for  
the choice  
of photon  
energy!

- $dN_i \propto$  (no. of atoms of species  $i$  at  $x, y, z$ )
- (photon flux at  $x, y, z$ )
  - (differential cross section of relevant level of species  $i$ )
  - (probability of no loss escape of electrons from  $x, y, z$ )
- {
- (acceptance solid angle of the electron analyzer)
  - (detection efficiency)

incoming flux  
& absorption  
coefficient

electron mean  
free path

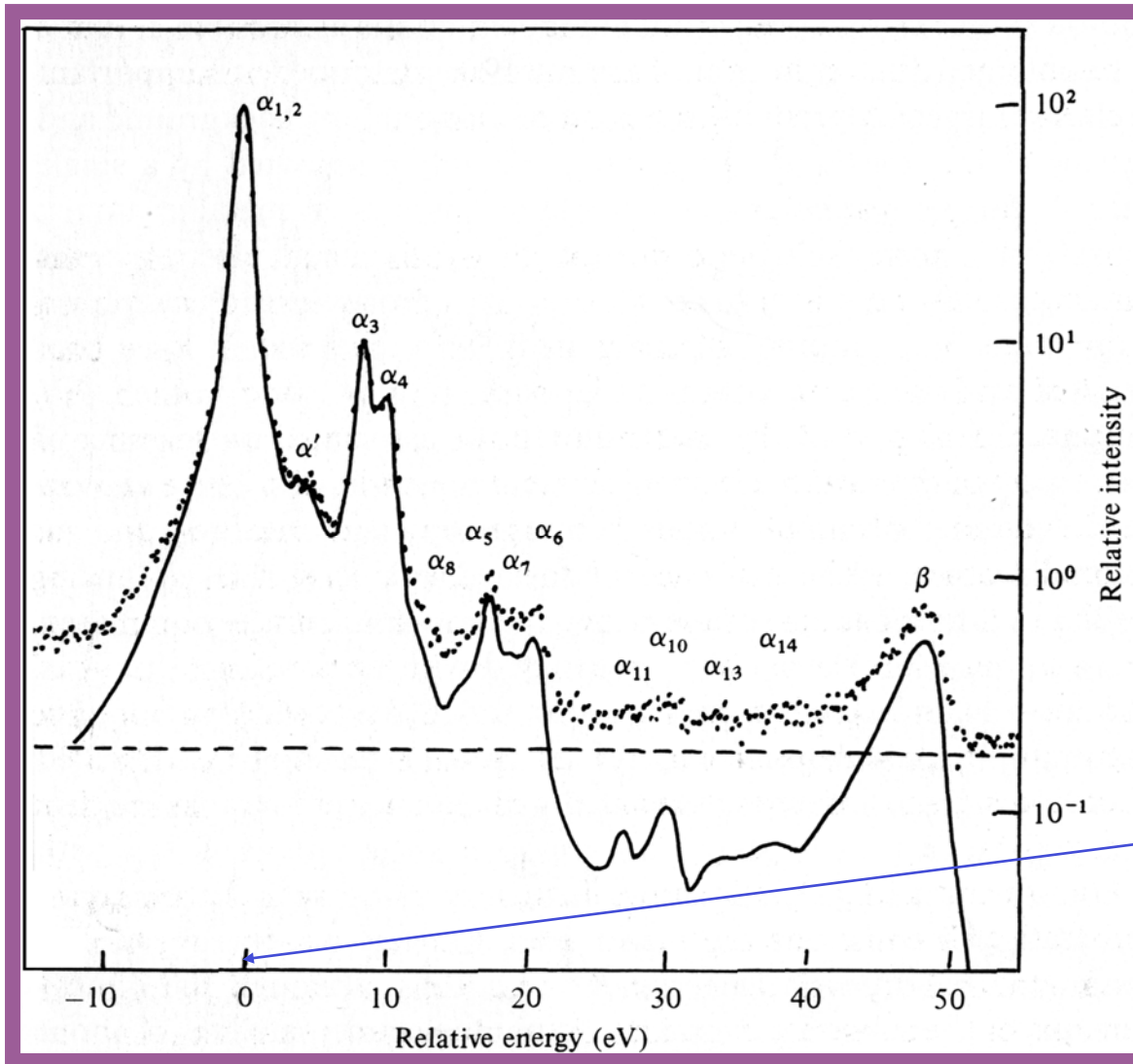


# The incoming photons

UV to soft x-rays (  $h\nu \sim 10$  to  $\sim 1500$  eV  
or  $\lambda \sim 1240$  to  $\sim 5$  Å)

- **Laboratory sources** (relatively cheap) **use characteristic transition lines:**
  - noble gas discharge (e.g.  $\text{HeI}_{\alpha} = 21.22$  eV)
  - solid target emission lines (Al  $\text{K}_{\alpha} = 1428$  eV; Mg  $\text{K}_{\alpha} = 1253$  eV)
- **Synchrotron radiation** (expensive!) **gives tunable, polarized and bright radiation**

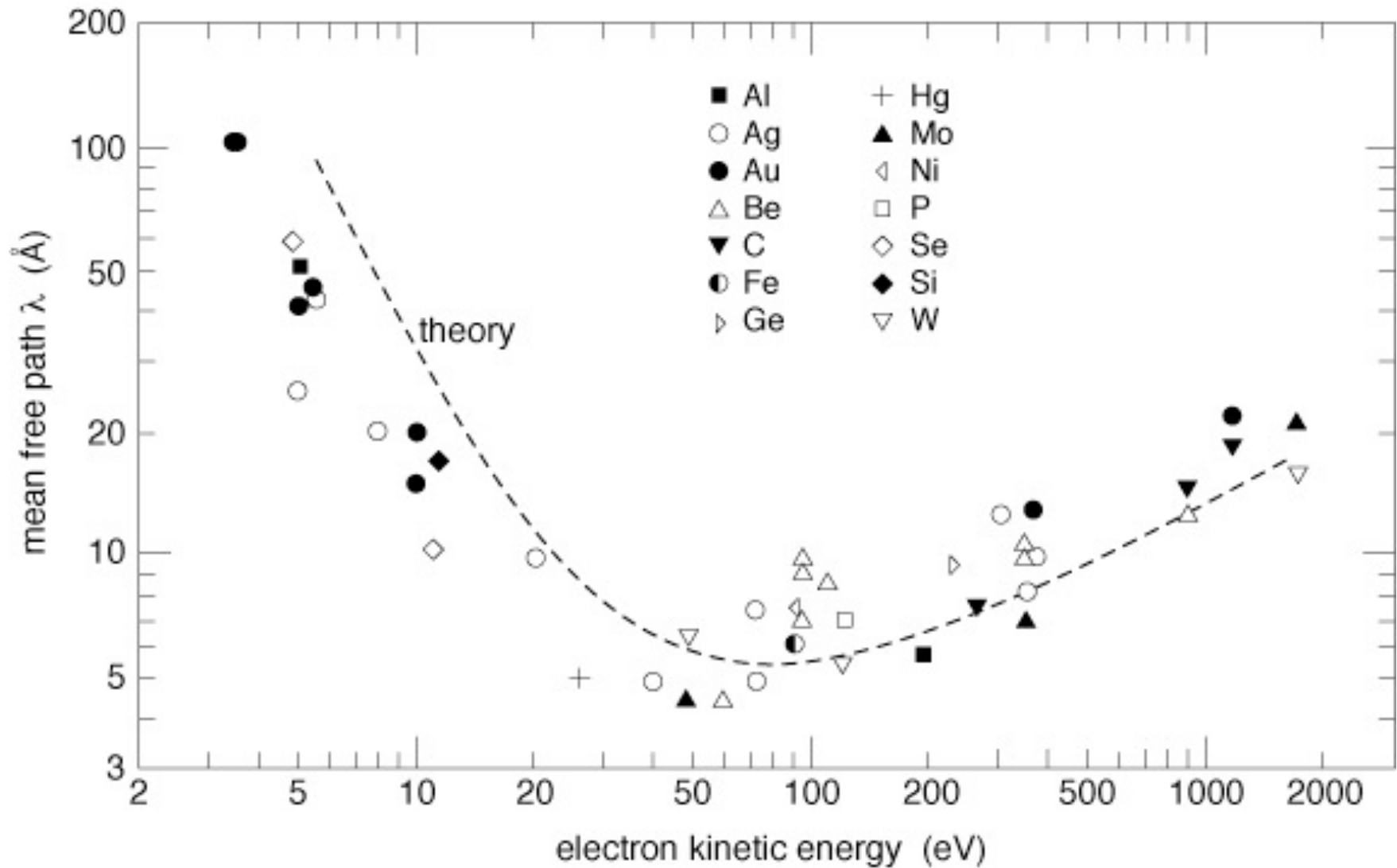
# The incoming photons



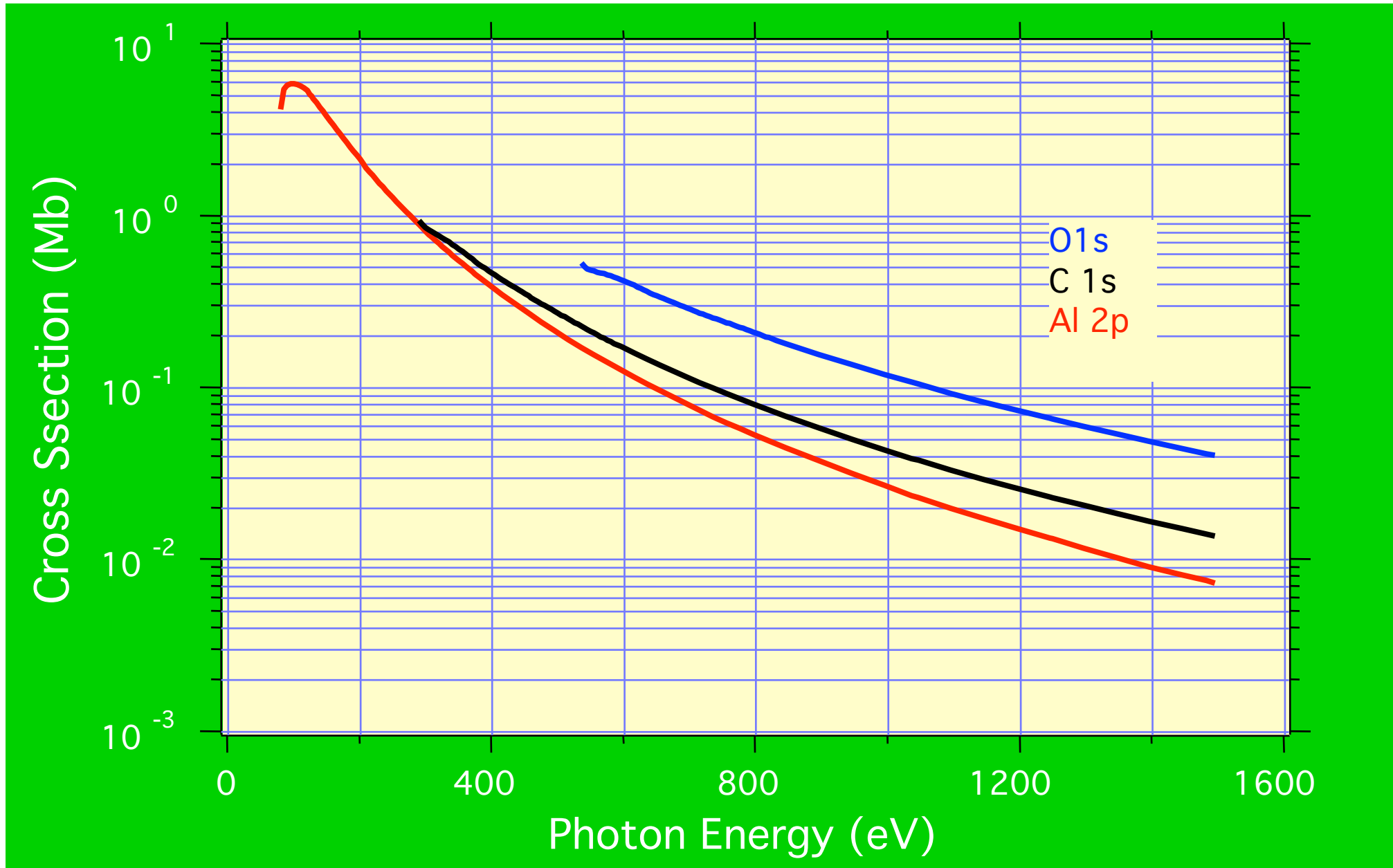
**A laboratory source:**  
the Mg K emission region before (dots) and after subtraction of the dashed background (line).

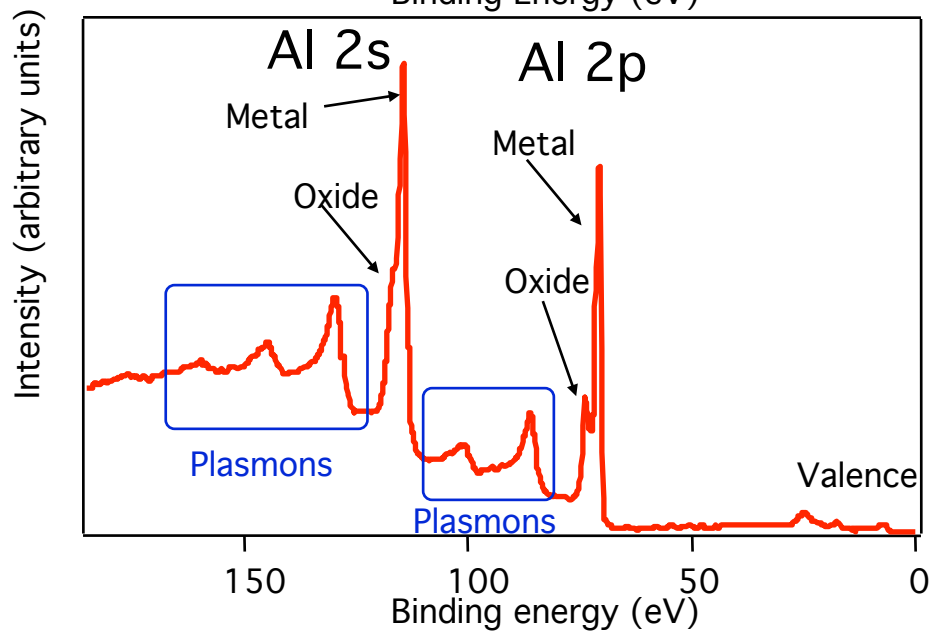
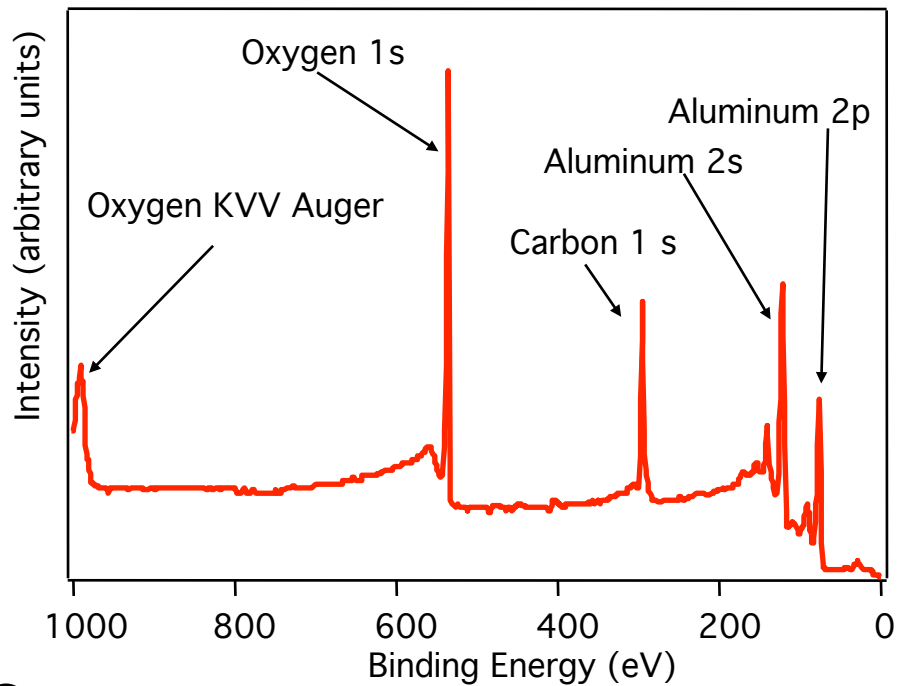
1253 eV

# Electron mean free path



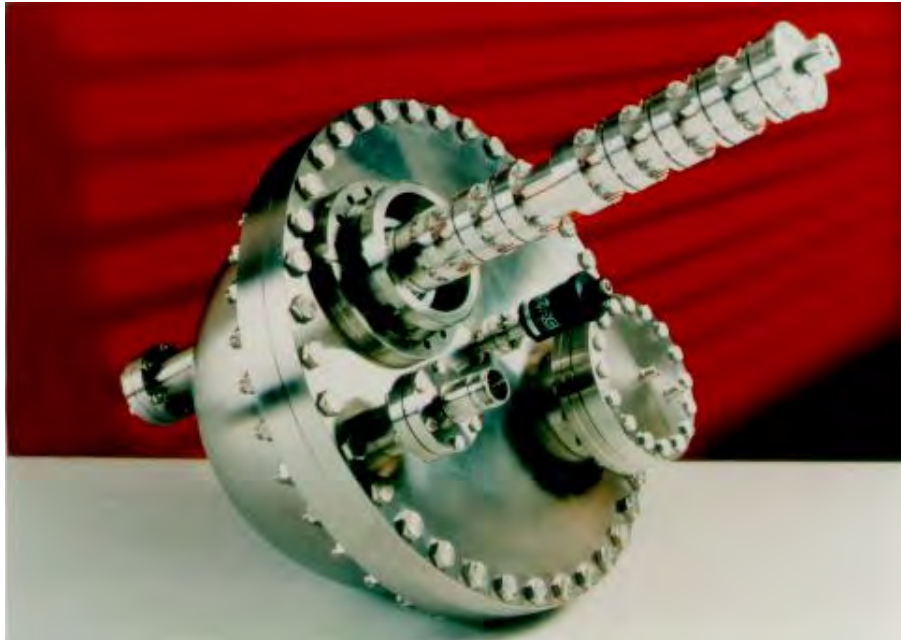
# Photoemission atomic cross section





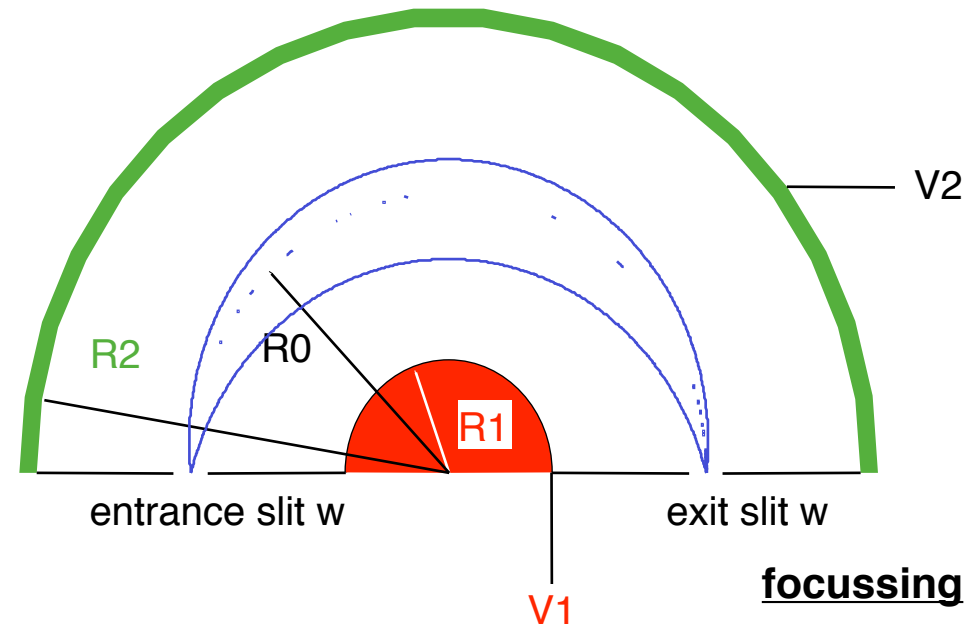
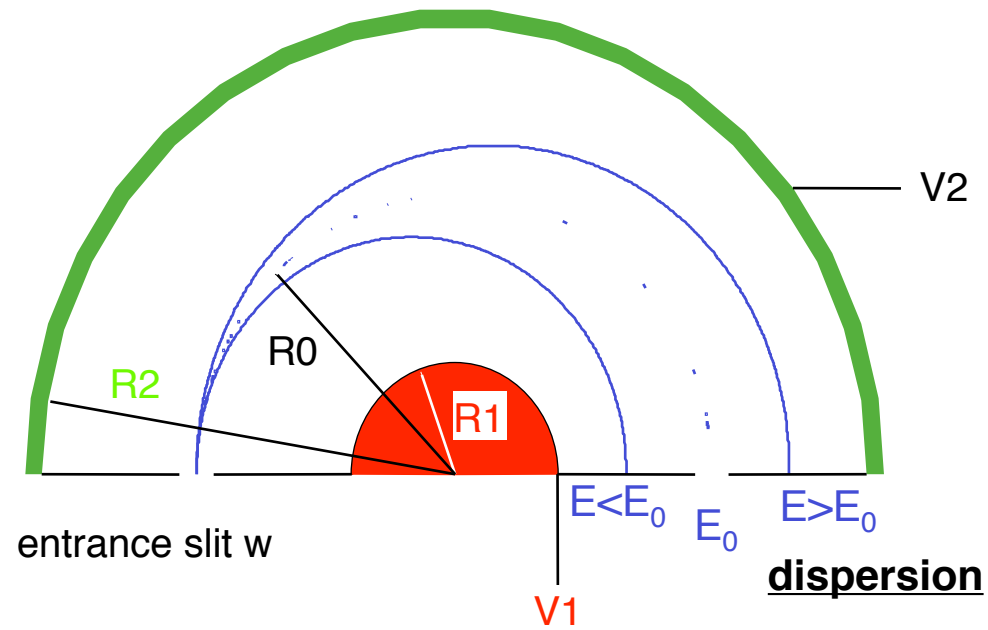
The photoemission spectrum of a “dirty” aluminum sample is dominated by the oxygen 1s level. The core levels of oxidized aluminum show a shift with respect to the metal.

# The spherical electron energy analyzer



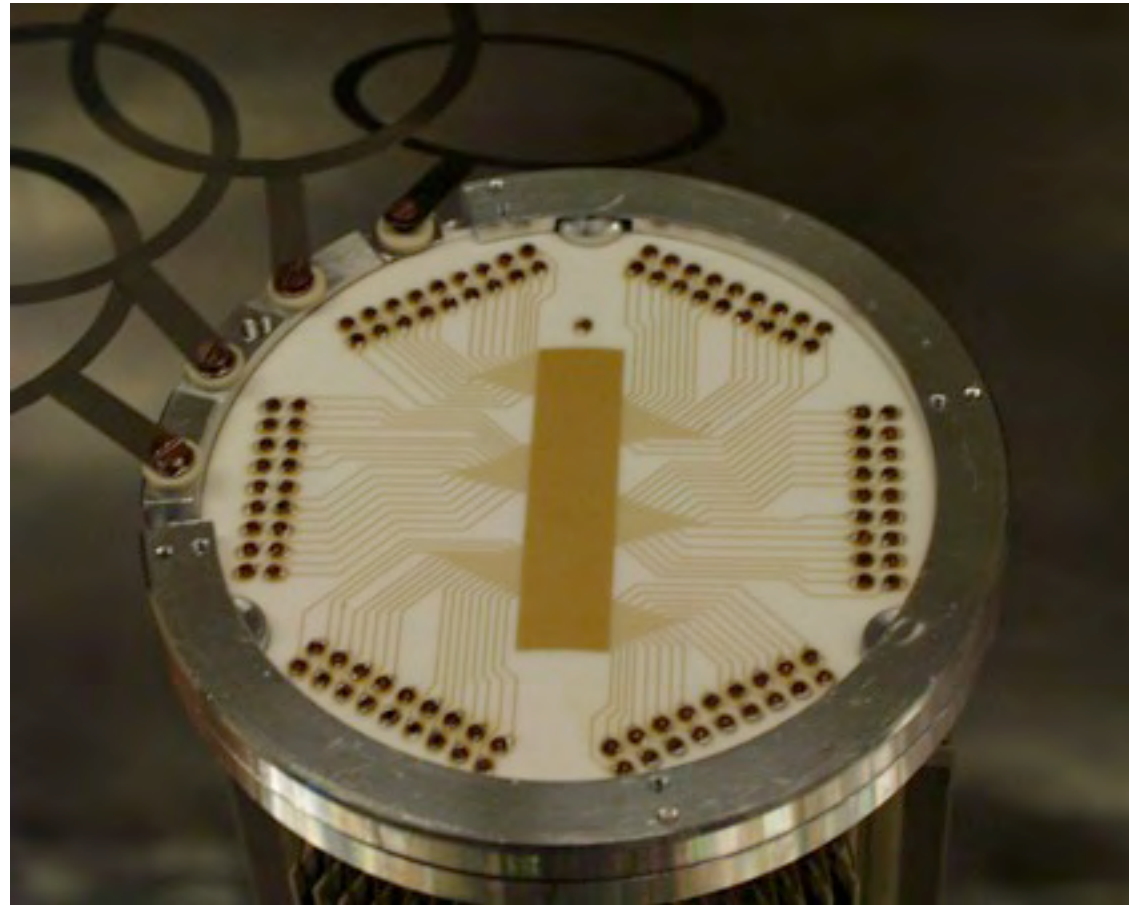
The pass energy  $E_0$  is the energy at which electrons follow a circular trajectory

$$E_0 = \frac{2\Delta V}{R_0} \left( \frac{1}{R_1} - \frac{1}{R_2} \right)^{-1}$$





# Position sensitive detection



# Theory

The hamiltonian for a system with an external em field, described by a vector potential  $\vec{A}$  and a scalar potential  $\phi$  is:

$$H = \frac{1}{2m} \left( \vec{p} + e \frac{\vec{A}(\vec{r}, t)}{c} \right)^2 - e\phi(\vec{r}, t) + V(\vec{r})$$

With the transverse gauge (no charges, no currents)

$$\left. \begin{array}{l} \vec{\nabla} \cdot \vec{A} = 0 \\ \phi(\vec{r}, t) = 0 \end{array} \right\} \rightarrow \nabla^2 \vec{A} + \frac{1}{c^2} \frac{\partial^2 \vec{A}}{\partial t^2} = 0$$

So the hamiltonian becomes:

$$H = \frac{1}{2m} p^2 + \frac{e}{2mc} (\vec{p} \cdot \vec{A} + \vec{A} \cdot \vec{p}) - \frac{e}{2mc^2} A^2 + V(\vec{r})$$

# Theory

The hamiltonian for a system with an external em field, described by a vector potential  $\vec{A}$  and a scalar potential  $\phi$  is:

$$H = \frac{1}{2m} \left( \vec{p} + e \frac{\vec{A}(\vec{r}, t)}{c} \right)^2 - e\phi(\vec{r}, t) + V(\vec{r})$$

With the transverse gauge (no charges, no currents)

$$\left. \begin{array}{l} \vec{\nabla} \cdot \vec{A} = 0 \\ \phi(\vec{r}, t) = 0 \end{array} \right\} \rightarrow \nabla^2 \vec{A} + \frac{1}{c^2} \frac{\partial^2 \vec{A}}{\partial t^2} = 0$$

So the hamiltonian becomes:

$$H = \frac{1}{2m} p^2 + \frac{e}{2mc} \left( \vec{p} \cdot \vec{A} + \vec{A} \cdot \vec{p} \right) - \frac{e}{2mc^2} A^2 + V(\vec{r})$$

$$\{ \vec{p}, \vec{A} \} = 0$$

# Theory

The hamiltonian for a system with an external em field, described by a vector potential  $\vec{A}$  and a scalar potential  $\phi$  is:

$$H = \frac{1}{2m} \left( \vec{p} + e \frac{\vec{A}(\vec{r}, t)}{c} \right)^2 - e\phi(\vec{r}, t) + V(\vec{r})$$

With the transverse gauge (no charges, no currents)

$$\left. \begin{array}{l} \vec{\nabla} \cdot \vec{A} = 0 \\ \phi(\vec{r}, t) = 0 \end{array} \right\} \rightarrow \nabla^2 \vec{A} + \frac{1}{c^2} \frac{\partial^2 \vec{A}}{\partial t^2} = 0$$

So the hamiltonian becomes:

$$H = \frac{1}{2m} p^2 + \frac{e}{2mc} (\vec{p} \cdot \vec{A} + \vec{A} \cdot \vec{p}) - \frac{e}{2mc^2} A^2 + V(\vec{r})$$

$\{\vec{p}, \vec{A}\} = 0$   $\sim 0$

# Theory

The hamiltonian for a system with an external em field, described by a vector potential  $\vec{A}$  and a scalar potential  $\phi$  is:

$$H = \frac{1}{2m} \left( \vec{p} + e \frac{\vec{A}(\vec{r}, t)}{c} \right)^2 - e\phi(\vec{r}, t) + V(\vec{r})$$

With the transverse gauge (no charges, no currents)

$$\left. \begin{array}{l} \vec{\nabla} \cdot \vec{A} = 0 \\ \phi(\vec{r}, t) = 0 \end{array} \right\} \rightarrow \nabla^2 \vec{A} + \frac{1}{c^2} \frac{\partial^2 \vec{A}}{\partial t^2} = 0$$

So the hamiltonian becomes:

$$H = \frac{1}{2m} p^2 + \frac{e}{2mc} (\vec{p} \cdot \vec{A} + \vec{A} \cdot \vec{p}) - \frac{e}{2mc^2} A^2 + V(\vec{r})$$

$\{\vec{p}, \vec{A}\} = 0$        $\sim 0$

$$H = \frac{1}{2m} p^2 + \frac{e}{mc} \vec{A} \cdot \vec{p} + V(\vec{r})$$

We can write:

$$H = H_0 + H_1$$

where

$$H_1 = \frac{ie\hbar}{mc} \vec{A} \cdot \vec{\nabla}$$

is the perturbation.

The incoming radiation can be described as a superposition of plane waves of the form:

$$\vec{A}(\vec{r}, t) = \vec{A}_\omega e^{i(\vec{q} \cdot \vec{r} - \omega t)}$$

We put all this into the time dependent perturbation theory to get:

$$c_{f,i} = -\frac{2\pi e}{mc} \vec{A}_\omega \cdot \langle f | e^{i\vec{q} \cdot \vec{r}} \vec{\nabla} | i \rangle \delta\left(\omega - \frac{E_f - E_i}{\hbar}\right)$$

For photoemission the wavelength  $\lambda = 2\pi/|q|$  is always much longer than the size of the atoms. So we can approximate the exponential with 1

$$c_{f,i} = -\frac{2\pi e}{mc} \vec{A}_\omega \cdot \langle f | \vec{\nabla} | i \rangle \delta\left(\omega - \frac{E_f - E_i}{\hbar}\right) = -\frac{2\pi ie}{m\hbar} \vec{A}_\omega \cdot \langle f | \vec{p} | i \rangle \delta\left(\omega - \frac{E_f - E_i}{\hbar}\right)$$

this formula represents the so-called **dipole approximation**

We define the photoionization cross section:

$$\sigma(\hbar\omega) = \frac{P(\hbar\omega)}{I(\hbar\omega)}$$

where  $P(\hbar\omega)$  is the number of photons absorbed by one atom per unit time at photon energy  $\hbar\omega$  (photxs<sup>-1</sup>) and  $I(\hbar\omega)$  is the incident photon flux (photxs<sup>-1</sup>×cm<sup>-2</sup>)

For a medium with  $n$  atoms per unit volume and photons traveling a distance  $dx$

$$\frac{dI}{I} = -n\sigma dx$$

or

$$I(x) = I_0 e^{-n\sigma x}$$

$$\eta = \frac{2\omega\kappa}{c} = n\sigma$$

$\sigma$  is generally measured in Megabarn (Mb, 1Mb=10<sup>-18</sup>cm<sup>2</sup>)

For a spherically symmetric system (isolated atom) the initial and final states can be expressed as product of a radial and angular part:

$$\Psi_i(\vec{r}) = \tilde{R}_{l_i}^i(r) Y_{L_i}(\hat{r})$$

$$\Psi_f(\vec{r}) = 4\pi \sum_L Y_L^*(\hat{k}_f) i^{-l} e^{i\delta_l} \tilde{R}_l^f(r) Y_L(\hat{r})$$

The  $\Psi_f$  can also be regarded as

$$\Psi_f(\vec{r}) = e^{-i\vec{k}_f \cdot \vec{r}} + f(E_f, \vec{k}_f) \frac{e^{ik_f r}}{r}$$



For a spherically symmetric system (isolated atom) the initial and final states can be expressed as product of a radial and angular part obtaining:

$$\frac{d\sigma_{nl}(h\nu)}{d\Omega} = \frac{\sigma_{nl}(h\nu)}{4\pi} [1 + \beta P_2(\cos \gamma)]$$

In which

$$\sigma_{nl}(h\nu) = \frac{4\pi^2 \alpha a_0^2}{3} \frac{N_{nl}}{2l+1} h\nu [lR_{l-1}^2(\epsilon_k) + (l+1)R_{l+1}^2(\epsilon_k)]$$

and

$$R_{l\pm 1}(\epsilon) = \int_0^\infty \tilde{R}_l^i(r) r \tilde{R}_{l\pm 1}^f(r) dr$$

For spherically symmetric systems (free atoms) the well known selection rules ( $\Delta l = \pm 1$ ) apply.

One can write the intensity for emission at a given angle  $\gamma$  from the polarization of the beam in the following form

$$\frac{d\sigma_{nl}(h\nu)}{d\Omega} = \frac{\sigma_{nl}(h\nu)}{4\pi} [1 + \beta P_2(\cos \gamma)]$$

$$\sigma_{nl}(h\nu) = \frac{4\pi^2 \alpha a_0^2}{3} \frac{N_{nl}}{2l+1} h\nu [lR_{l-1}^2(\epsilon_k) + (l+1)R_{l+1}^2(\epsilon_k)]$$

$$P_2(\cos \gamma) = \frac{3\cos^2 \gamma - 1}{2}$$

This term controls the weight of  $\Delta l = +1$  and  $\Delta l = -1$  channels

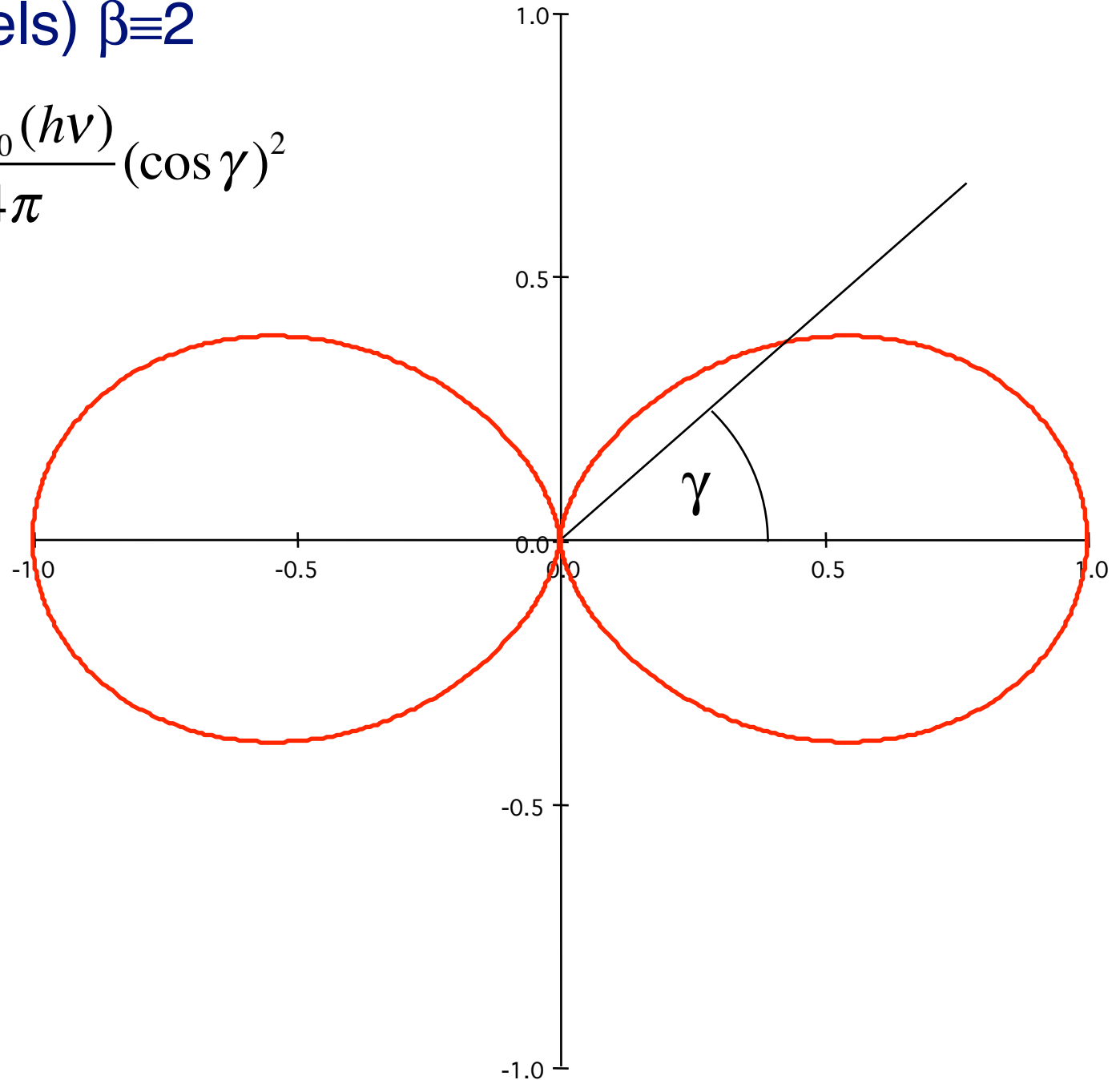
$$-1 \leq \beta \leq 2$$

At  $\gamma = 54.7^\circ$  (magic angle)  $P_2 = 0$ : the measurement is independent of  $\beta$

For  $l=0$  (s levels)  $\beta = 2$

For  $l=0$  (s levels)  $\beta \equiv 2$

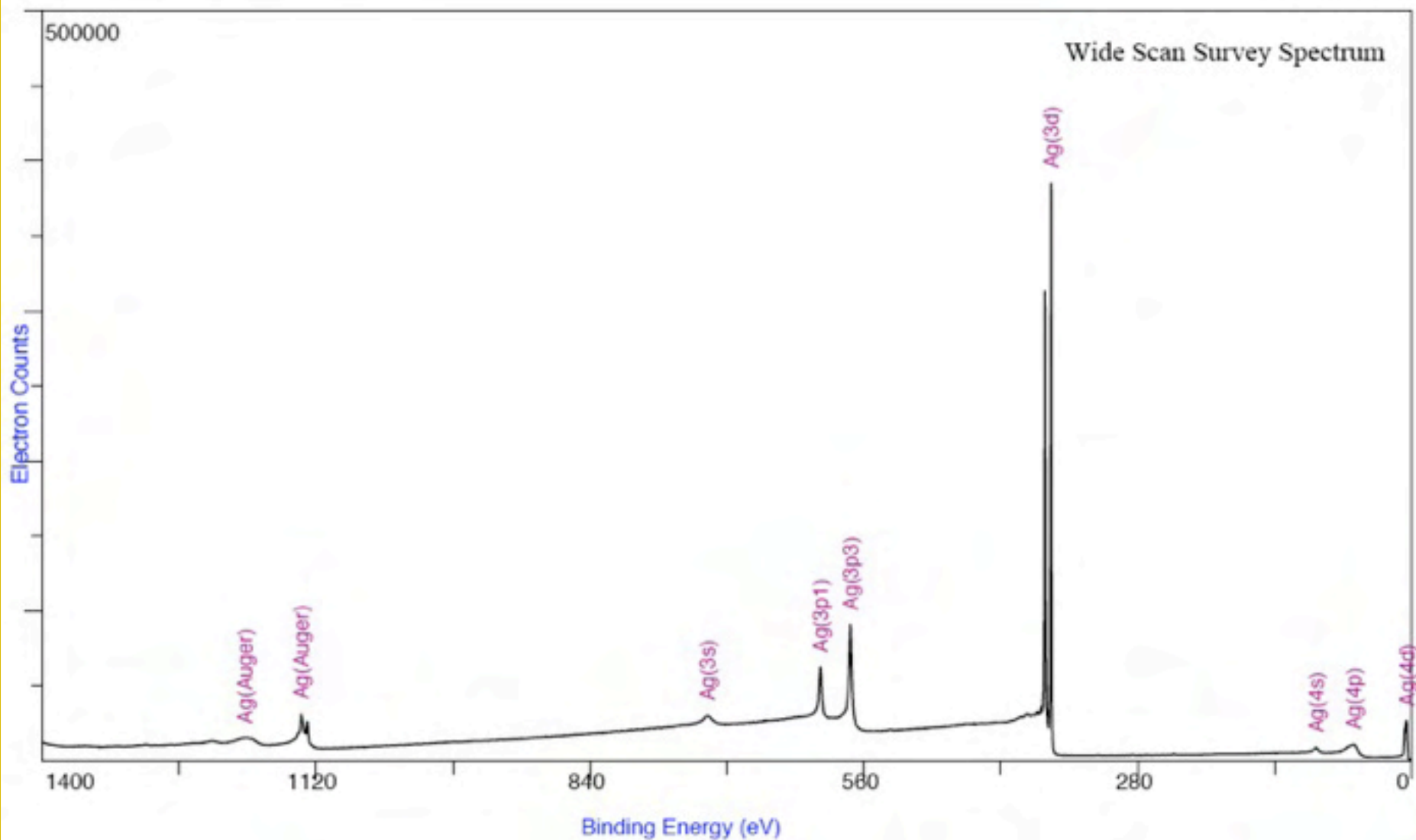
$$\frac{d\sigma_{nl=0}(h\nu)}{d\Omega} = \frac{\sigma_{nl=0}(h\nu)}{4\pi} (\cos\gamma)^2$$



# The Ag XPS spectrum

Silver Metal (Z=47)

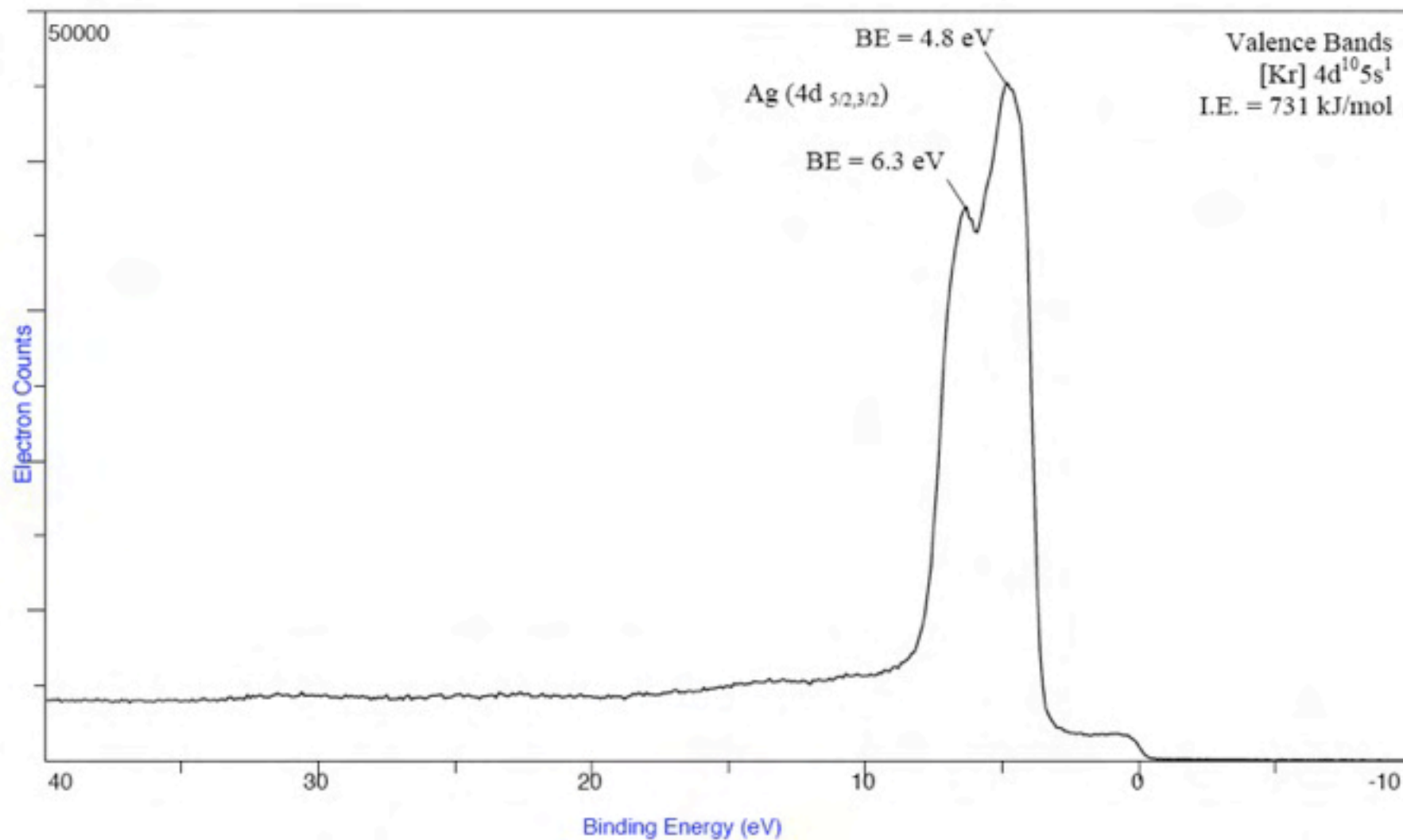
Ag<sup>0</sup>  
[CAS# 7440-22-4]



# The Ag XPS spectrum

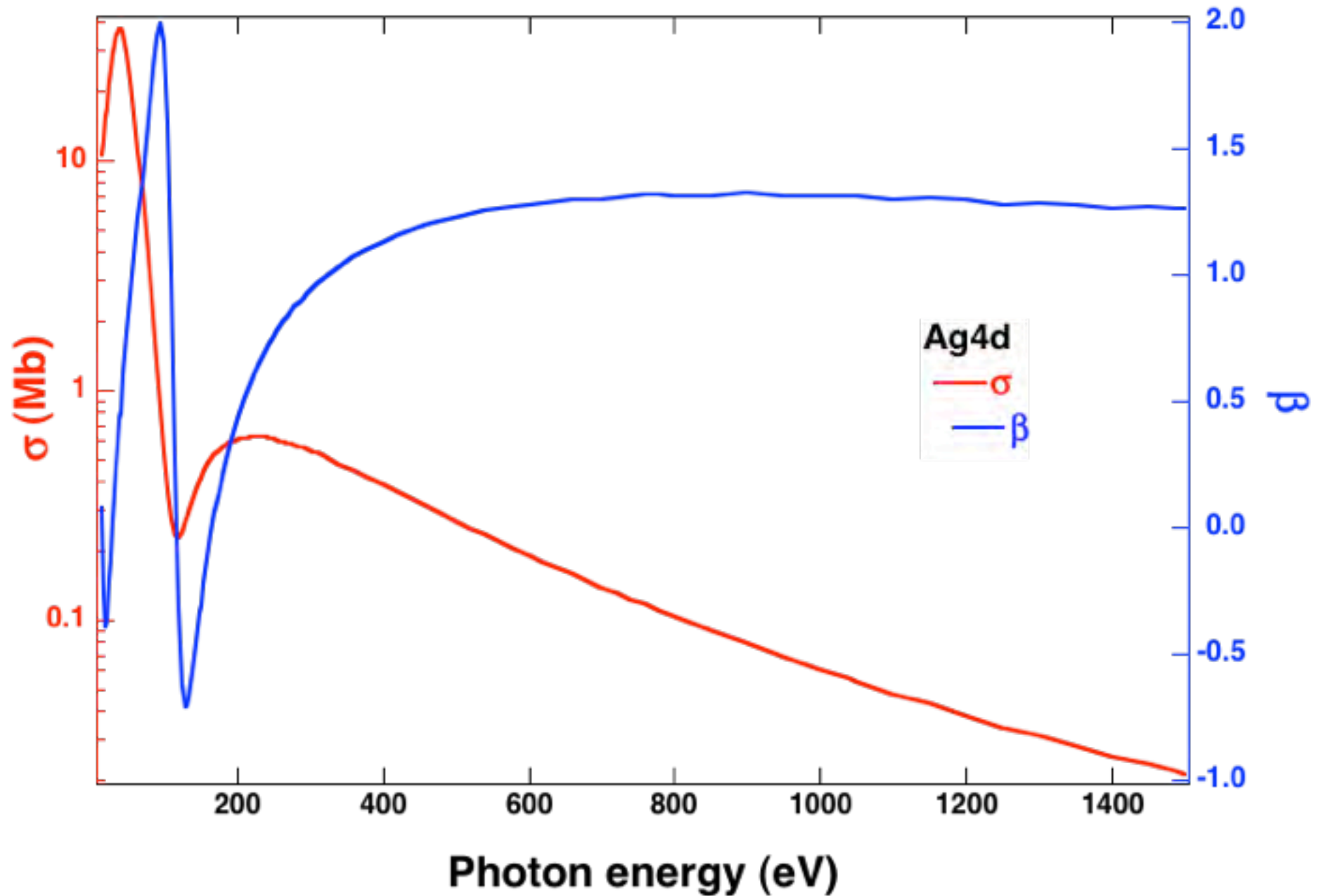
Silver Metal (Z=47)

$\text{Ag}^0$   
[CAS# 7440-22-4]



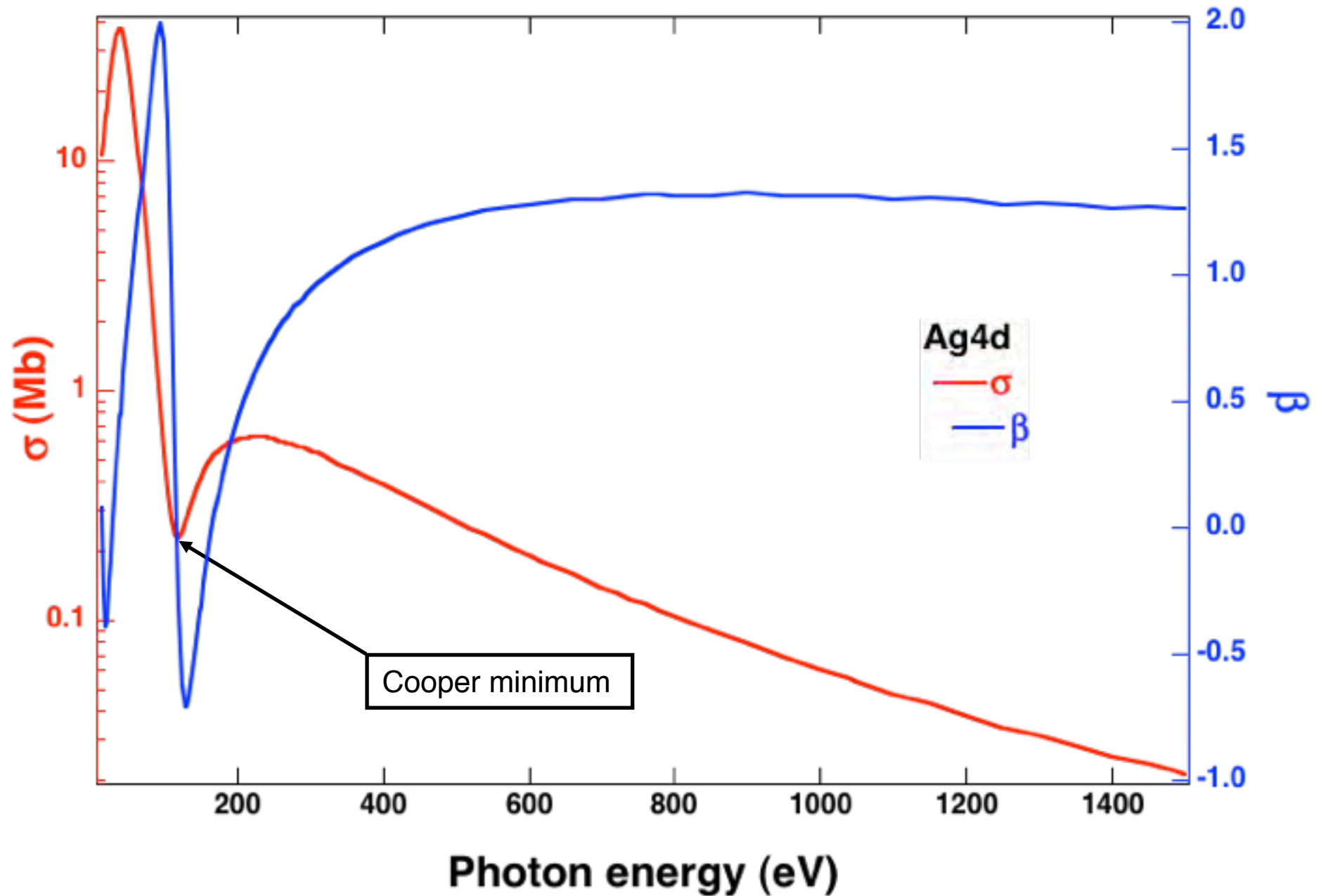
# Example: the Ag 4d level

(from J.J. Yeh: "Atomic calculation of photoionization cross sections and asymmetry parameters", Gordon Breach)

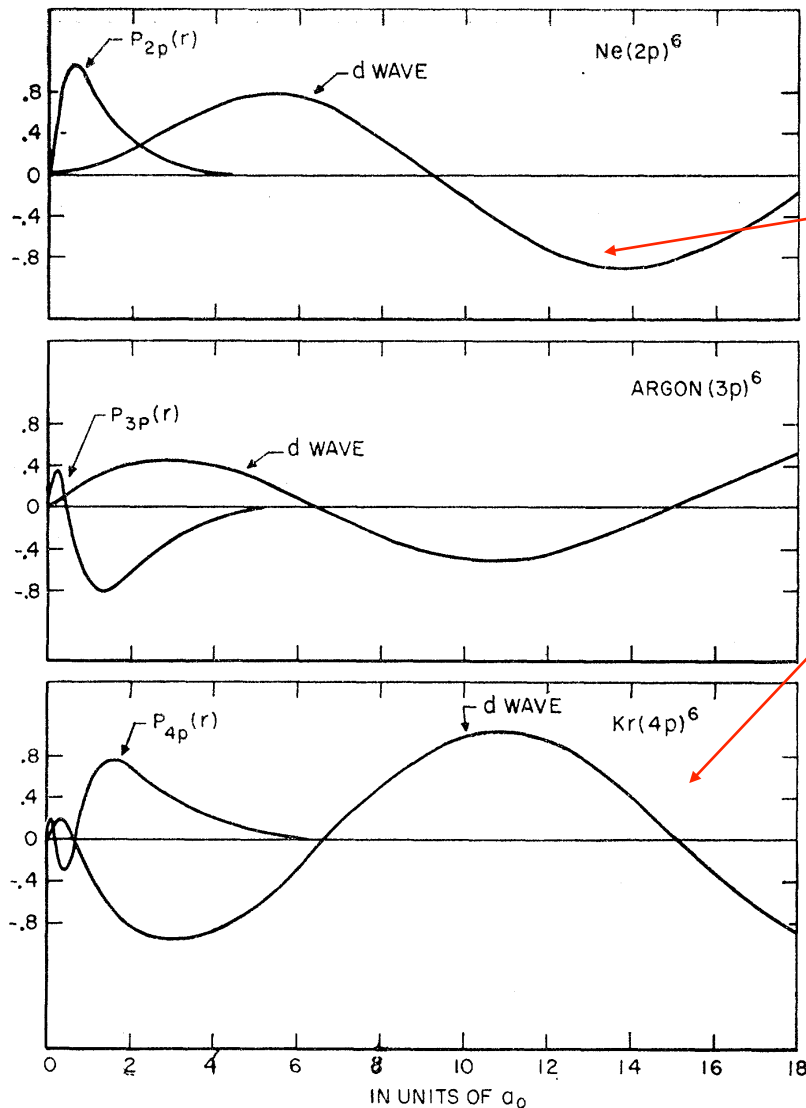


# Example: the Ag 4d level

(from J.J. Yeh: "Atomic calculation of photoionization cross sections and asymmetry parameters", Gordon Breach)



# The Cooper minimum is due to a node in the initial state



$\Delta l = +1, E_k = 0$  (i.e. at threshold)

$$\langle f(E_k = 0) | \vec{p} | i \rangle > 0$$

$$\langle f(E_k = 0) | \vec{p} | i \rangle < 0$$

At some kinetic energy  
the integral will become  
positive!

FIG. 2. Outer subshell radial wave functions and  $d$  waves for  $\epsilon = 0$  for Ne, Ar, and Kr.



# The Cooper minimum

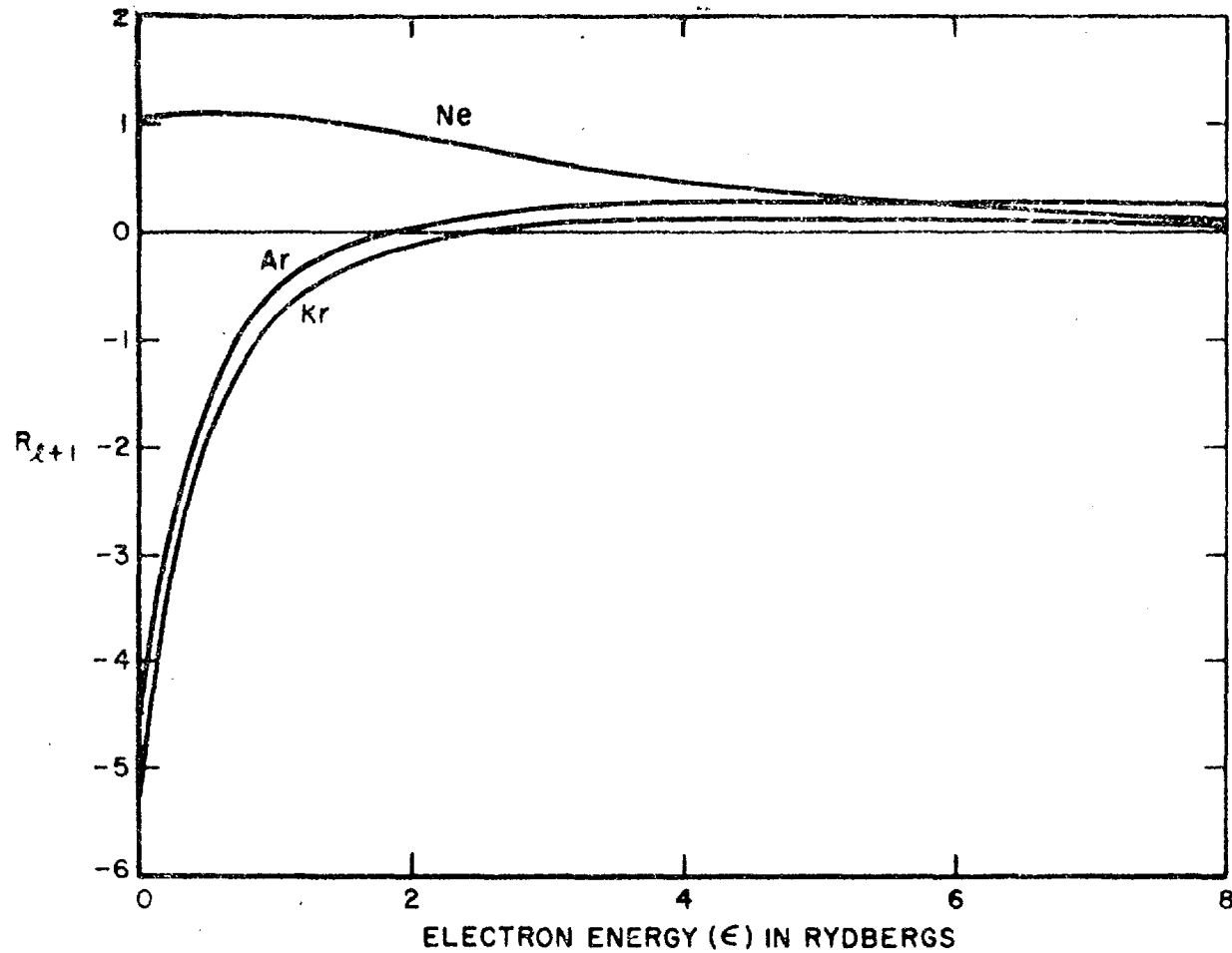
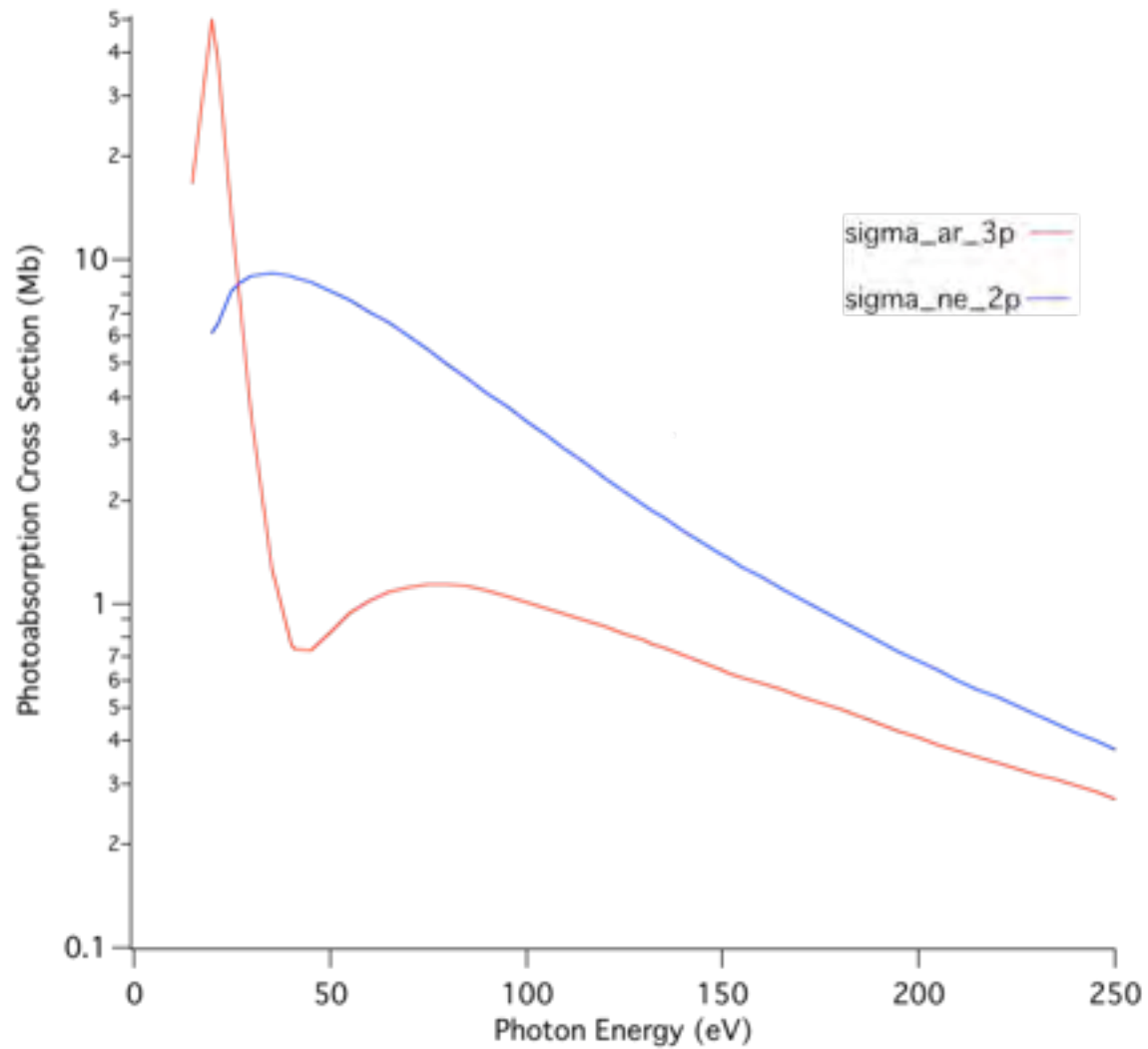


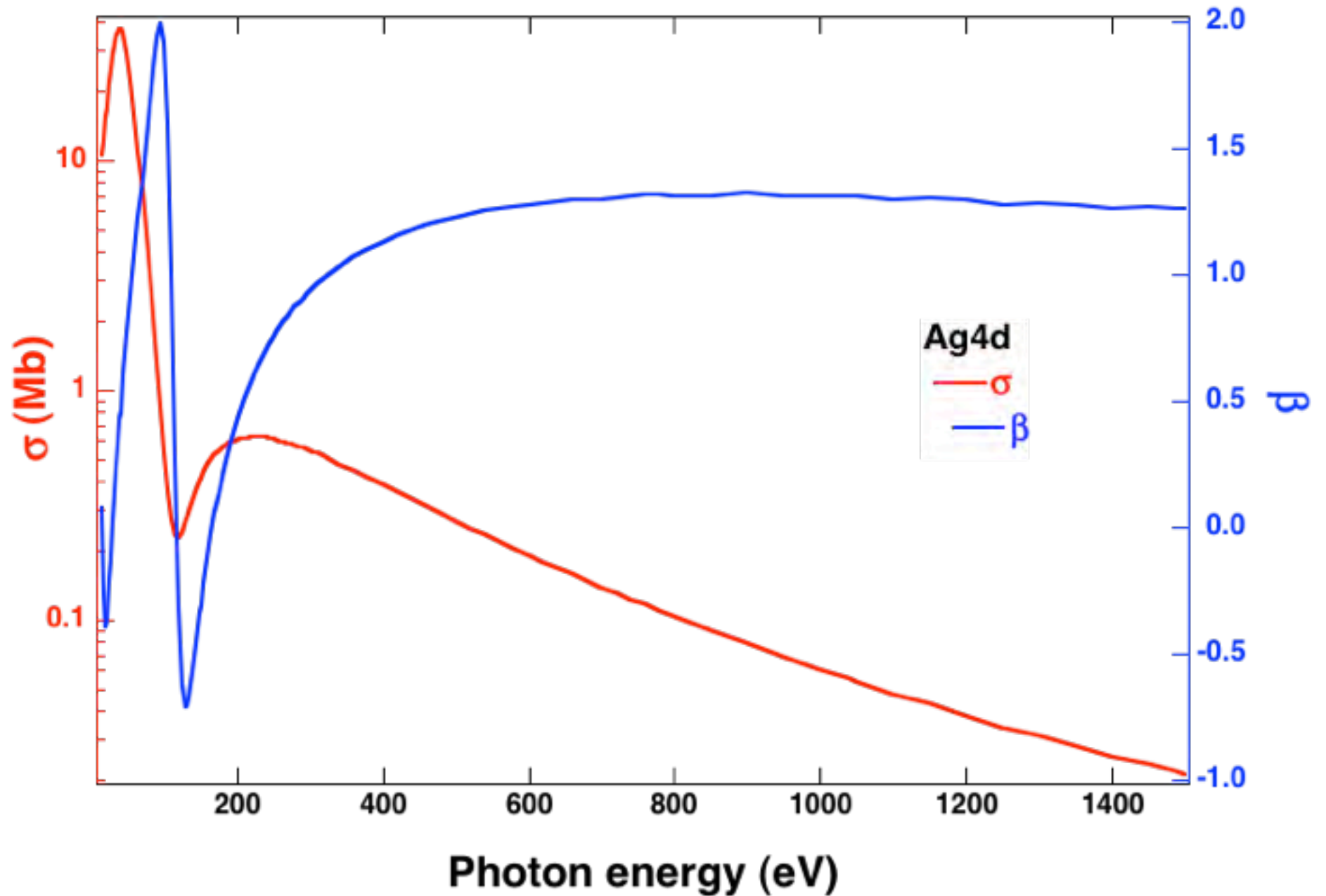
FIG. 3. Matrix elements for  $p \rightarrow d$  transitions in Ne, Ar, and Kr.

# The Cooper minimum



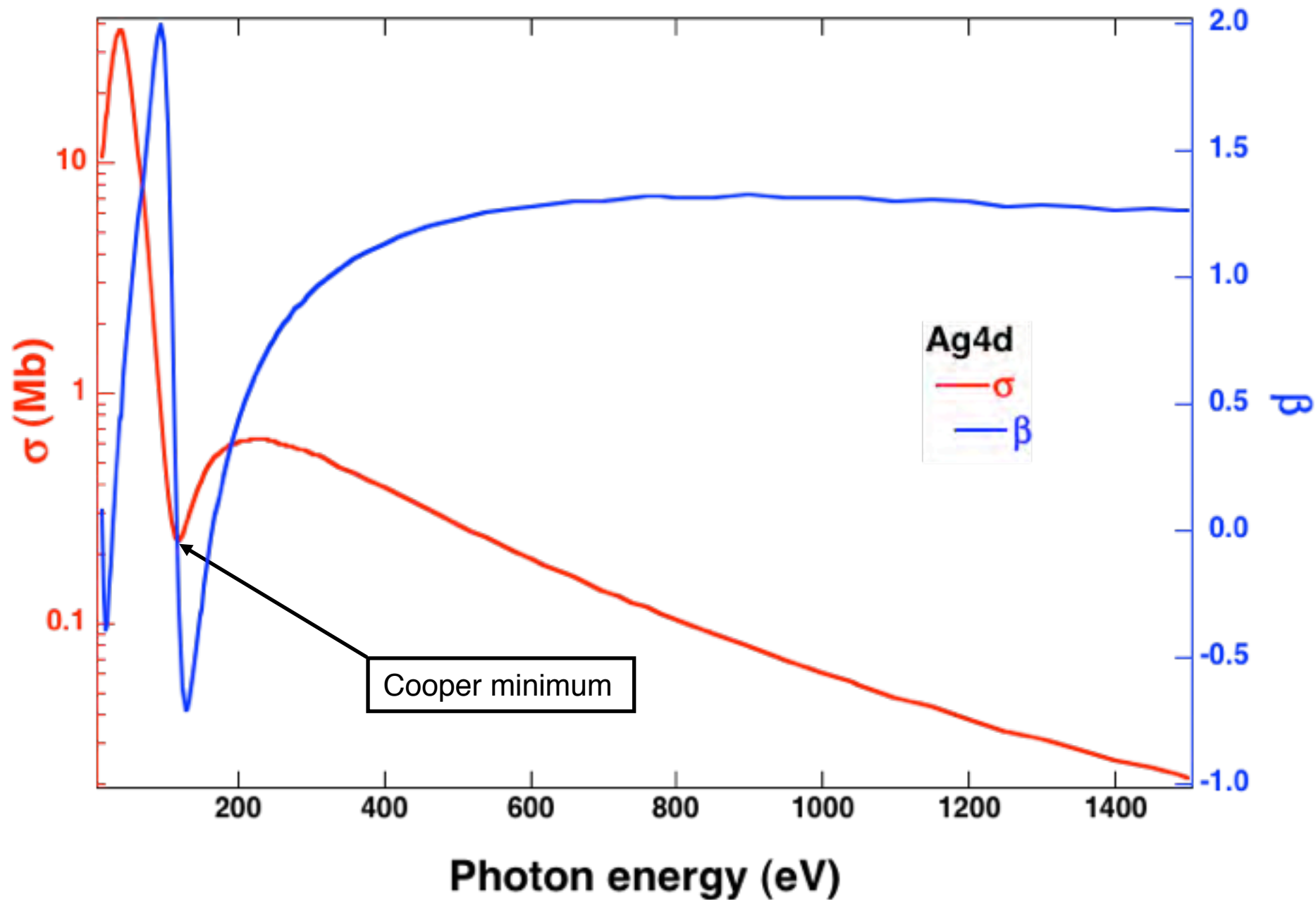
# Example: the Ag 4d level

(from J.J. Yeh: "Atomic calculation of photoionization cross sections and asymmetry parameters", Gordon Breach)

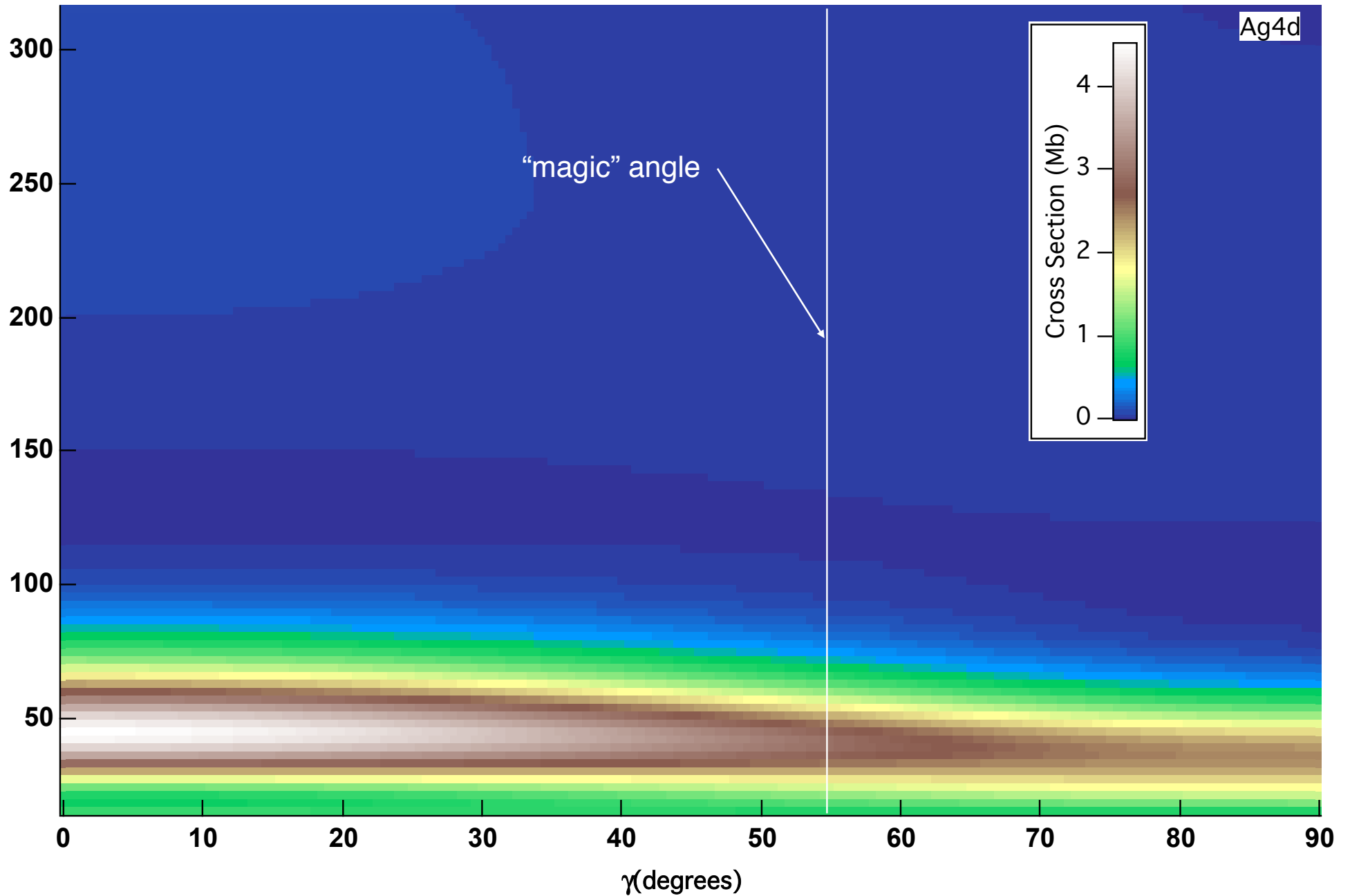


# Example: the Ag 4d level

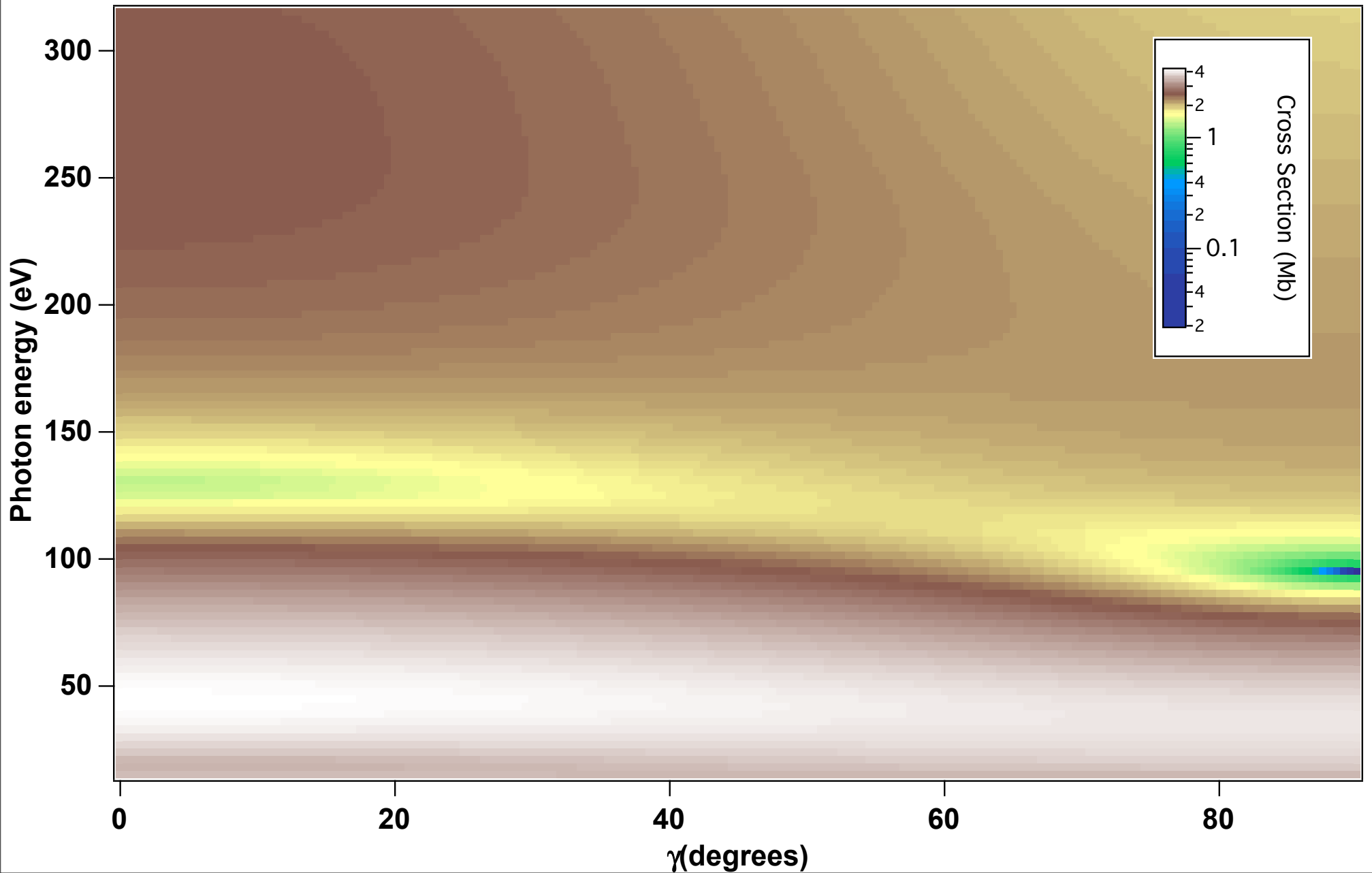
(from J.J. Yeh: "Atomic calculation of photoionization cross sections and asymmetry parameters", Gordon Breach)



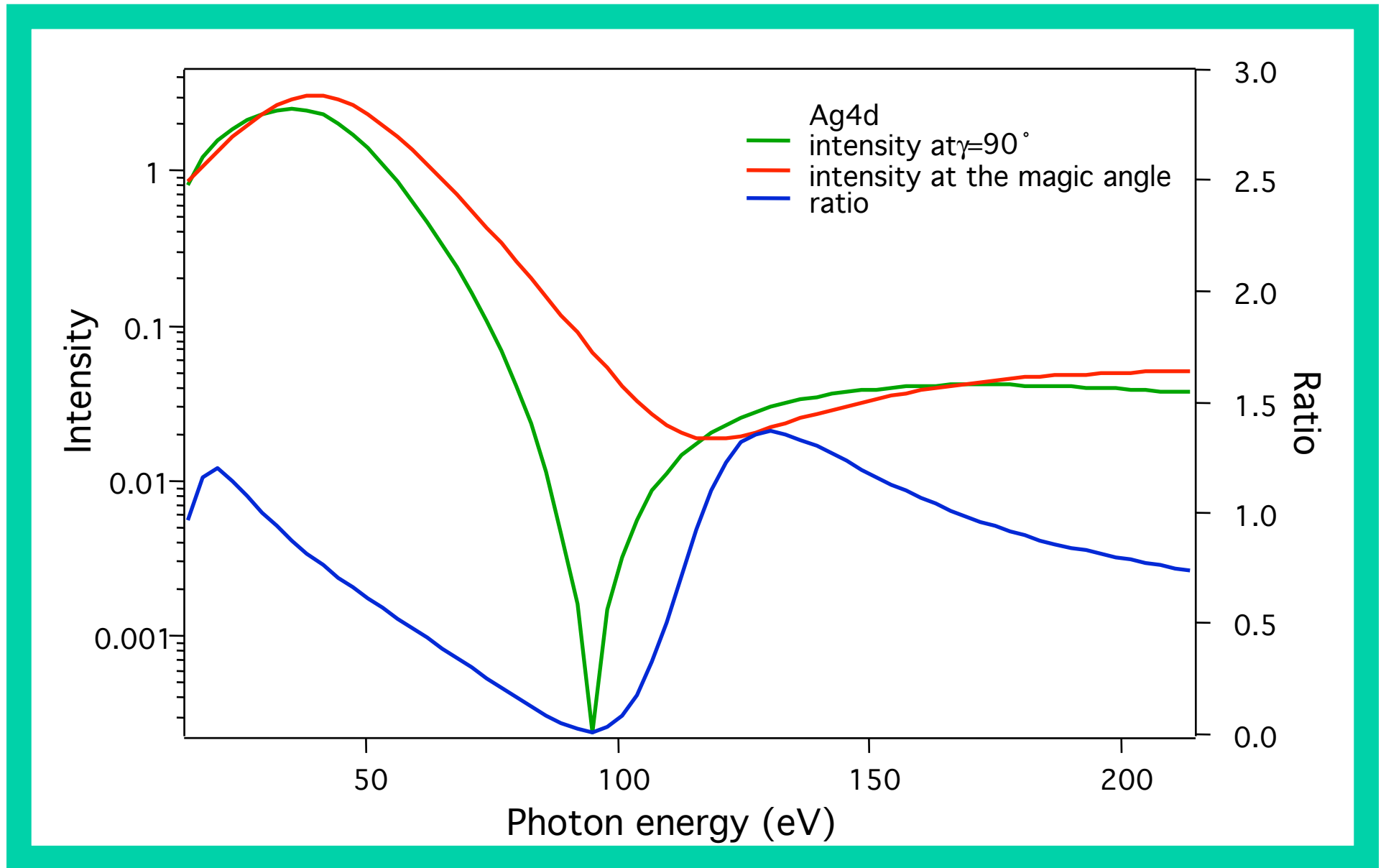
# Example: the Ag 4d level



# Example: the Ag 4d level (log scale)



# Example: the Ag 4d level

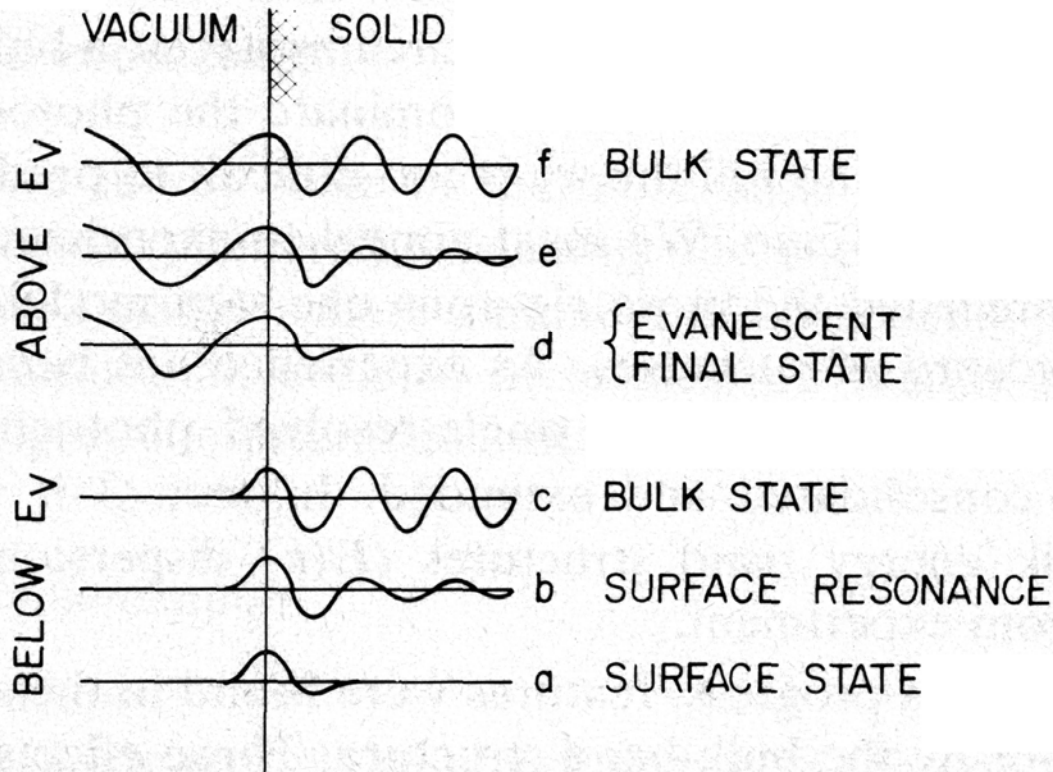


# Valence band angle resolved photoemission (ARUPS)

- Bulk and surface states
- Band mapping
- Selection rules
  - determination of the symmetry
  - determination of adsorption geometry



## WAVE FUNCTIONS AT THE SURFACE



Schematic representation of the wave functions of initial states (a), (b) and (c), and final states (d), (e) and (f), involved in optical transitions giving rise to photoelectron emission. States (c) and (f) correspond to bulk Bloch states hardly modified by the presence of the surface. States (b) and (e) are more strongly evanescent (surface resonances). States (a) and (d) have essentially no amplitude in the interior of the solid and correspond respectively to a true bound surface state and the case of band-gap emission.

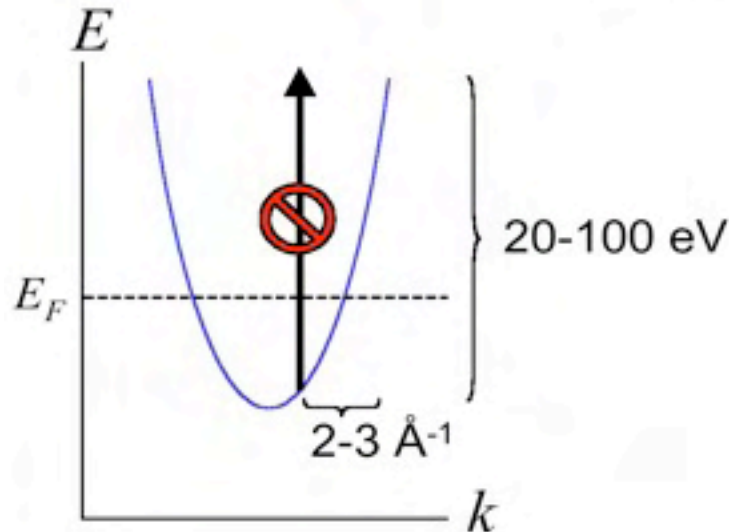
1

## Photoexcitation process: Momentum conservation

Photon Momentum  $p = \hbar q = h / \lambda$

Photon Energy  $E = h\nu = hc / \lambda$

Typical photon wavenumber  $q = 2\pi \frac{E}{hc} = 2\pi \frac{E [\text{eV}]}{12400 [\text{eV} \cdot \text{\AA}]}$   
 $= .01 \text{ to } .05 \text{ \AA}^{-1}$  (for  $E = 20 \text{ to } 100 \text{ eV}$ )

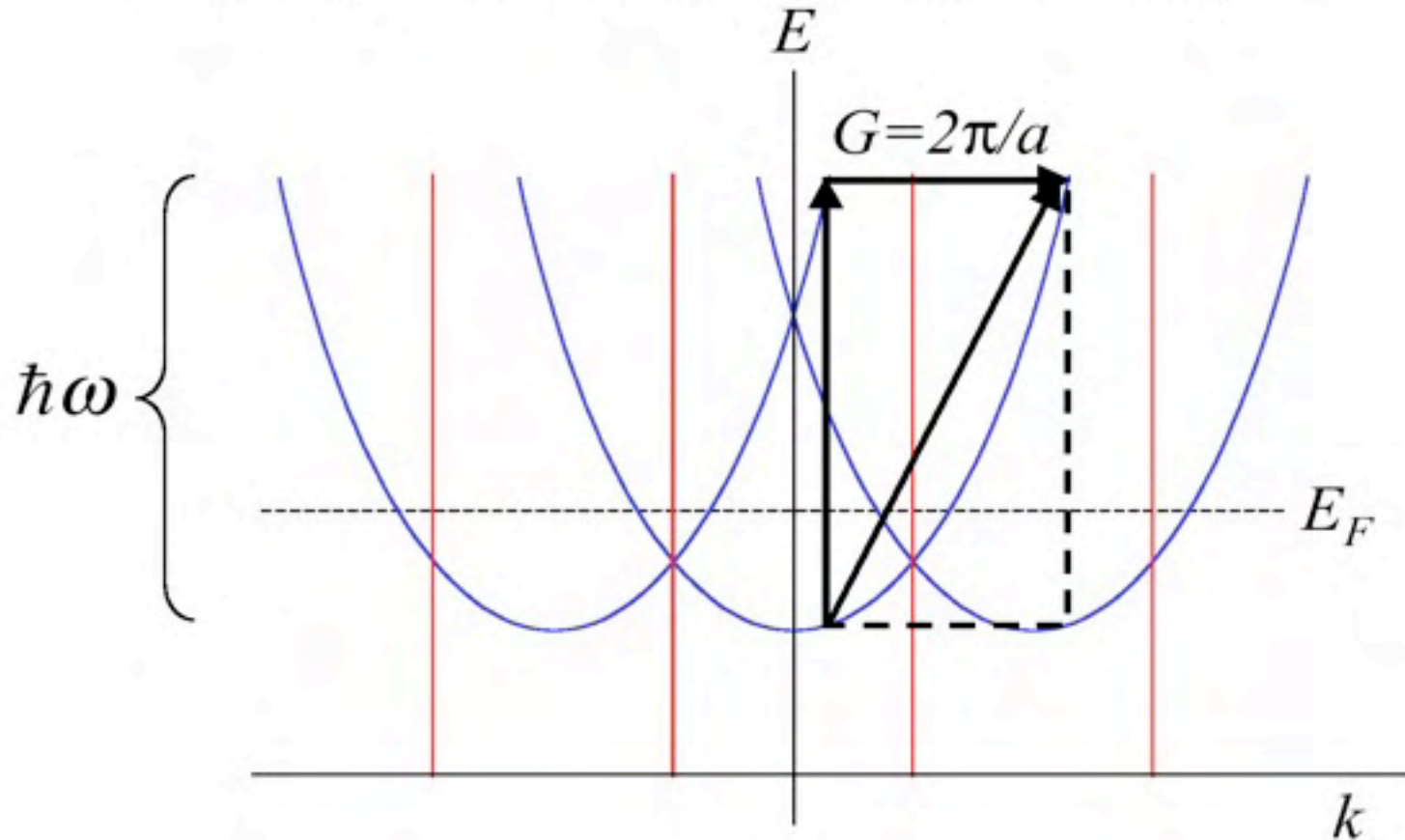


- The photons impart very little momentum in the photoemission process, i.e. **vertical transitions**
- Therefore photon-stimulated transitions are not allowed for free electrons (**energy and momentum conservation laws cannot be satisfied at the same time**).

## In order to satisfy both energy and momentum conservation

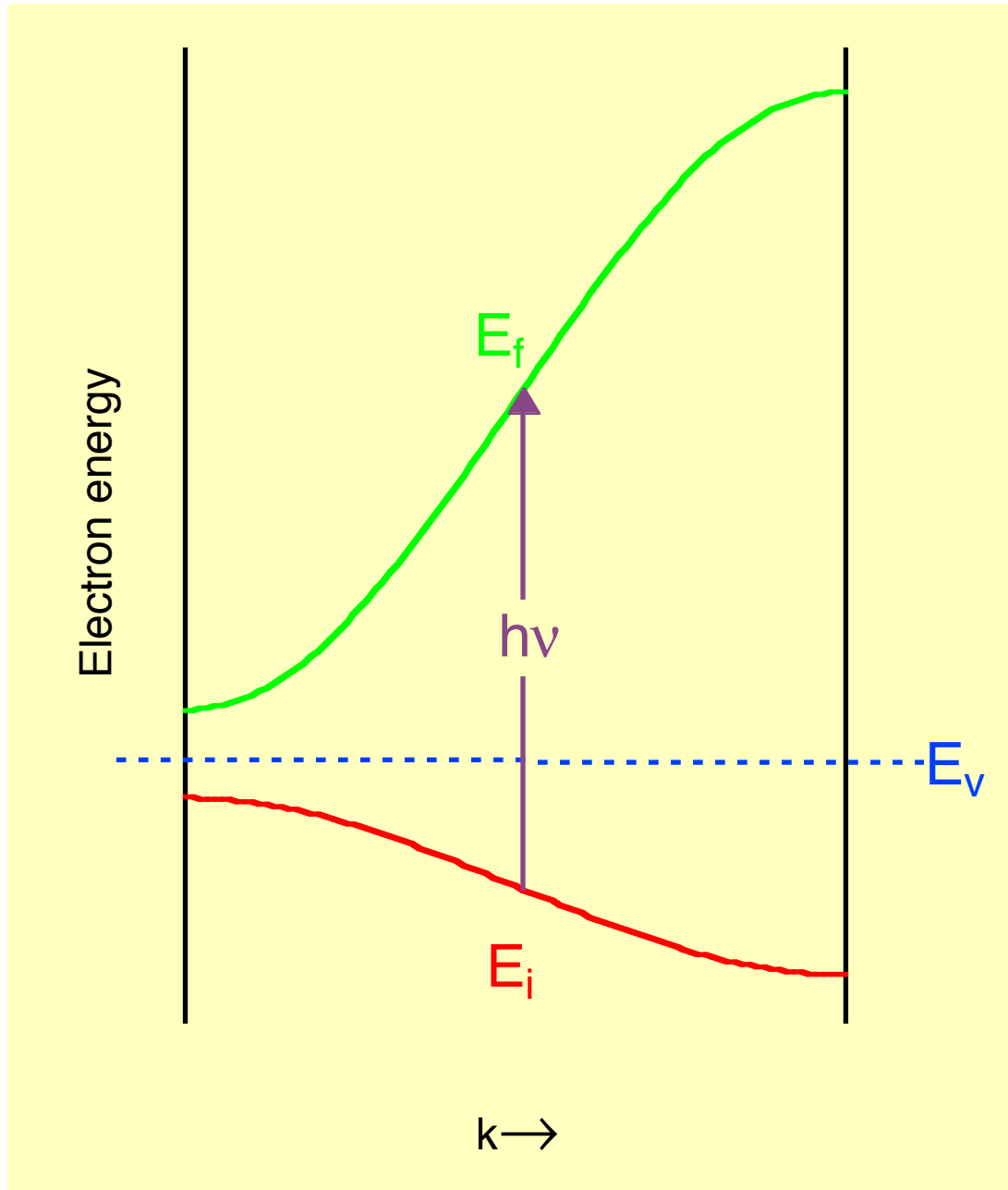
The role of crystal translational symmetry is crucial

- i.e. no photoemission is allowed from truly free electrons.



$$E_f = E_i + \hbar\nu \quad \& \quad \mathbf{k}_f = \mathbf{k}_i + \mathbf{G}$$

# Direct transitions

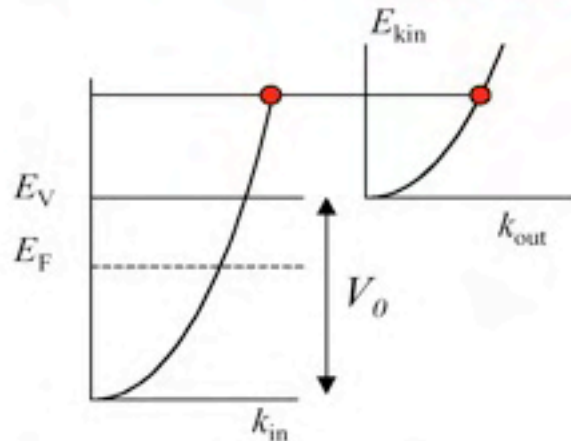


At the surface the crystal symmetry is conserved in the surface plane but is broken perpendicularly to the surface: the component of the electron momentum parallel to the surface plane ( $k_{//}$ ) is conserved, but  $k_{\perp}$  is not

The potential barrier at the surface slows the electron in the direction normal to the surface.



**Free-electron final state model**

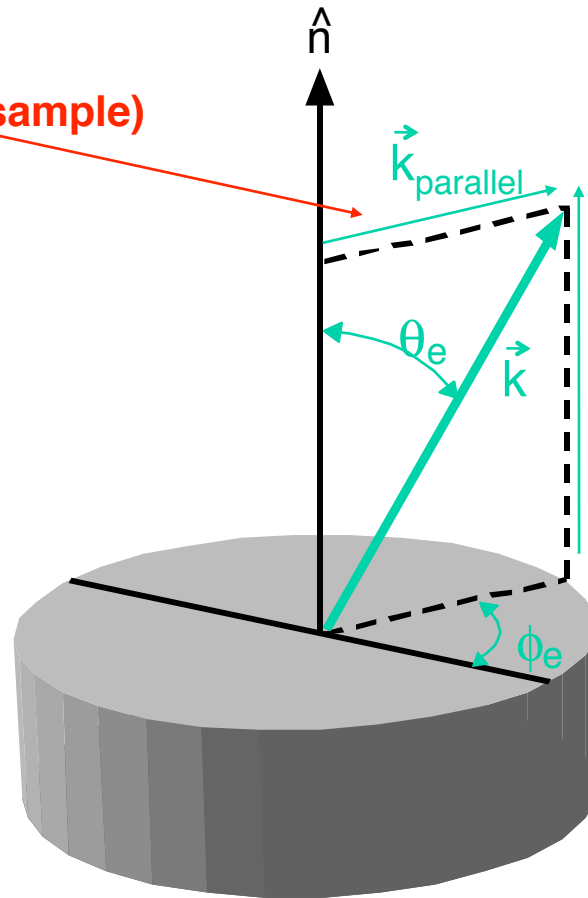


We match the free-electron parabolas inside and outside the solid to obtain the wavevector  $k$  inside the solid

# Momentum conservation

The surface breaks the translational symmetry along  $\hat{n}$

Conserved (i.e.  $\vec{k}_{\text{parallel}}$  in the sample)



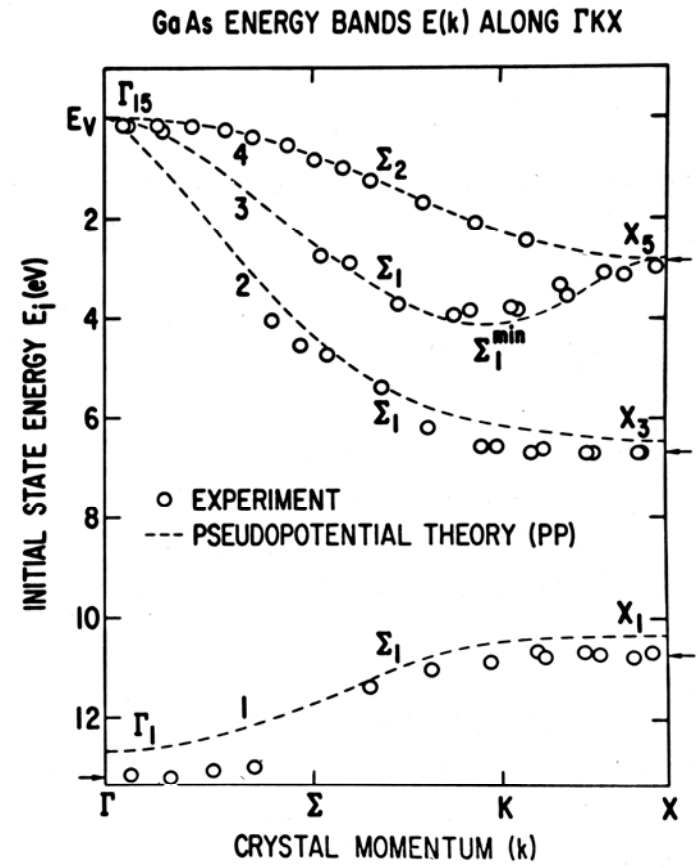
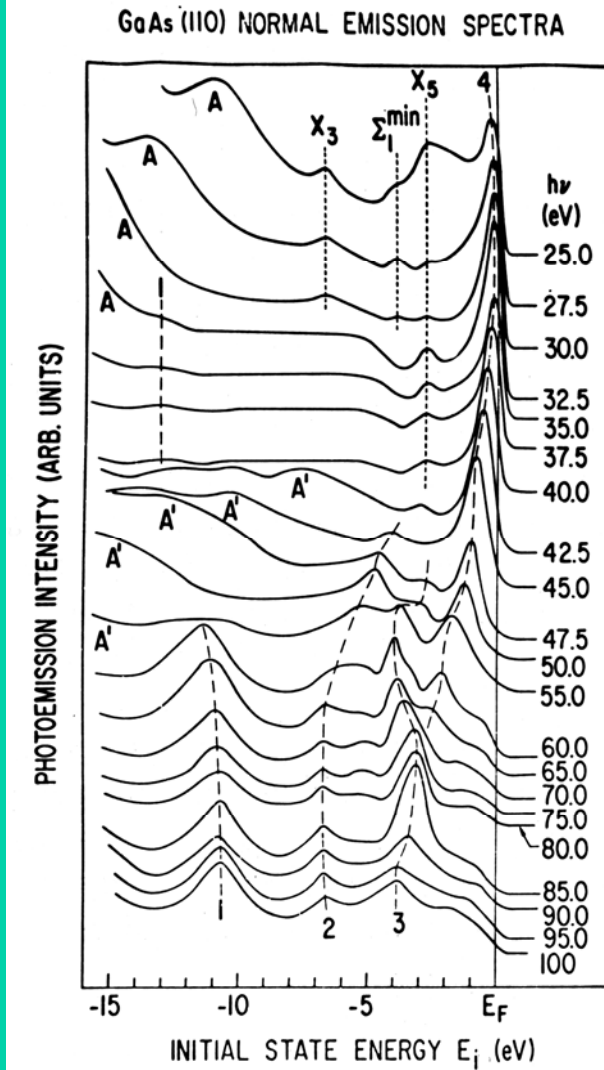
$$E_k = \frac{\hbar^2 k^2}{2m}$$

Outgoing electron

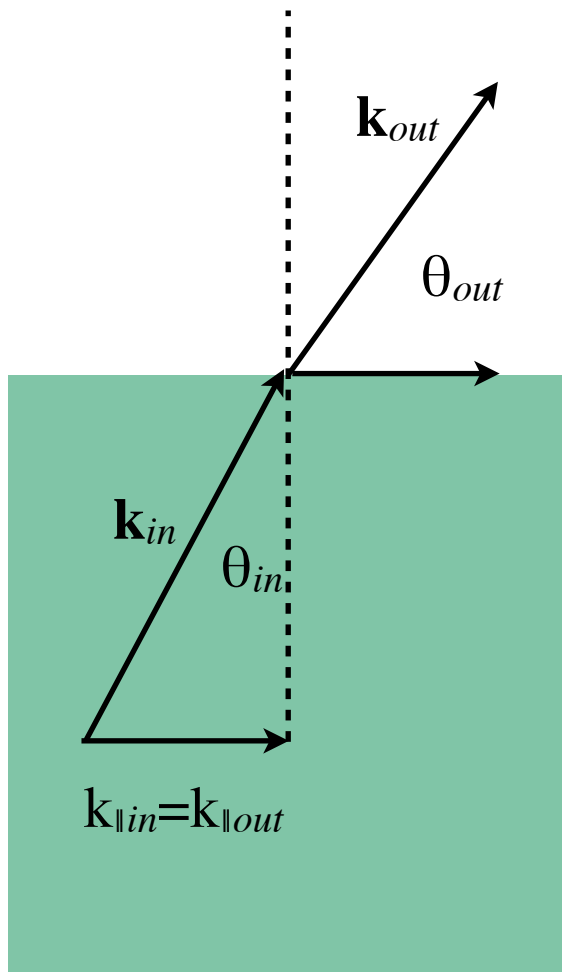
NOT Conserved

Oriented single crystal

# Band mapping: GaAs



At the surface the crystal symmetry is conserved in the surface plane but is broken perpendicularly to the surface: the component of the electron momentum parallel to the surface plane ( $k_{\parallel}$ ) is conserved, but  $k_{\perp}$  is not



### *Kinematic relations*

$$k_{out} = \sqrt{\frac{2m^*}{\hbar^2} E_{kin}}$$

$$k_{in} = \sqrt{\frac{2m^*}{\hbar^2} (E_{kin} + V_0)}$$

$$k_{out\parallel} = k_{in\parallel} = k_{\parallel}$$

### *"Snell's law"*

$$k_{\parallel} = \sin \theta_{out} \sqrt{\frac{2m^*}{\hbar^2} E_{kin}} = \sin \theta_{in} \sqrt{\frac{2m^*}{\hbar^2} (E_{kin} + V_0)}$$

### *Critical angle for emission from bulk states*

$$(\sin \theta_{in})_{max} = \sqrt{\frac{E_{kin}}{E_{kin} + V_0}}$$



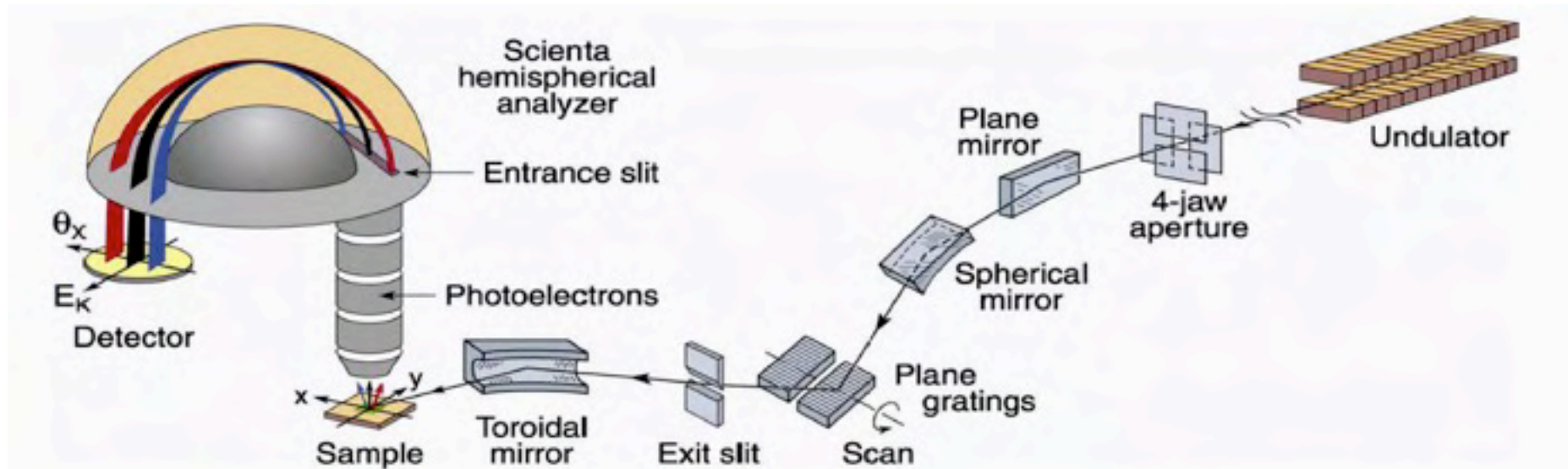
## First important results:

$$E_k = h\nu - |E_B| - \Phi_{Analyzer}$$

$$k_{//} = \sqrt{\frac{2m^* E_k}{\hbar^2}} \sin \theta_{out} \approx 0.512 \sqrt{E_k} \sin \theta_{out}$$

Band mapping is therefore completely determined for 2D systems and surface states for which  $k_{//}$  is a good quantum number

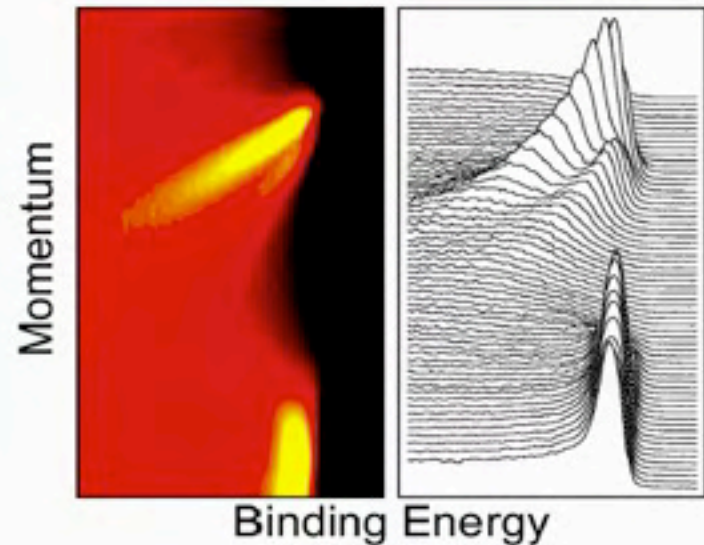
# State-of-the-art



## Parallel multi-angle recording

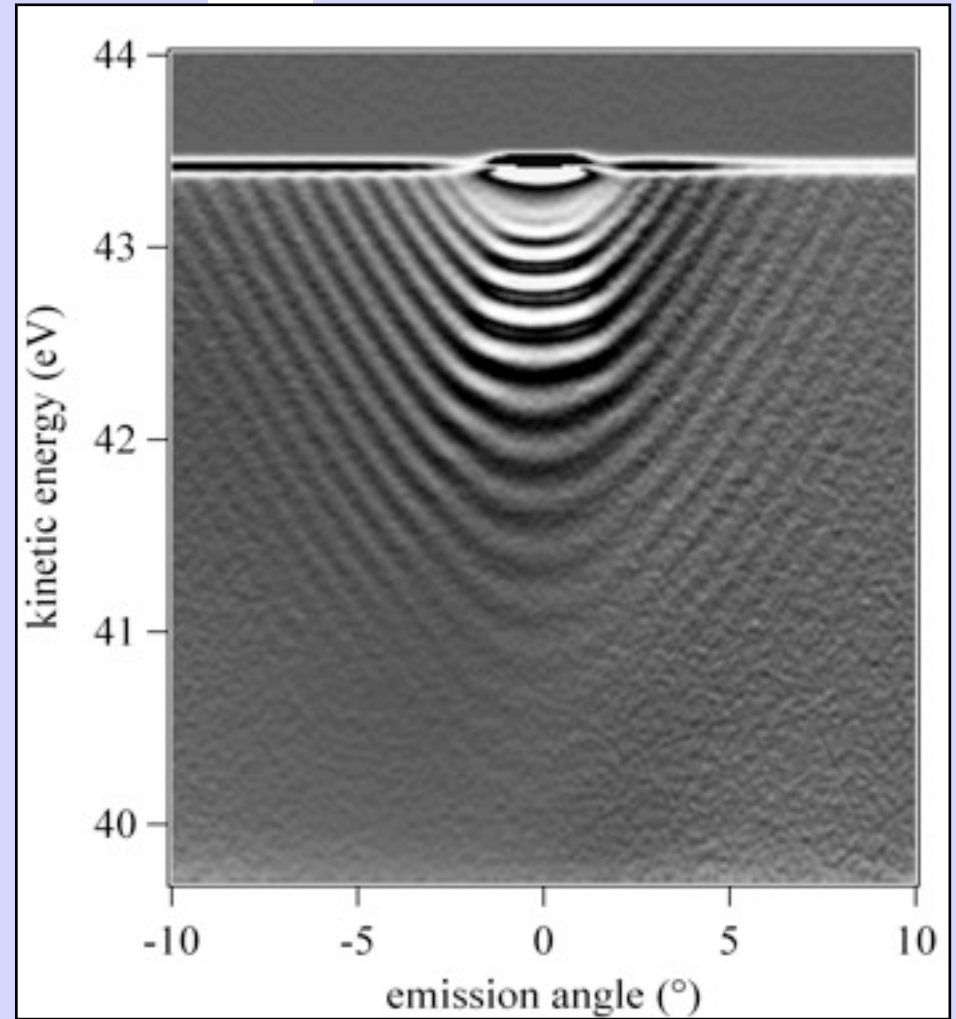
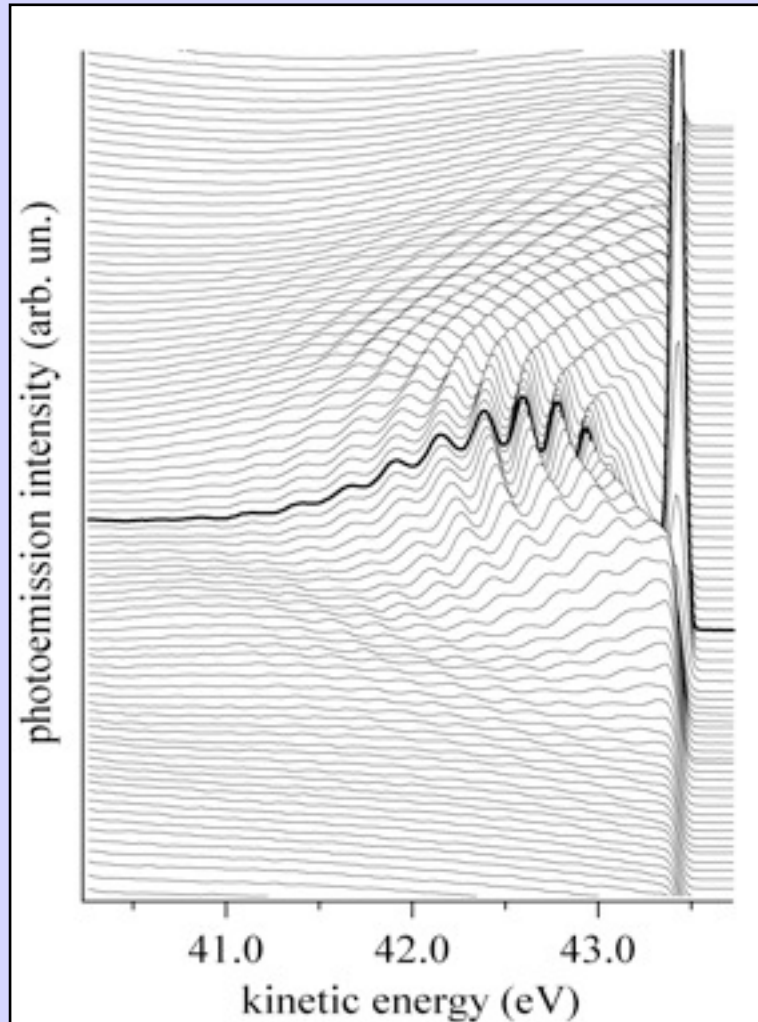
- Improved **energy resolution**
- Improved **momentum resolution**
- Improved **data-acquisition efficiency**

	$\Delta E$ (meV)	$\Delta\theta$
<b>past</b>	<b>20-40</b>	<b>2°</b>
<b>now</b>	<b>2-10</b>	<b>0.2°</b>



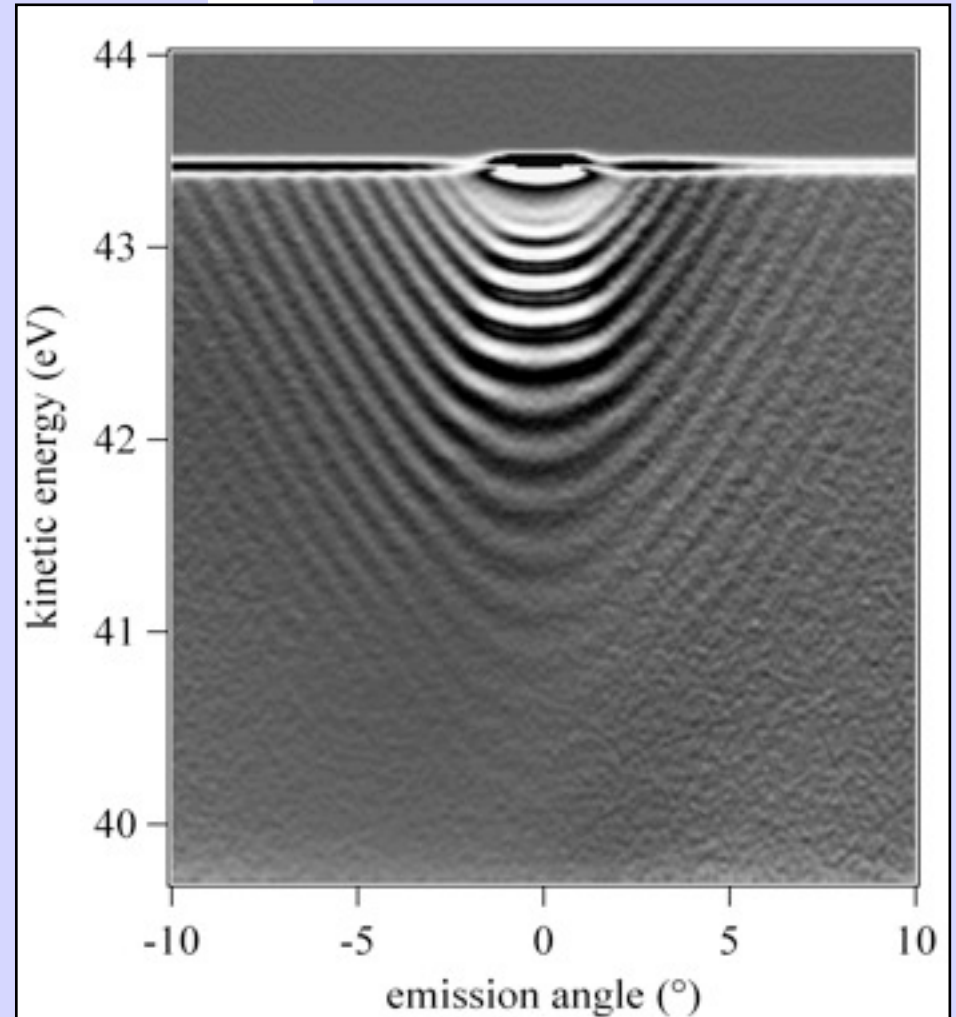
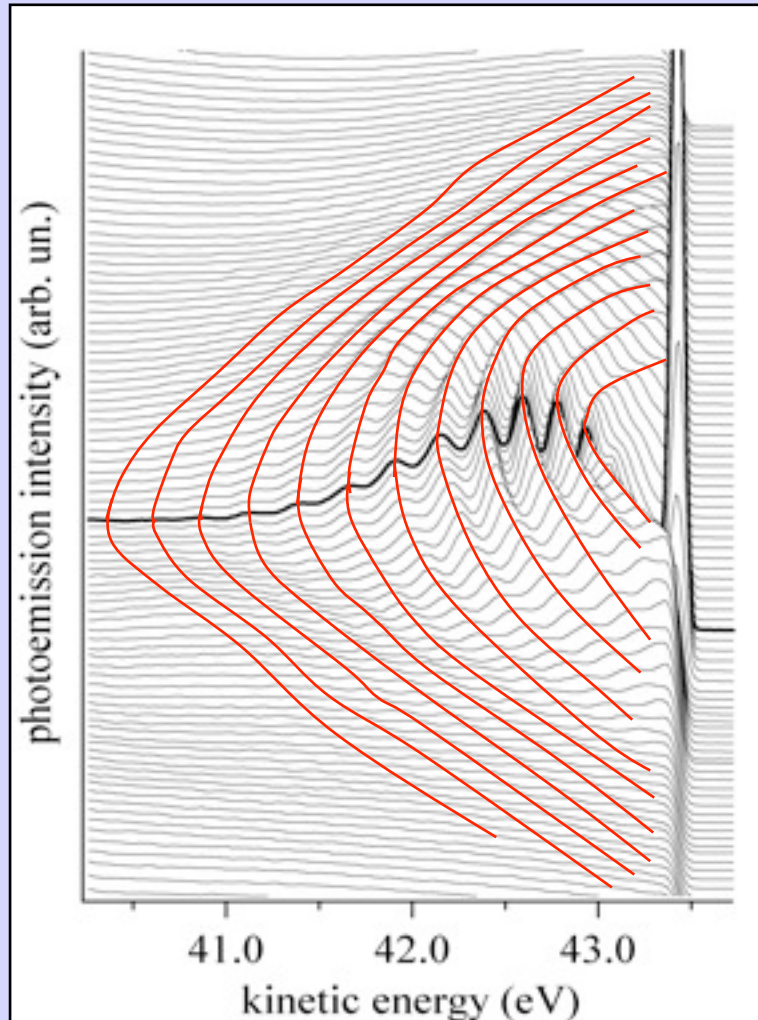
courtesy of A. Damascelli

## Discrete quantum well states of an atomically flat 150 Å Ag film on Pt(111)

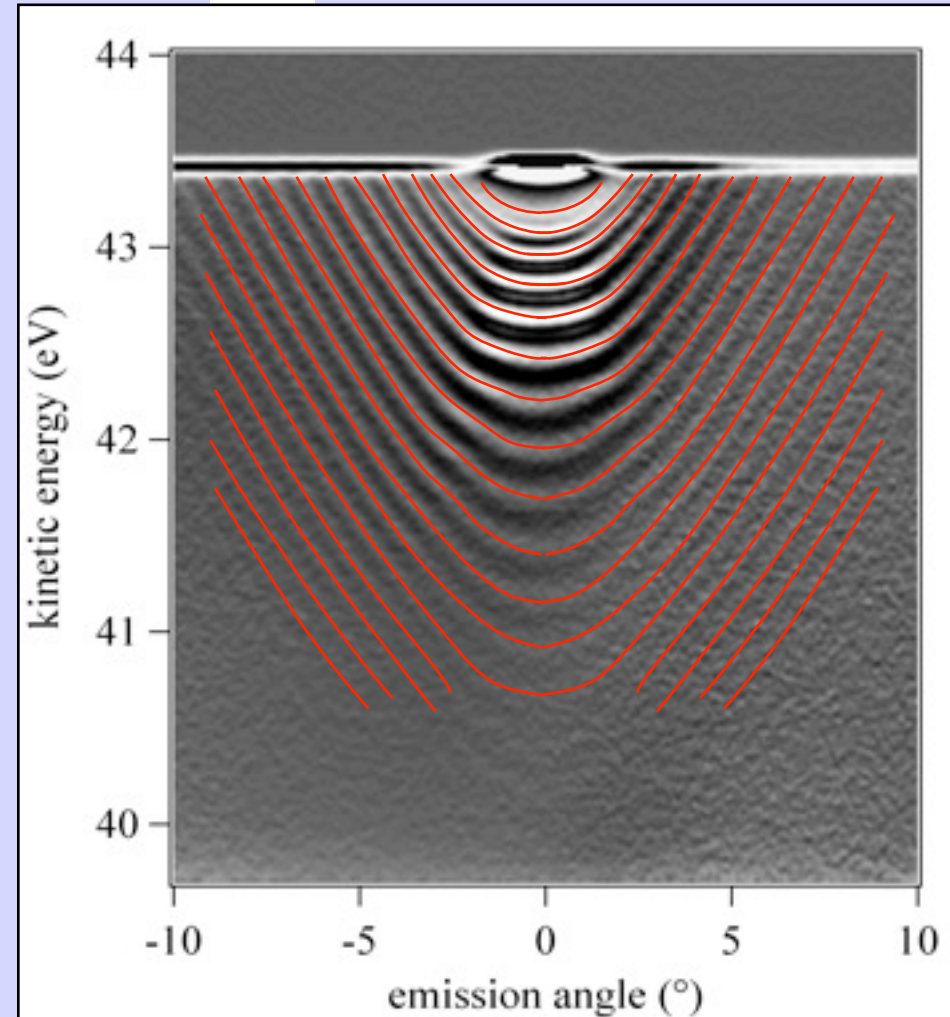
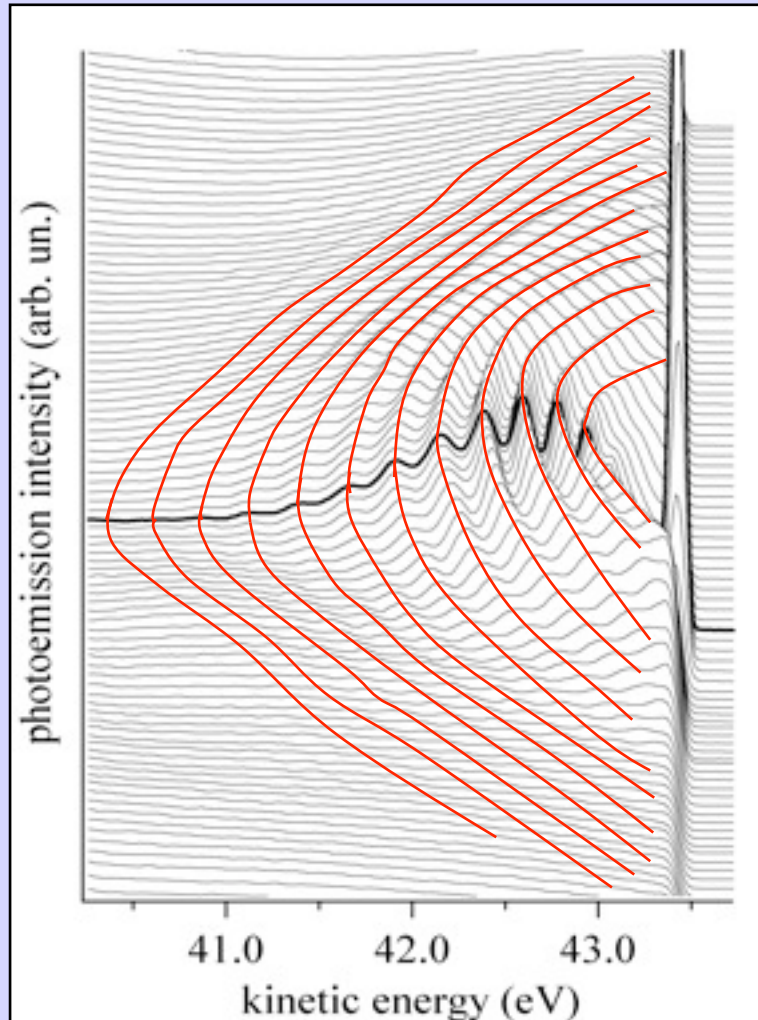




Discrete quantum well states of an atomically flat 150 Å Ag film on Pt(111)



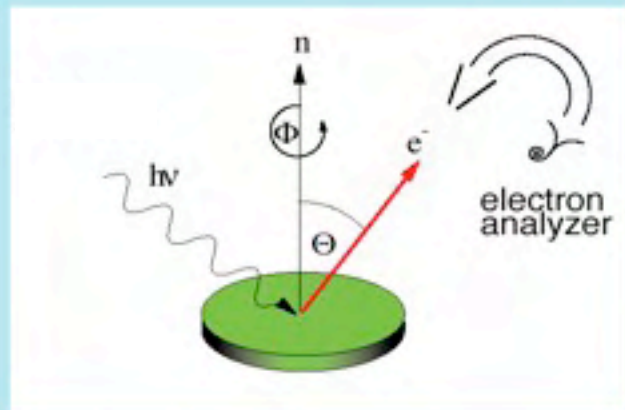
## Discrete quantum well states of an atomically flat 150 Å Ag film on Pt(111)





# Angle-resolved photoemission from (quasi) 2D systems: a simple picture

Example: Cu(111) surface state

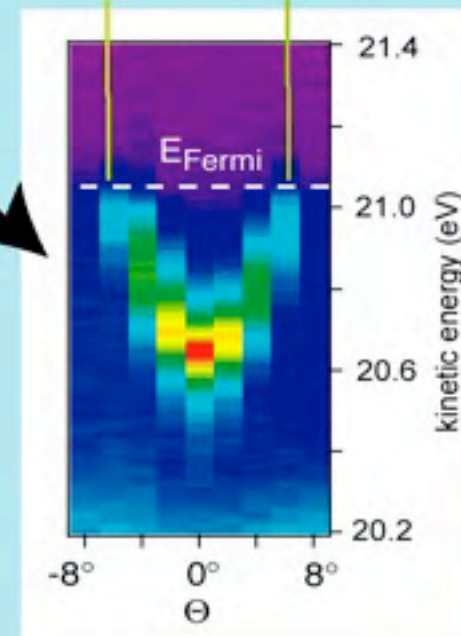
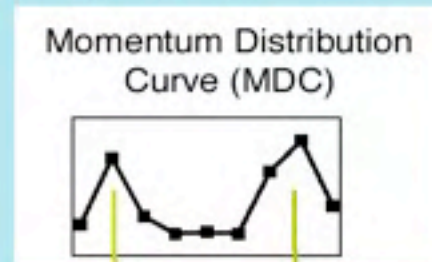
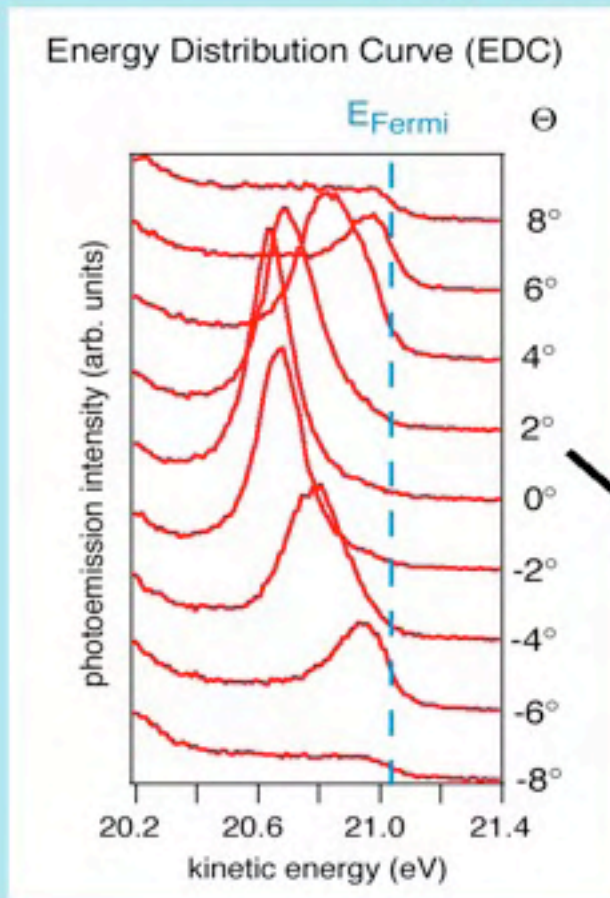


- measure  $E_{kin}$ ,  $\Theta$ ,  $\Phi$ .

$$k_x = \sqrt{\frac{2m}{\hbar^2}} \sin \Theta \cos \Phi \sqrt{E_{kin}}$$

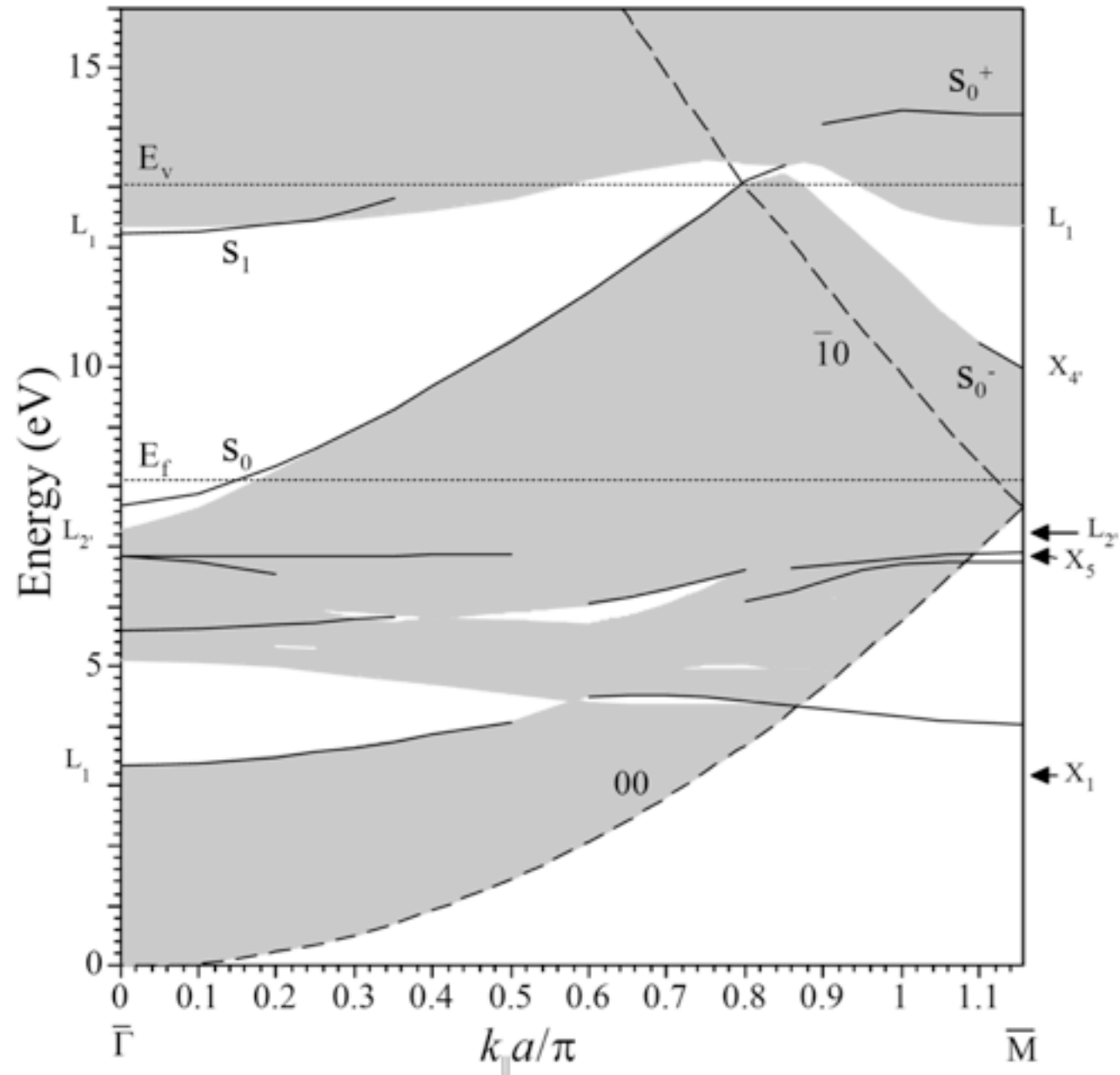
$$k_y = \sqrt{\frac{2m}{\hbar^2}} \sin \Theta \sin \Phi \sqrt{E_{kin}}$$

obtain  $E_{bin}(k_x, k_y)$ , i.e. the occupied band structure



Courtesy of Ph. Hofmann

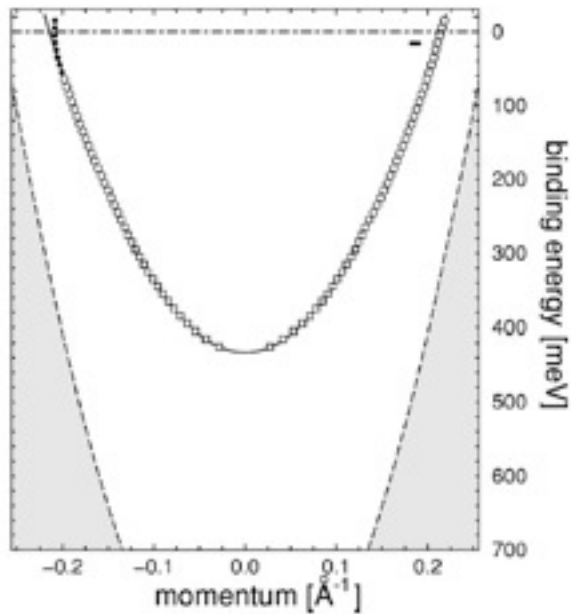
# Cu (111) surface band structure



# Shockley Surface States of Noble Metal (111) Surfaces

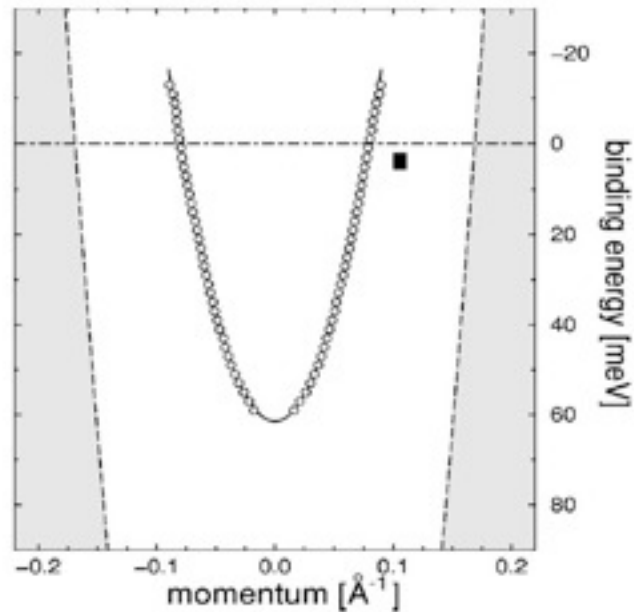
Cu(111)

Z=29



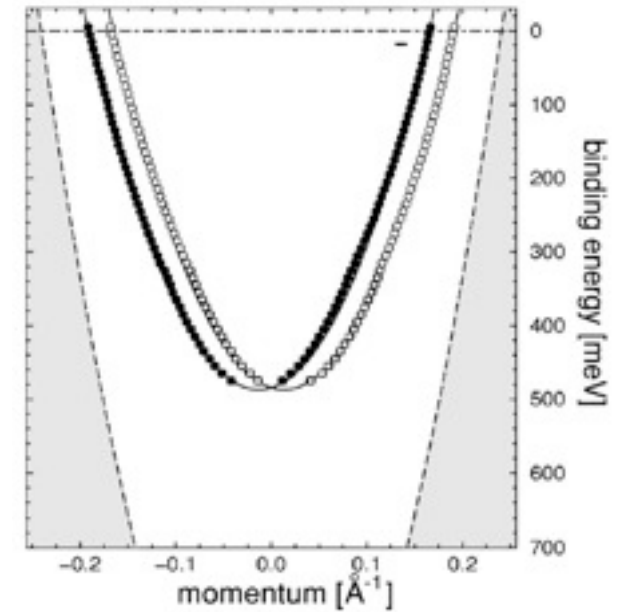
Ag(111)

Z=47



Au(111)

Z=79



Two parabolas: spin-orbit splitting

PES Experiment, Reinert, Nicolay, Ehm, and Hüfner, PRB 63, 115415 (2001)



# Bandgap opening in graphene induced by patterned hydrogen adsorption

Richard Balog<sup>1</sup>, Bjarke Jørgensen<sup>1</sup>, Louis Nilsson<sup>1</sup>, Mie Andersen<sup>1</sup>, Emile Rienks<sup>2</sup>, Marco Bianchi<sup>3</sup>, Mattia Fanetti<sup>4</sup>, Erik Lægsgaard<sup>1</sup>, Alessandro Baraldi<sup>3,4</sup>, Silvano Lizzit<sup>5</sup>, Zeljko Sljivancanin<sup>6</sup>, Flemming Besenbacher<sup>1</sup>, Bjørk Hammer<sup>1</sup>, Thomas G. Pedersen<sup>7</sup>, Philip Hofmann<sup>2</sup> and Liv Hornekær<sup>1\*</sup>

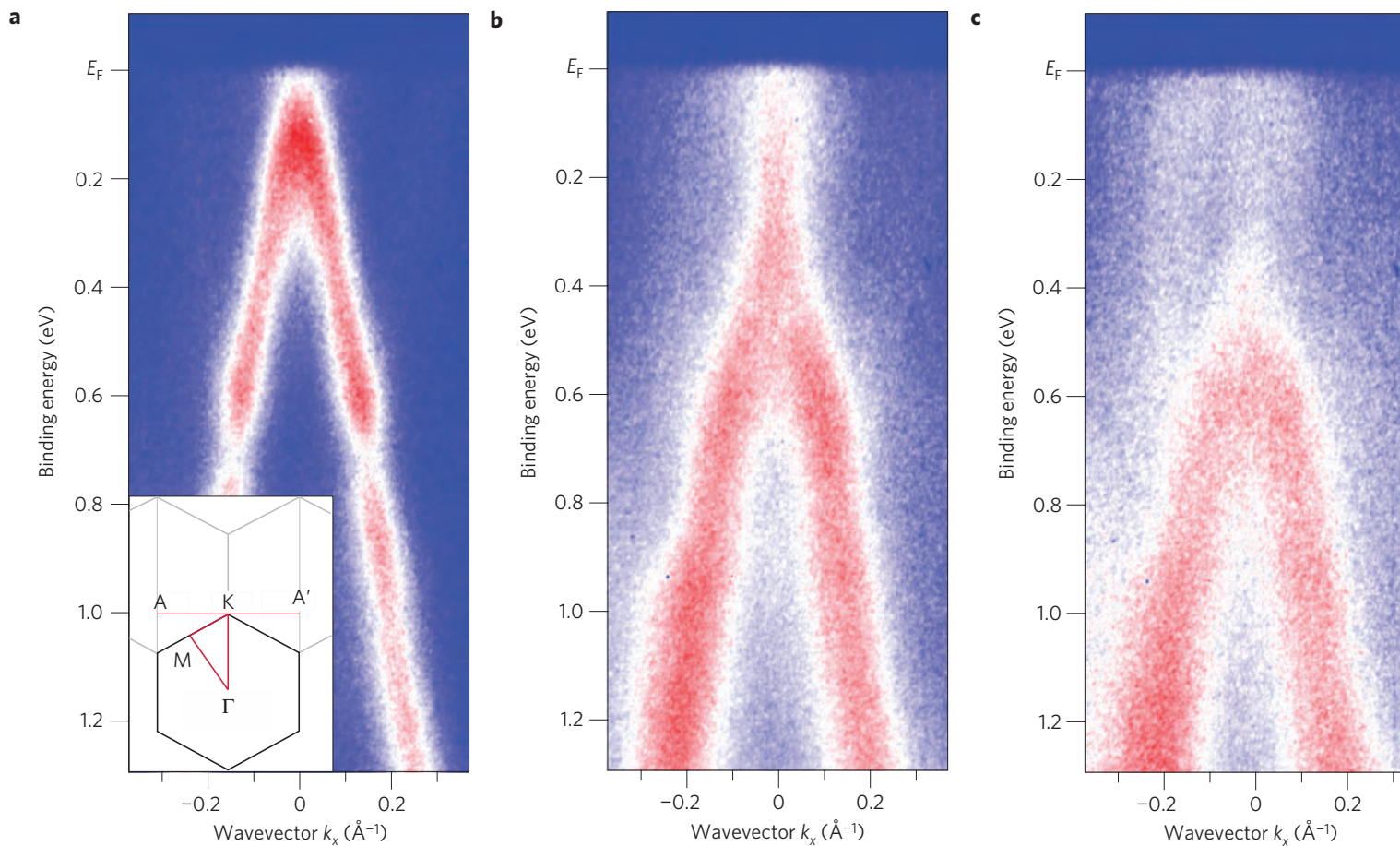


**Figure 1 | Observation of a gap opening in hydrogenated graphene.** a–c, Photoemission intensity along the A–K–A' direction of the Brillouin zone (see inset) for clean graphene on Ir(111) (a), graphene exposed to a 30 s dose of atomic hydrogen (b) and graphene exposed to a 50 s dose of atomic hydrogen (c).

# Bandgap opening in graphene induced by patterned hydrogen adsorption

Richard Balog<sup>1</sup>, Bjarke Jørgensen<sup>1</sup>, Louis Nilsson<sup>1</sup>, Mie Andersen<sup>1</sup>, Emile Rienks<sup>2</sup>, Marco Bianchi<sup>3</sup>, Mattia Fanetti<sup>4</sup>, Erik Lægsgaard<sup>1</sup>, Alessandro Baraldi<sup>3,4</sup>, Silvano Lizzit<sup>5</sup>, Zeljko Sljivancanin<sup>6</sup>, Flemming Besenbacher<sup>1</sup>, Bjørk Hammer<sup>1</sup>, Thomas G. Pedersen<sup>7</sup>, Philip Hofmann<sup>2</sup> and Liv Hornekær<sup>1\*</sup>

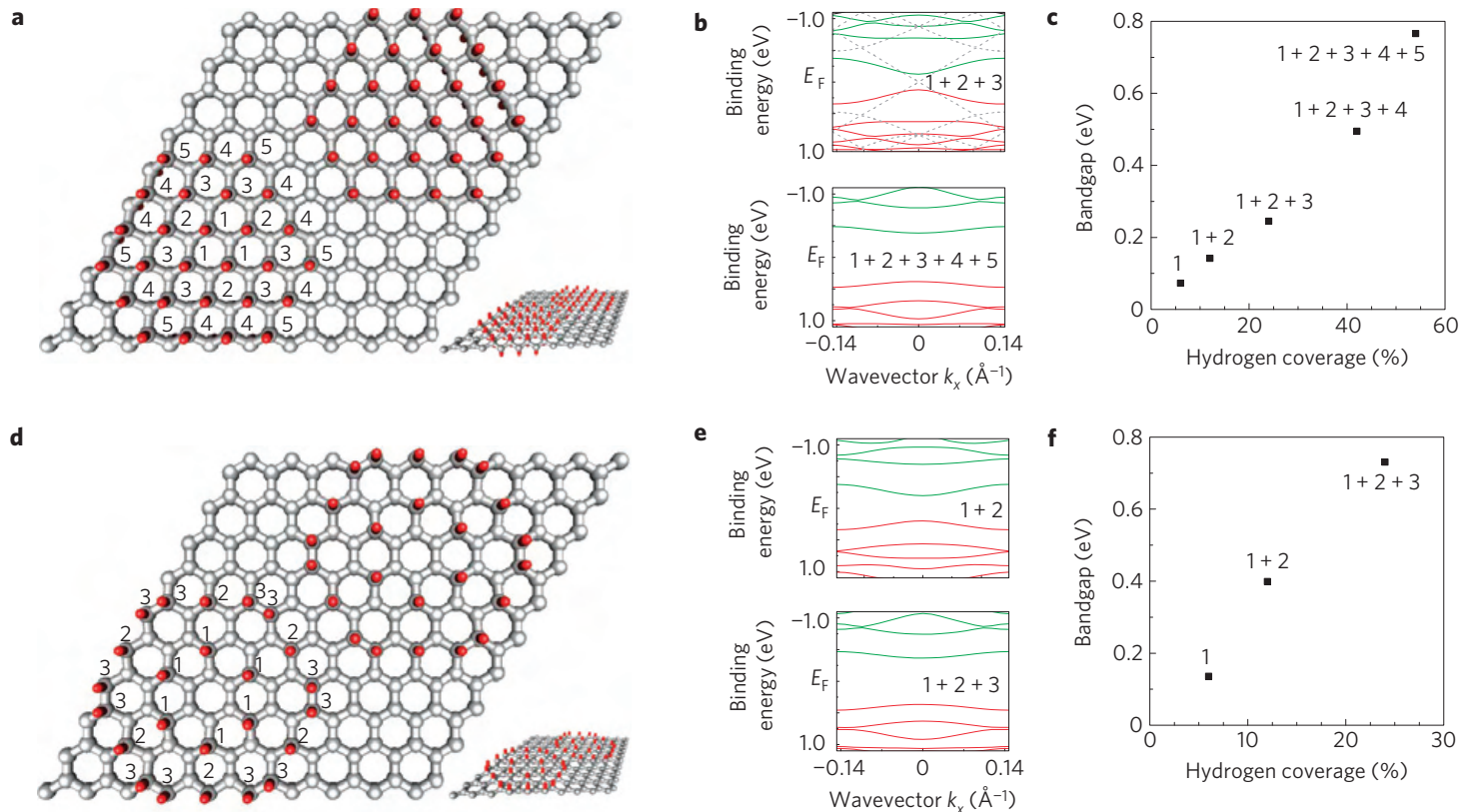
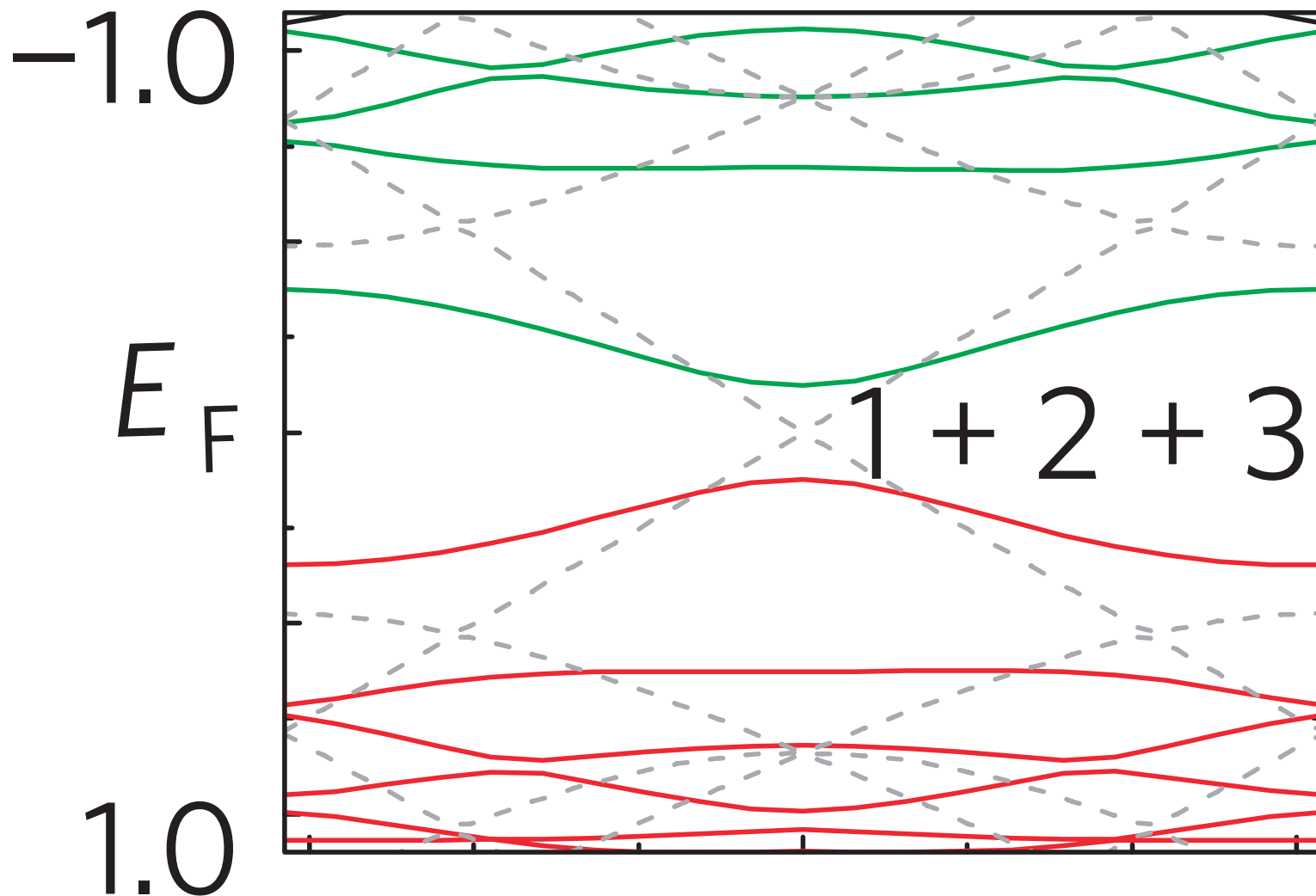


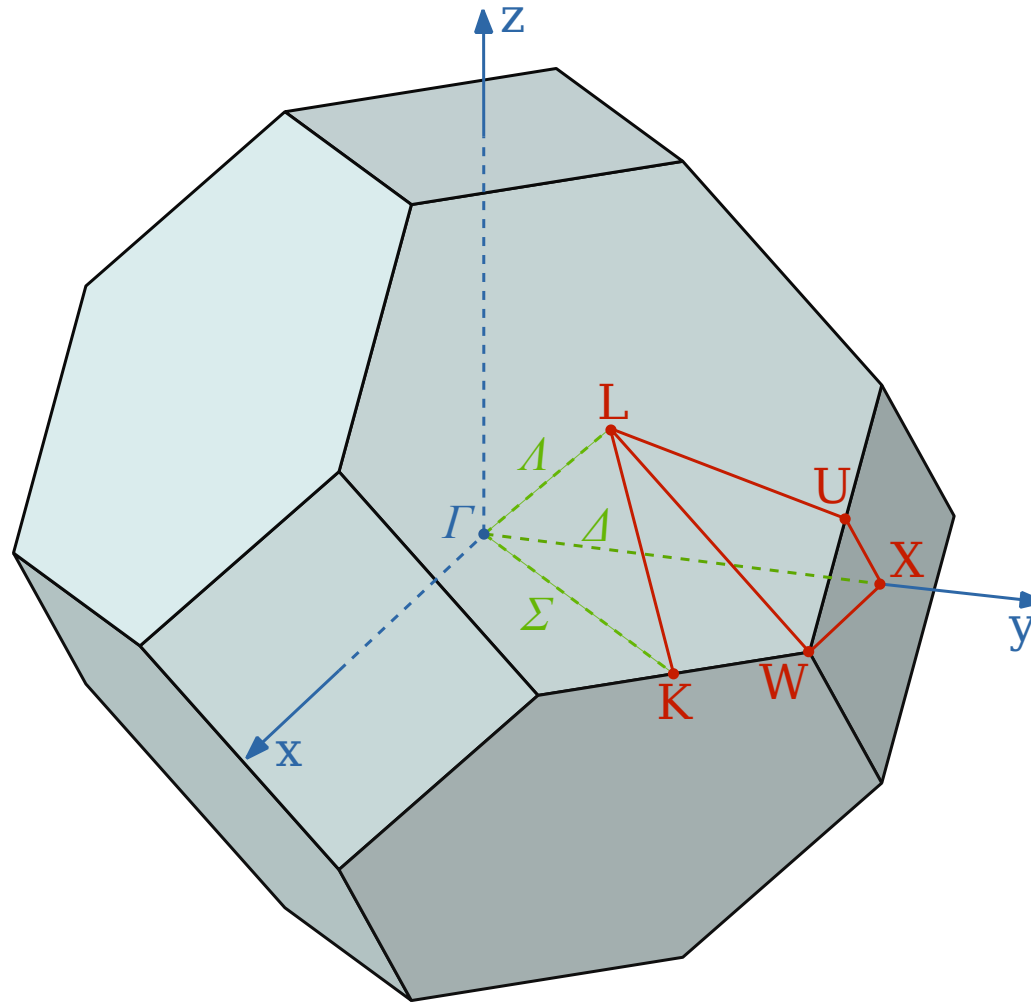
**Figure 4 | Hydrogen adsorbate structures, calculated band structures and bandgaps.** **a**, Hydrogen atom adsorbate structures forming graphane islands with hydrogen coverage ranging between 6% and 54% (corresponding to 3%–27% of the top sites) following the Moiré superlattice periodicity. **b**, Band structures for graphane-like islands with medium and high hydrogen coverage. Filled and empty bands are shown in red and green, respectively. For comparison, the band structure of intact graphene is shown in grey (dashed). **c**, Bandgap opening as a function of hydrogen coverage. A maximum of 0.77 eV is reached with 54% coverage (corresponding to 27% top site coverage). **d**, Adsorbate structures composed of increasing amounts of hydrogen pairs in *para* and *ortho* dimer configurations. **e**, Band structures with and without *ortho*-hydrogen dimers. **f**, Bandgap opening as a function of hydrogen coverage. At 23% coverage a bandgap opening as large as 0.73 eV is obtained. In **b**, **c**, **e** and **f**, numbers 1–5 refer to adsorbate structures formed by hydrogen atoms at all the positions marked by the corresponding numbers in **a** and **d** respectively.

# Bandgap opening in graphene induced by patterned hydrogen adsorption

Richard Balog<sup>1</sup>, Bjarke Jørgensen<sup>1</sup>, Louis Nilsson<sup>1</sup>, Mie Andersen<sup>1</sup>, Emile Rienks<sup>2</sup>, Marco Bianchi<sup>3</sup>,  
Mattia Fanetti<sup>4</sup>, Erik Lægsgaard<sup>1</sup>, Alessandro Baraldi<sup>3,4</sup>, Silvano Lizzit<sup>5</sup>, Zeljko Sljivancanin<sup>6</sup>,  
Flemming Besenbacher<sup>1</sup>, Bjørk Hammer<sup>1</sup>, Thomas G. Pedersen<sup>7</sup>, Philip Hofmann<sup>2</sup> and Liv Hornekær<sup>1\*</sup>



# The fcc Brillouin zone



Valence-band structure of silver along  $\Lambda$  from angle-resolved photoemissionP. S. Wehner,\* R. S. Williams,<sup>†</sup> S. D. Kevan, D. Denley,<sup>‡</sup> and D. A. ShirleyMaterials and Molecular Research Division, Lawrence Berkeley Laboratory and Department of Chemistry,  
University of California, Berkeley, California 94720

(Received 20 November 1978)

# Ag band structure

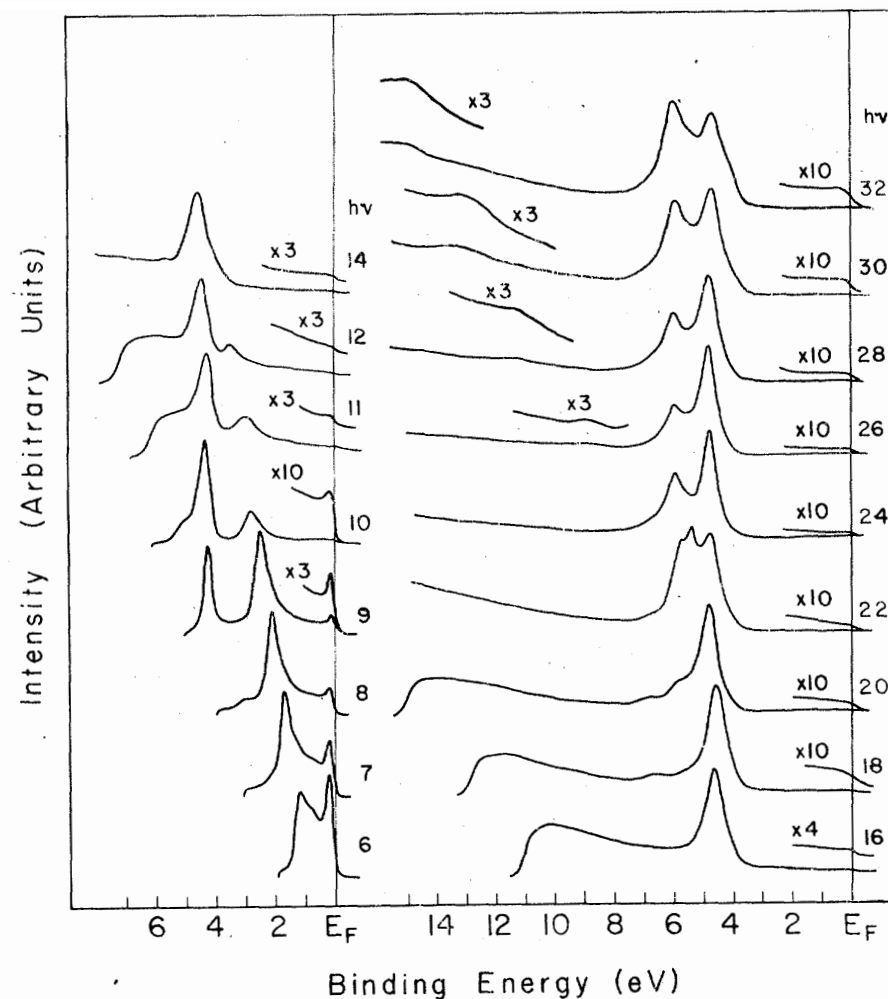


FIG. 1. Electron energy distributions at normal emission for Ag(111) in the range  $h\nu = 6$  to 32 eV. The region of predominantly  $sp$  emission near  $E_F$  is magnified for most spectra. For  $h\nu = 26$  to 32 eV the region containing the constant final-state feature is also magnified.

Valence-band structure of silver along  $\Lambda$  from angle-resolved photoemissionP. S. Wehner,\* R. S. Williams,<sup>†</sup> S. D. Kevan, D. Denley,<sup>‡</sup> and D. A. ShirleyMaterials and Molecular Research Division, Lawrence Berkeley Laboratory and Department of Chemistry,  
University of California, Berkeley, California 94720

(Received 20 November 1978)

# Ag band structure

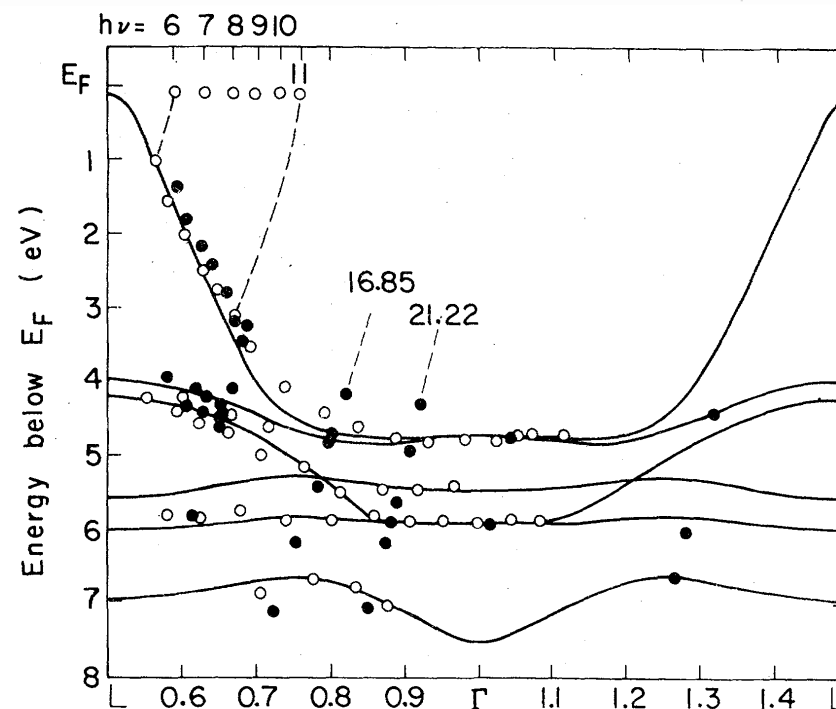


FIG. 2. Valence-band energies of silver along  $\Lambda$  vs the  $k$  point along  $\Lambda$  in the second zone that corresponds to each photoemission peak. A partial photon energy scale is indicated along the top, together with dashed curves for the conduction band (band 7) displaced down by 6 eV and by 10 eV. Christensen's band structure is plotted, together with our data (open circles) and those of Hansson and Flodström (filled circles from 7 to 11.6 eV); Roloff and Neddermeyer (filled circles at 11.83, 16.85, and 21.22 eV); and Liebowitz and Shevchik (filled circles at 26.9 and 40.8 eV).

**Valence-band structure of silver along  $\Lambda$  from angle-resolved photoemission**

P. S. Wehner,\* R. S. Williams,<sup>†</sup> S. D. Kevan, D. Denley,<sup>‡</sup> and D. A. Shirley  
*Materials and Molecular Research Division, Lawrence Berkeley Laboratory and Department of Chemistry,  
University of California, Berkeley, California 94720*  
(Received 20 November 1978)

# Ag band structure

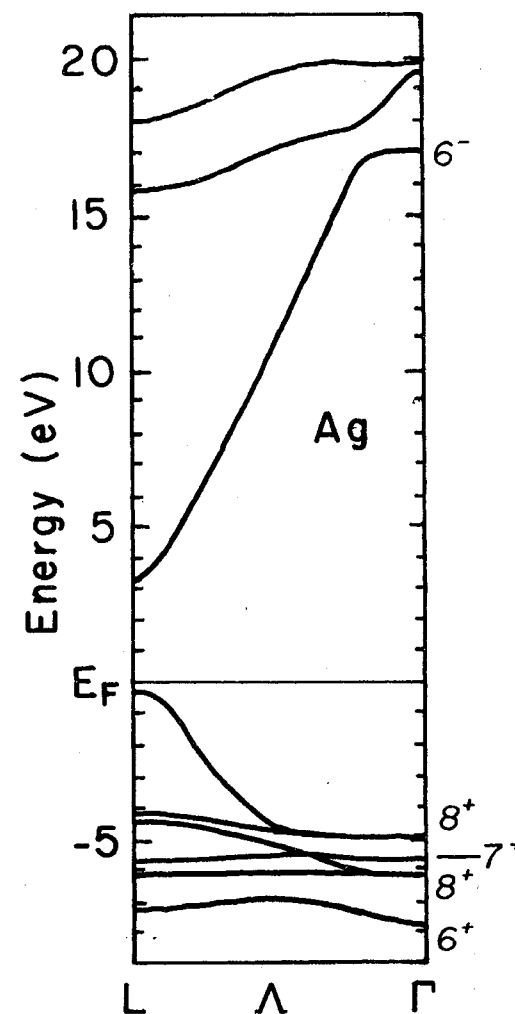
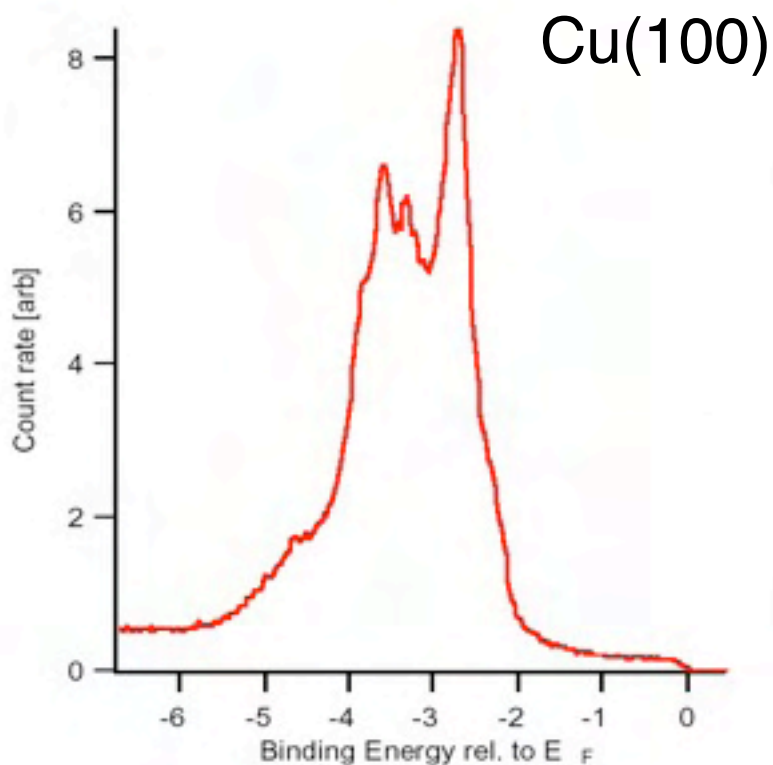


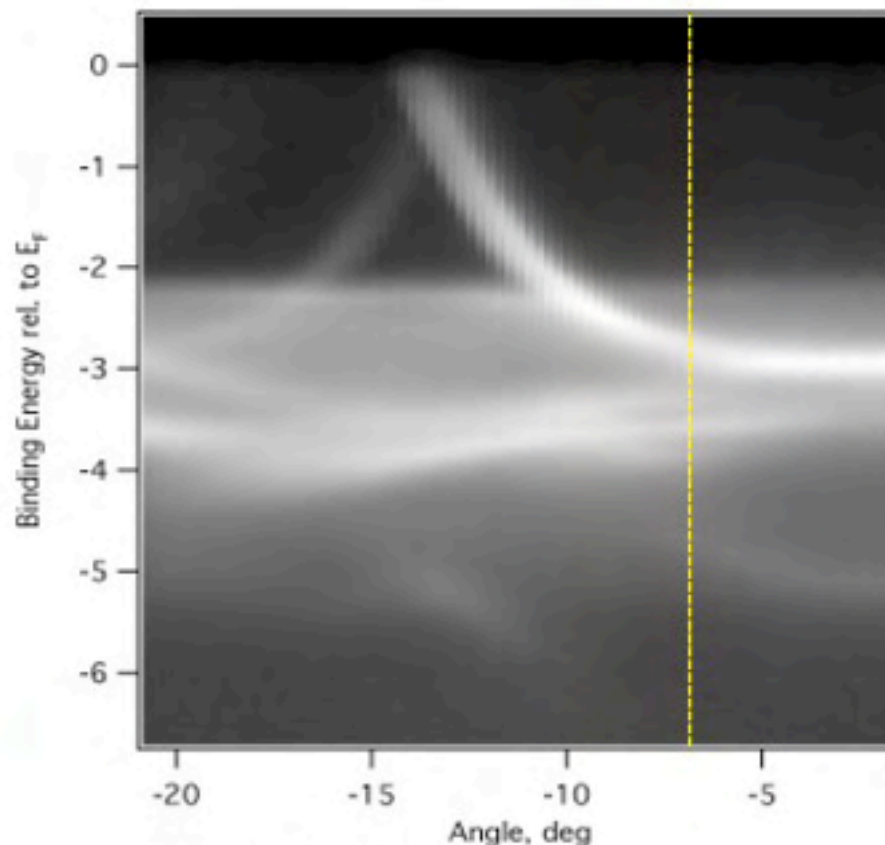
FIG. 5. Ag band structure along  $\Lambda$  as calculated in Ref. 15.



# What does a photoemission spectrum look like?



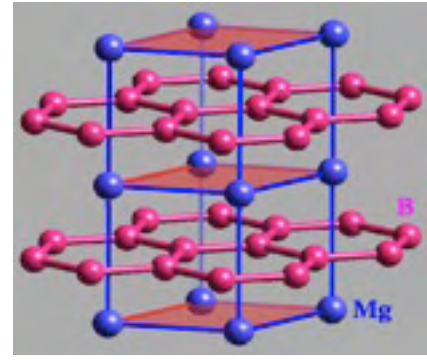
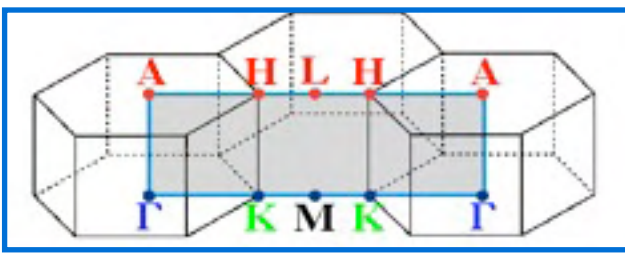
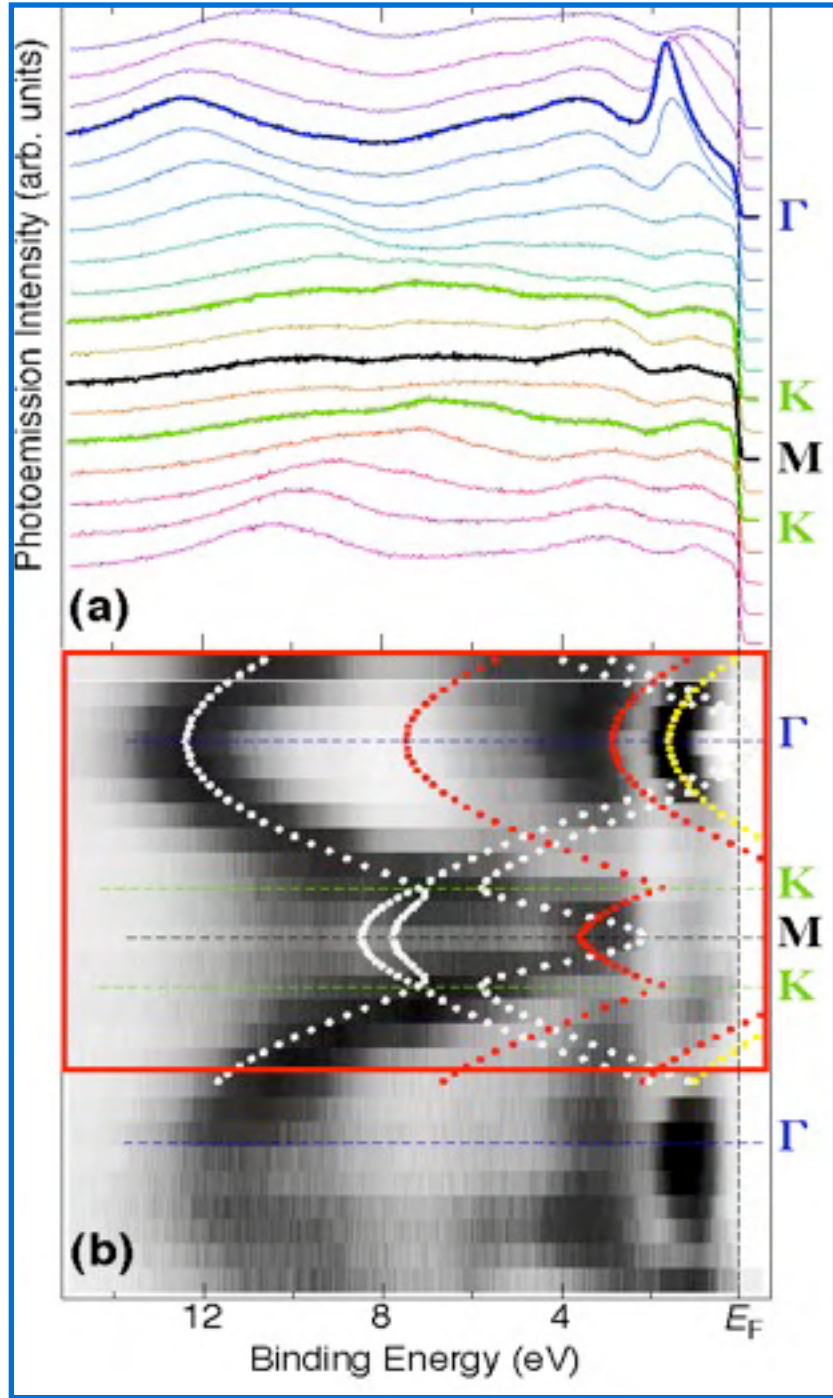
**A spectrum at a single polar angle**



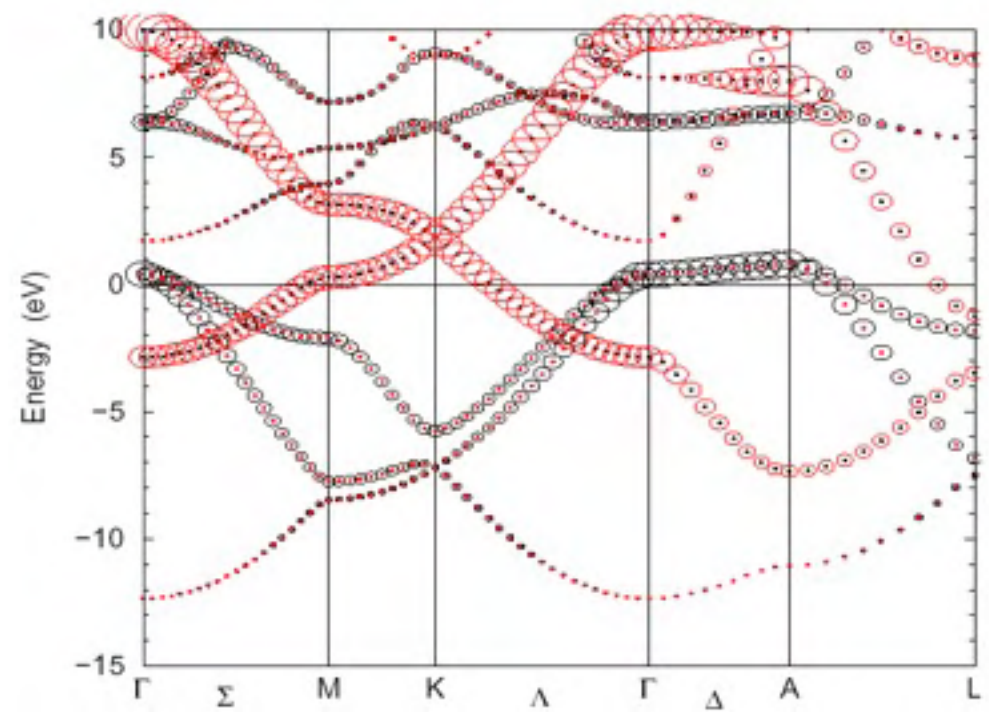
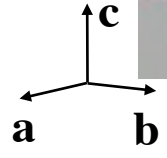
**Accumulate spectra as the angle is scanned**

Bulk or surface states? Why are bulk bands quite sharp anyway?





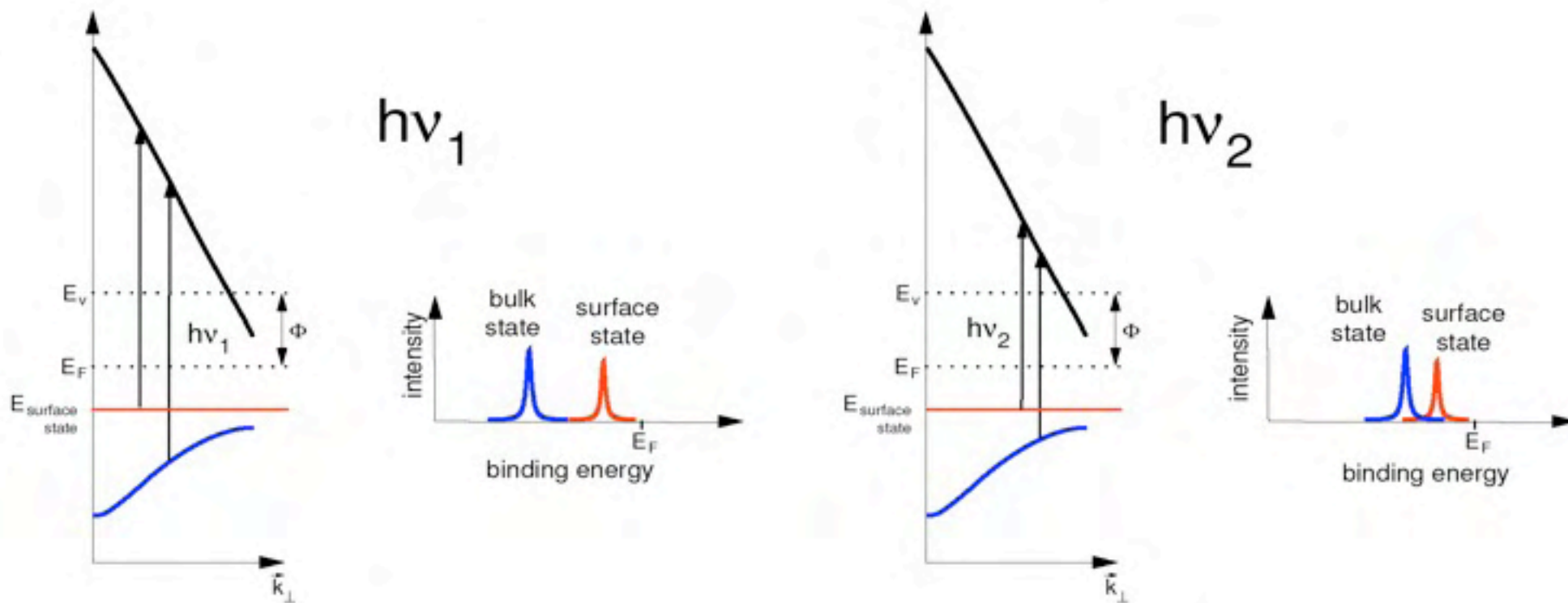
$MgB_2$



*Photon energy: 105eV ( $\Delta E \approx 50meV$ )*  
*in-plane dispersion along  $\Gamma-K-M-K-\Gamma$*

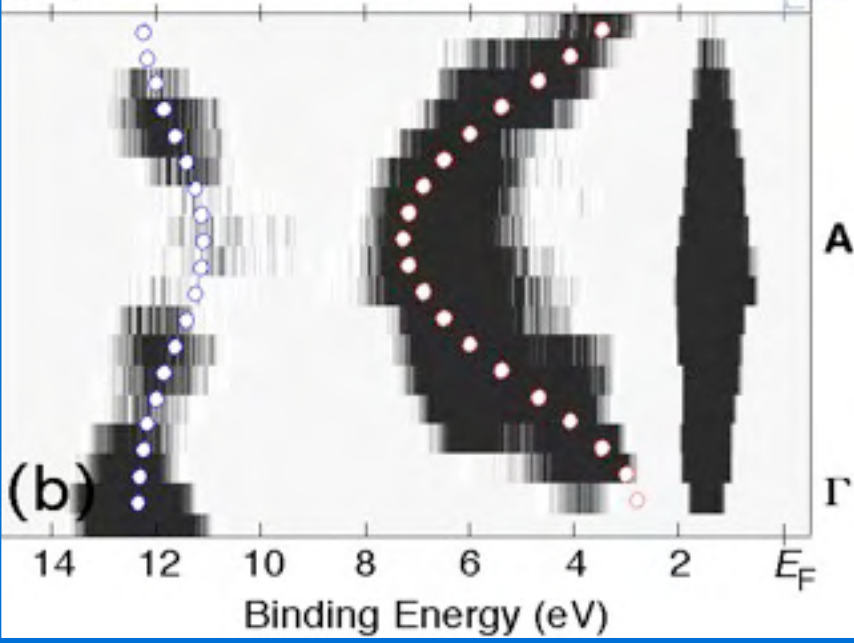
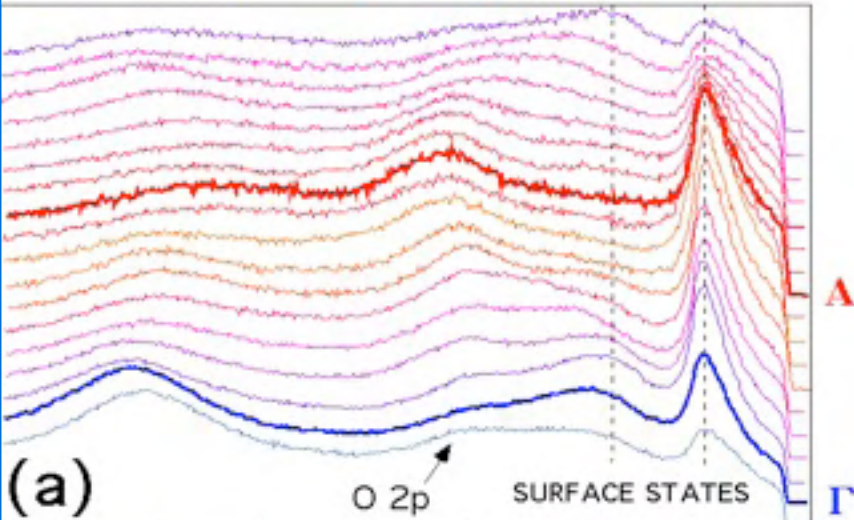
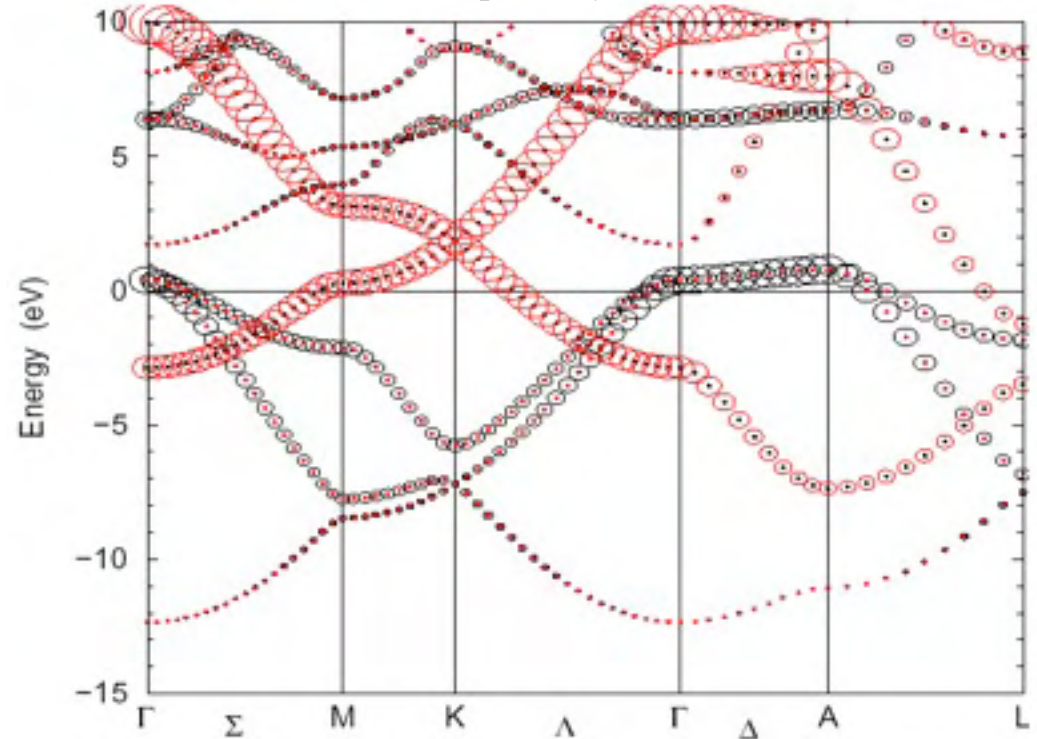
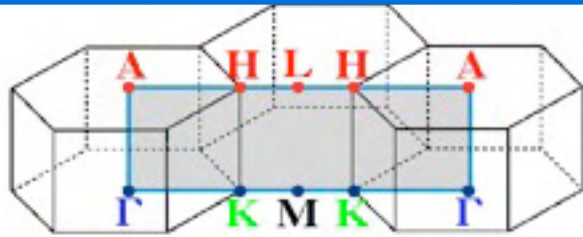
# Recognize surface states from bulk bands

fix  $k_{//}$  and change  $k_{\perp}$ . Bulk states should have dispersion, surface states should not.



**Easiest way:** fix  $k_{//}=0$  ( $\Gamma$ , normal emission) and change the photon energy





$\Gamma$ -A direction

Normal emission geometry

Photon energy: 95 eV - 185 eV ( $\Delta E \approx 50$  meV)

No dispersive peak at 1.65 eV:

Mg terminated  $MgB_2(0001)$  surface state

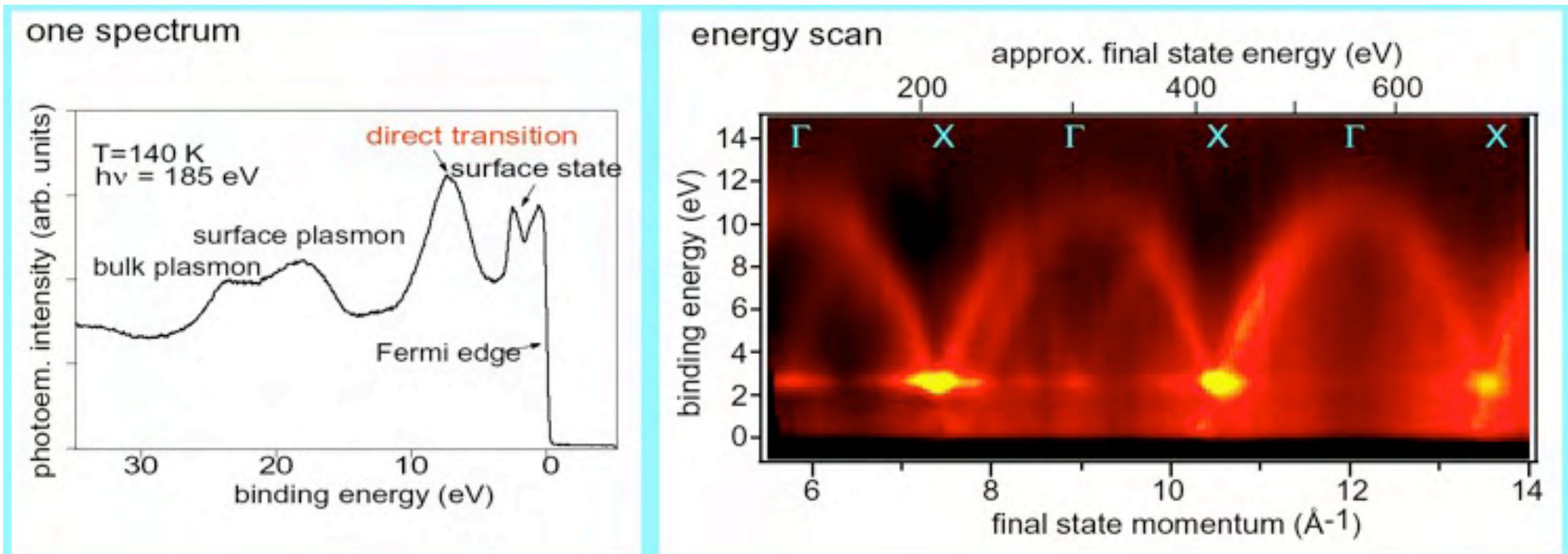
Weak no dispersive peak at 3.2 eV:

B terminated  $MgB_2(0001)$  surface state

(B terminated domains)

# Surface states and $k_{\parallel}$ mapping: example Al(100)

Photon energy changed at normal emission  $k_{\parallel}=0$

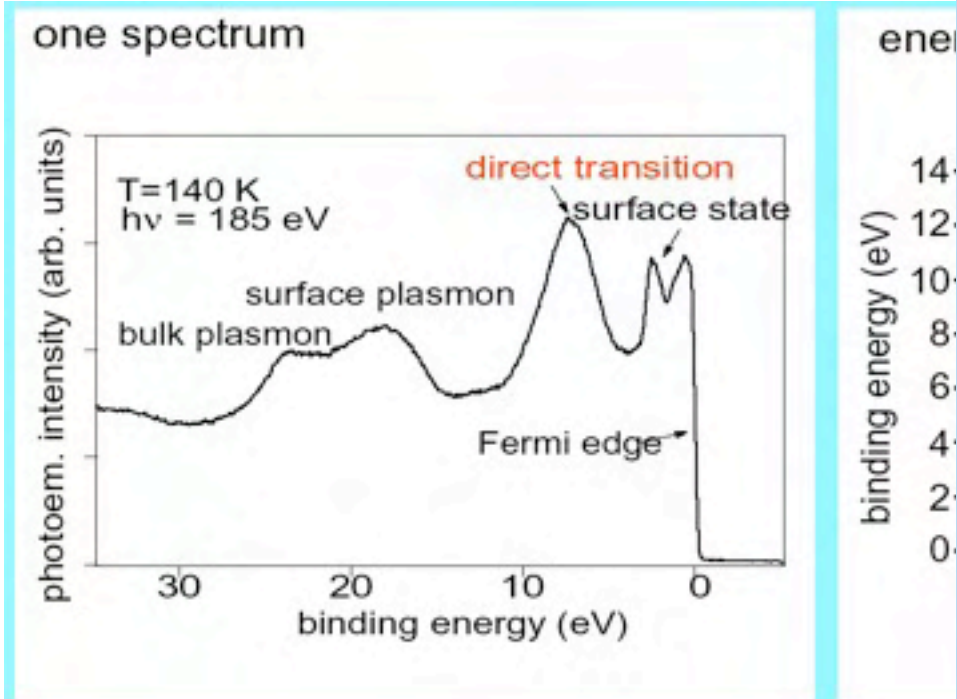


- The free electron-like band structure is evident but there are also some "ghost" bands caused by surface umklapp processes
- The surface state intensity is observable at all energies but resonantly enhanced at the X points.



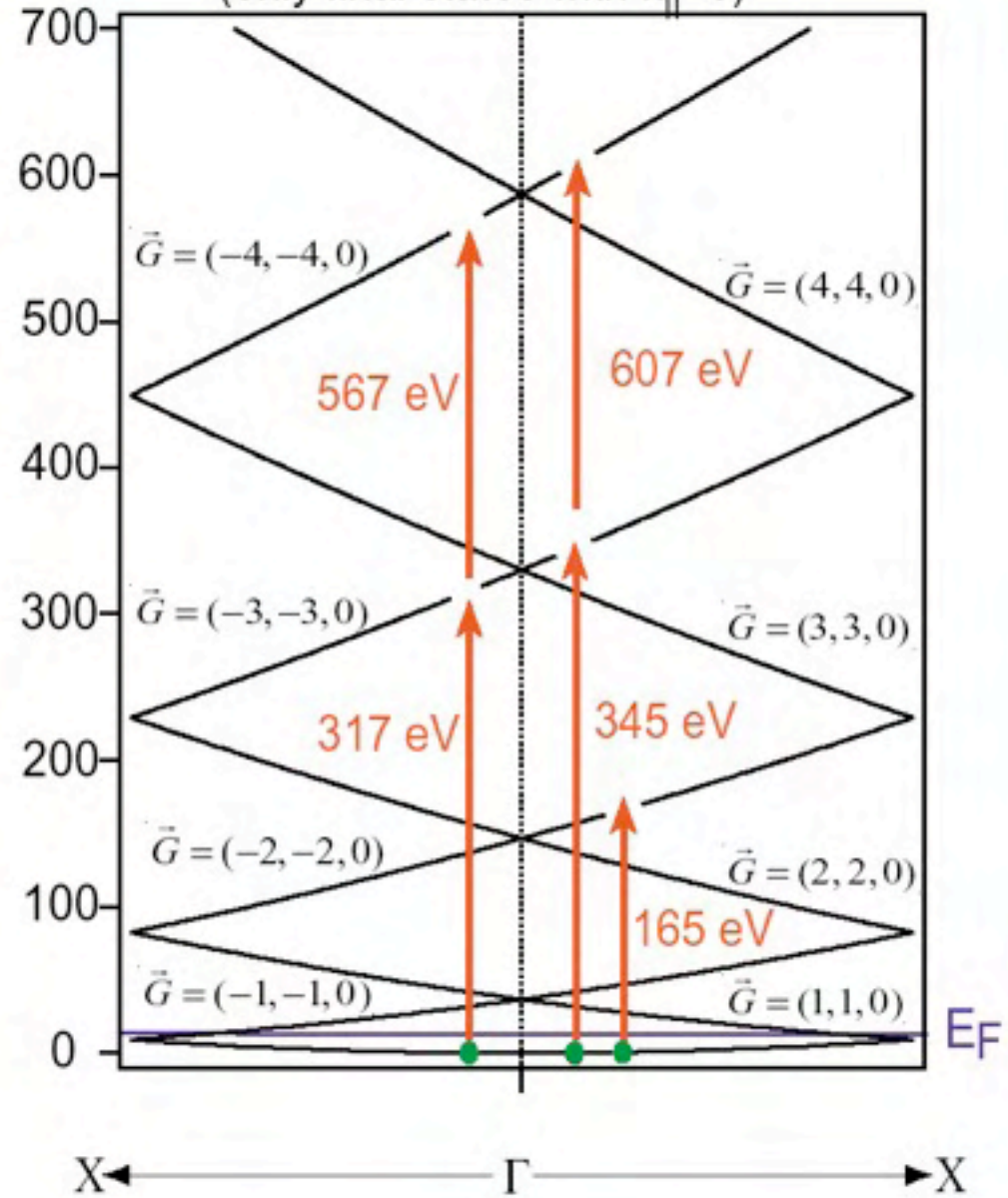
# Surface states and $k_{\perp}$ map example Al(100)

Photon energy changed at normal emission  $k_{\parallel}$



- The free electron-like band structure is evident from surface umklapp processes
- The surface state intensity is observable at all

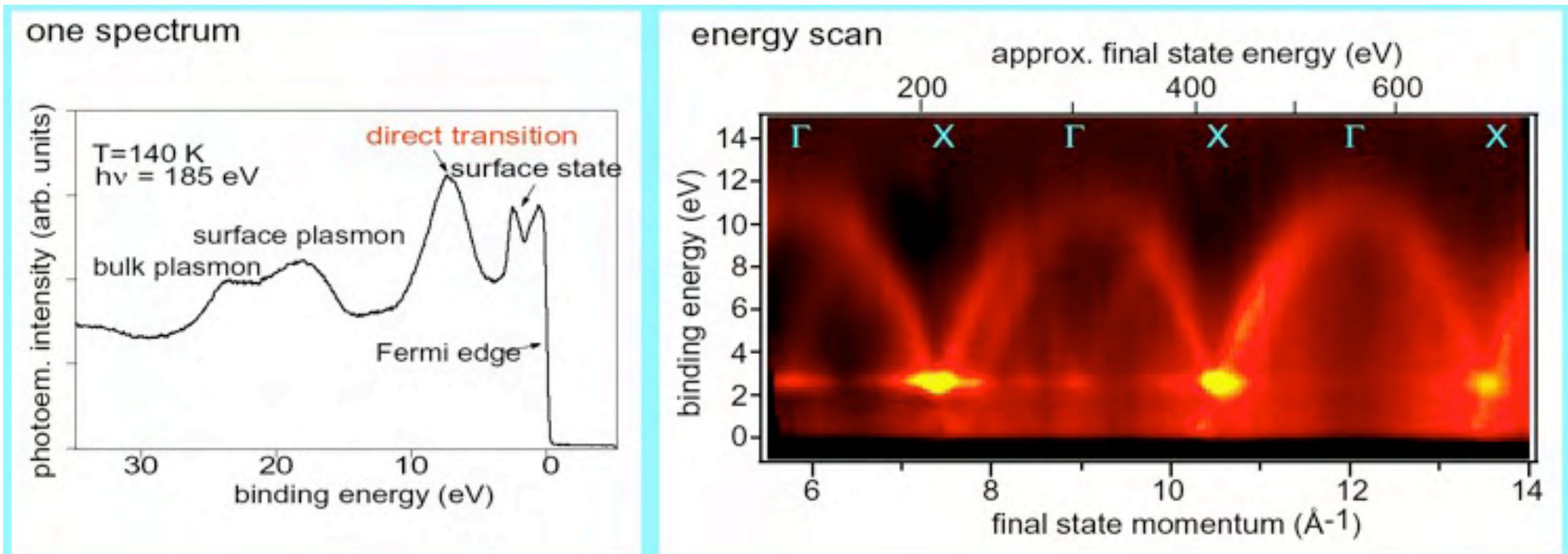
Free electron bandstructure ( $\Gamma$ -X) for Al  
(only final states with  $k_{\parallel}=0$ )



Reduced zone scheme - Normal emission direction

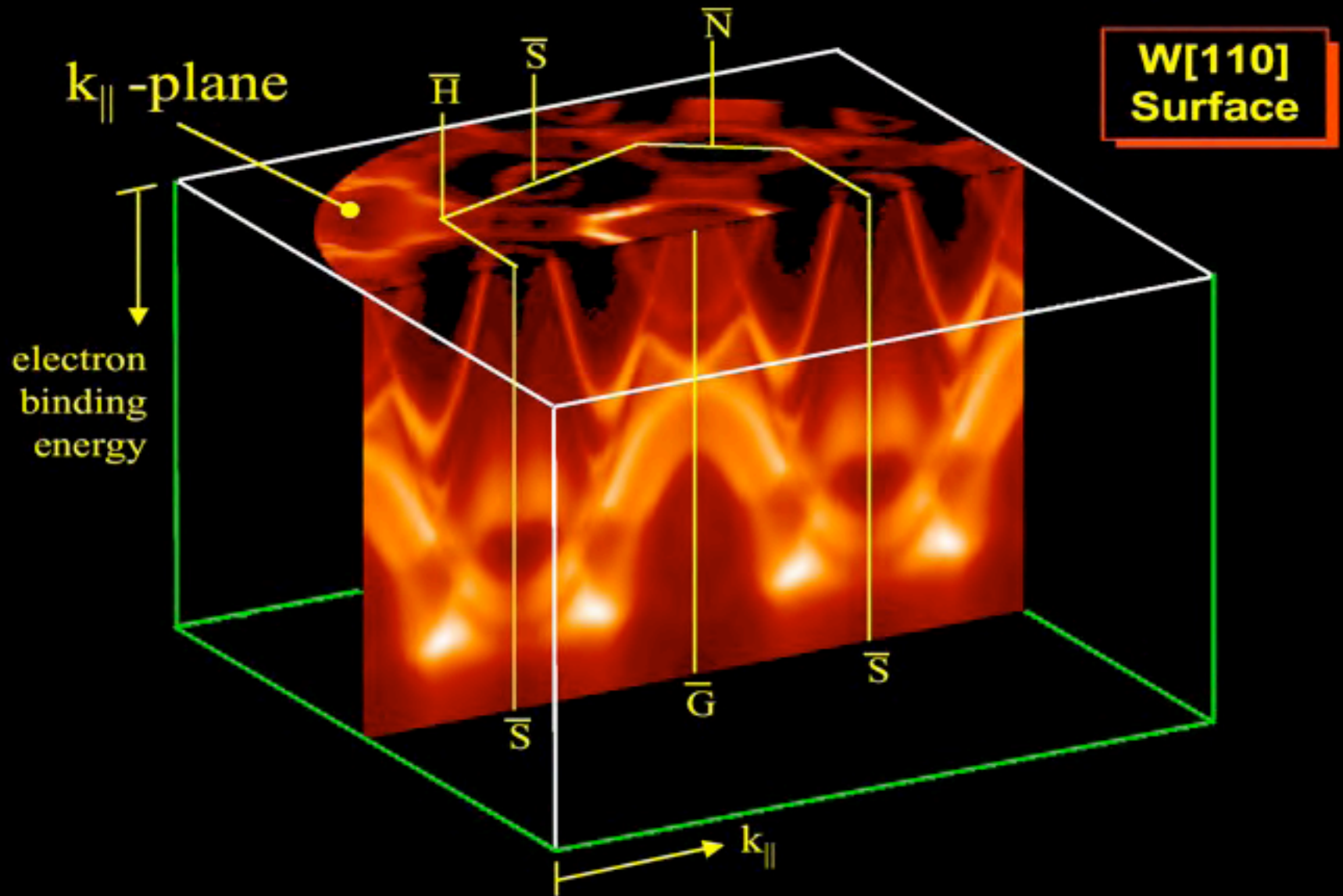
# Surface states and $k_{\parallel}$ mapping: example Al(100)

Photon energy changed at normal emission  $k_{\parallel}=0$



- The free electron-like band structure is evident but there are also some "ghost" bands caused by surface umklapp processes
- The surface state intensity is observable at all energies but resonantly enhanced at the X points.

# Band Mapping and Fermi Contours





# Determining Fermi vectors by angle resolved photoemission

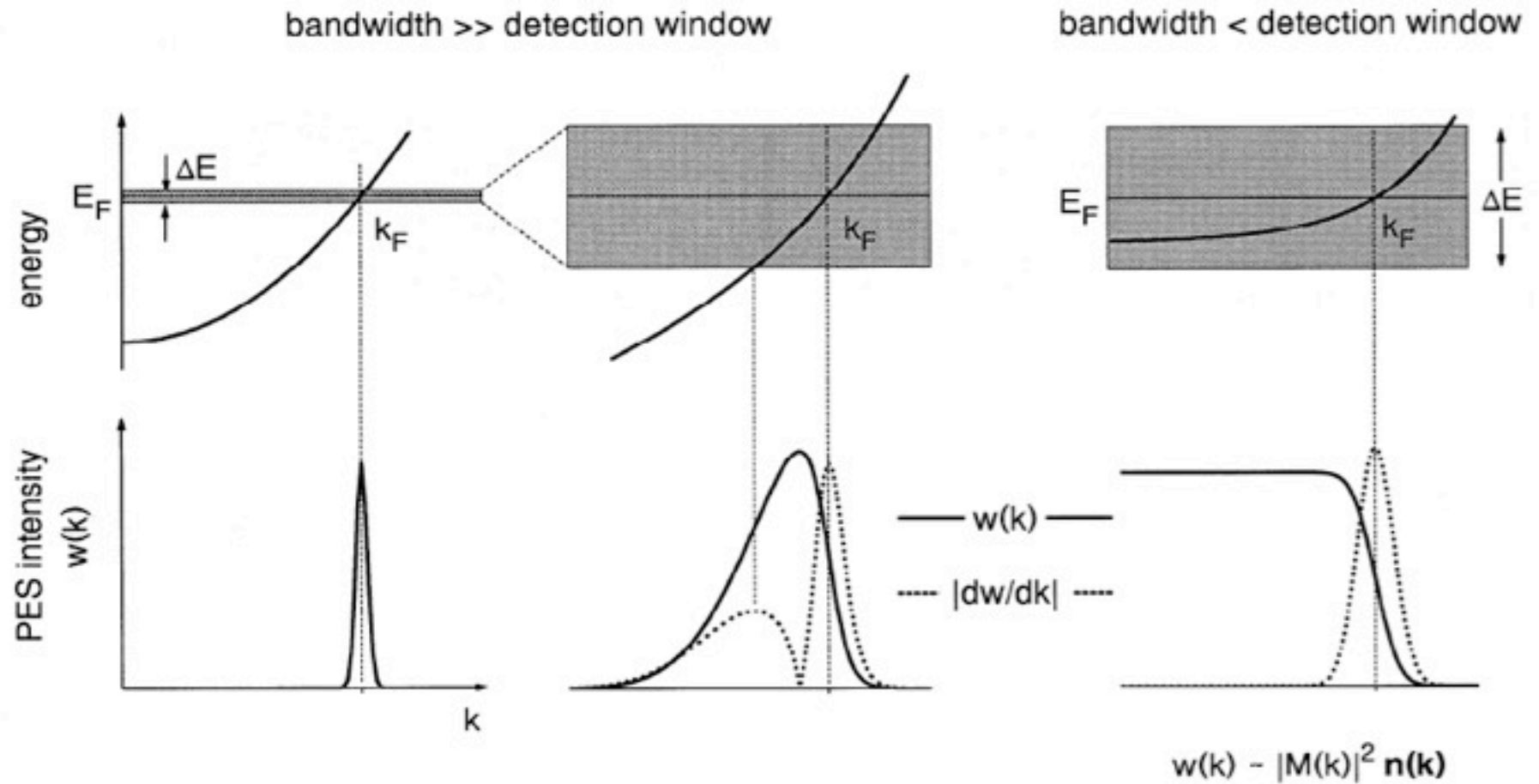


Fig. 8. Schematic behavior of the detected photoelectron intensity near a Fermi level crossing for wide band (left and center) and narrow band systems (right).



# Determining Fermi vectors by angle resolved photoemission

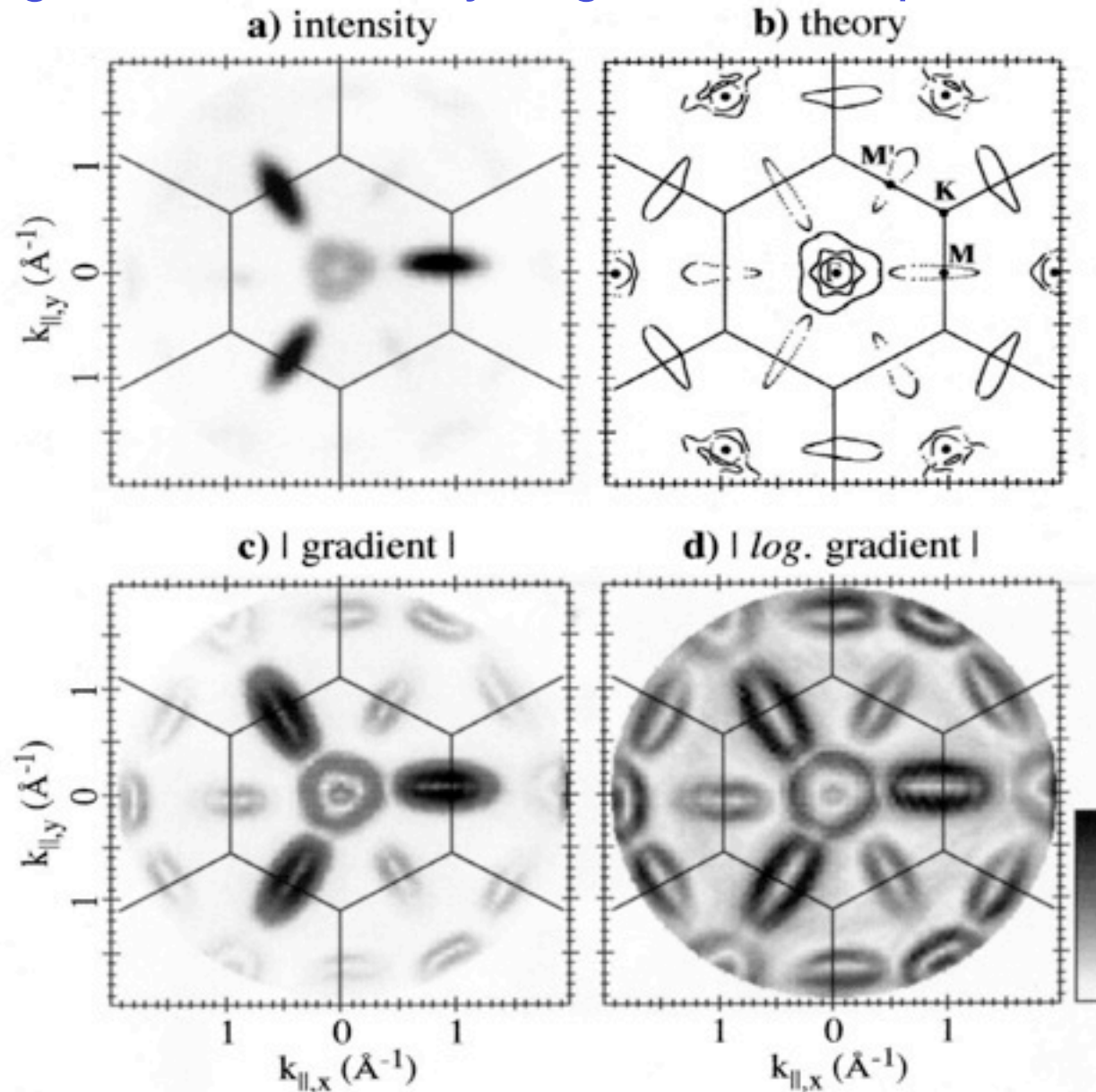
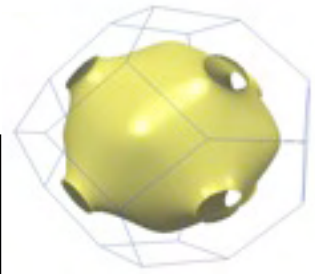


Fig. 9. Analysis of the He I FSM data on  $\text{TiTe}_2$ ; see text for details. (From Ref. [45]).

# Bulk Fermi Surface mapping: case studies Cu

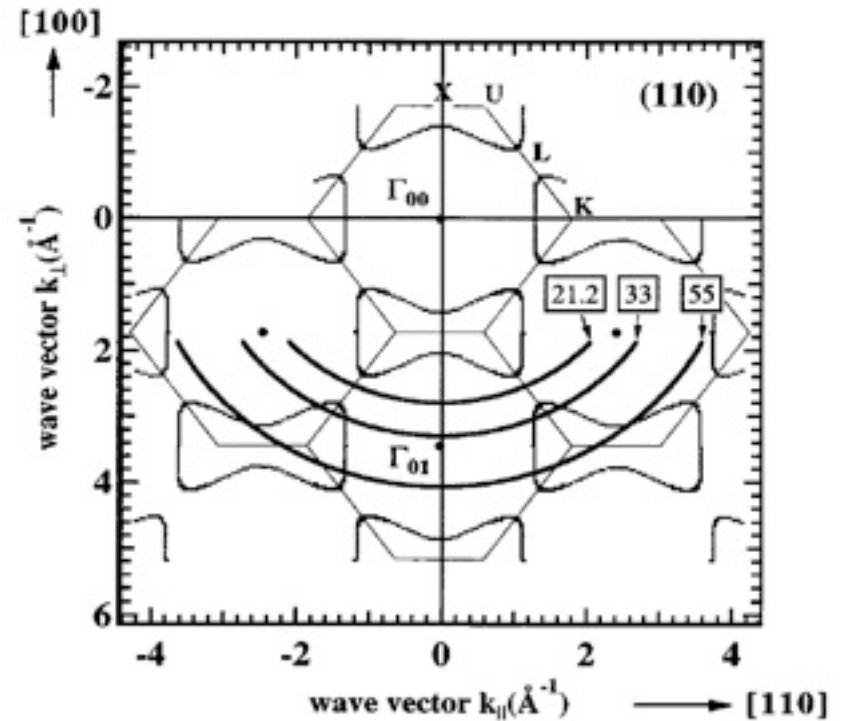
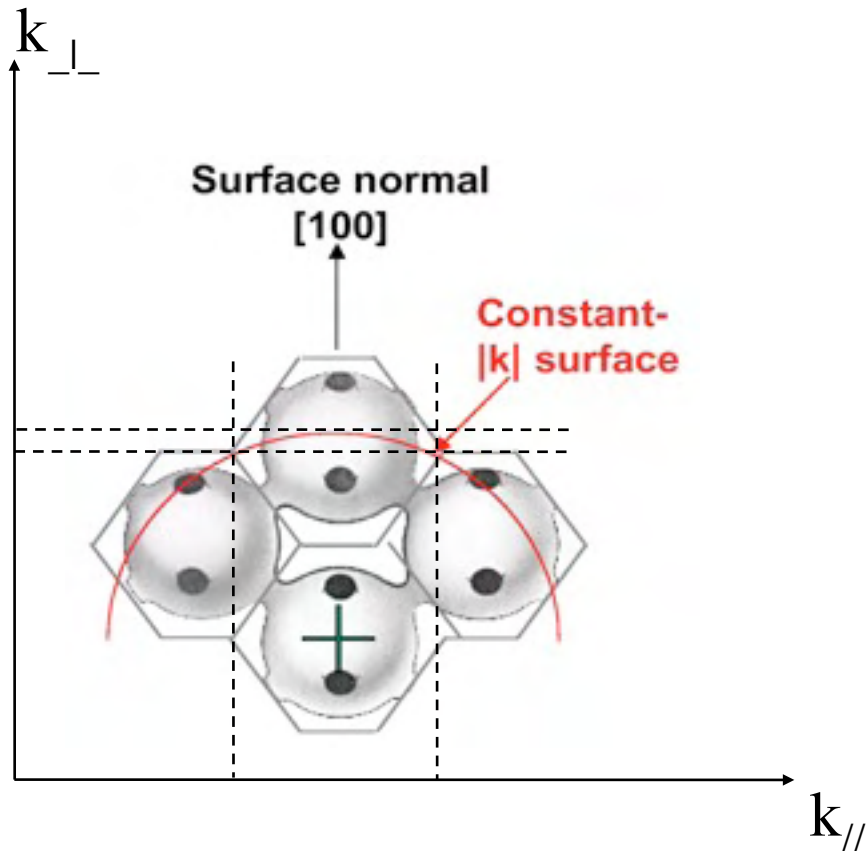


$$k_{out} = \sqrt{\frac{2m^*}{\hbar^2} E_{kin}}$$

$$k_{in} = \sqrt{\frac{2m^*}{\hbar^2} (E_{kin} + V_0)}$$

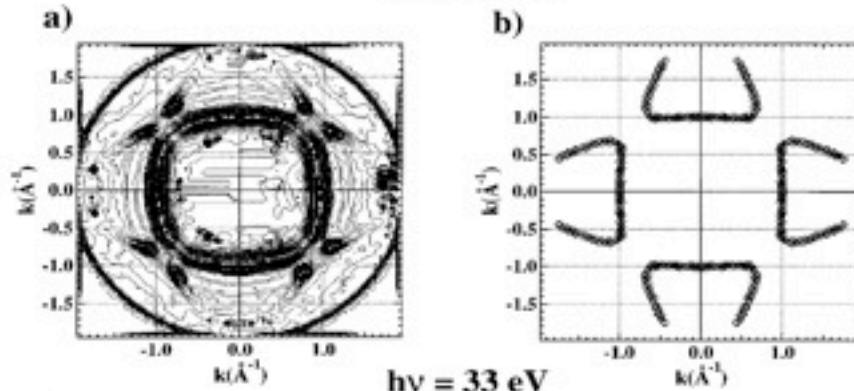
$$k_{\parallel out} = k_{\parallel in} = \sin \theta_{out} \sqrt{\frac{2m^*}{\hbar^2} E_{kin}}$$

$$k_{in \perp} = \sqrt{\frac{2m^*}{\hbar^2} (E_{kin} \cos^2 \theta_{out} + V_0)}$$



# Cu (100)

$h\nu = 21.2 \text{ eV}$



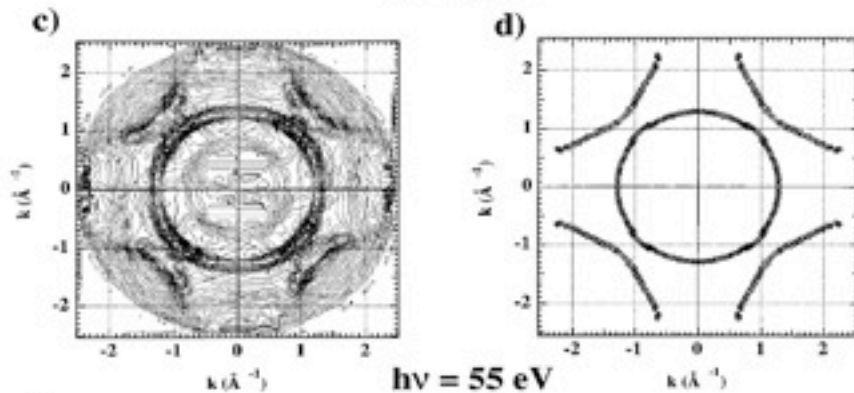
Slices of the Fermi surface  
in the  $k_{//}$  plane at different  $k_{\perp}$

$$k_{\perp} = 2.83 \text{ \AA}^{-1}$$

Less defined  $k_{\perp}$  at low  
kinetic energy (broader  
Fermi contours, ie.  
thicker slices).

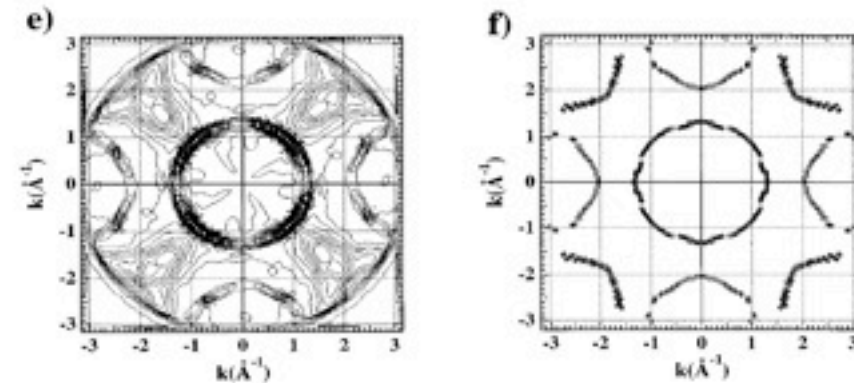
$$k_{\perp} = 3.33 \text{ \AA}^{-1}$$

$h\nu = 33 \text{ eV}$



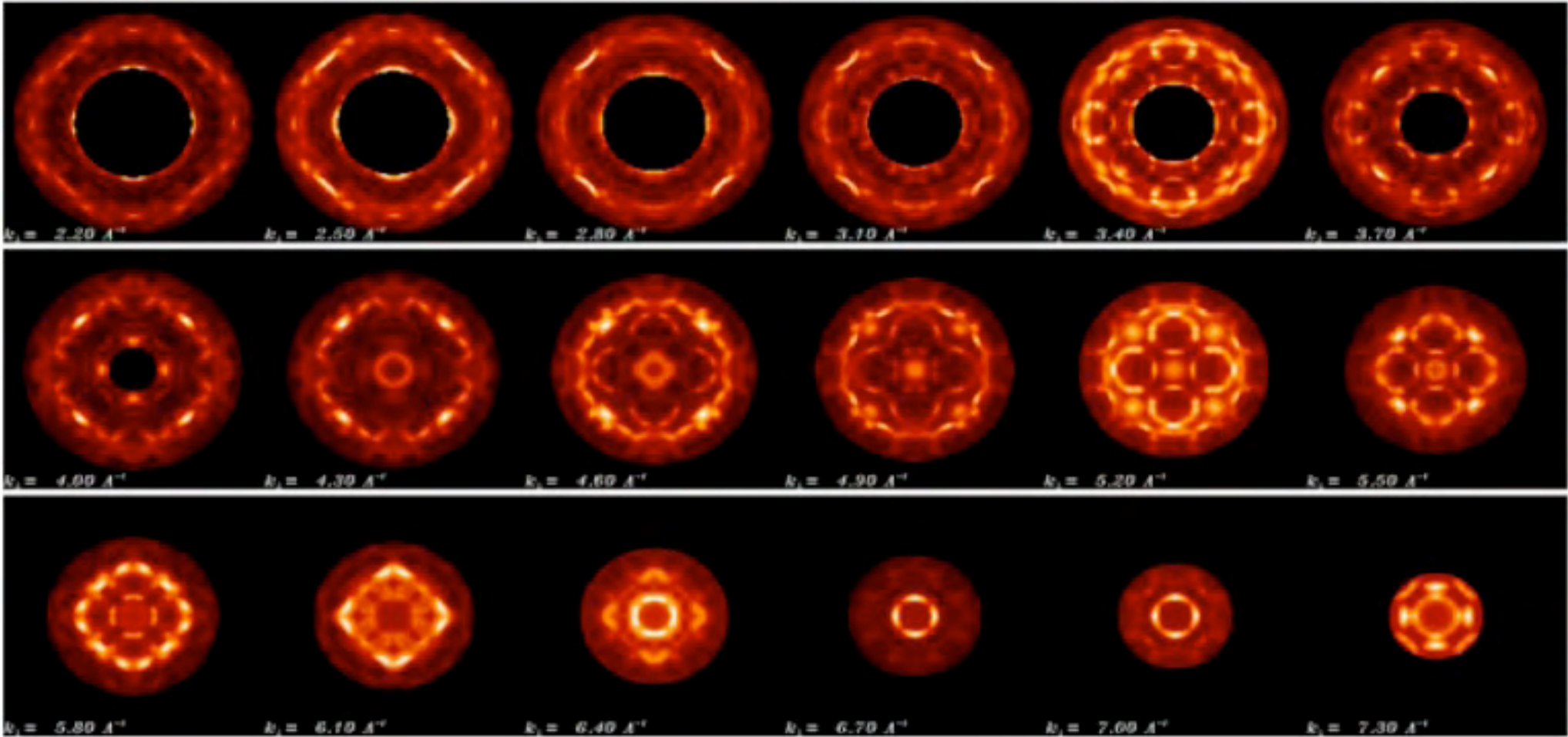
3D reconstruction of the  
Fermi surface shape is  
possible

$h\nu = 55 \text{ eV}$

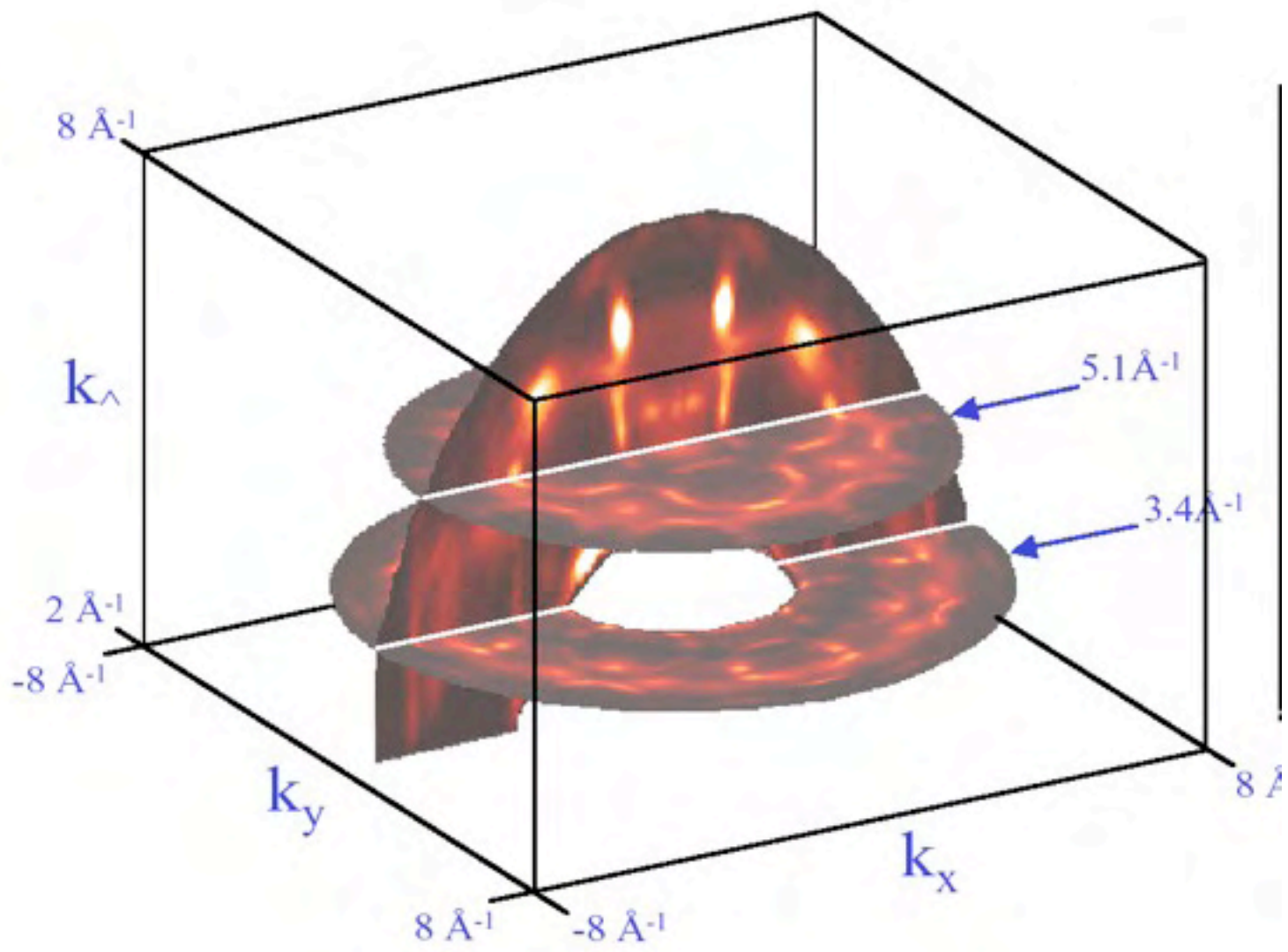


$$k_{\perp} = 4.11 \text{ \AA}^{-1}$$

FIG. 3. On the left side, experimental photoelectron angular distributions from the Cu(100) Fermi surface at 21, 33, and 55 eV kinetic energies. On the right side, the results of a tight binding theoretical calculation for the same energies are indicated.

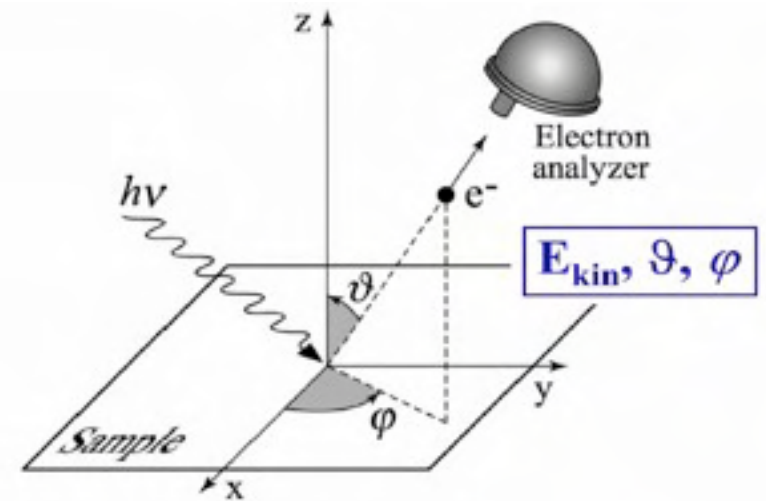
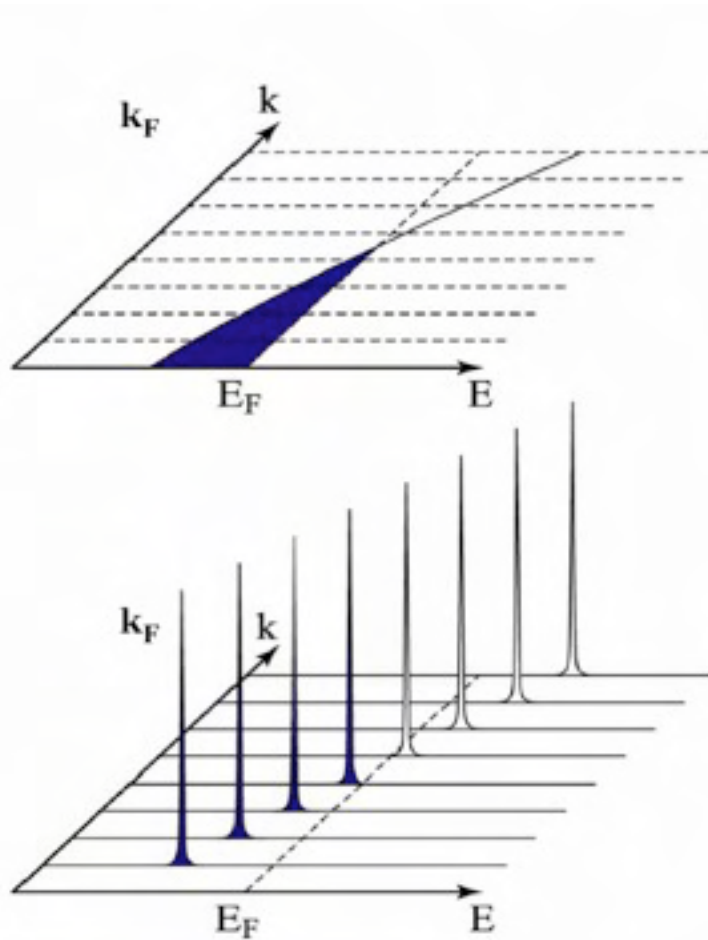


$$k_z = 2.2 \text{ to } 7.0 \text{ \AA}^{-1}, \Delta k_z = 0.3 \text{ \AA}^{-1}$$





The photoelectron spectrum consists of “spikes” at energies  $E_{kin}$



Energy Conservation

$$E_{kin} = h\nu - \phi - |E_B|$$

Momentum Conservation

$$p_{||} = \hbar k_{||} = \sqrt{2mE_{kin}} \cdot \sin \vartheta$$

The intensity is modulated by the matrix element  $|M_{fi}|^2 = |\langle k_f | A_0 p | k_i \rangle|^2$

# Selection rules

In the dipole matrix element:

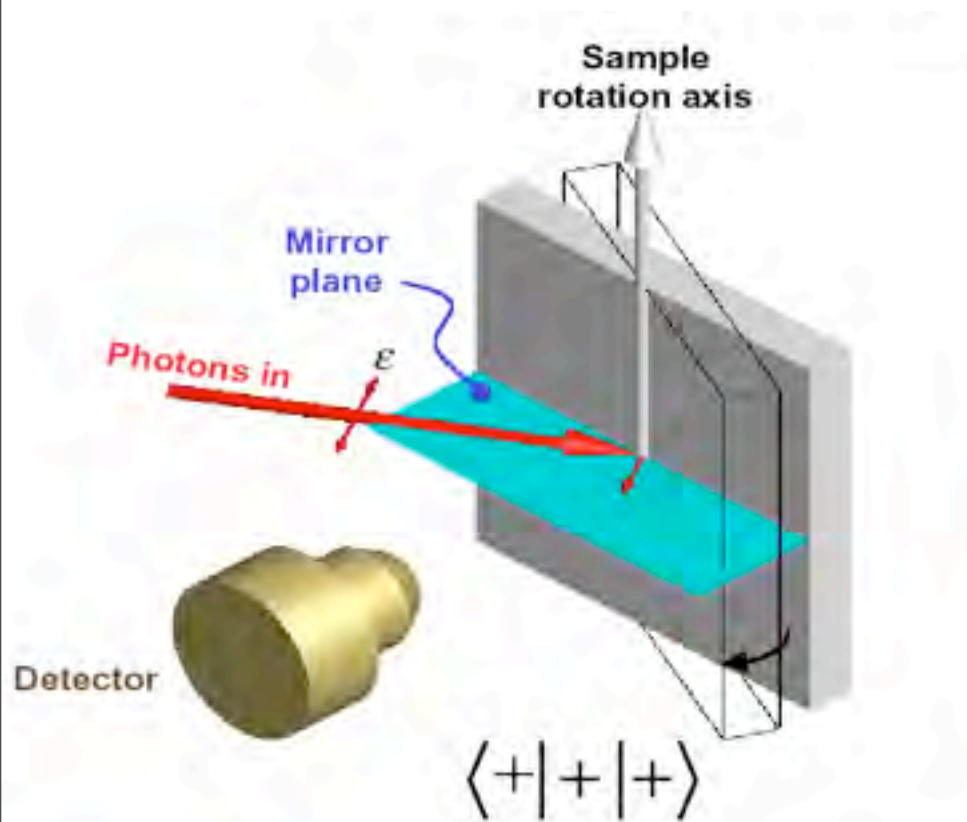
$$c_{f,i} \propto \vec{A} \cdot \langle f | \vec{\nabla} | i \rangle \delta(\omega - \omega_{i,f}) = \left[ A_x \langle f | \frac{\partial}{\partial x} | i \rangle + A_y \langle f | \frac{\partial}{\partial y} | i \rangle + A_z \langle f | \frac{\partial}{\partial z} | i \rangle \right] \delta(\omega - \omega_{i,f})$$

both  $|i\rangle$  and  $|f\rangle$  must belong to irreducible representations of the symmetry operations of the surface.

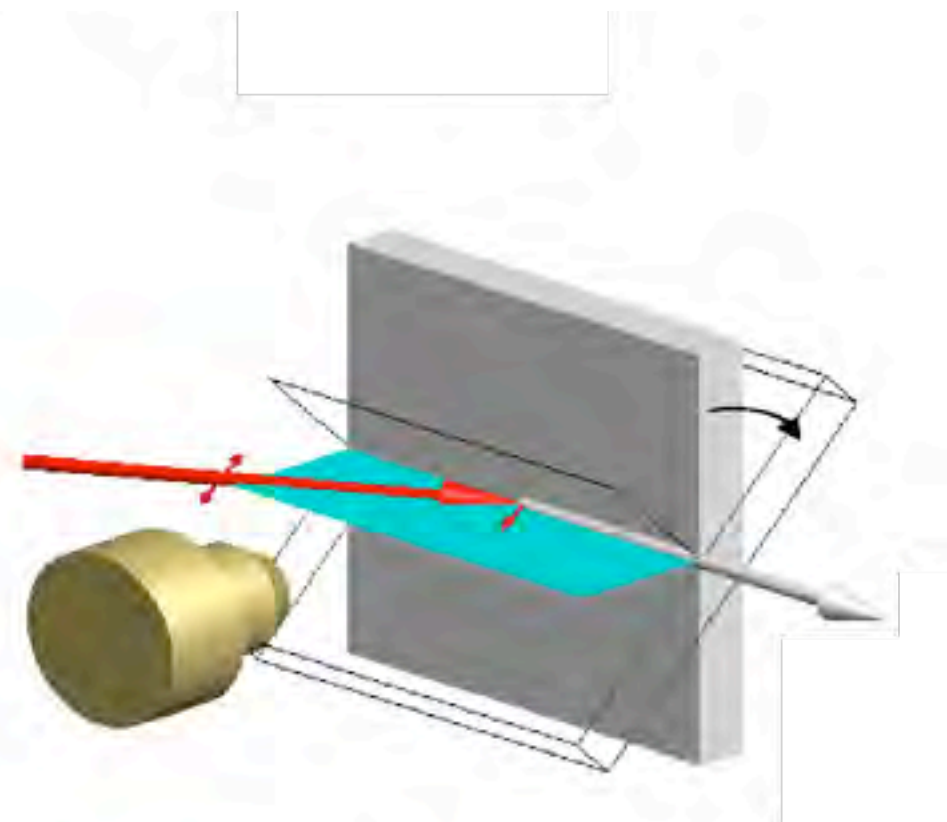
If electrons are collected along a direction contained for example in a mirror plane,  $|f\rangle$  has even parity with respect to mirroring: an odd function has node in the plane.

By orienting the polarization in a direction contained in the same mirror plane (even operator) only even initial states contribute to the spectrum. if the polarization is perpendicular only odd states are seen.



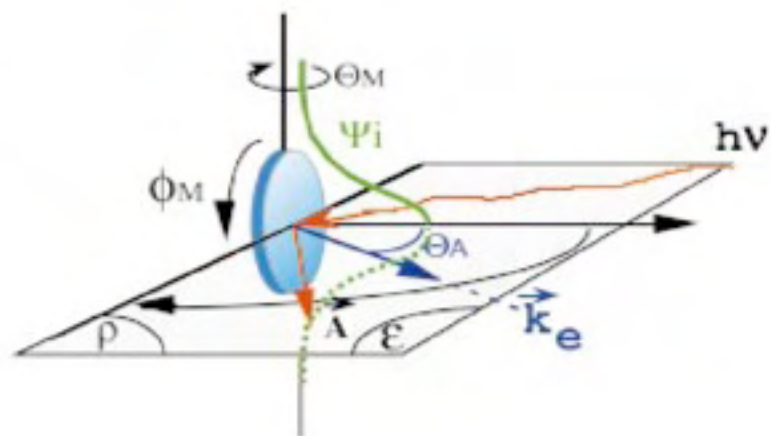


**Only even initial states are observed at all rotation angles**



**Mixture of even and odd states**

a) even detection



b) odd detection

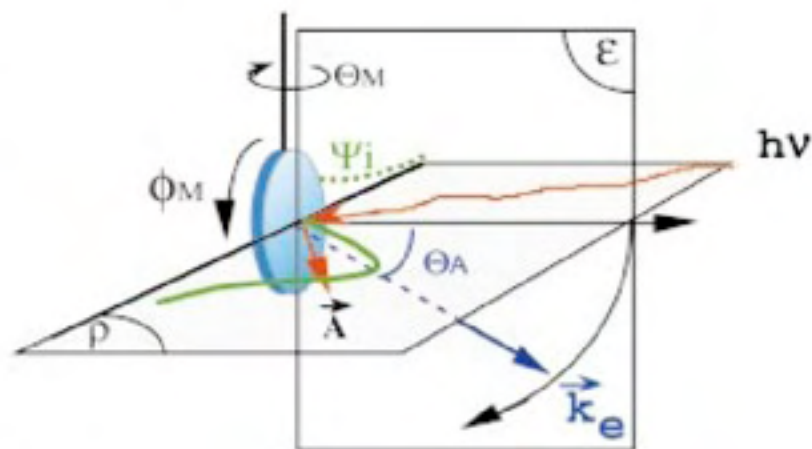
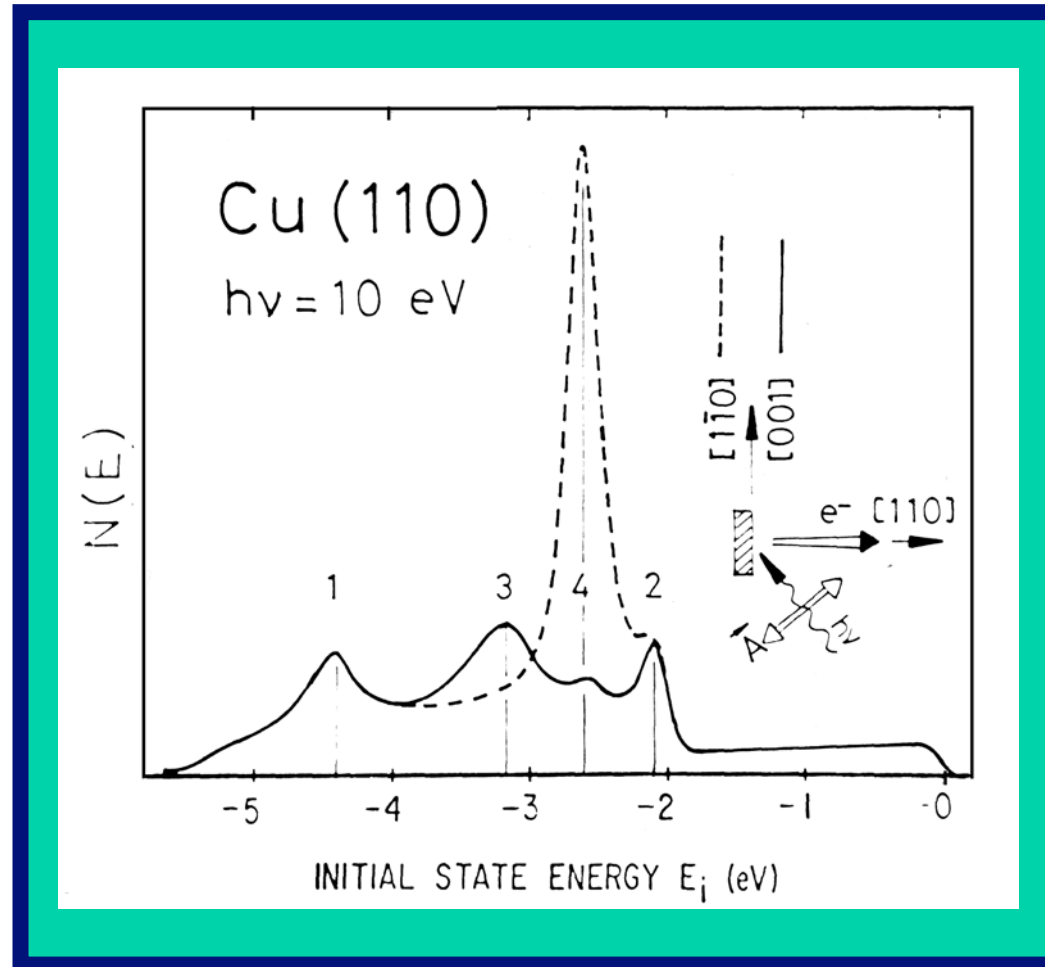


FIG. 1. (Color) The meaning of “even” and “odd” detection geometry in the present ARPES experiments is explained.  $\vec{k}_e$  points toward the detector. In the even case, the detector moves in the plane of incident light (horizontal plane) in which the synchrotron light is polarized. In the odd case, the detector moves in a perpendicular plane as shown. The sample is kept fixed. For initial states lying in a mirror plane (e.g., along the  $\Gamma$ - $\bar{M}$  line), the even polarization selects emission only from states symmetric with respect to the mirror plane, while the odd polarization couples to antisymmetric states as discussed in the text. The detector is rotated along the vertical and horizontal axis to access states throughout the  $(k_x, k_y)$  plane.

# Applications of selection rules

a) knowing the geometry one can determine the symmetry of the states: Cu(110)

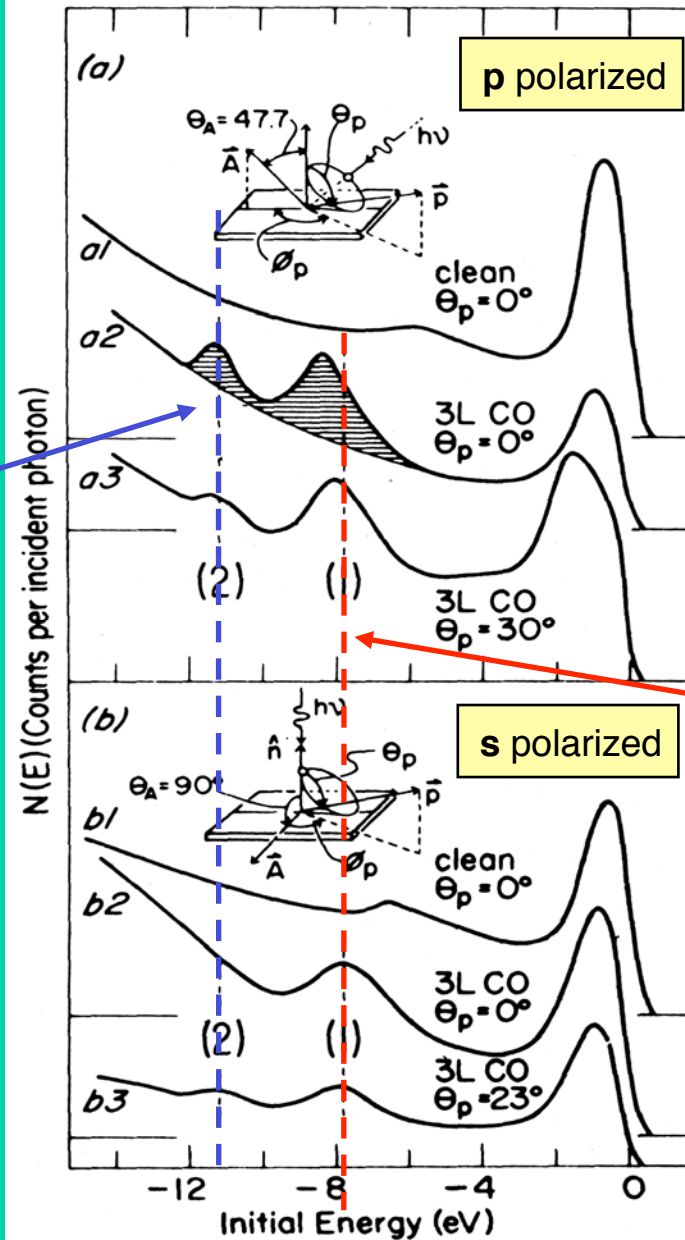


# Applications of selection rules

b) knowing the symmetry of the states one can determine the geometry: orientation of CO/Ni(100)

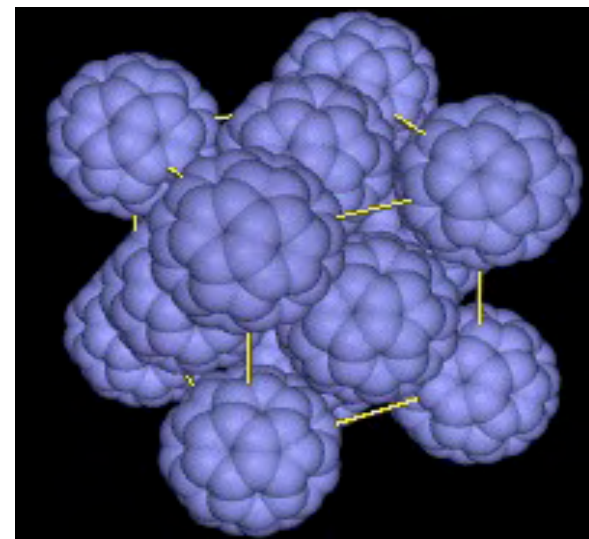
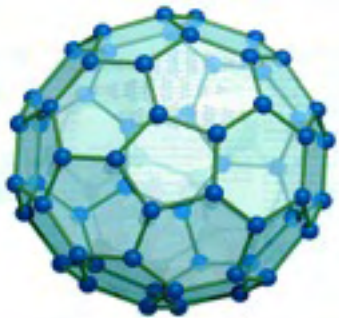
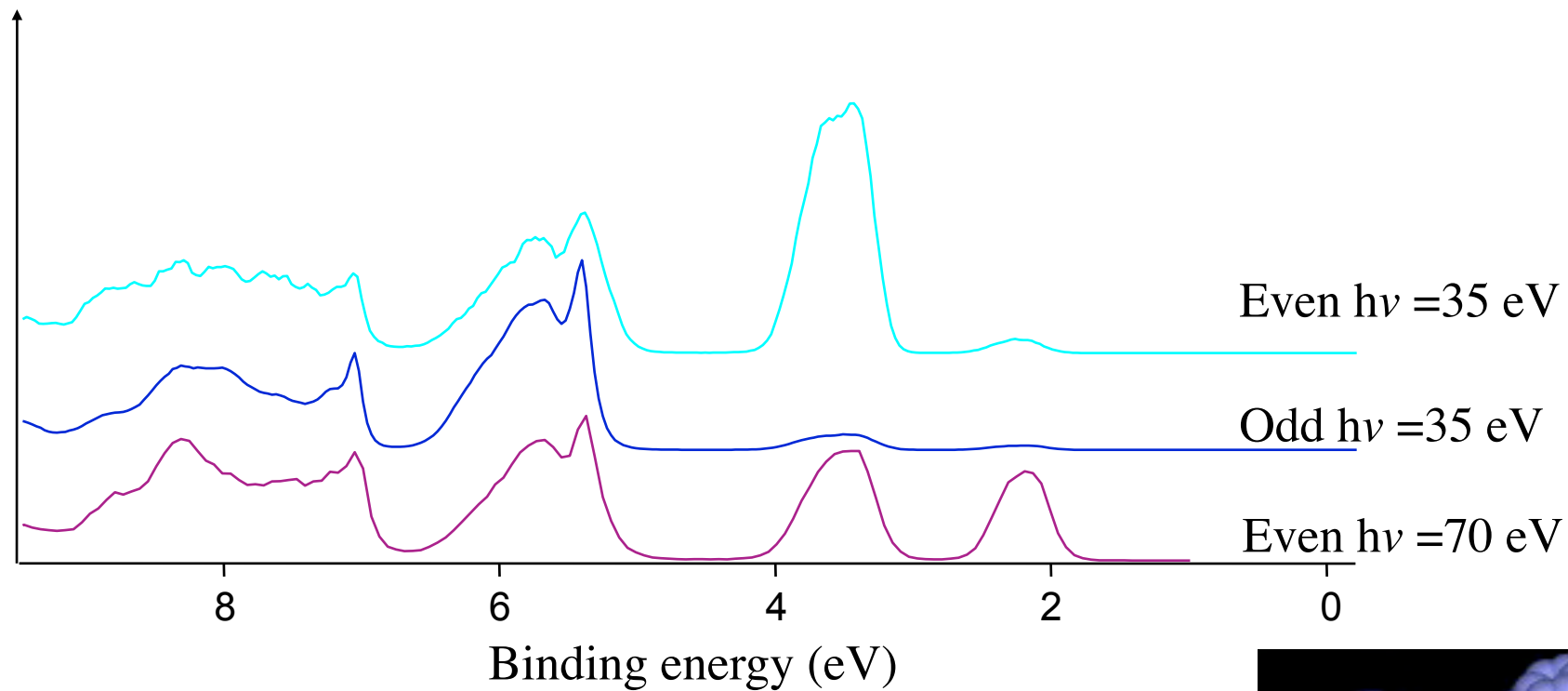
$4\sigma$

the  $4\sigma$  disappears for an antisymmetric geometry: CO is standing upright

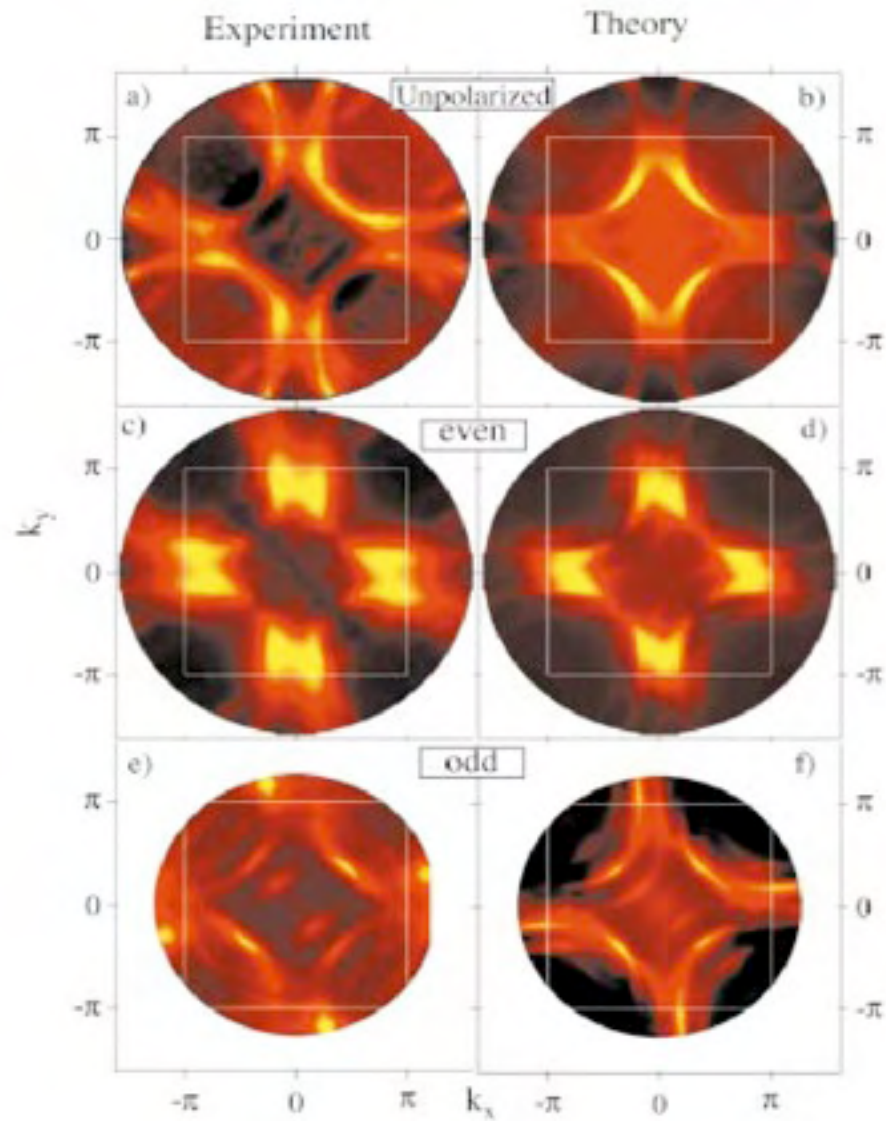


$1\pi+5\sigma$

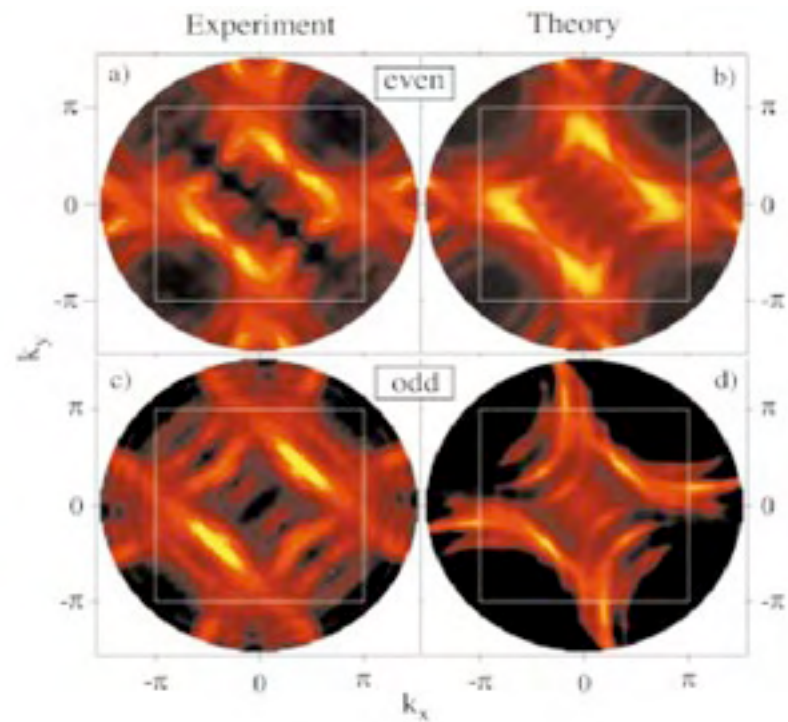
# Matrix effects on a molecular crystal: C<sub>60</sub>







$h\nu = 21.2 \text{ eV}$



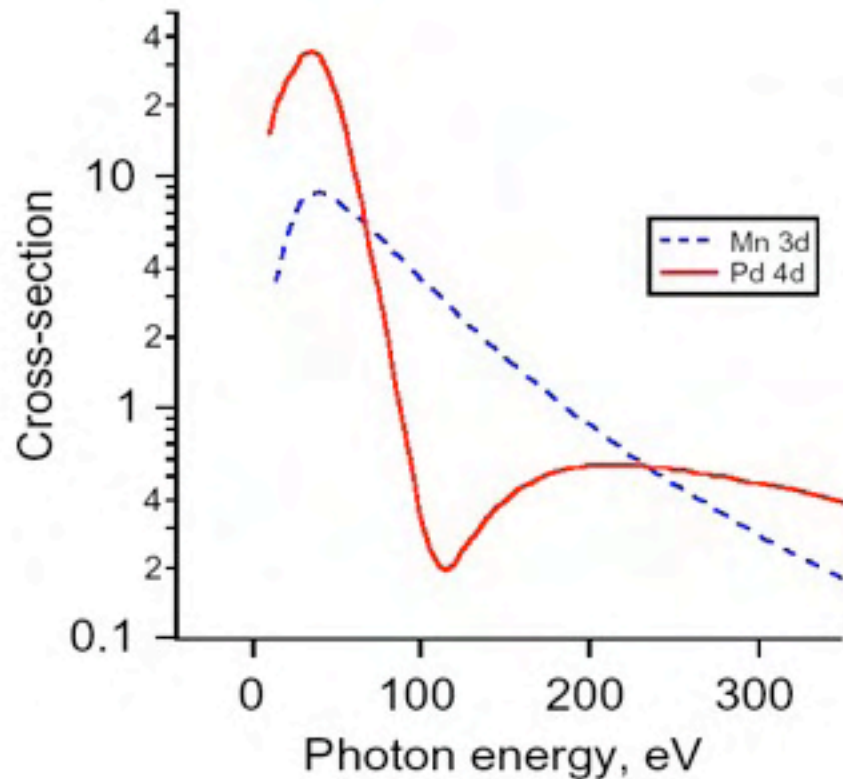
$h\nu = 35 \text{ eV}$

M.C. Asensio et al., PRB (2003)

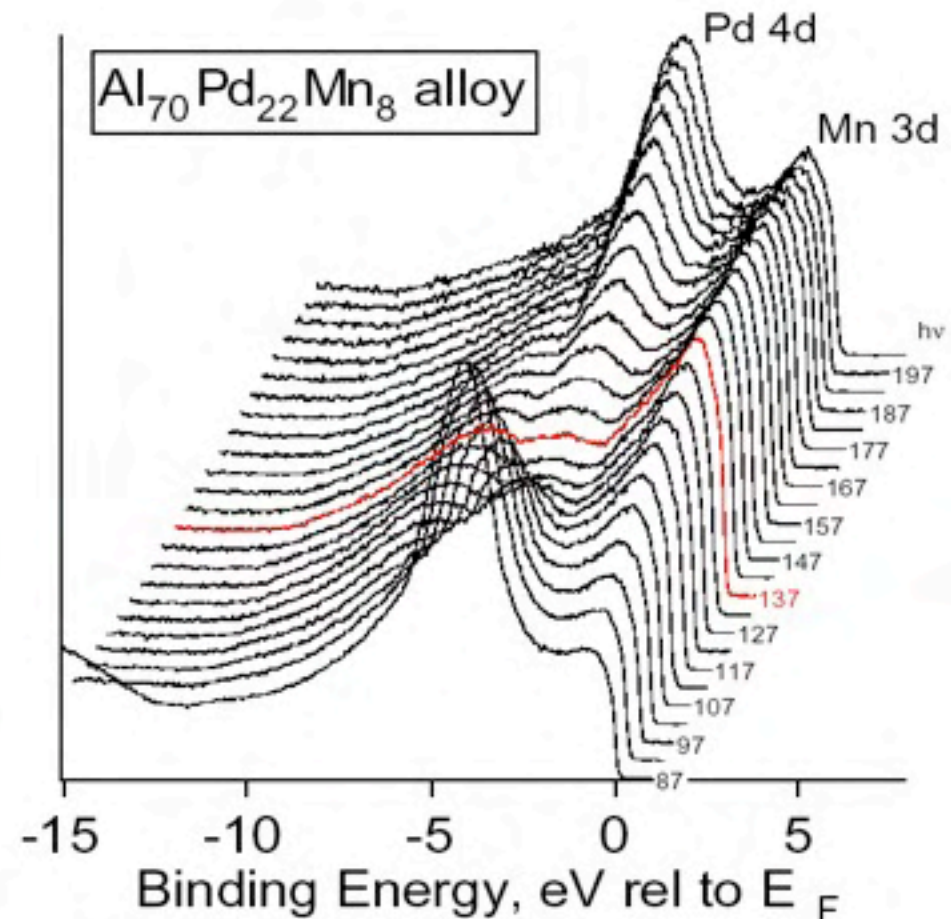
Matrix effects on the Fermi surface shape in Bi2212

# Application of the Cooper minimum effect to alloys

Calculation  
J.J.Yeh

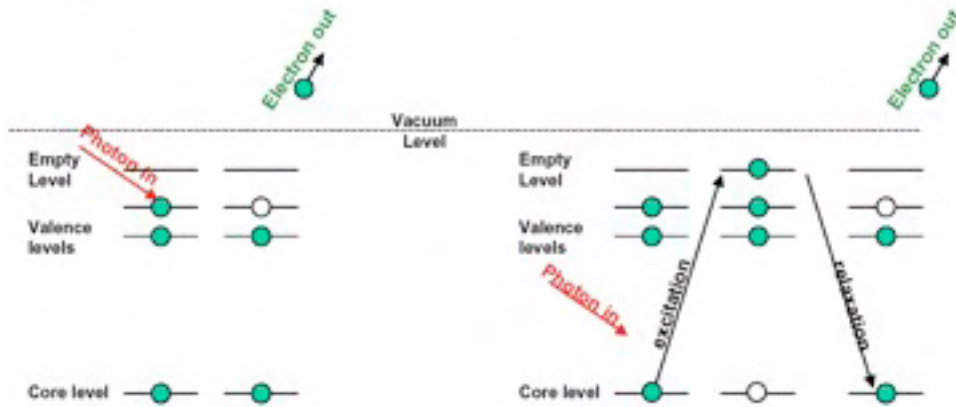


Expt.  
Rotenberg et al





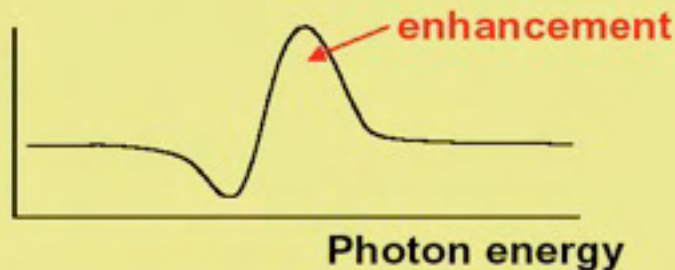
# Resonant photoemission



- These processes (non-resonant and resonant photoemission) have the same initial and final states.
- As quantum mechanics dictates, these independent channels will interfere when added coherently

$$|M_f|^2 = \left| \langle f | H_{NR} | i \rangle + \langle f | H_R | i \rangle \right|^2$$

Photoemission yield or absorption



- Not all valence electrons are enhanced equally!
- Only those with overlap to the core hole are enhanced
- This can be very useful to get projections of the valence bands to the individual atoms.

Two constraints on the time scale of the process:

- 1) To have a coherent interfering process the time scale of the two channels must be comparable.
- 2) The excited electron must remain localized on the same atom of the core hole for a time scale bigger or comparable to the core hole lifetime

# Gd@C<sub>82</sub> resonant photoemission

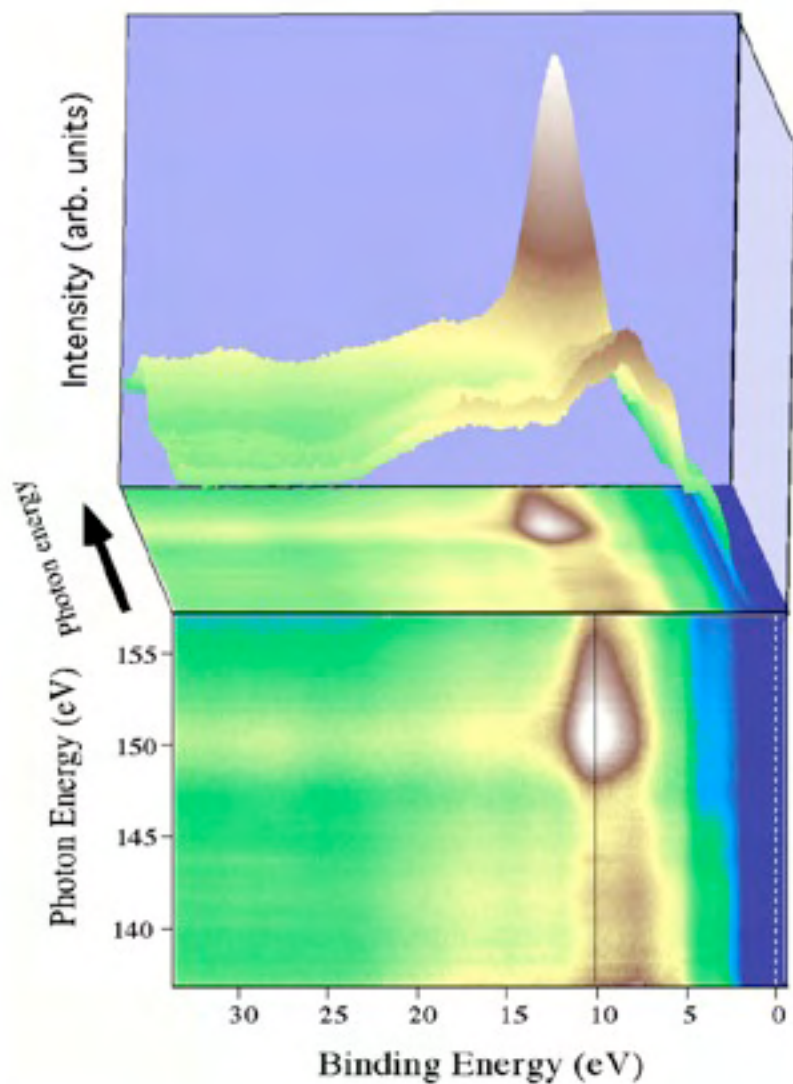
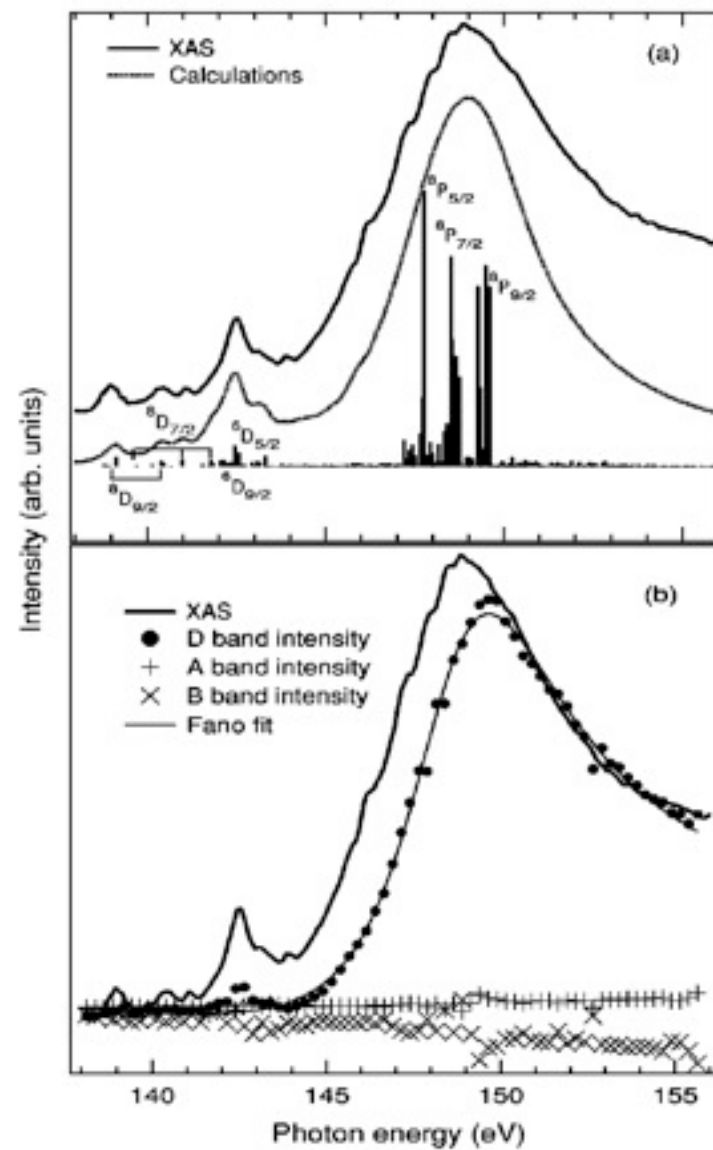
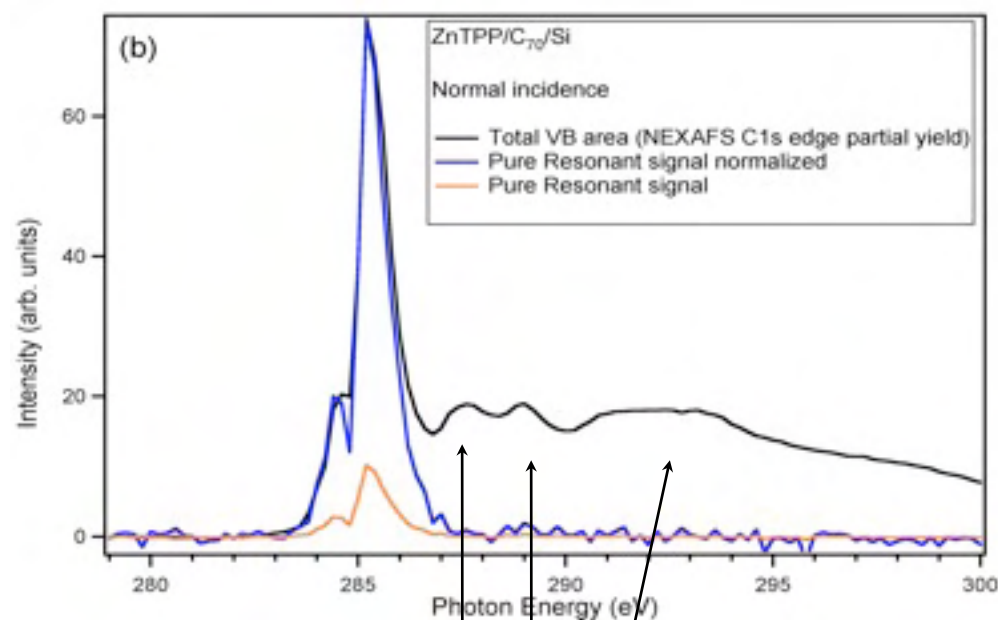
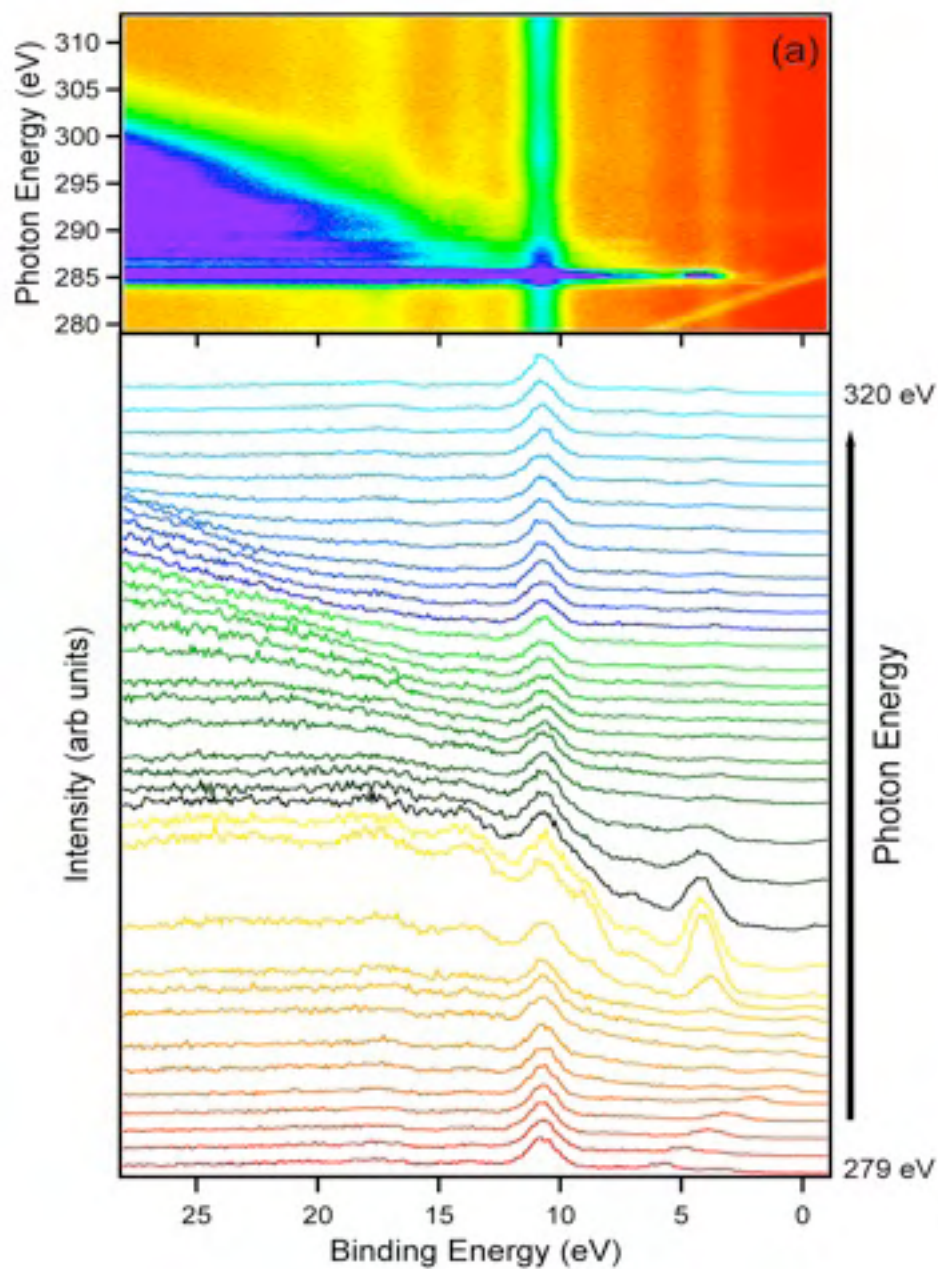


FIG. 3. (Color online) Resonant photoemission valence band spectra collected at the Gd  $4d \rightarrow 4f$  edge.



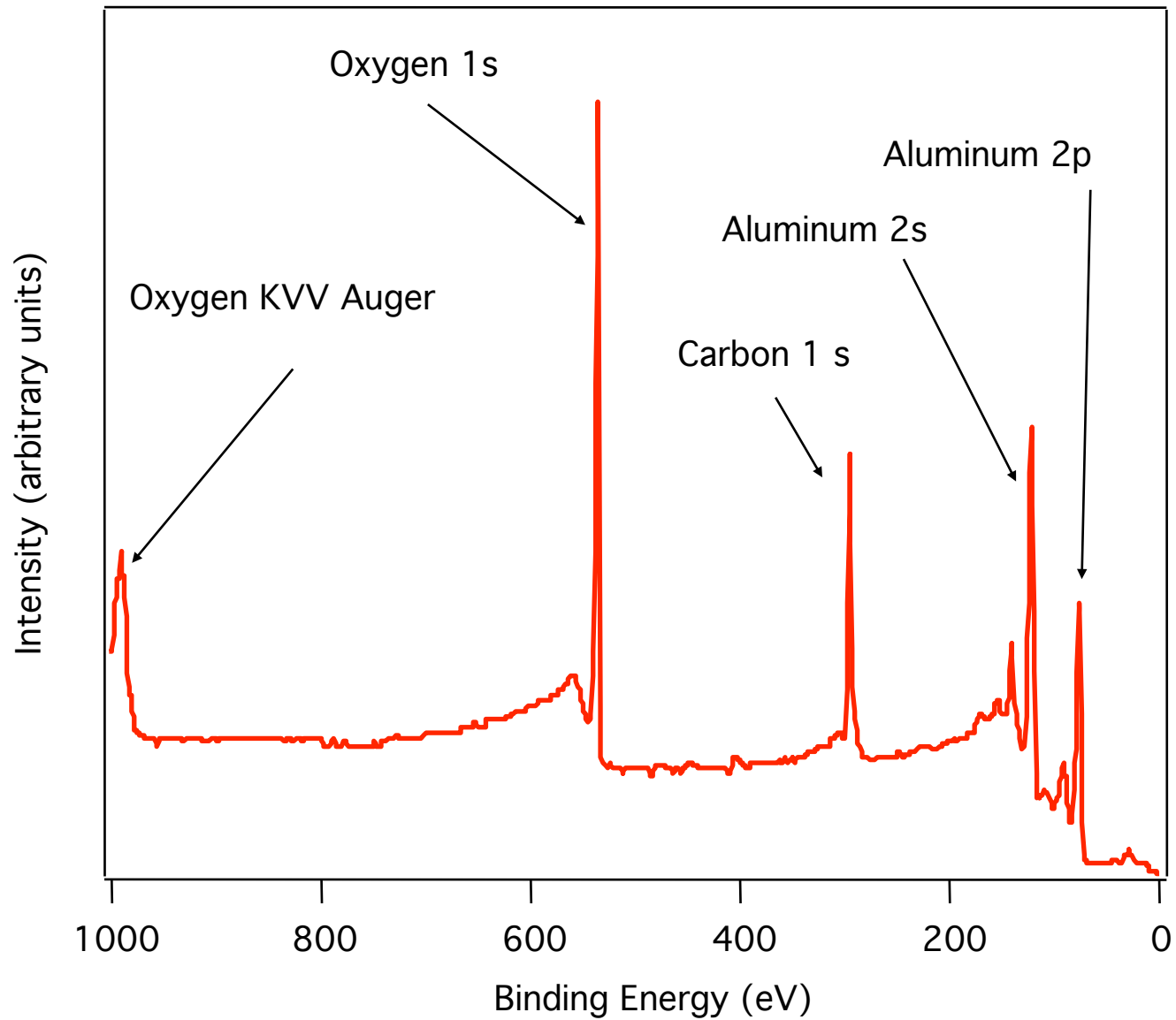


When excited to these states, C1s core electrons delocalize well before the core hole decay.

# Core level photoemission (XPS or ESCA)

- Element specificity
- Sensitivity to chemical environment
  - the core level shift
- Photoelectron diffraction
- Examples

# Surface chemical analysis.

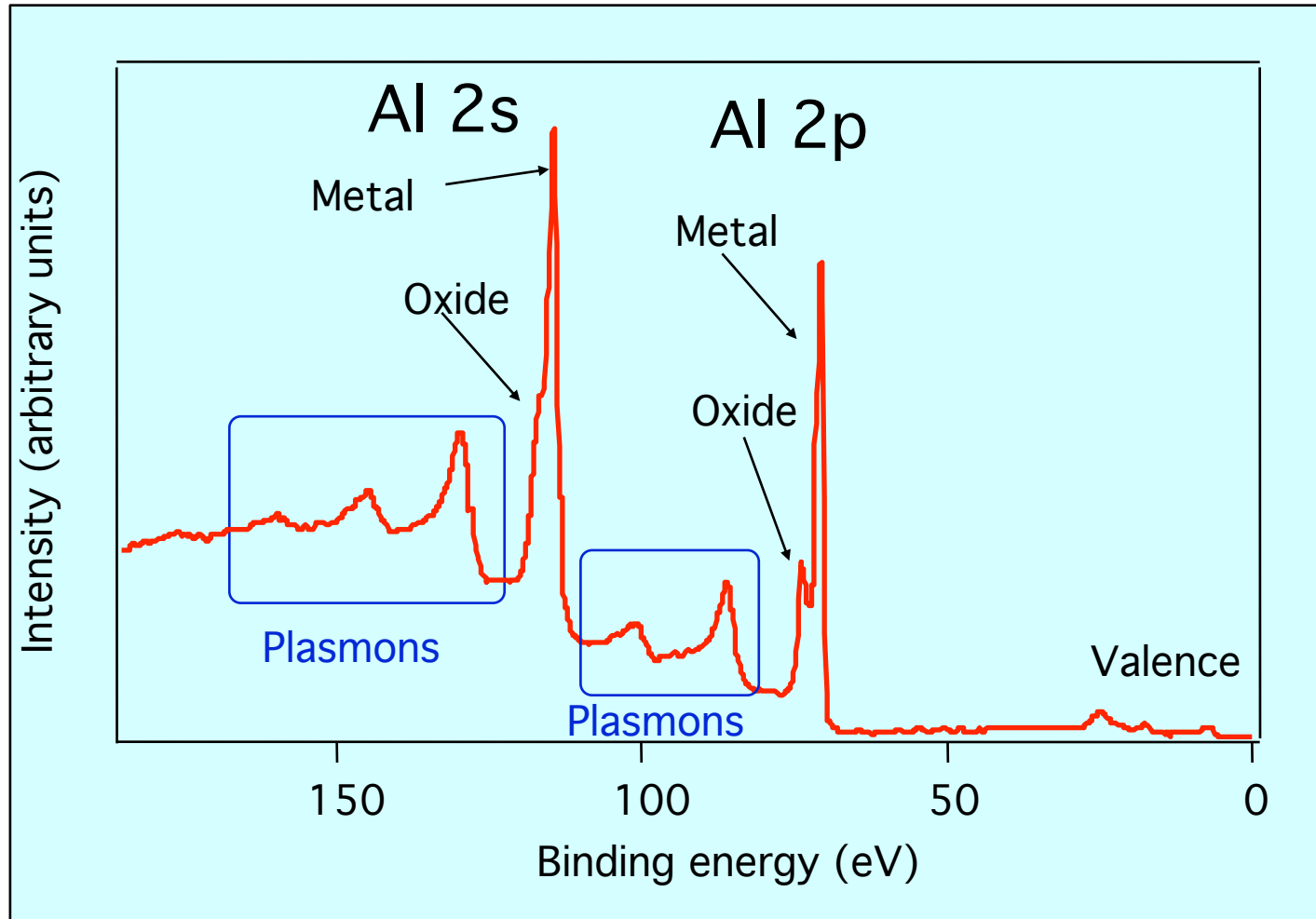


# Each element has a specific set of accessible core levels

	K 1s	L-I 2s	L-II 2p <sub>1/2</sub>	L-III 2p <sub>3/2</sub>	M-I 3s	M-II 3p <sub>1/2</sub>	M-III 3p <sub>3/2</sub>	M-IV 3d <sub>3/2</sub>	M-V 3d <sub>5/2</sub>
1	H	13.6							
2	He	24.6*							
3	Li	54.7*							
4	Be	111.5*							
5	B	188*							
6	C	284.2*							
7	N	409.9*	37.3*						
8	O	543.1*	41.6*						
9	F	696.7*							
10	Ne	870.2*	48.5*	21.7*	21.6*				
11	Na	1070.8+	63.5+	30.4+	30.5*				
12	Mg	1303.0+	88.6*	49.6+	49.21				
13	Al	1559	117.8*	72.9*	72.5*				
14	Si	1839	149.7*b	99.8*	99.2*				
15	P	2145.5	189*	136*	135*				
16	S	2472	230.9	163.6*	162.5*				
17	Cl	2822	270*	202*	200*				
18	Ar	3205.9*	326.3*	250.6+	248.4*	29.3*	15.9*	15.7*	
19	K	3608.4*	378.6*	297.3*	294.6*	34.8*	18.3*	18.3*	
20	Ca	4038.5*	438.4+	349.7+	346.2+	44.3+	25.4+	25.4+	
21	Sc	4492	498.0*	403.6*	398.7*	51.1*	28.3*	28.3*	
22	Ti	4966	560.9+	460.2+	453.8+	58.7+	32.6+	32.6+	
23	V	5465	626.7+	519.8+	512.1+	66.3+	37.2+	37.2+	
24	Cr	5989	696.0+	583.8+	574.1+	74.1+	42.2+	42.2+	
25	Mn	6539	769.1+	649.9+	638.7+	82.3+	47.2+	47.2+	
26	Fe	7112	844.6+	719.9+	706.8+	91.3+	52.7+	52.7+	
27	Co	7709	925.1+	793.2+	778.1+	101.0+	58.9+	59.9+	
28	Ni	8333	1008.6+	870.0+	852.7+	110.8+	68.0+	66.2+	
29	Cu	8979	1096.7+	952.3+	932.7	122.5+	77.3+	75.1+	
30	Zn	9659	1196.2*	1044.9*	1021.8*	139.8*	91.4*	88.6*	10.2*
31	Ga	10367	1299.0*b	1143.2+	1116.4+	159.51	103.5+	100.0+	18.7+
32	Ge	11103	1414.6*b	1248.1*b	1217.0*b	180.1*	124.9*	120.8*	29.8*
33	As	11867	1527.0*b	1359.1*b	1323.6*b	204.7*	146.2*	141.2*	41.7*
34	Se	12658	1652.0*b	1474.3*b	1433.9*b	229.6*	166.5*	160.7*	55.5*
35	Br	13474	1782*	1596*	1550*	257*	189*	182*	70*



Energy of core level peaks.



$$E_k = h\nu - E_b + E_a + E_r$$

Koopman (initial state) binding energy

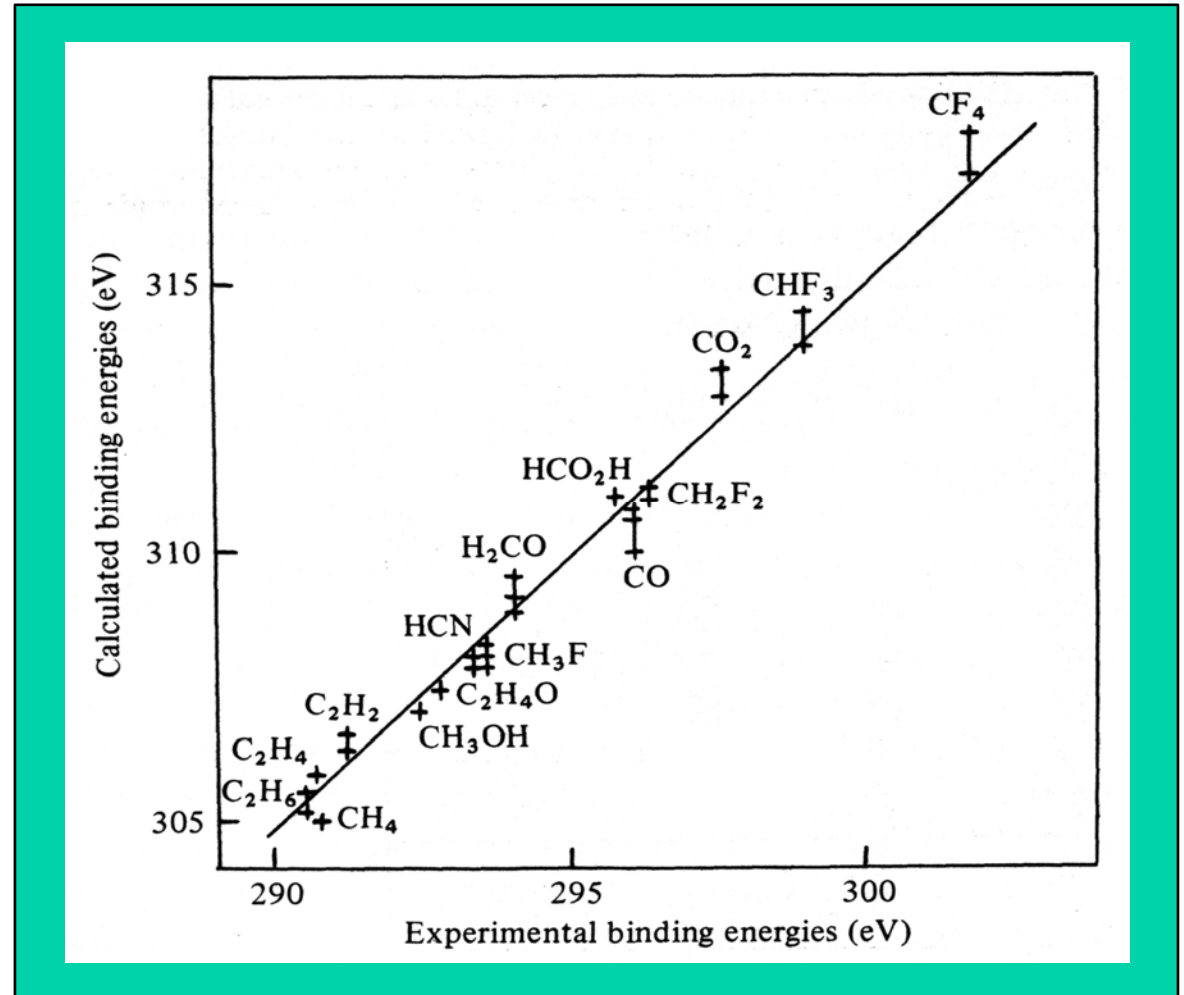
Intraatomic relaxation

Extraatomic relaxation

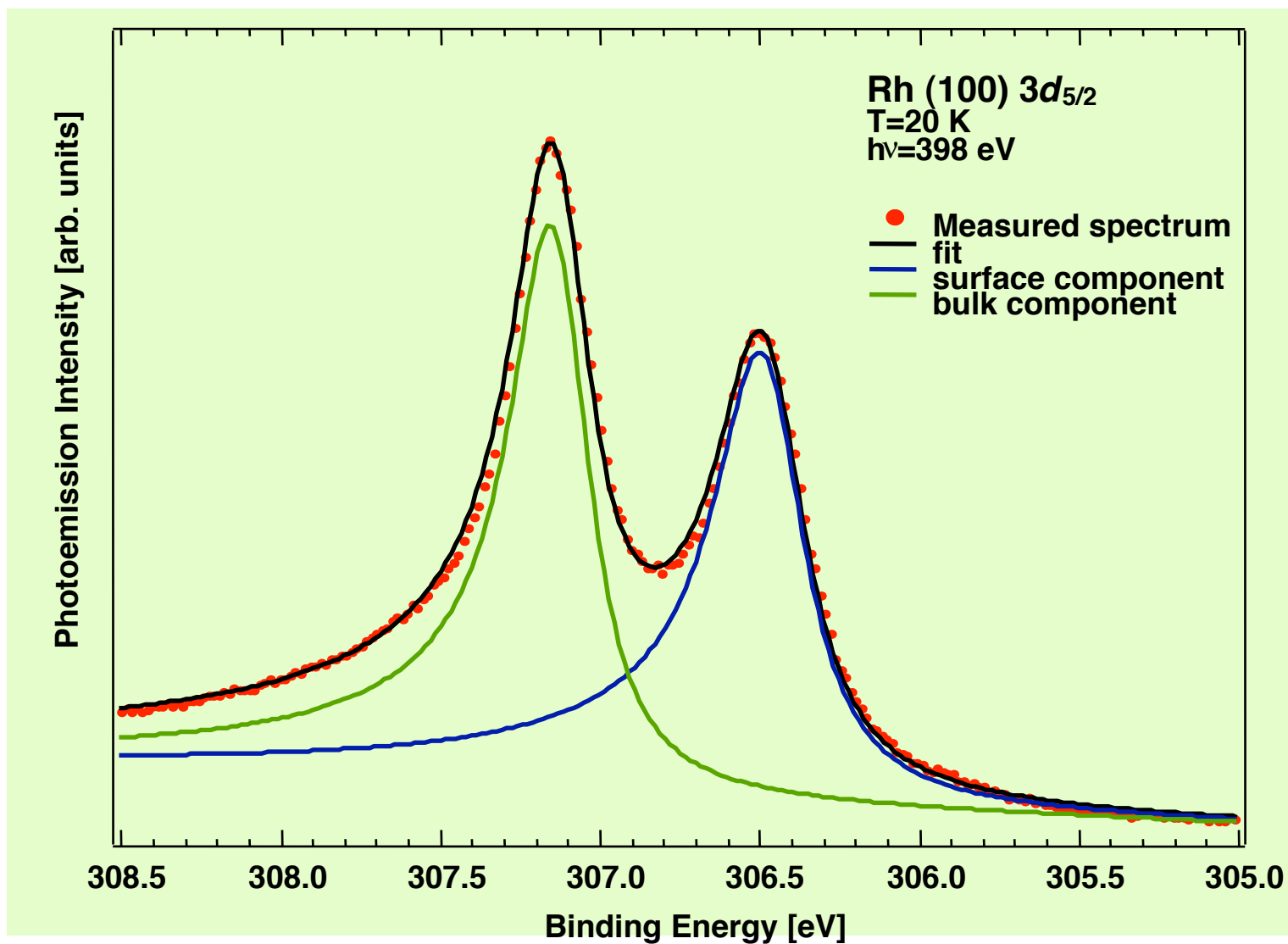


# Neglecting relaxation...

Comparison of experimental XPS C 1s binding energies with those calculated via Koopman's theorem for C in a range of molecules. Although experimental and theoretical values differ by 15 eV (associated with relaxation effects) the systematic comparison is excellent as indicated by the straight line of unity slope



# A particular case of core level shift: the *surface* core level shift



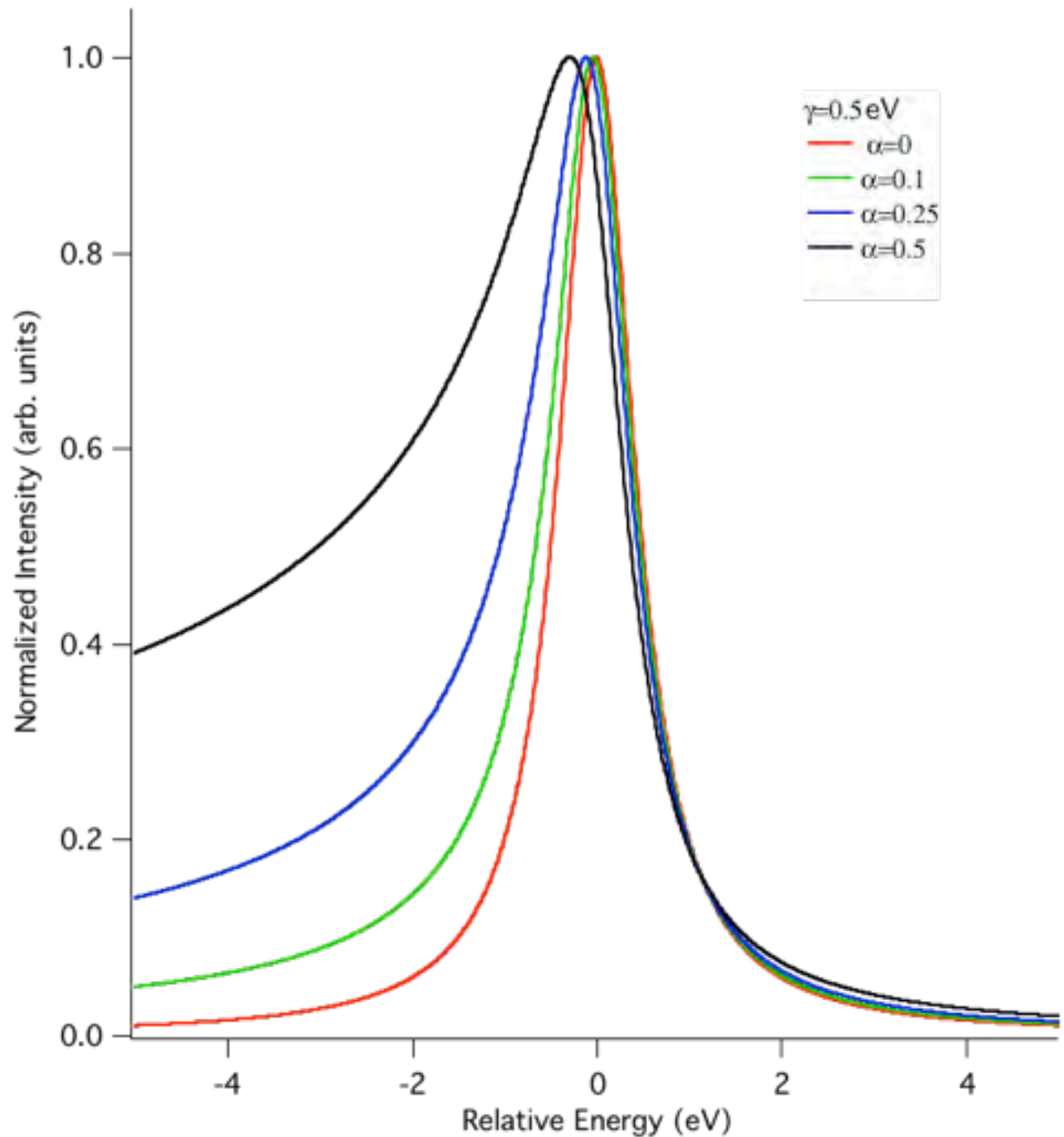
# The Doniach-Šunjić lineshape

J. Phys. C **3**, 285 (1970)

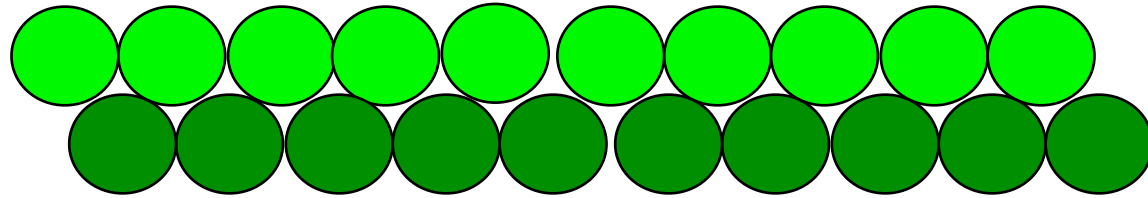
$$Y(E) = \frac{\Gamma(1 - \alpha)}{(E^2 + \gamma^2)^{\frac{(1-\alpha)}{2}}} \cos \left[ \frac{\pi\alpha}{2} + (1 - \alpha) \arctan \left( \frac{E}{\gamma} \right) \right]$$

# The Doniach- Šunjić lineshape

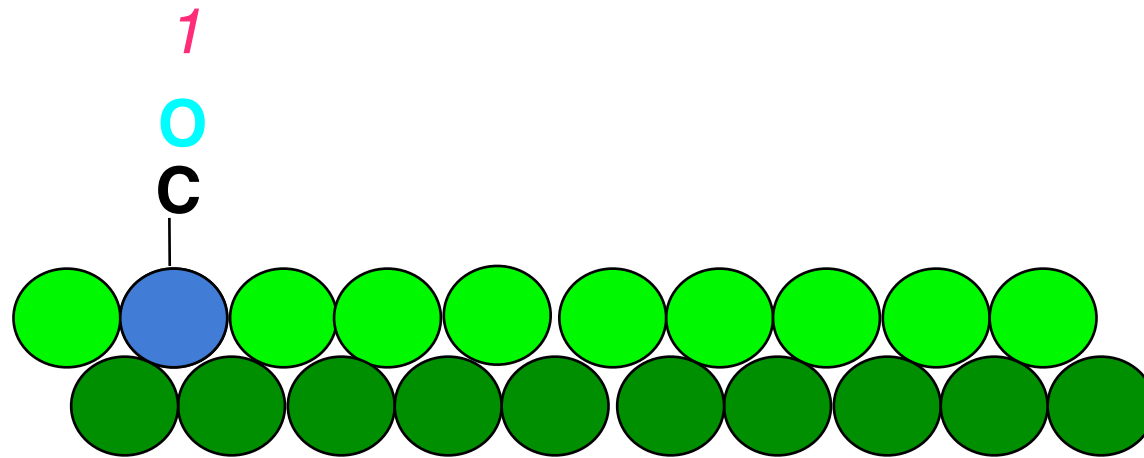
J. Phys. C **3**, 285  
(1970)



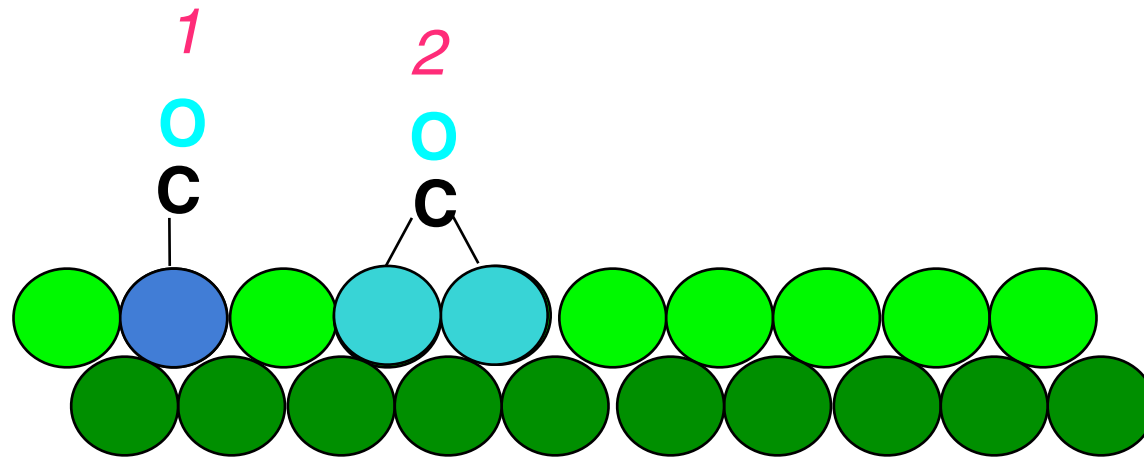
# Reactions on surfaces



# Reactions on surfaces

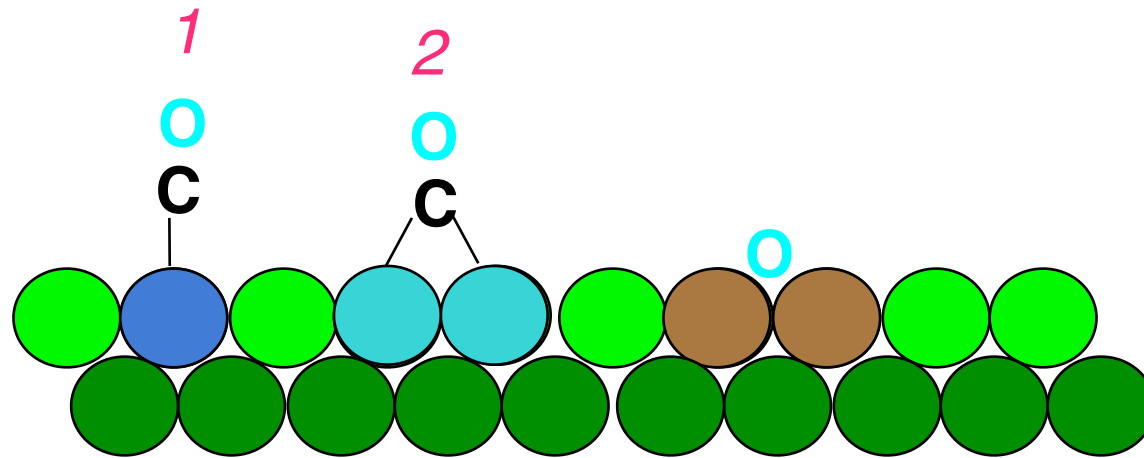


# Reactions on surfaces

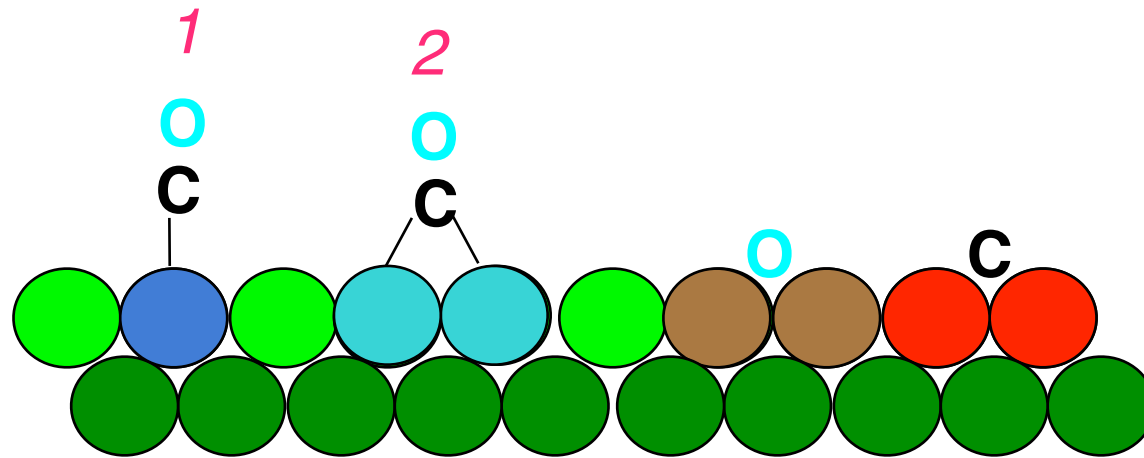




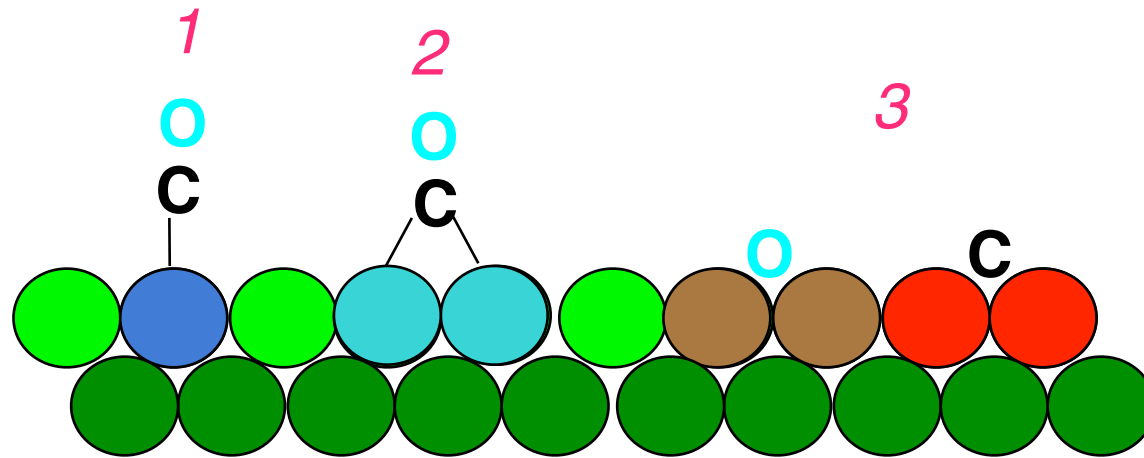
# Reactions on surfaces



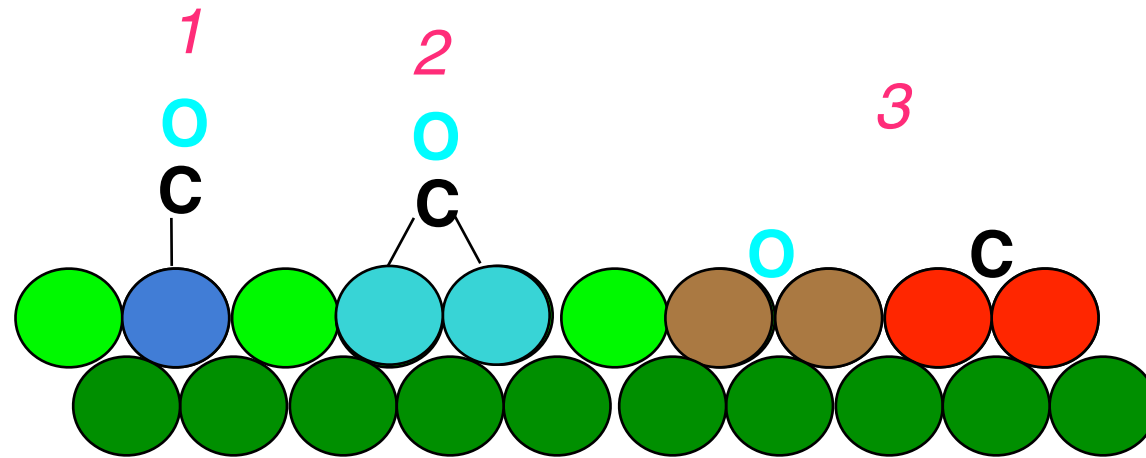
# Reactions on surfaces



# Reactions on surfaces

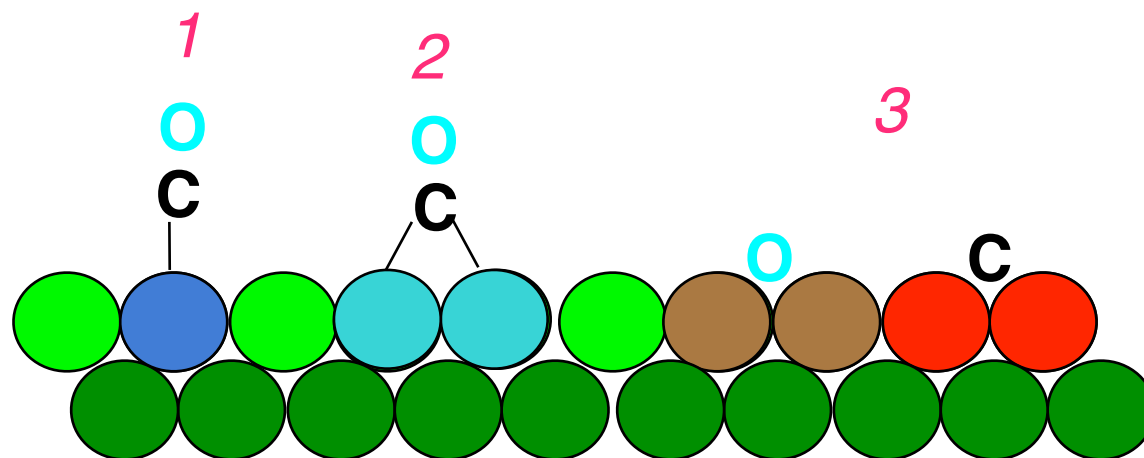


# Reactions on surfaces



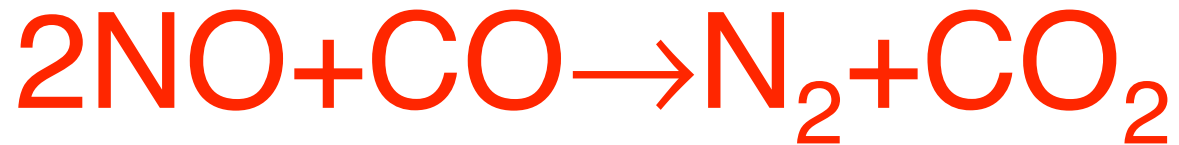
- Distinguish **1** (CO on top) from **2** (CO on a bridge site) and from **3** (dissociated CO)

# Reactions on surfaces

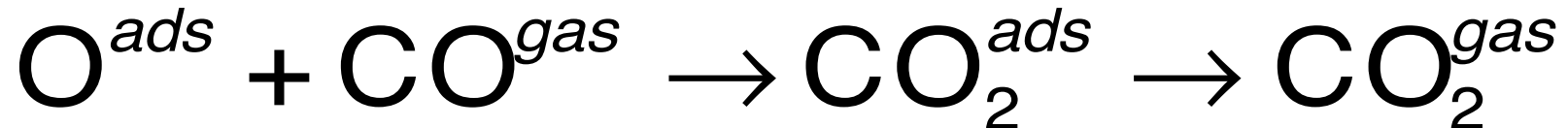
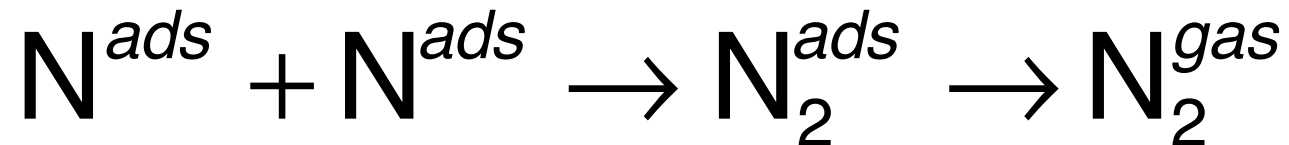
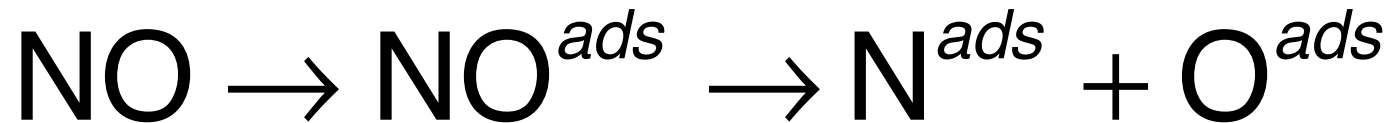


- Distinguish **1** (CO on top) from **2** (CO on a bridge site) and from **3** (dissociated CO)
- Follow changes from **1** to **2** and/or to **3**

# Example of surface reaction



Intermediate reactions:



# Why XPS?

- has unambiguous correspondence between surface species and spectral features;
- is quantitative;
- is applicable to both molecular and atomic adsorbates;
- changes in both adsorbate and substrate can be detected.



# For $t < 1994$ XPS used to be a “slow” technique

Typical acquisition time  $\sim 30$  minutes for adsorbates



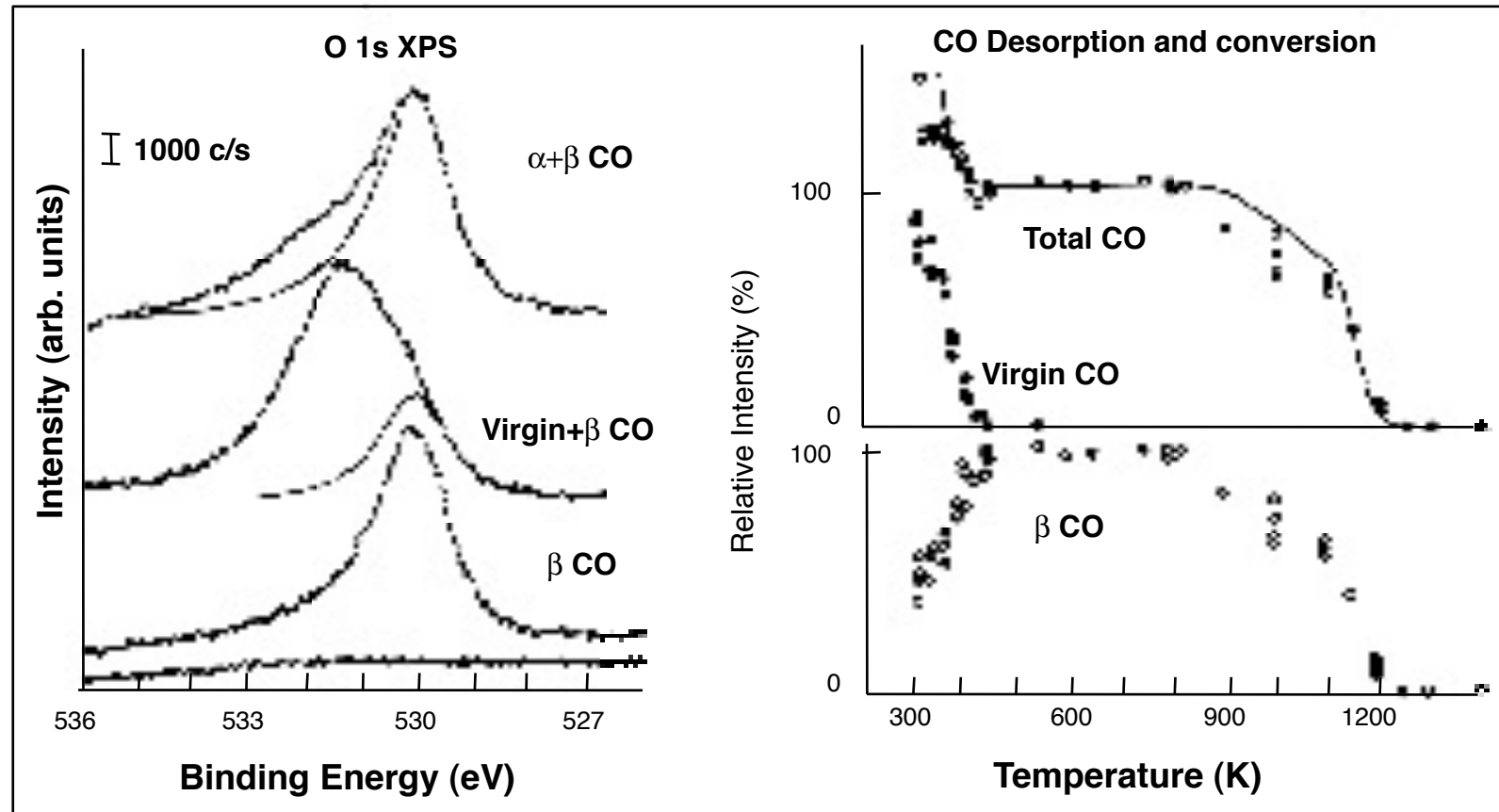
only “*frozen*” and/or low resolution experiments were possible



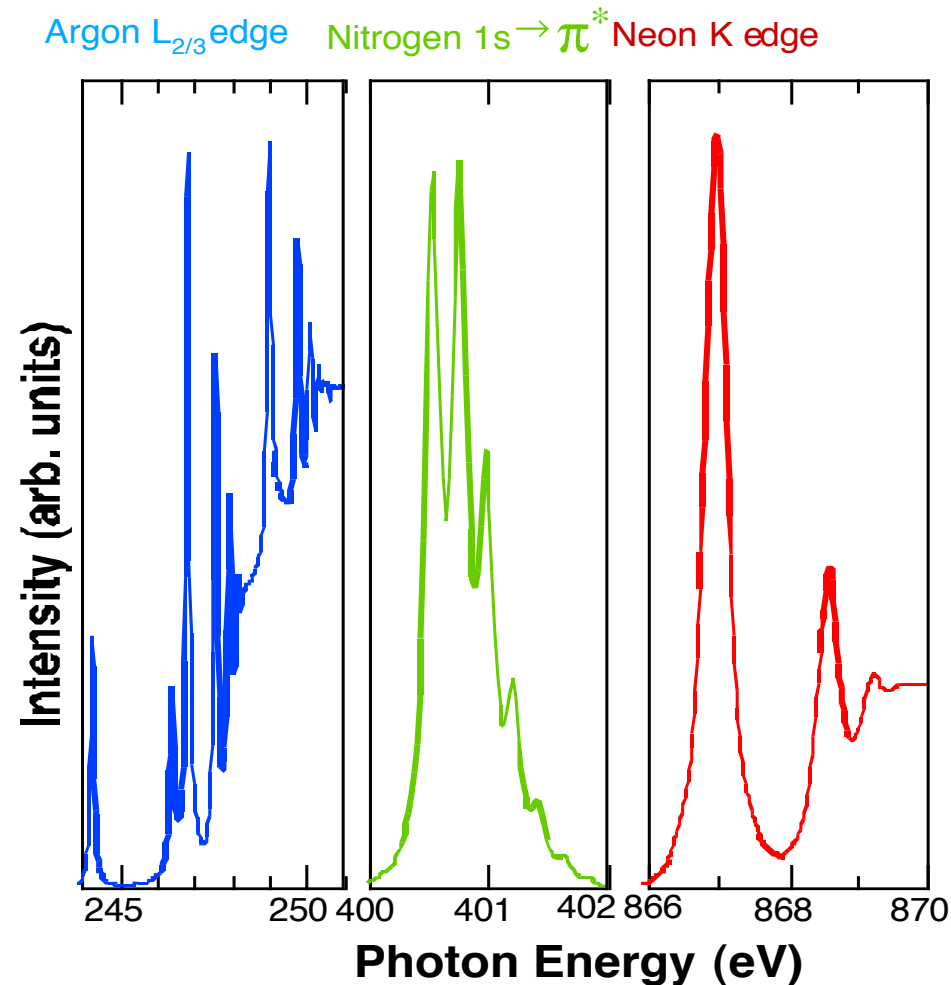
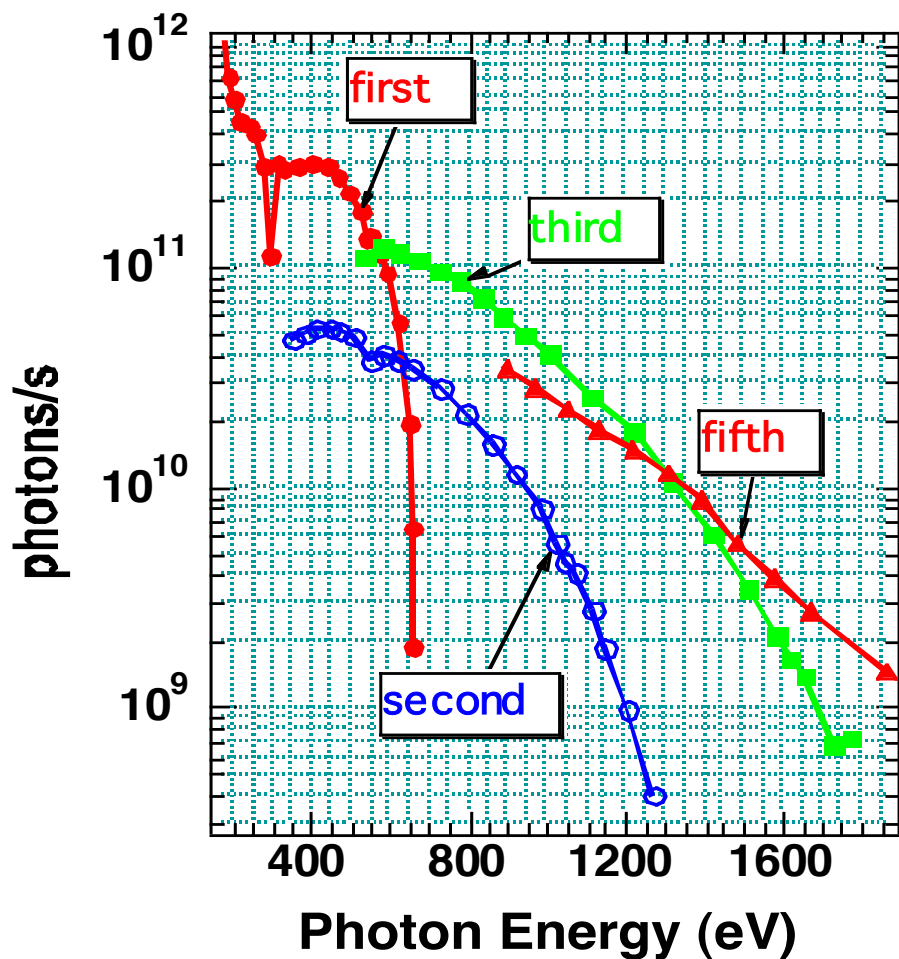
better to go for vibrational spectroscopies!

# First attempts to use XPS to follow surface reactions: dissociation of CO/W(110)

E. Umbach, J.C. Fuggle, D. Menzel, J. Electron Spectrosc. **10**,15 (1977)



# With 3rd generation SR sources: flux & resolution at the same time



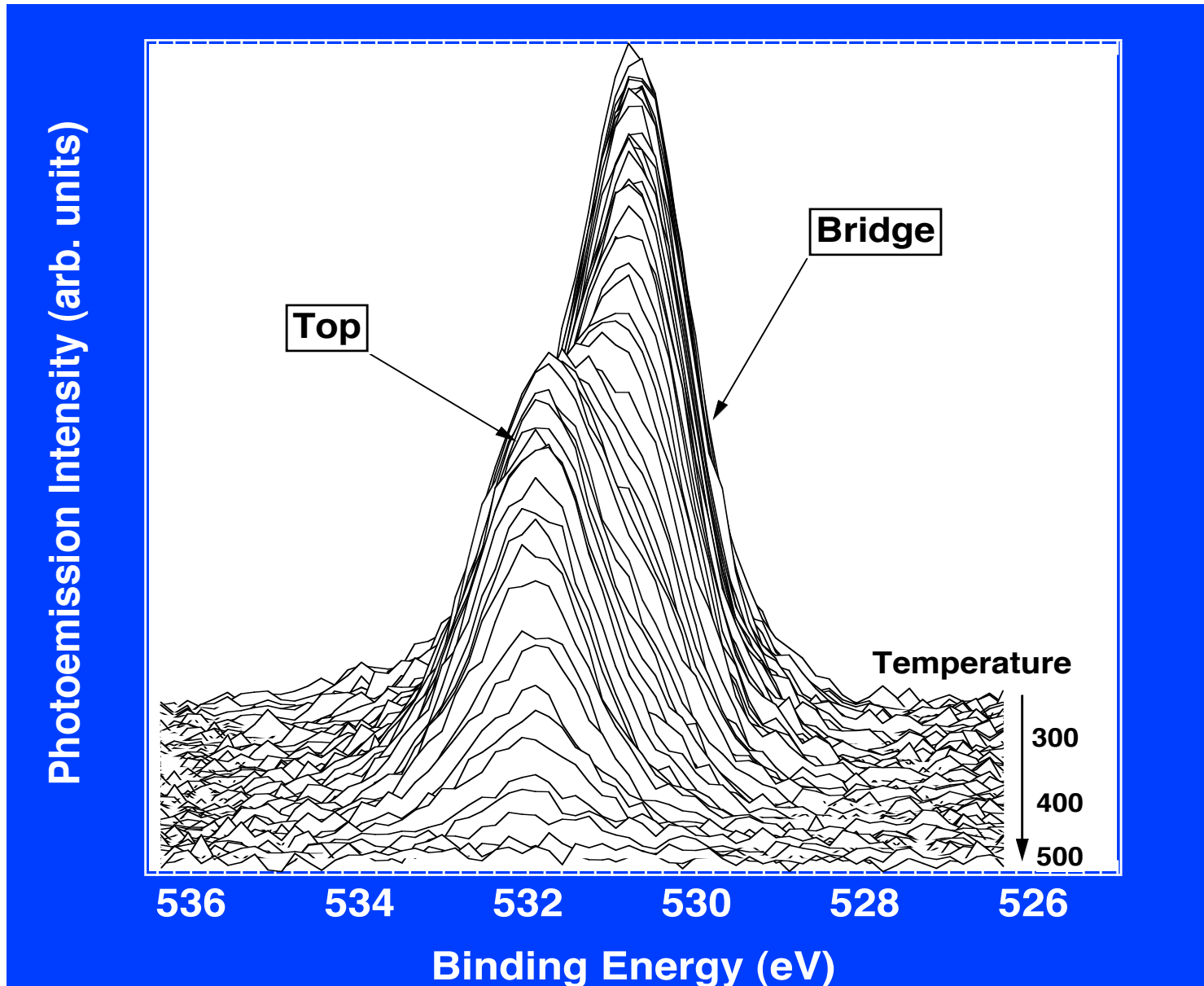
# Measure surface time-dependent phenomena

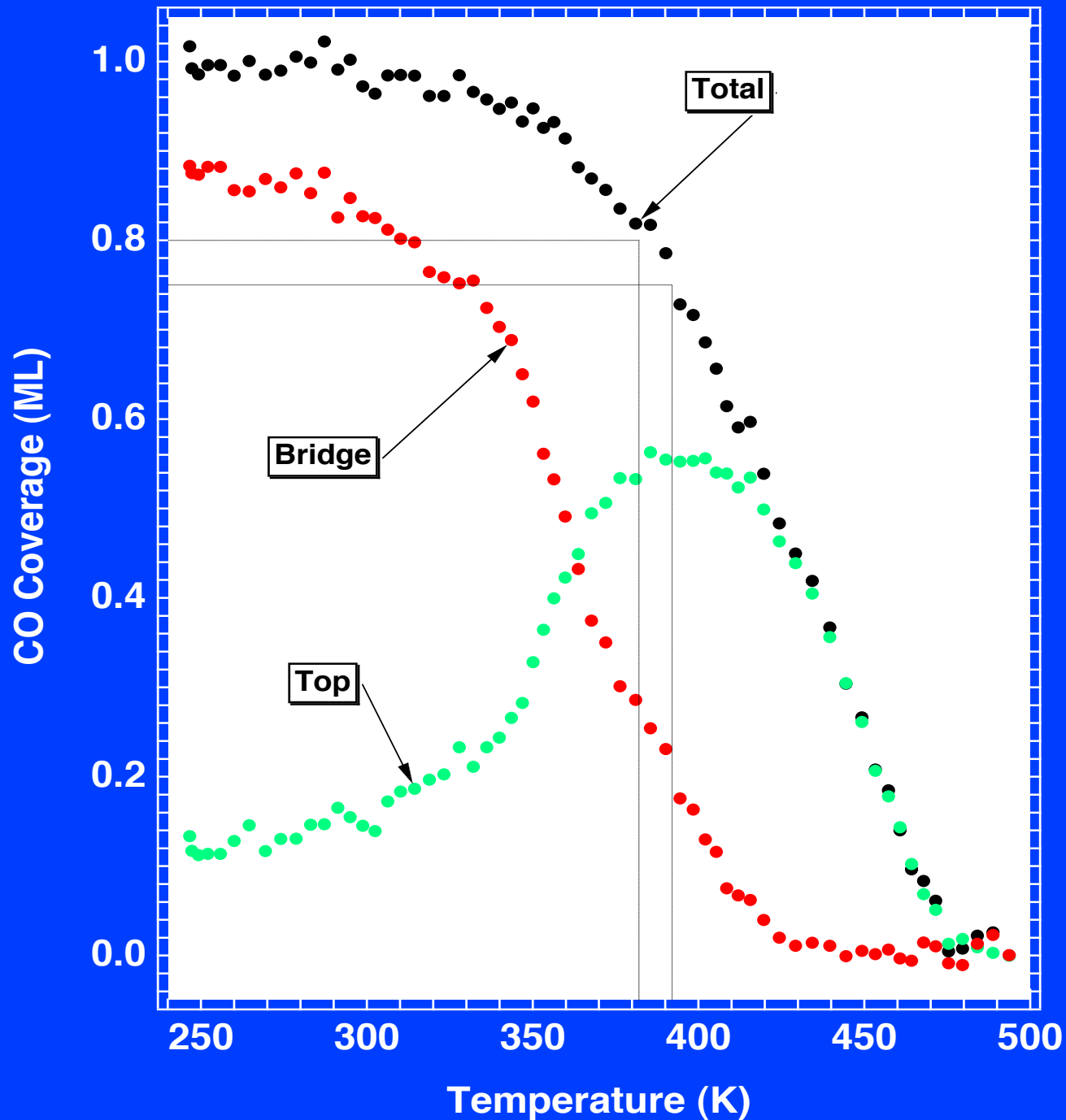
- Trigger the phenomenon (e.g. open a leak valve!)
- Measure a lot of spectra
- Analyze them to get quantitative information

# CO thermal desorption from Rh (110)

- Two adsorption sites
- Migration and desorption

# Desorption of CO/Rh(110)

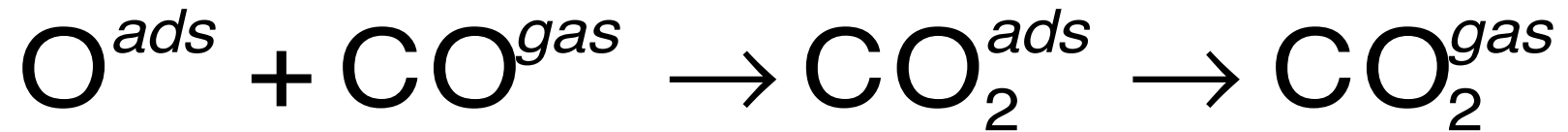




CO/Rh(110):  
CO desorption  
& migration



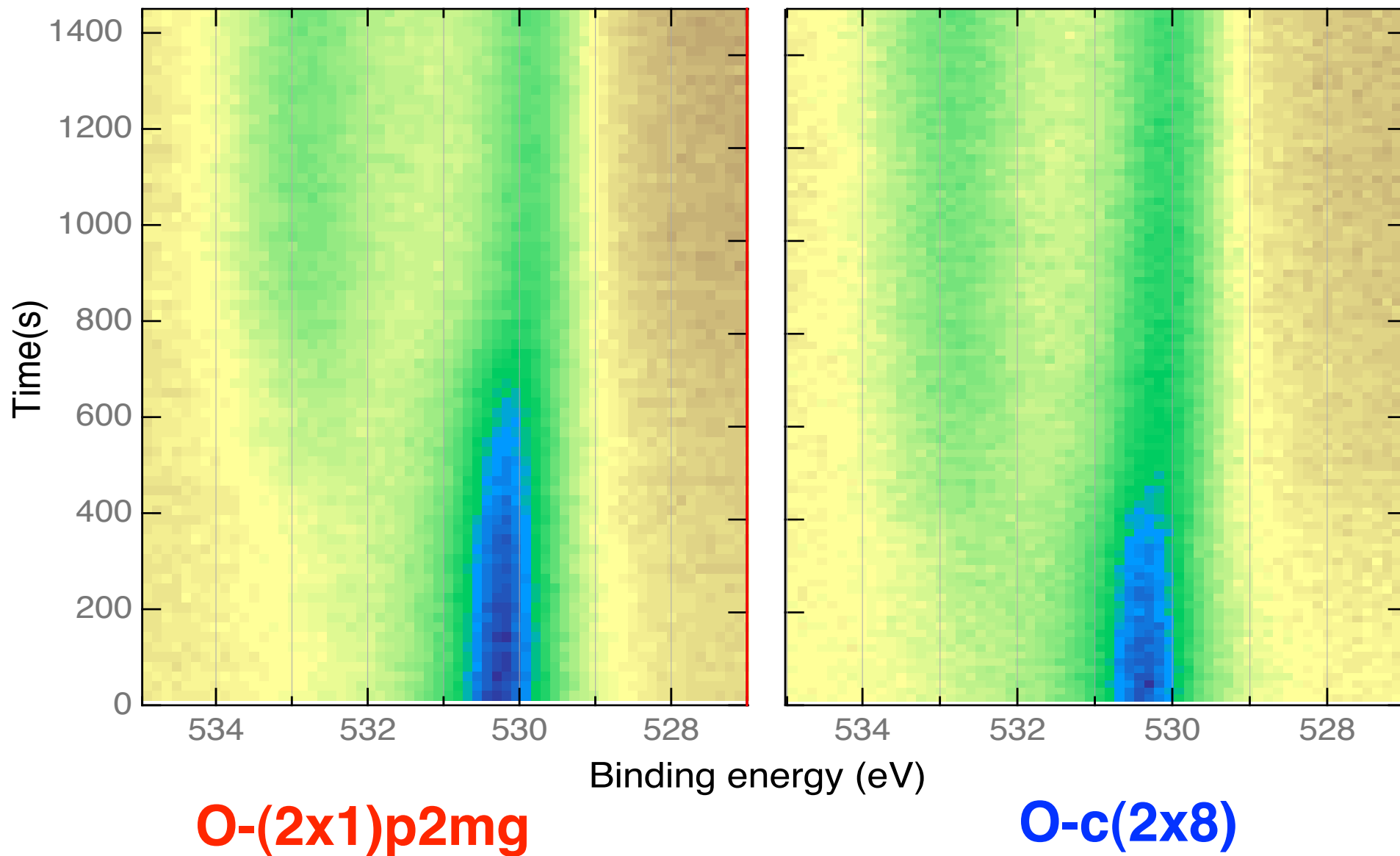
# CO titration of oxygen overlayers on Rh (110) at T=200 K

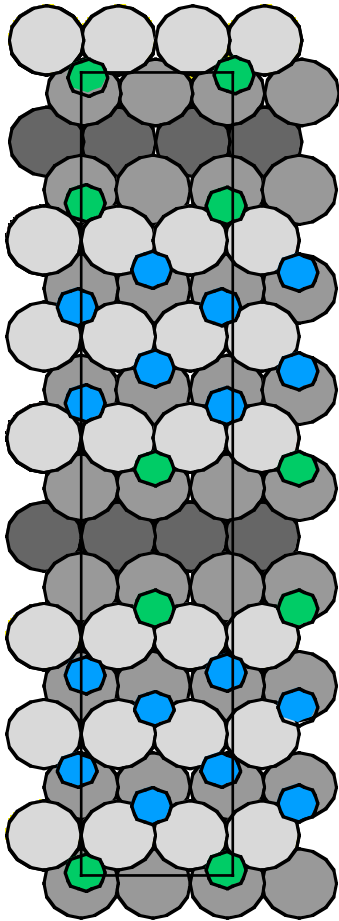


Effect of surface restructuring on reaction rate

# CO titration of oxygen overlayers on Rh (110)

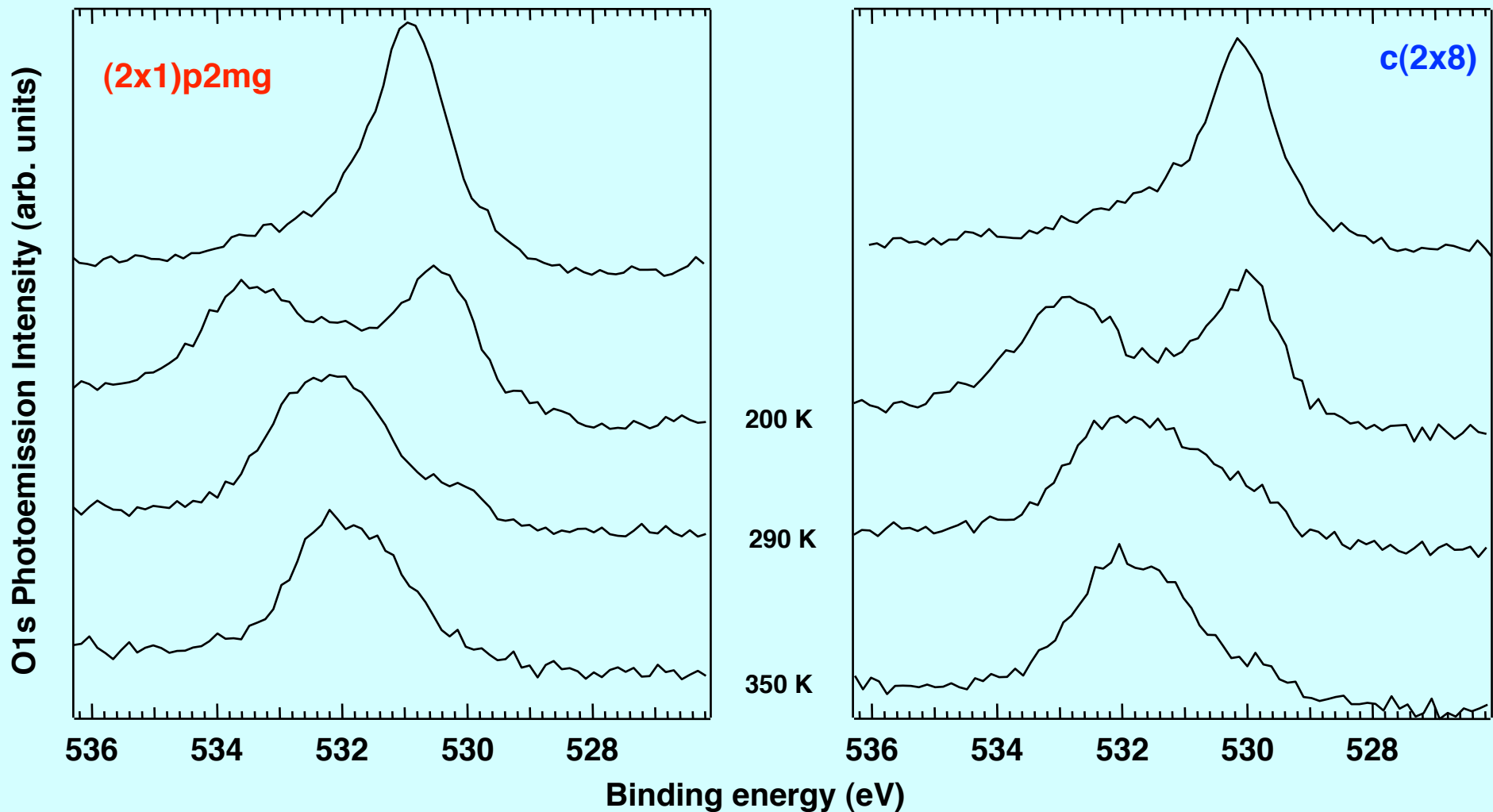
T=200 K





La struttura O-c(2x8) con gli atomi di ossigeno nei siti *threefold* nei solchi non ricostruiti (azzurri-più reattivi) e nei solchi ricostruiti (verdi-meno reattivi)

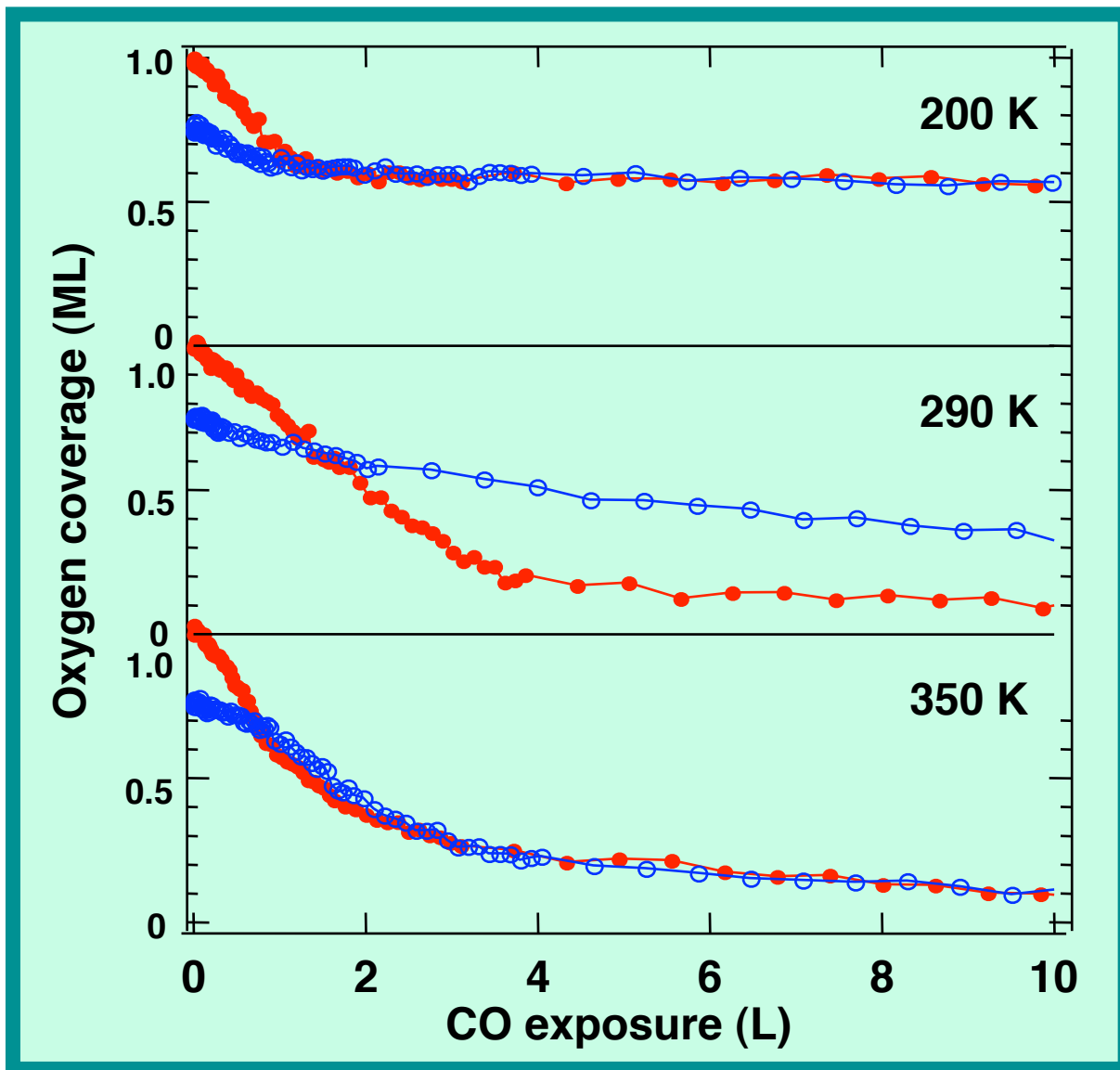
# CO titration of oxygen overlayers on Rh (110)



spectra taken after 20 L CO exposure

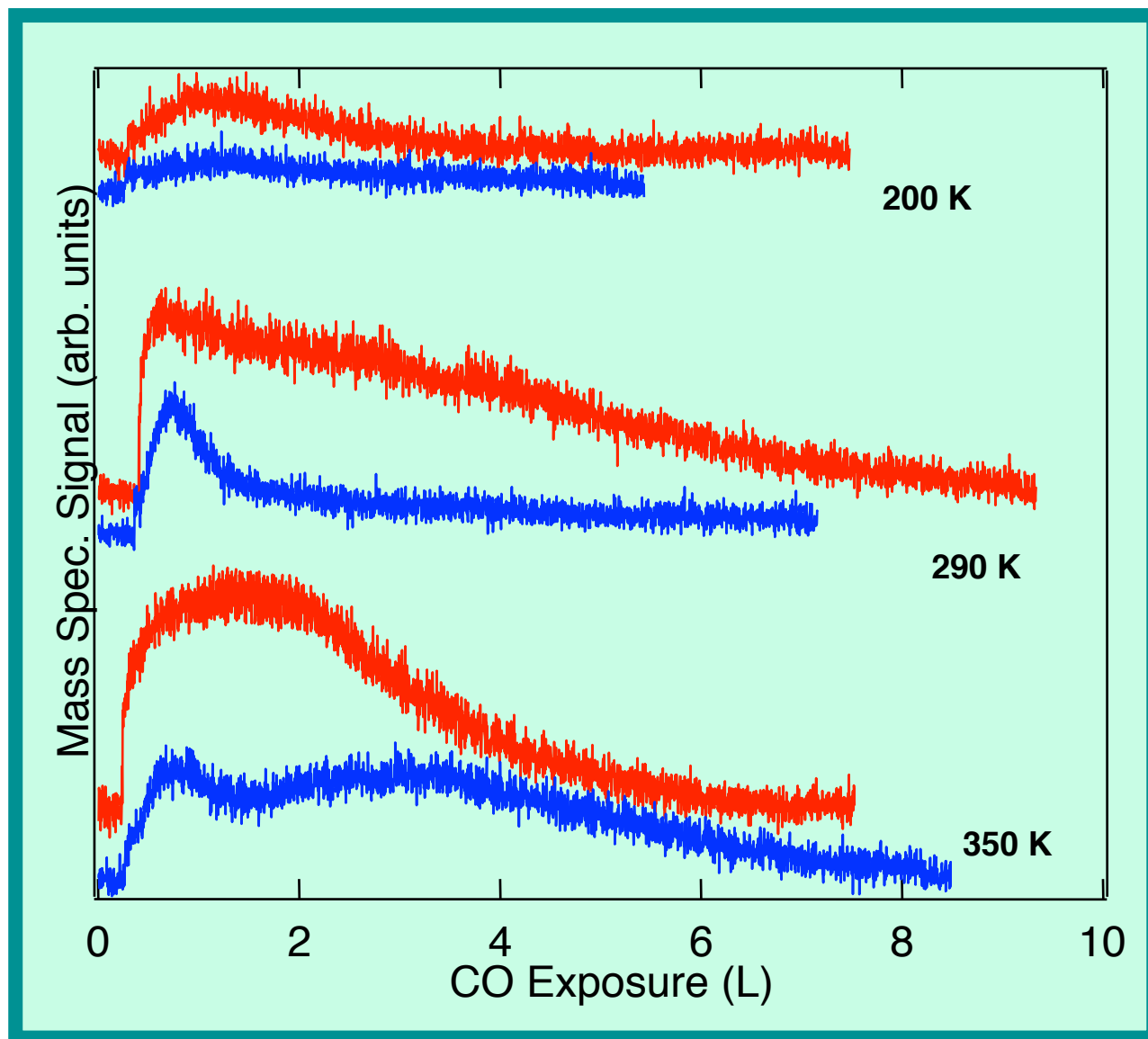
# CO titration of oxygen overlayers on Rh (110)

O decay for  
**O-(2x1)p2mg**  
and  
**O-c(2x8)**



# CO titration of oxygen overlayers on Rh (110)

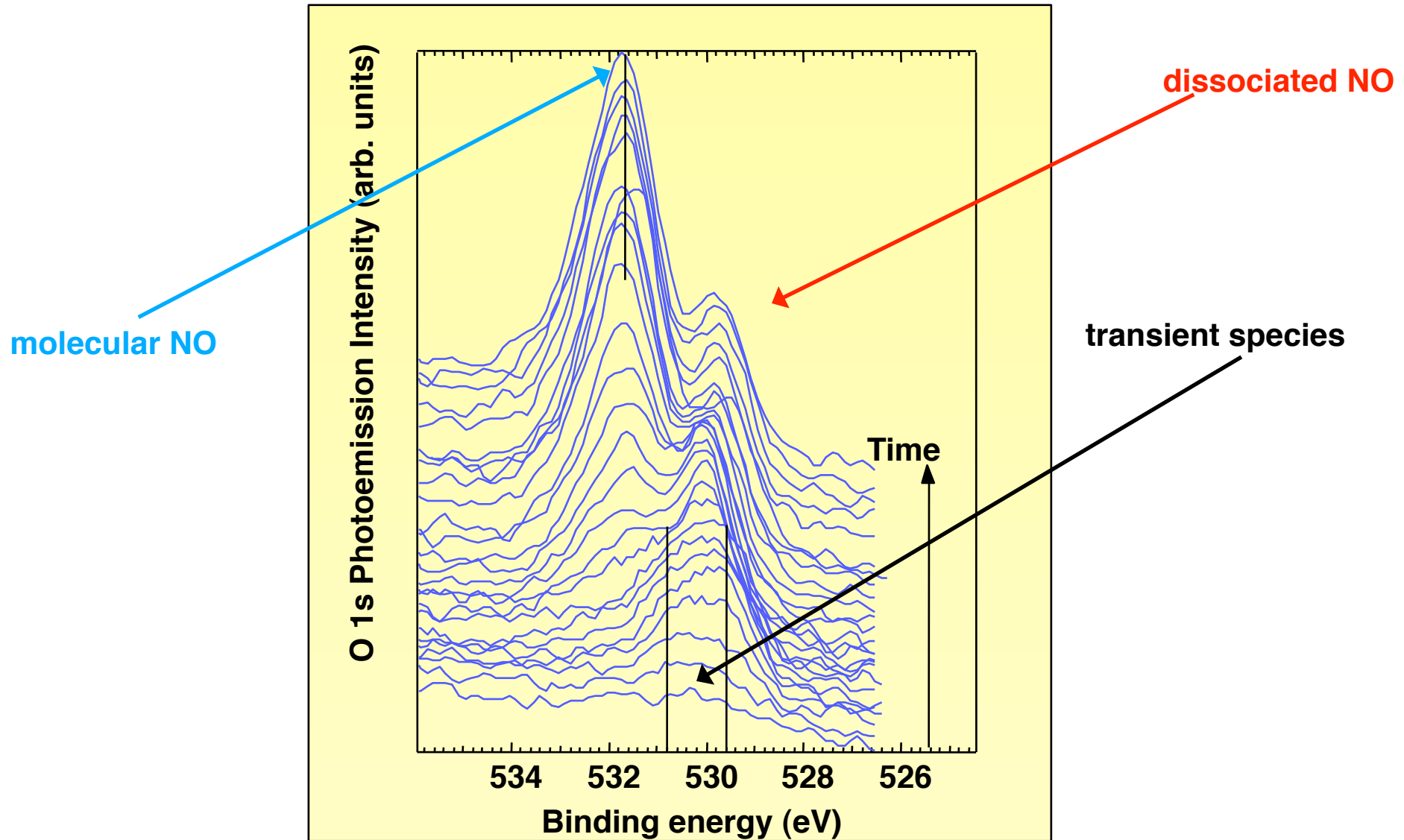
CO<sub>2</sub> production  
from  
**O-(2x1)p2mg**  
and  
**O-c(2x8)**



# Adsorption and dissociation of Nitric Oxide on Rh(110)

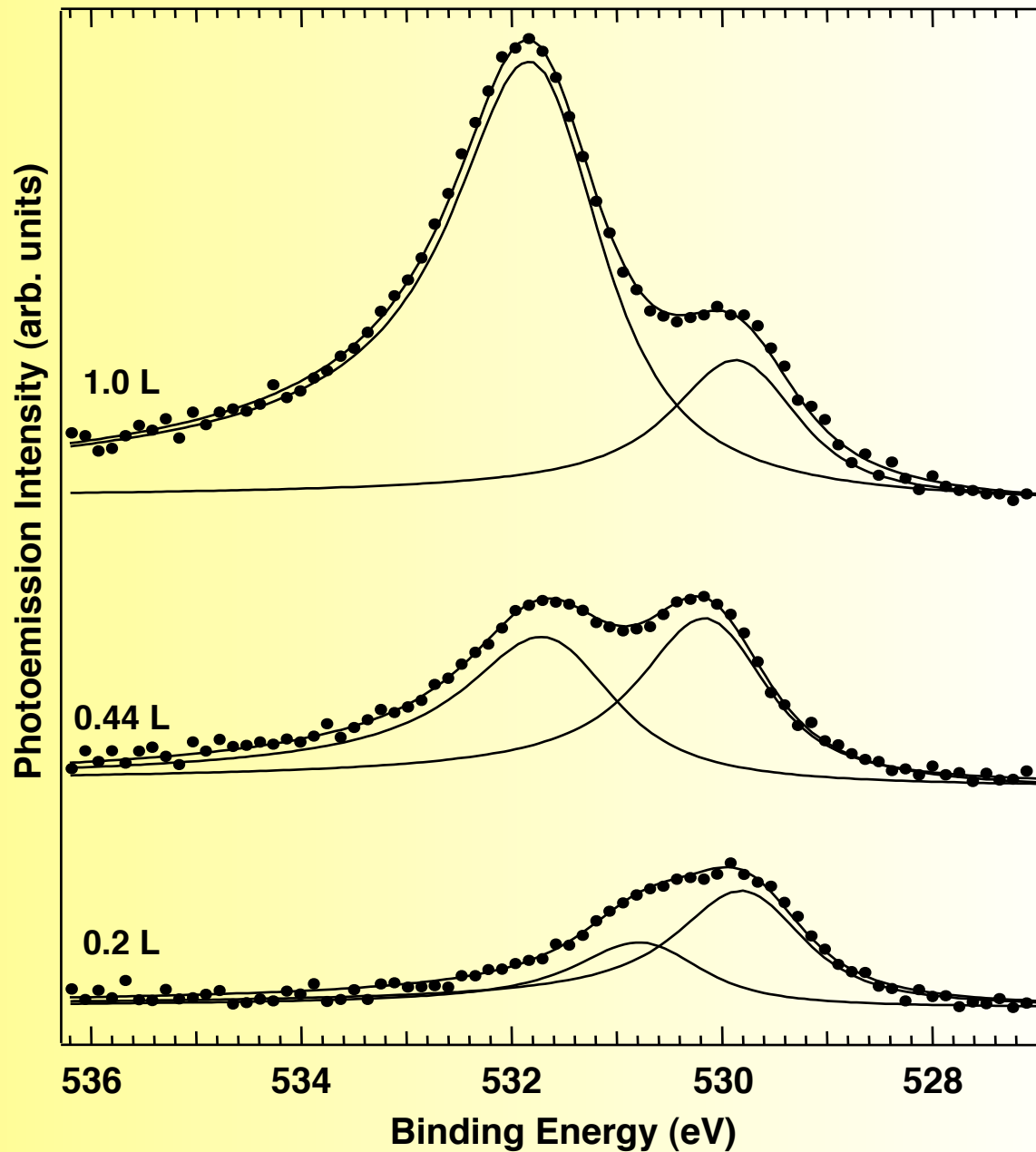
Observation of an adsorption state precursor  
to dissociation

# O 1s spectra during NO exposure at 270 K



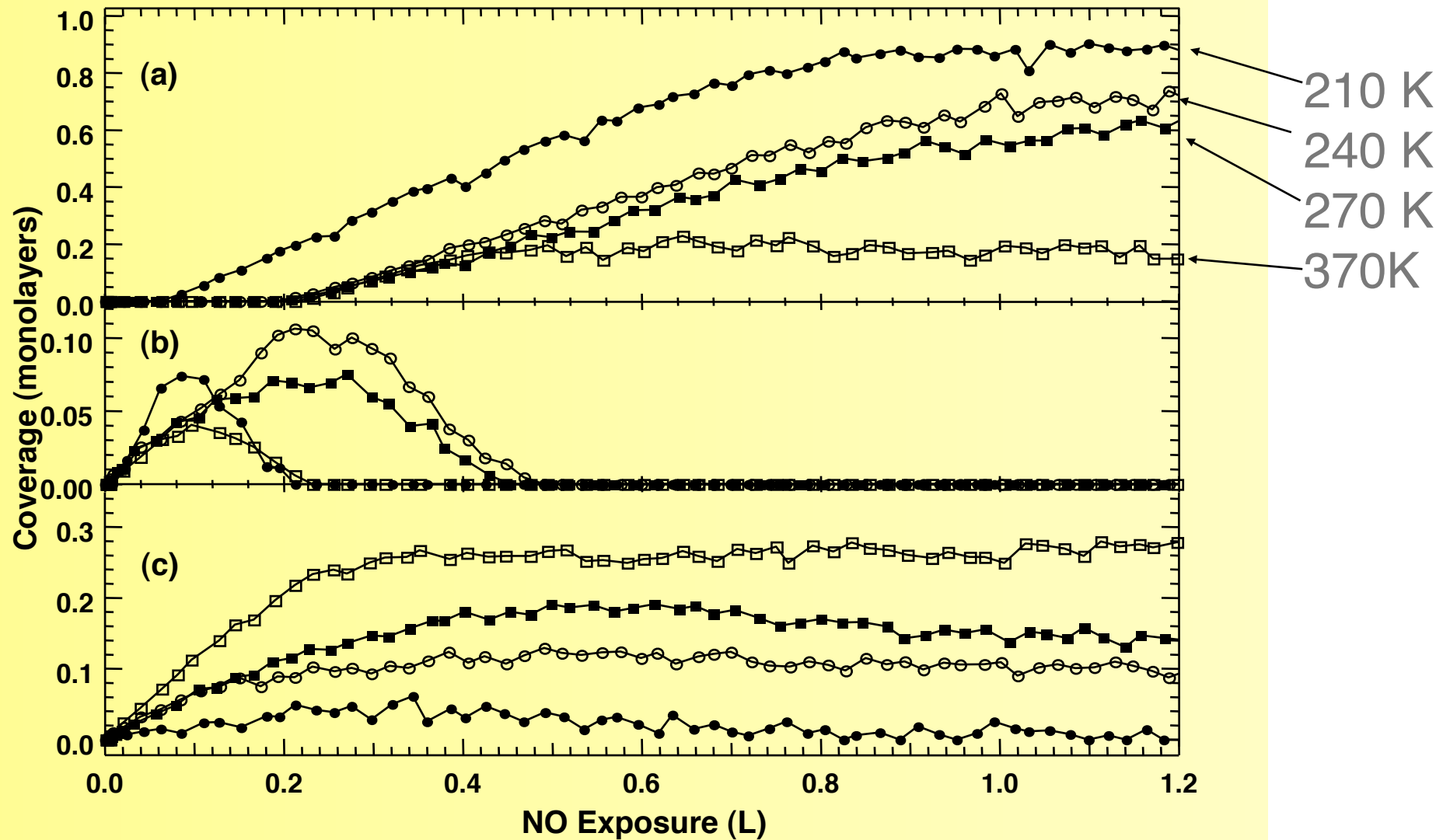


# NO dissociation on Rh (110)



**Selection of O  
1s spectra  
during NO  
exposure at  
270 K**

# NO dissociation on Rh (110)

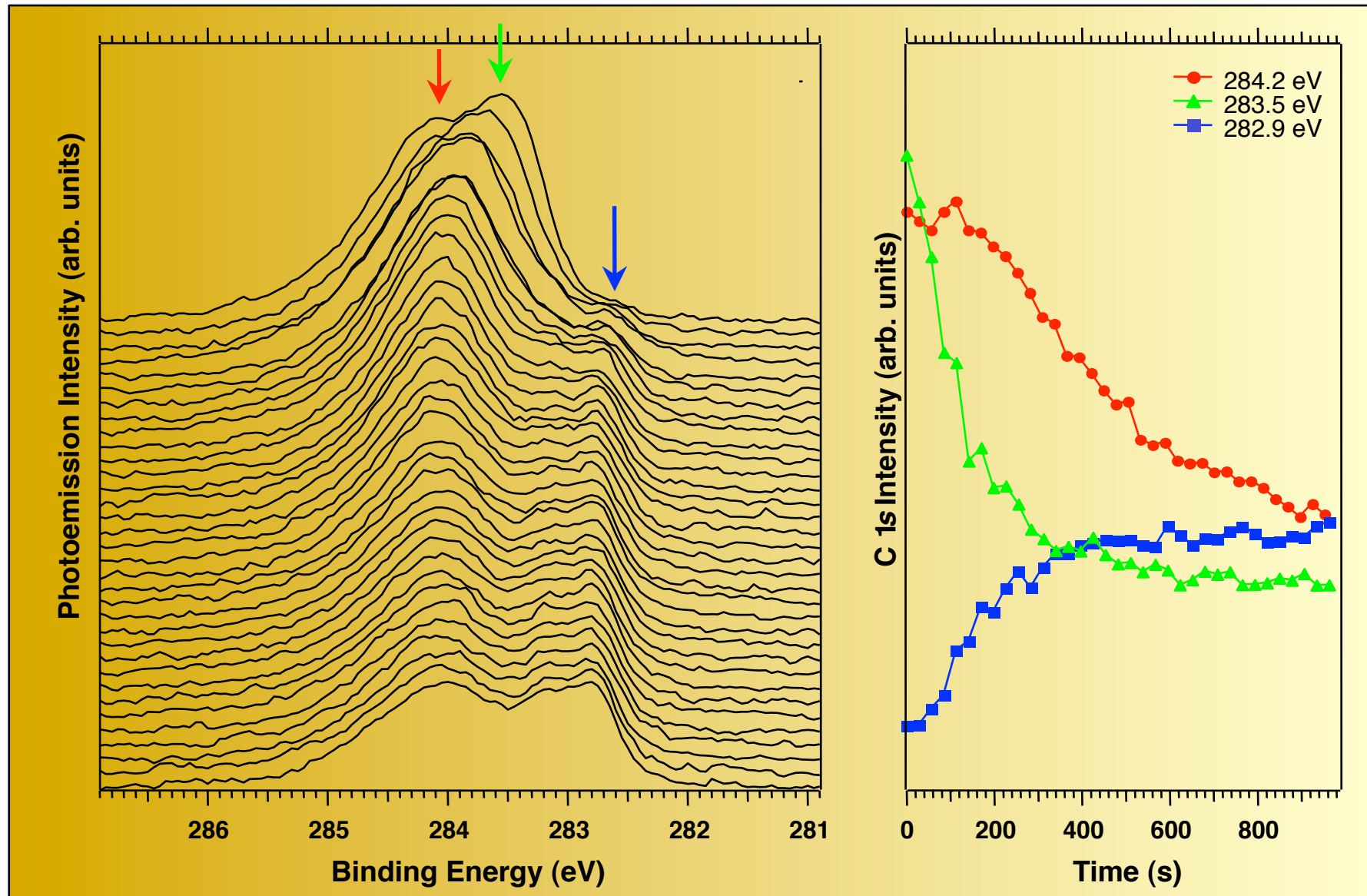


# Photochemistry of CH<sub>4</sub> on Pt (111)

Photodesorption of multilayers

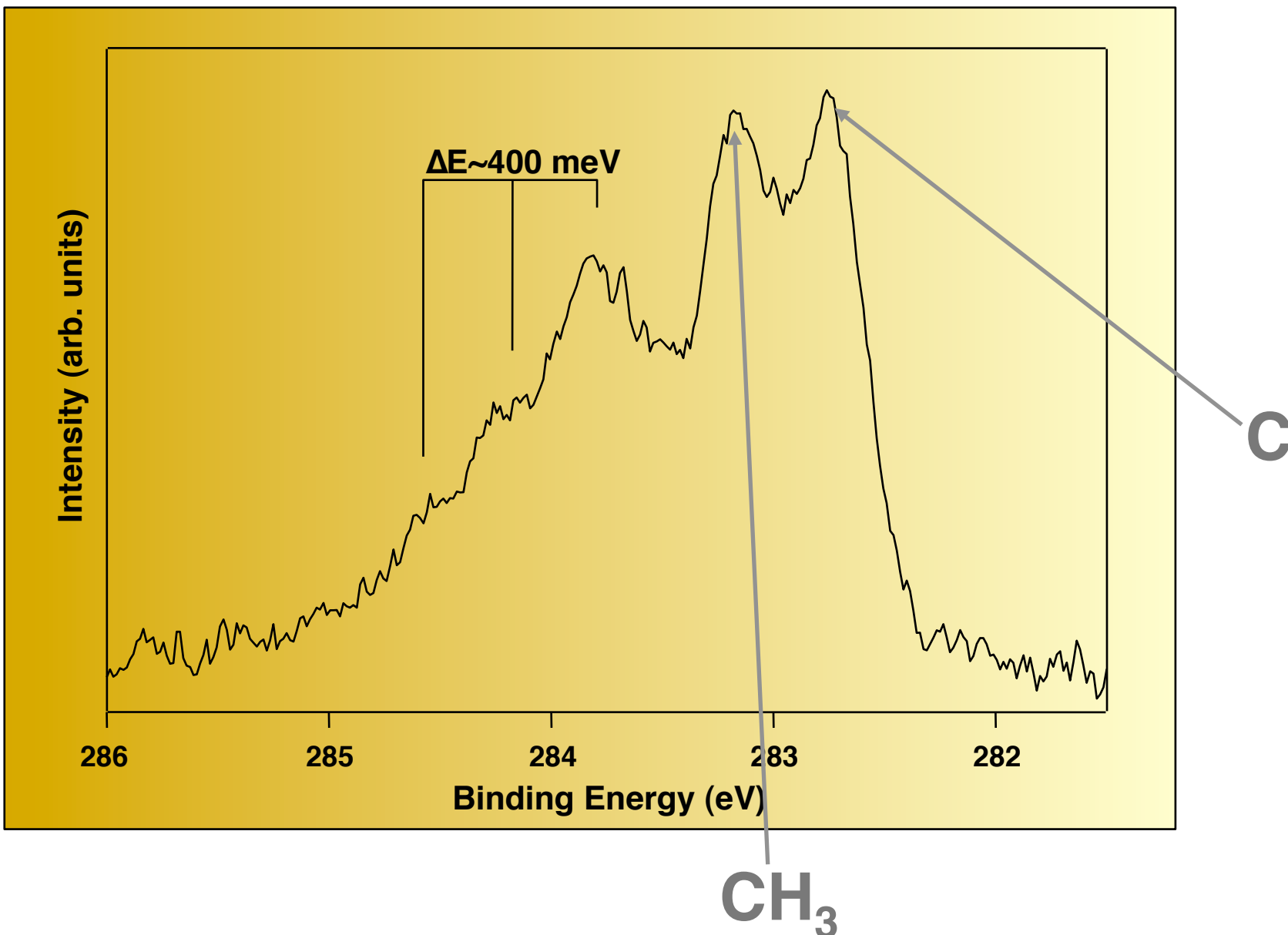
Dissociation into C+CH<sub>3</sub> species

# Photochemistry of CH<sub>4</sub> on Pt(111)

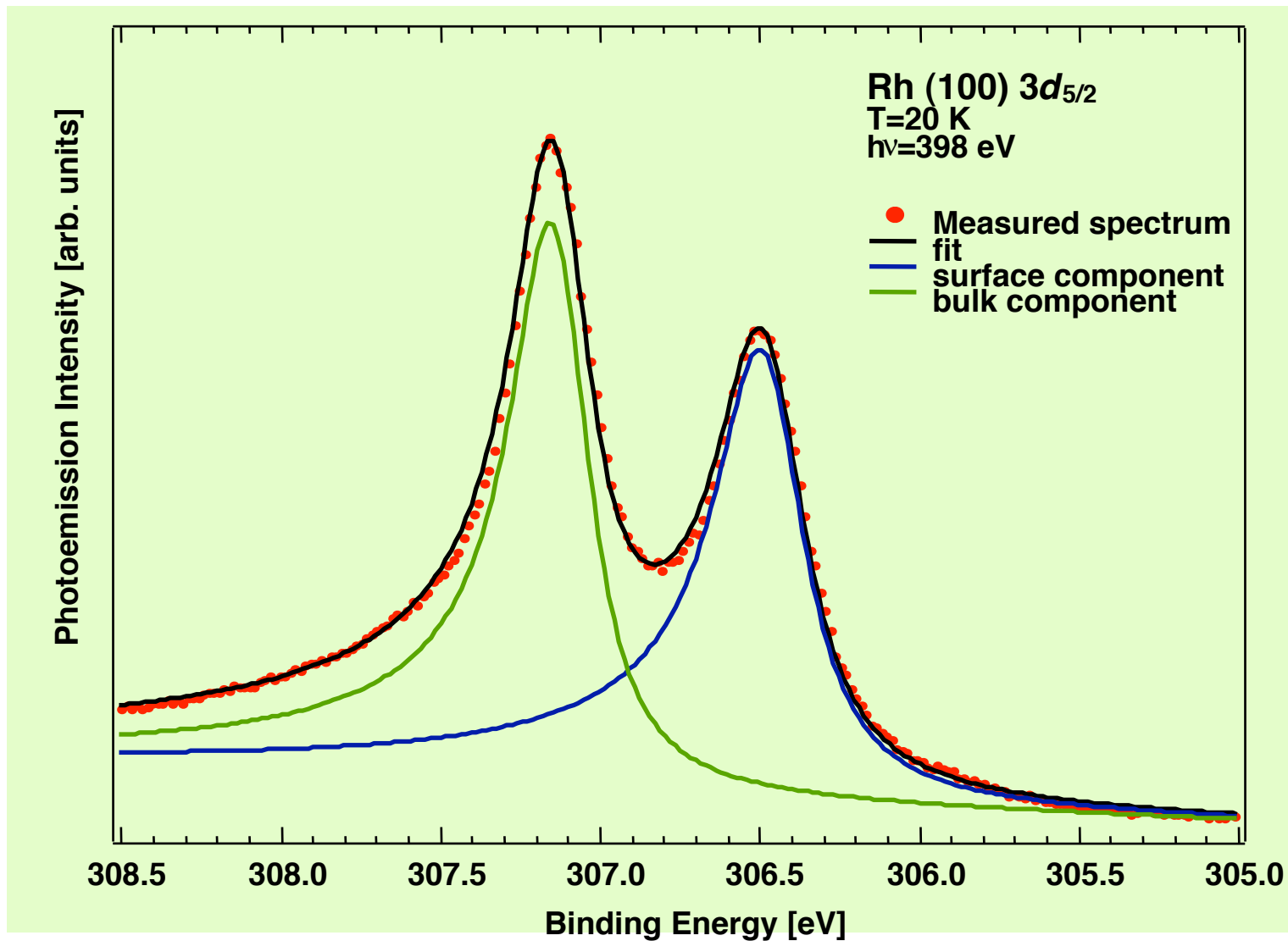


# Photochemistry of CH<sub>4</sub> on Pt(111)

High resolution C 1s spectrum after long exposure to  $h\nu$



# The surface core level shift



# Identification of adsorbate bonding by changes in the substrate *Surface* *Core level Shift*

Evolution of the del SCLS of low Miller indices Rh surfaces  
as a function of O<sub>2</sub> dose

# Surface Core Level Shift

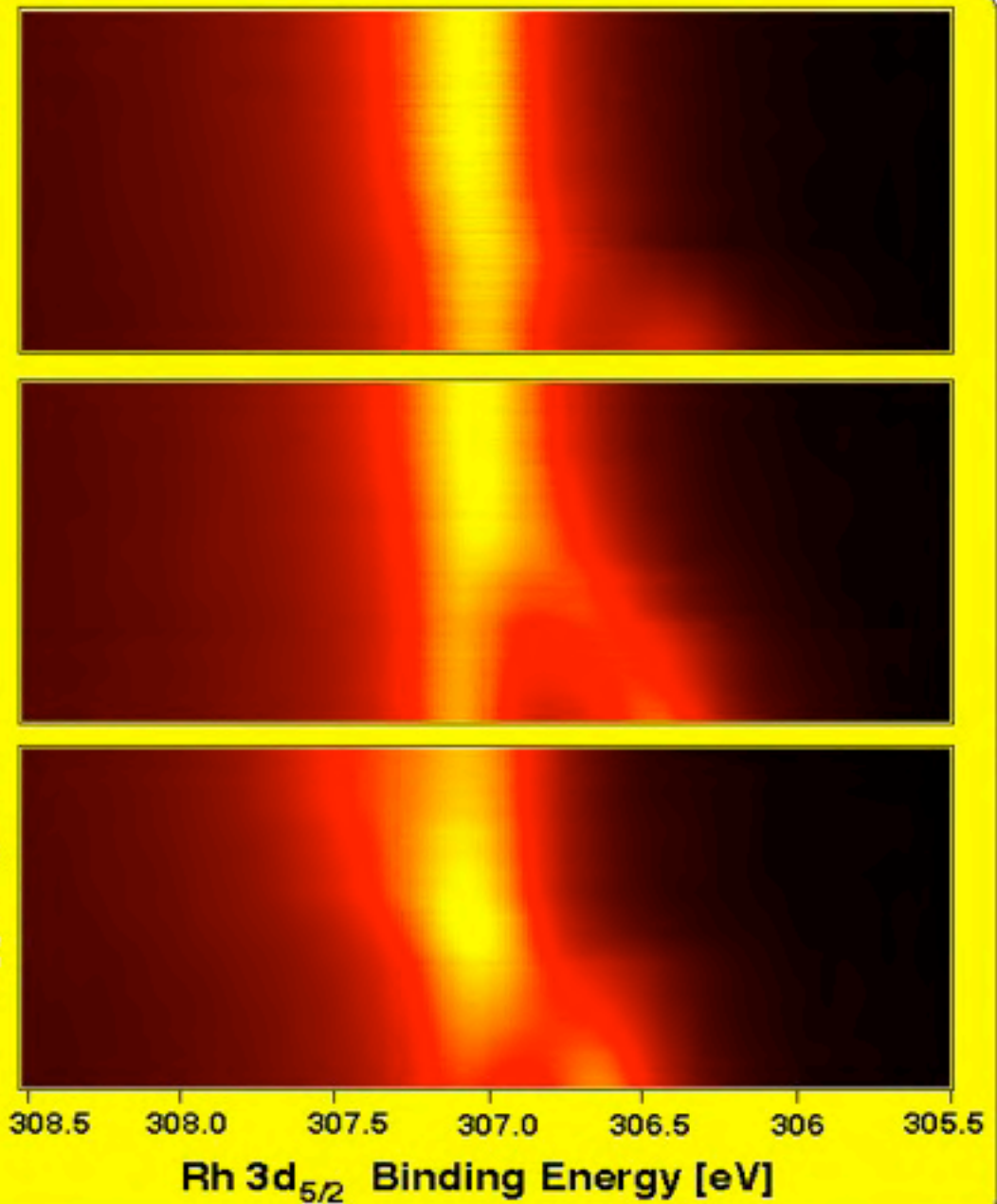
## Rh surfaces

Rh(110)

Rh(100)

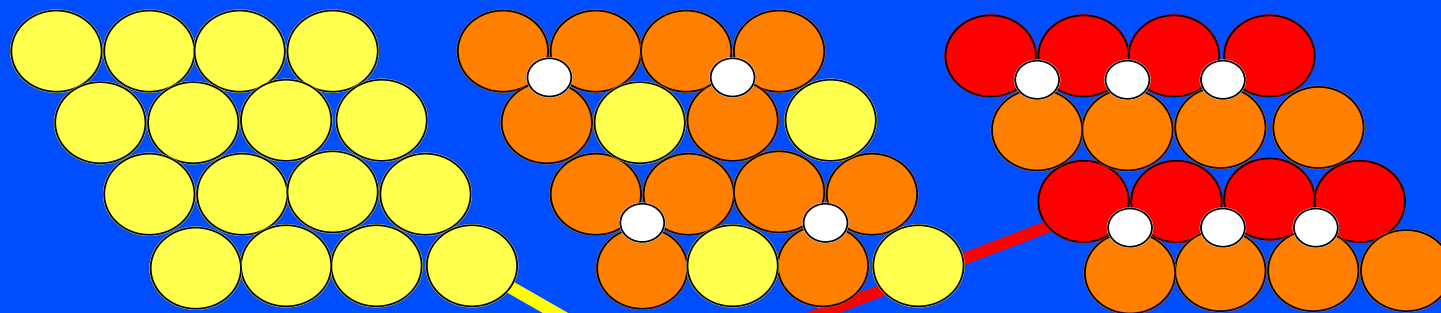
Rh(111)

Oxygen exposure

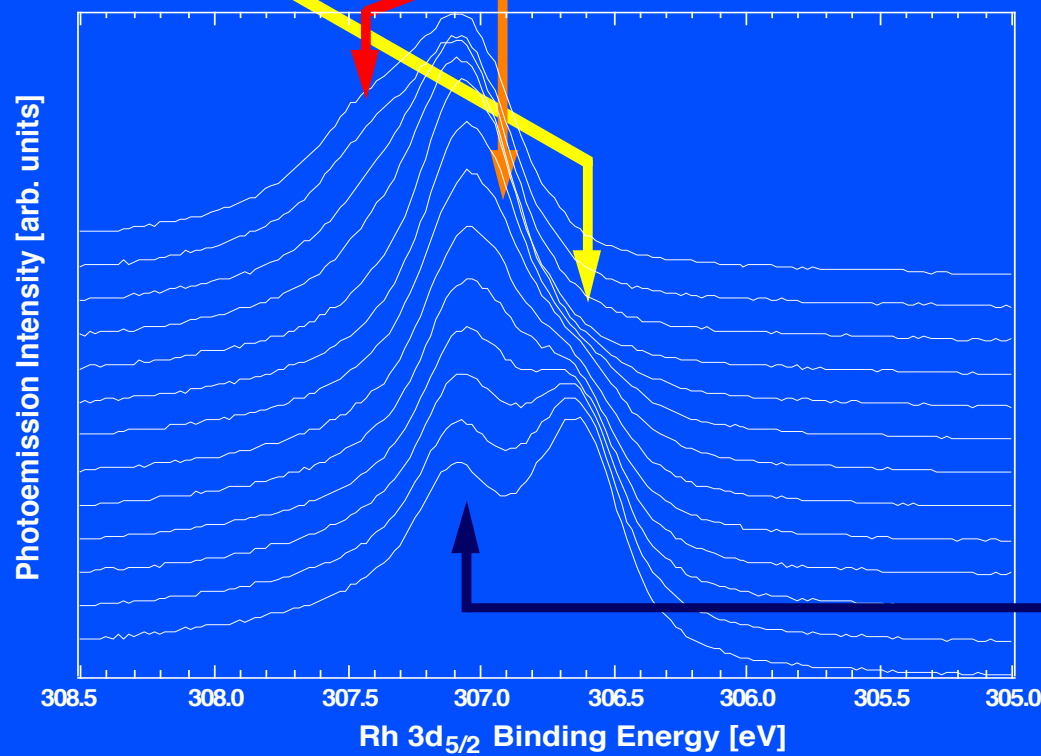




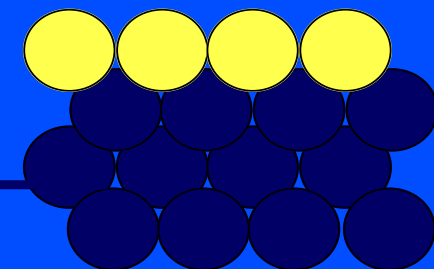
# SCLS study of oxygen adsorption on Rh(111)



○ Oxygen

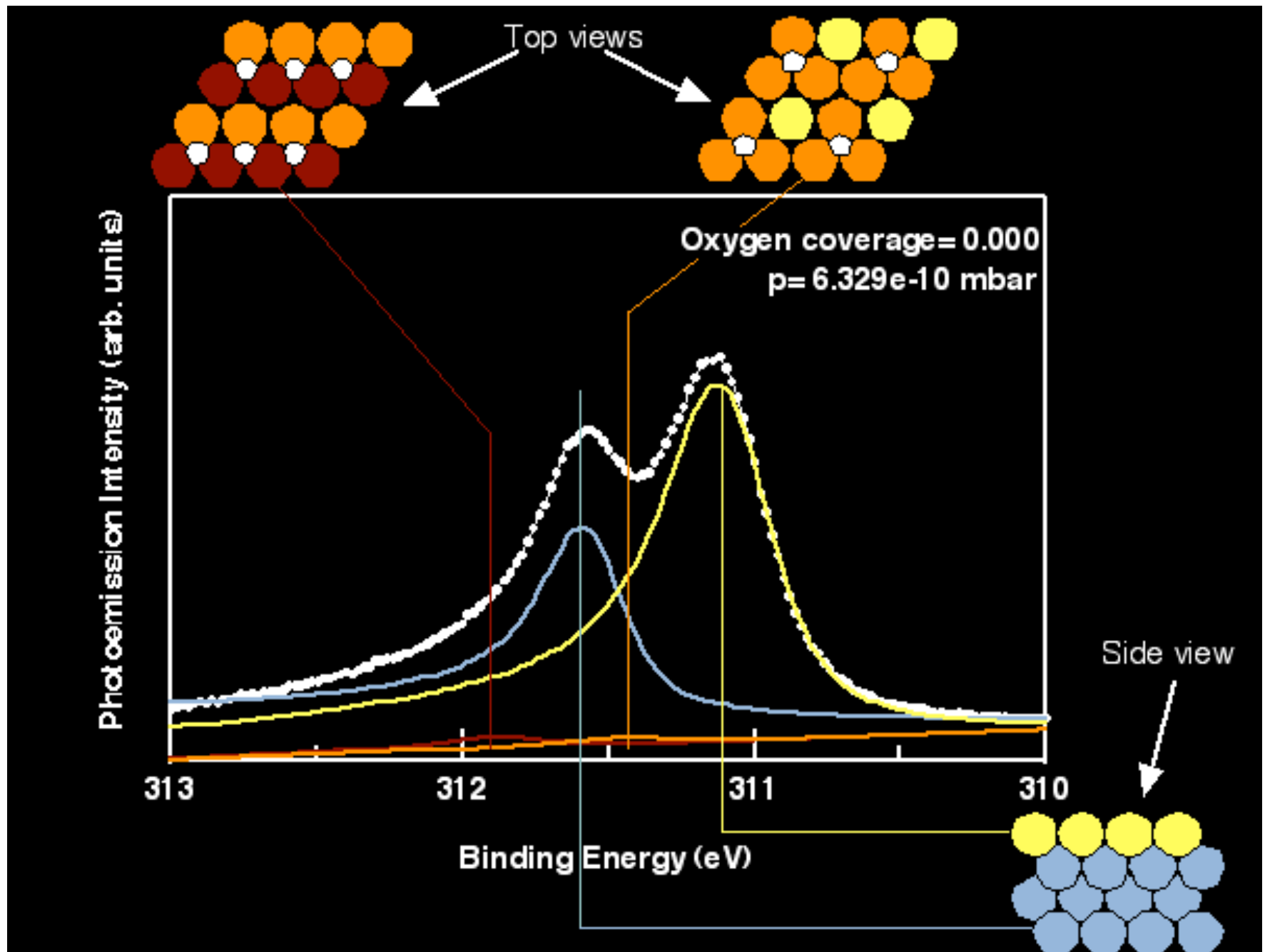


side view

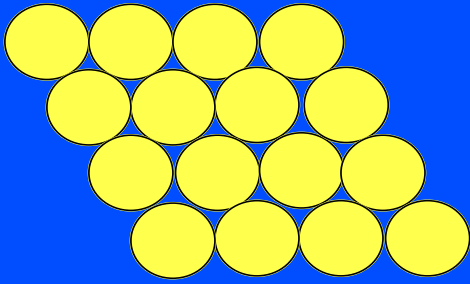


# Rh(111): evolution of the Rh $3d_{5/2}$ peak during exposure to $O_2$

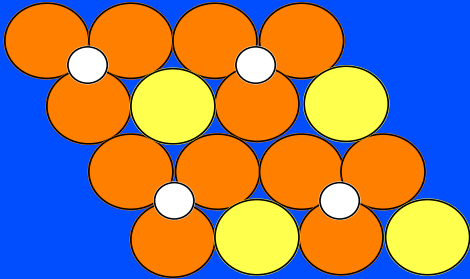
# Rh(111): evolution of the Rh 3d<sub>5/2</sub> peak during exposure to O<sub>2</sub>



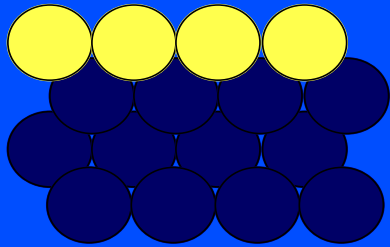
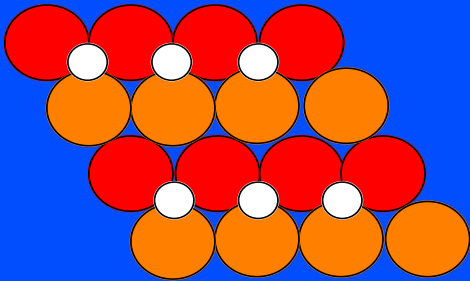
(1x1)



$p(2 \times 2)$



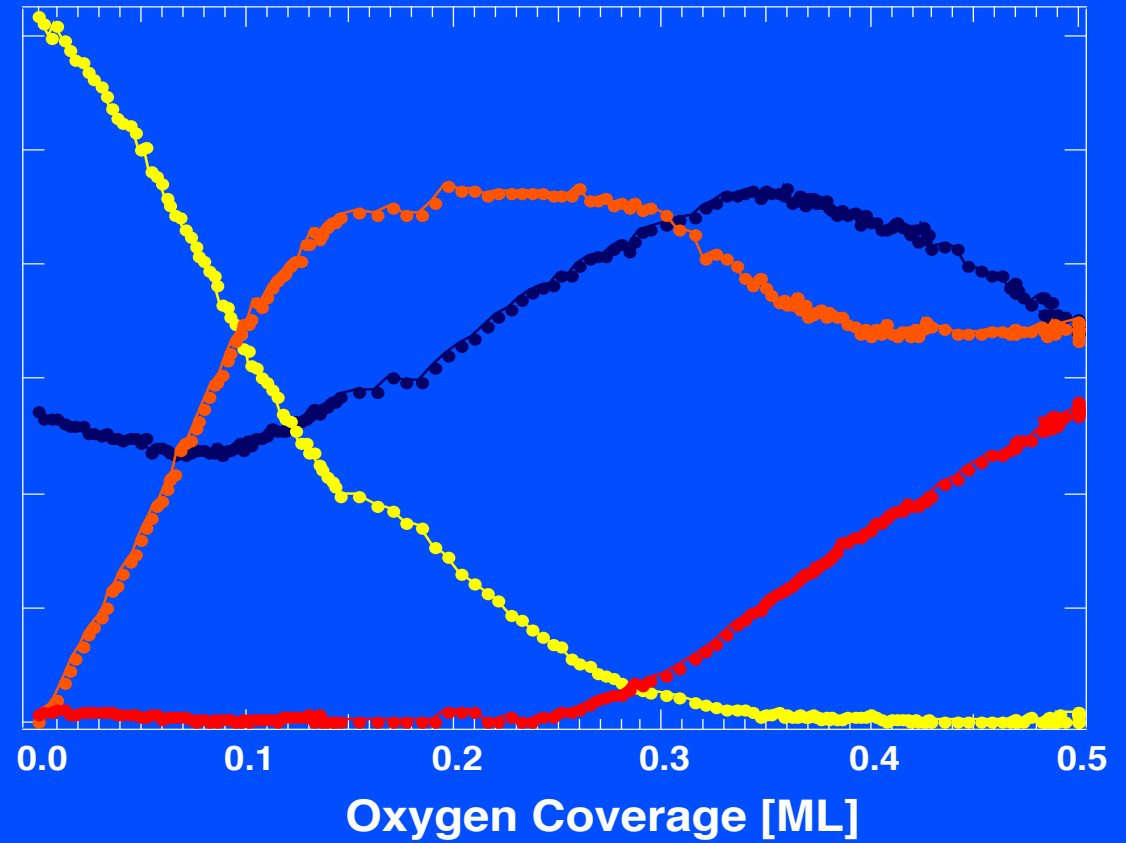
$p(2 \times 1)$



$p(2 \times 2)$   
 $\Theta = 0.25$  ML

$p(2 \times 1)$   
 $\Theta = 0.5$  ML

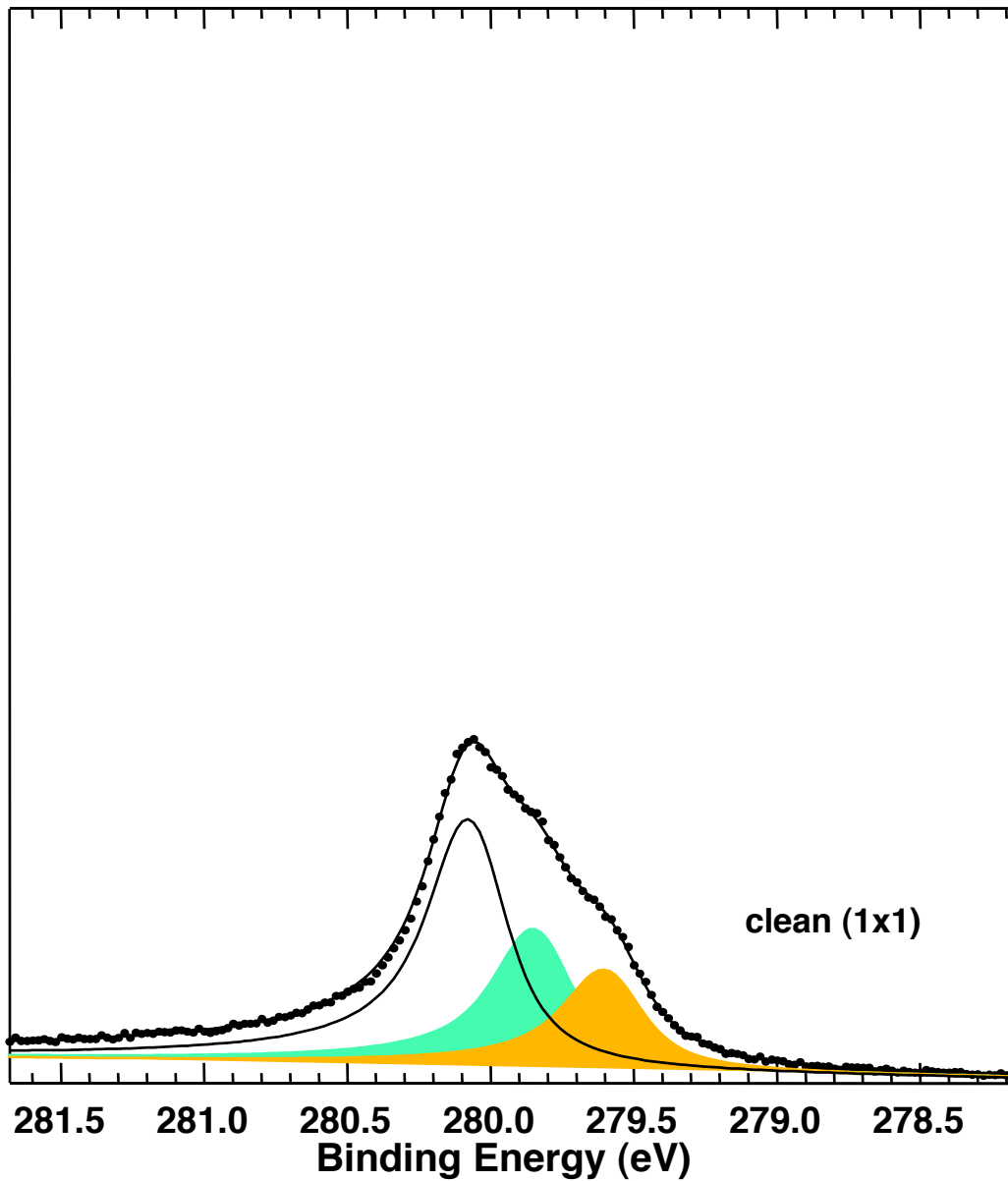
SCLS Intensity [arb. units]



# Identification of adsorbate bonding by the substrate SCLS

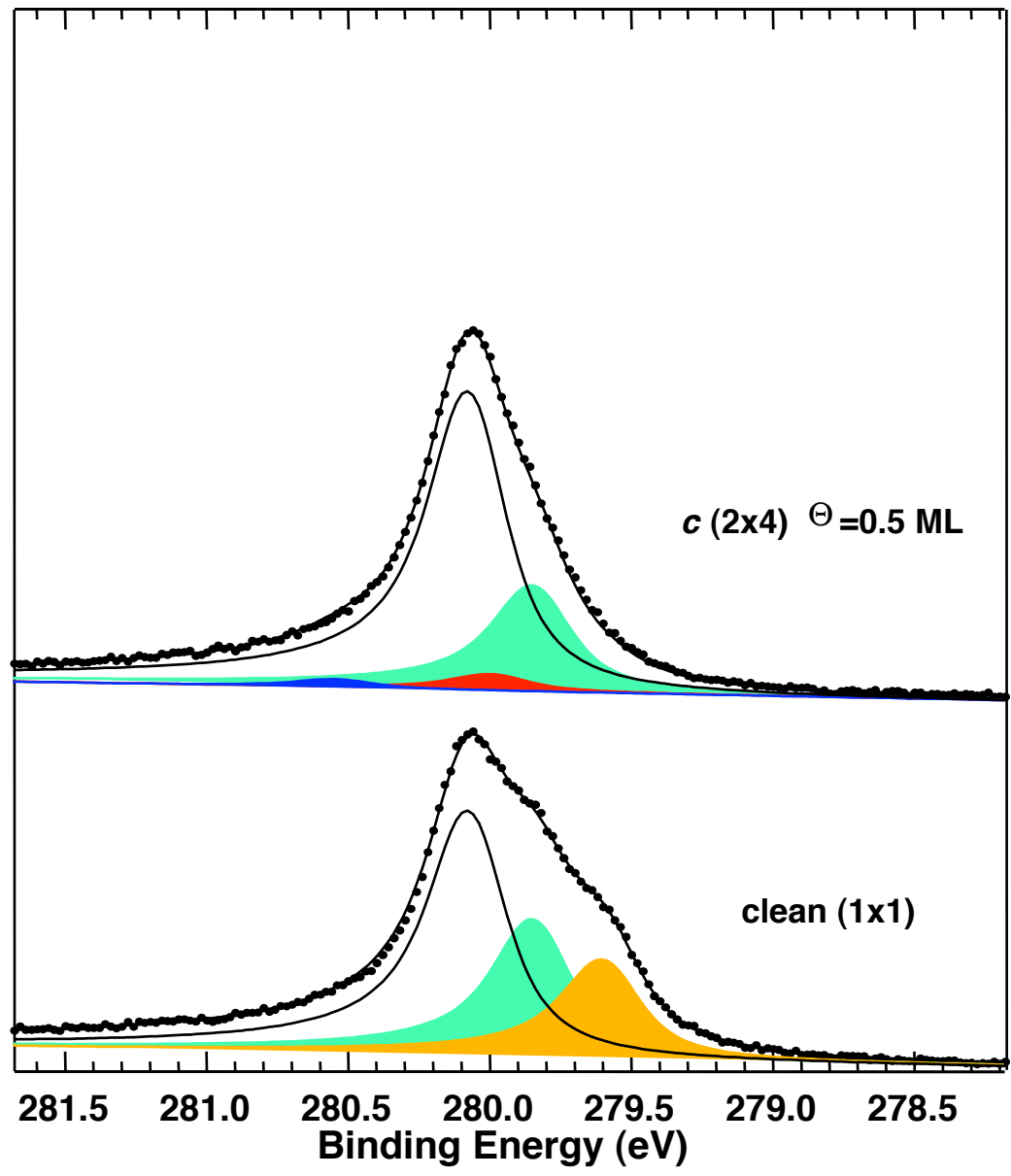
2) O on Ru(101 $\bar{0}$ )

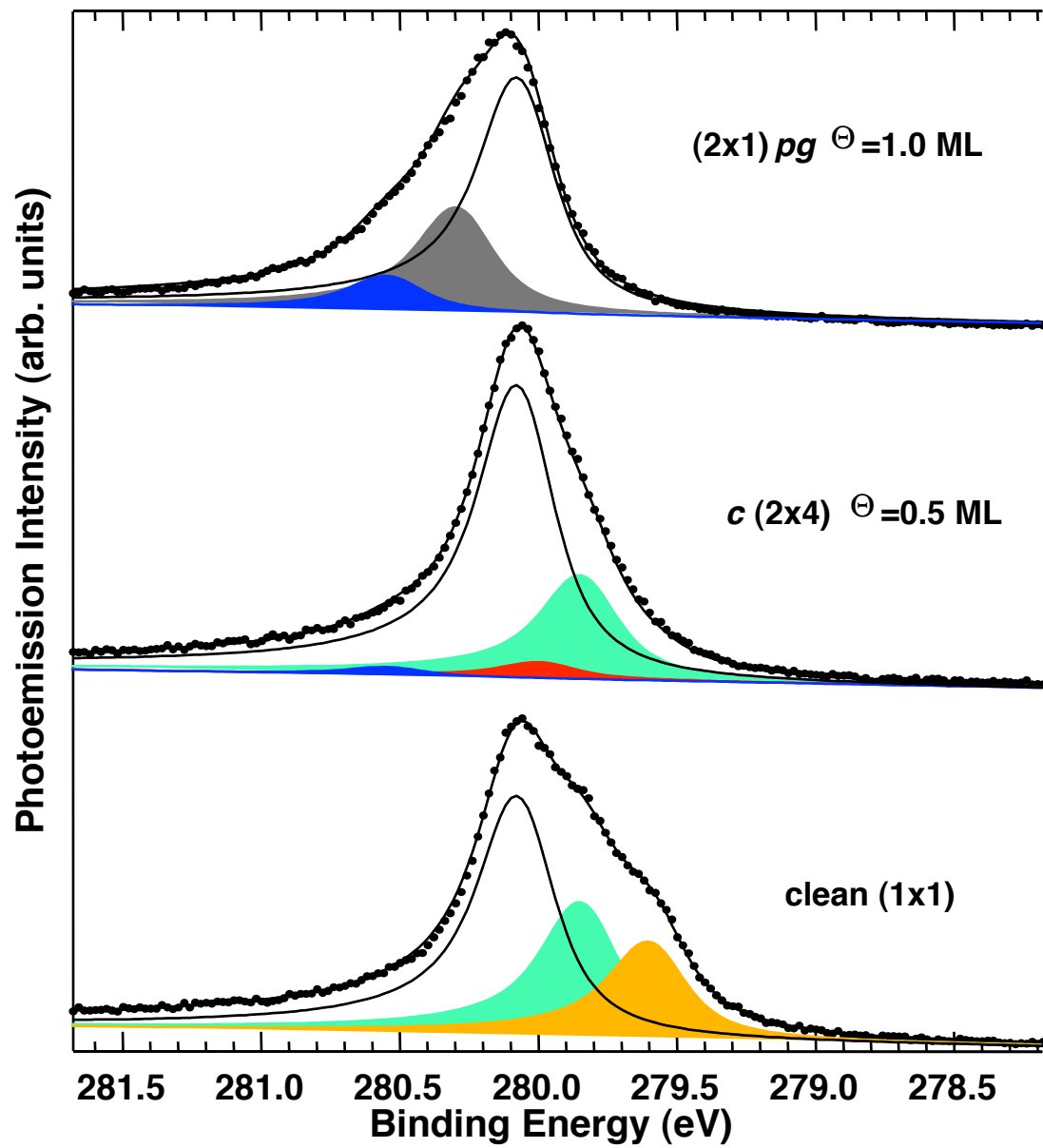
Photoemission Intensity (arb. units)



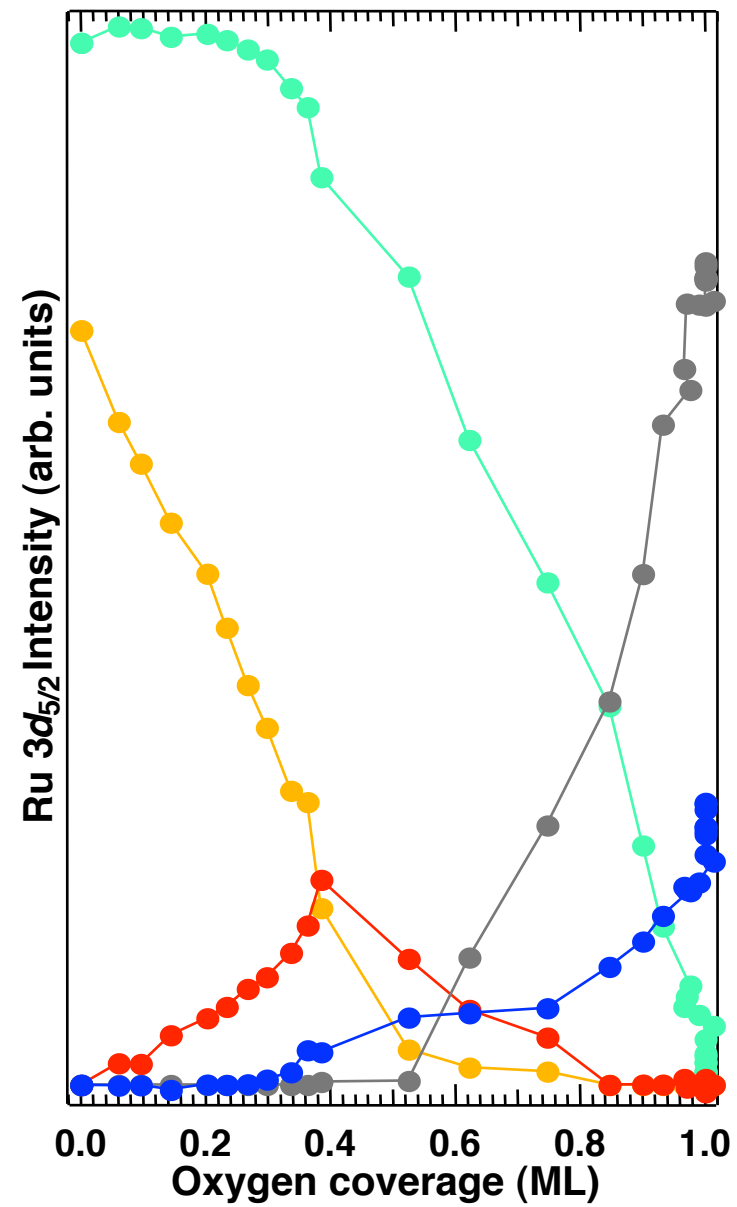
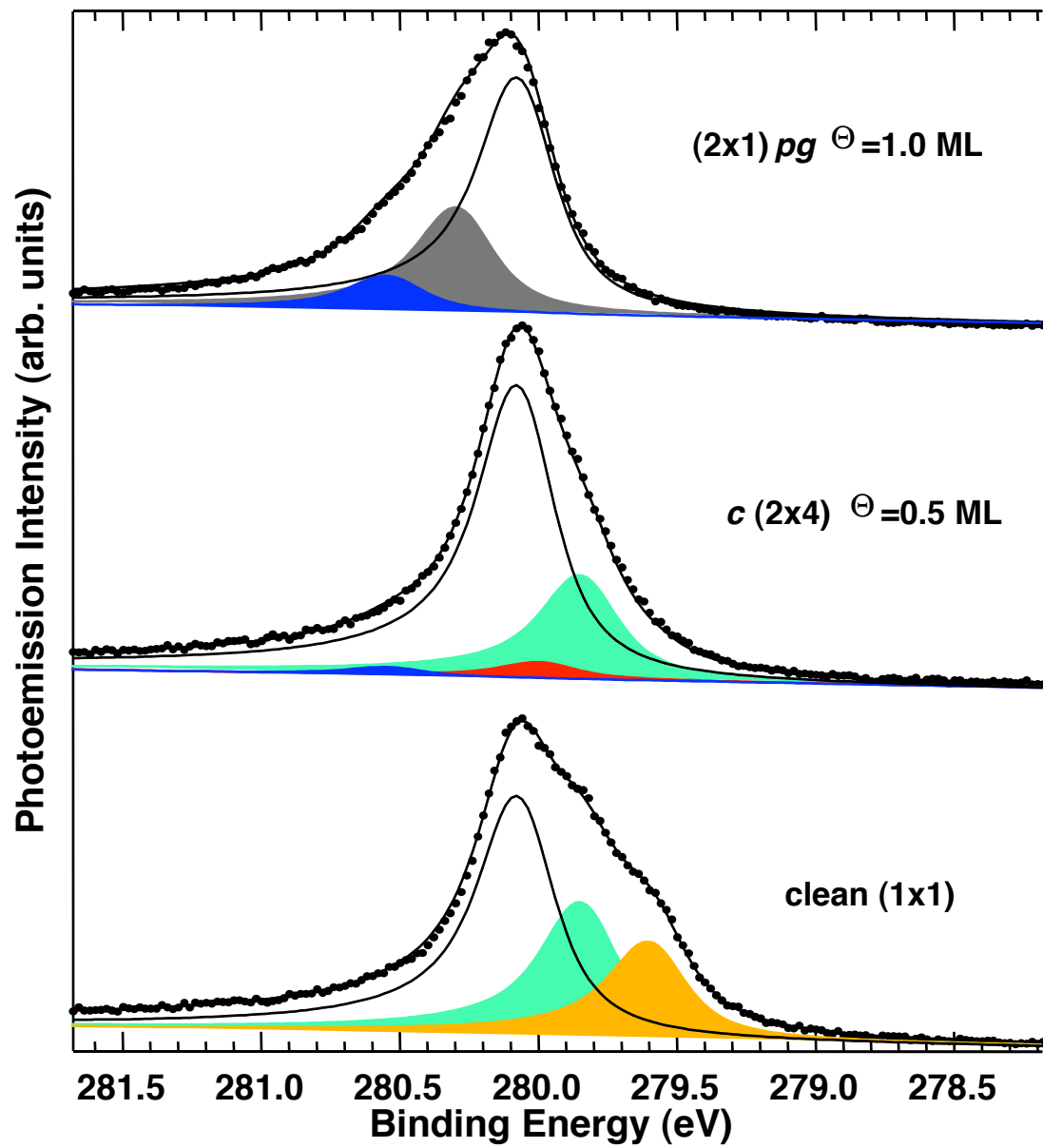
clean (1x1)

Photoemission Intensity (arb. units)

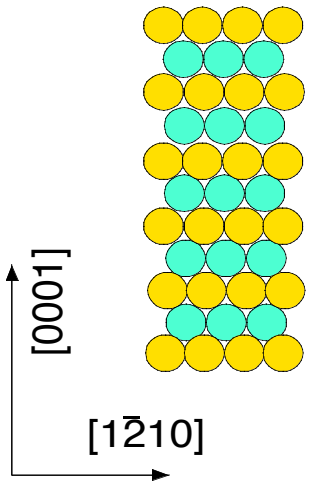






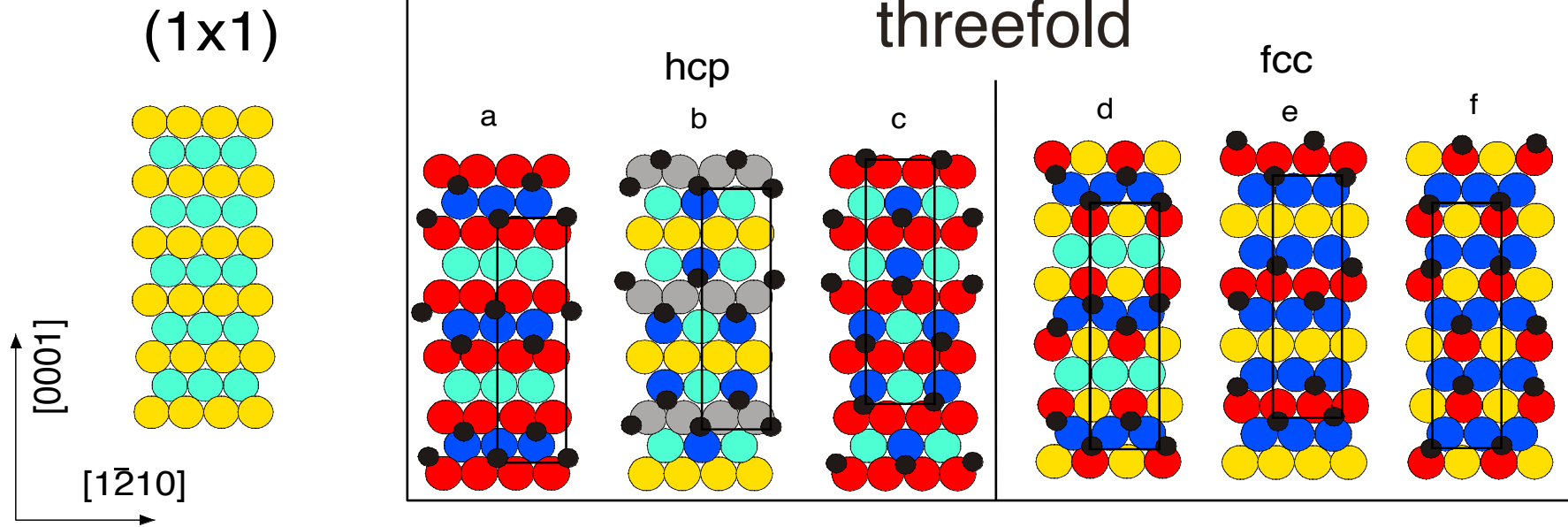


(1x1)





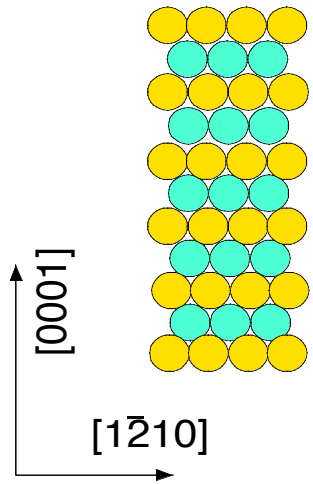
# Ru(10 $\bar{1}0$ )-c(2x4)-2O



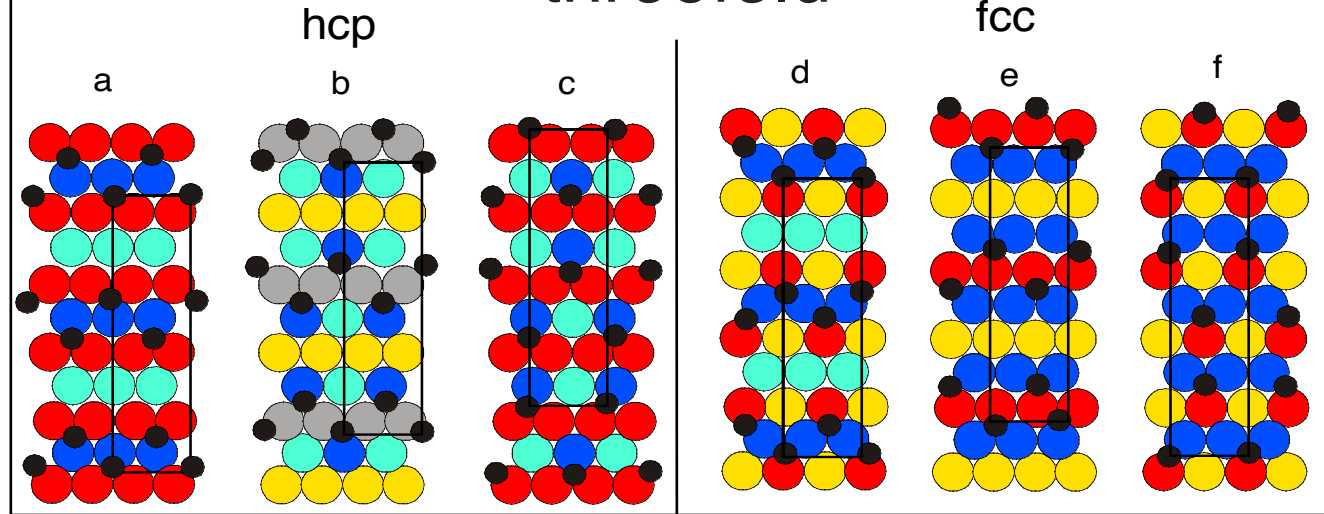
- oxygen
- Ru<sub>1</sub>
- Ru<sub>2</sub>
- Ru<sub>1</sub>-O
- Ru<sub>1</sub>-2O
- Ru<sub>2</sub>-O

# Ru(10 $\bar{1}0$ )-c(2x4)-2O

(1x1)

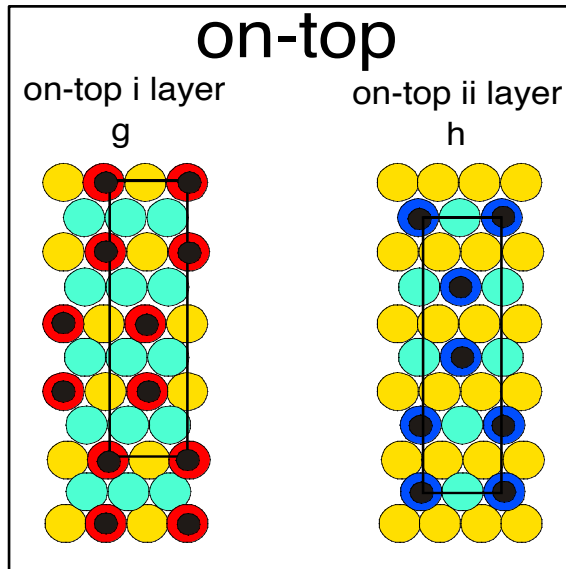


threefold



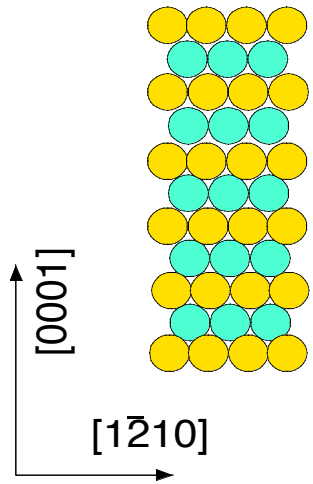
- oxygen
- Ru<sub>1</sub>
- Ru<sub>2</sub>
- Ru<sub>1</sub>-O
- Ru<sub>1</sub>-2O
- Ru<sub>2</sub>-O

on-top

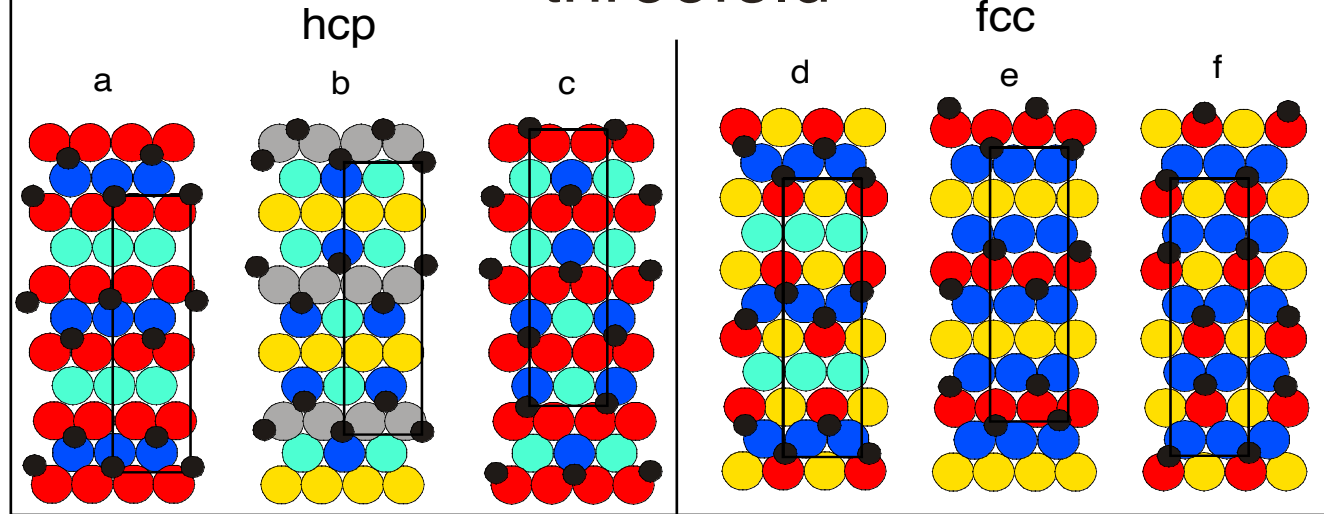


# Ru(10 $\bar{1}0$ )-c(2x4)-2O

(1x1)

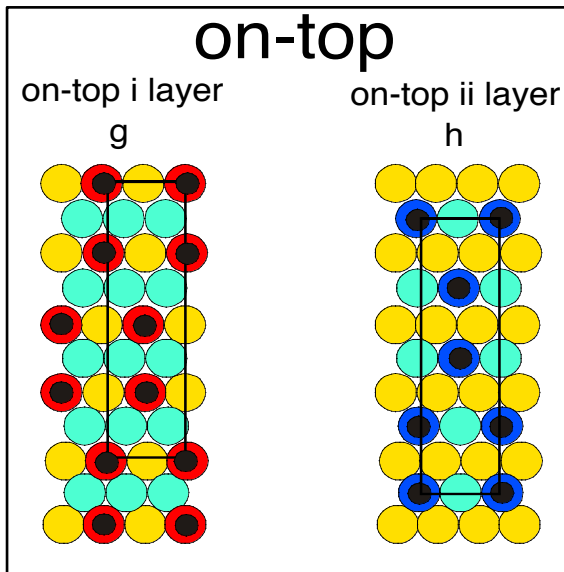


threefold

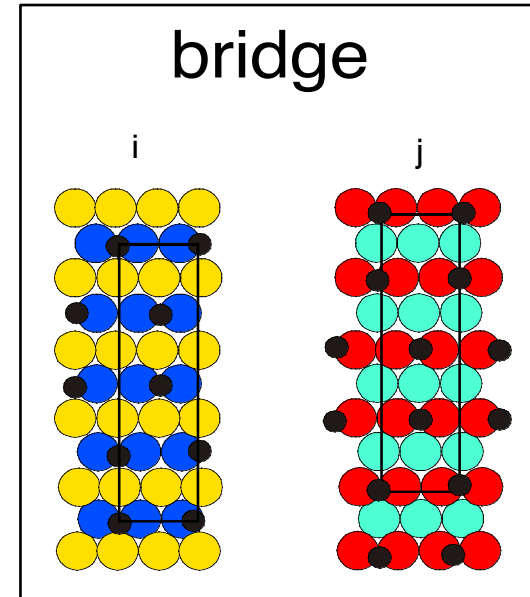


- oxygen
- Ru<sub>1</sub>
- Ru<sub>2</sub>
- Ru<sub>1</sub>-O
- Ru<sub>1</sub>-2O
- Ru<sub>2</sub>-O

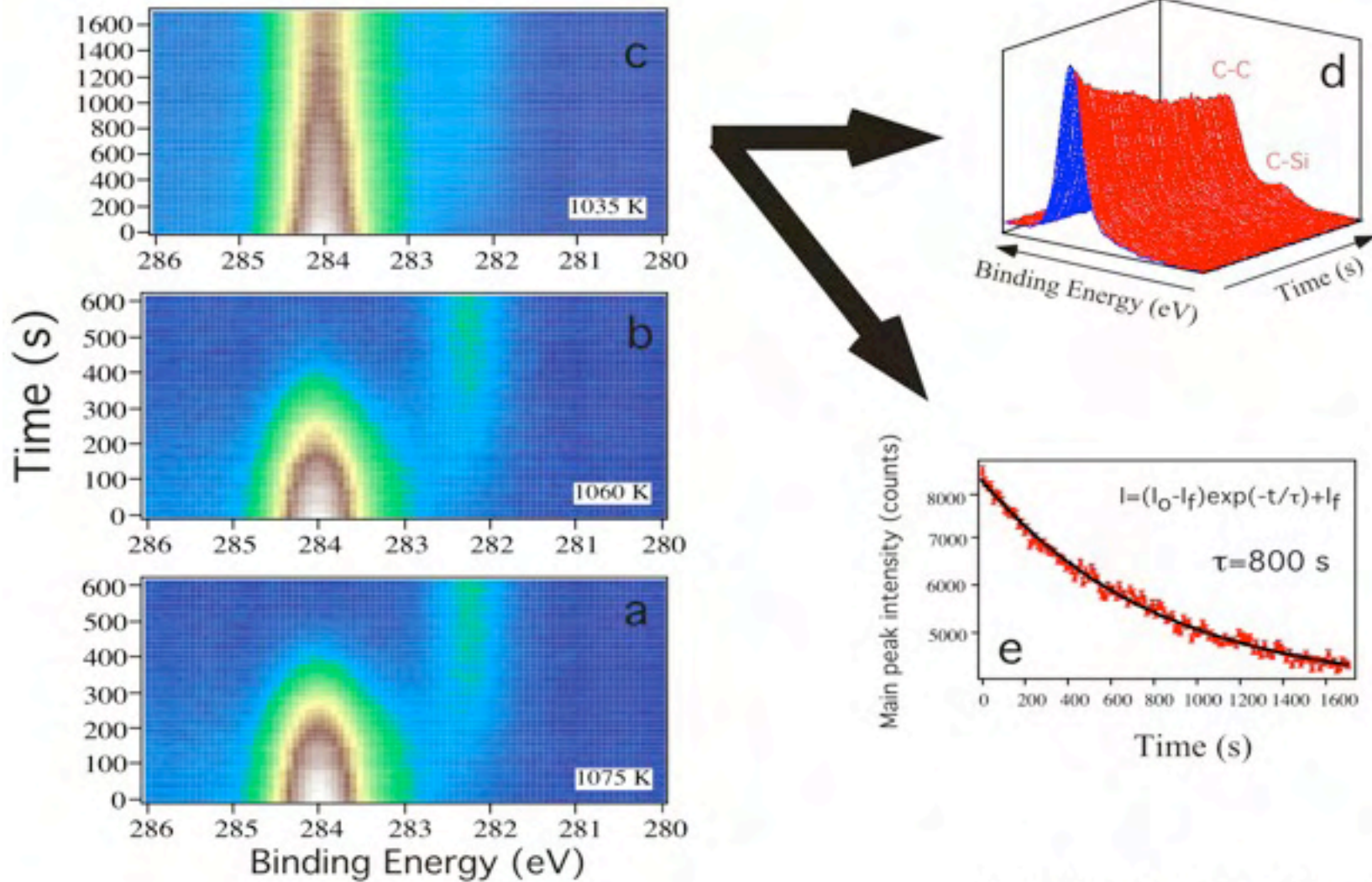
on-top



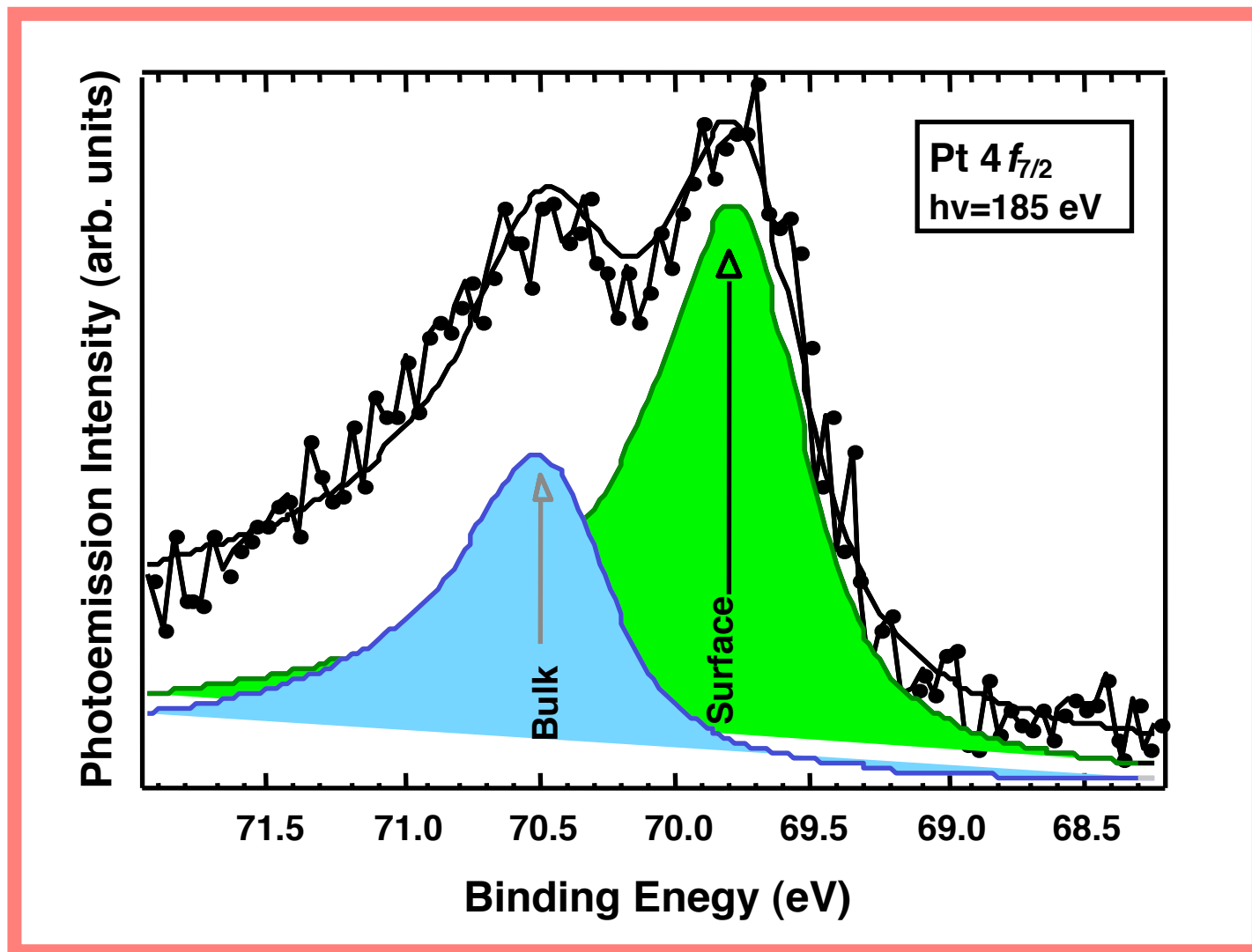
bridge



# SiC formation by decomposition of C<sub>60</sub>/Si

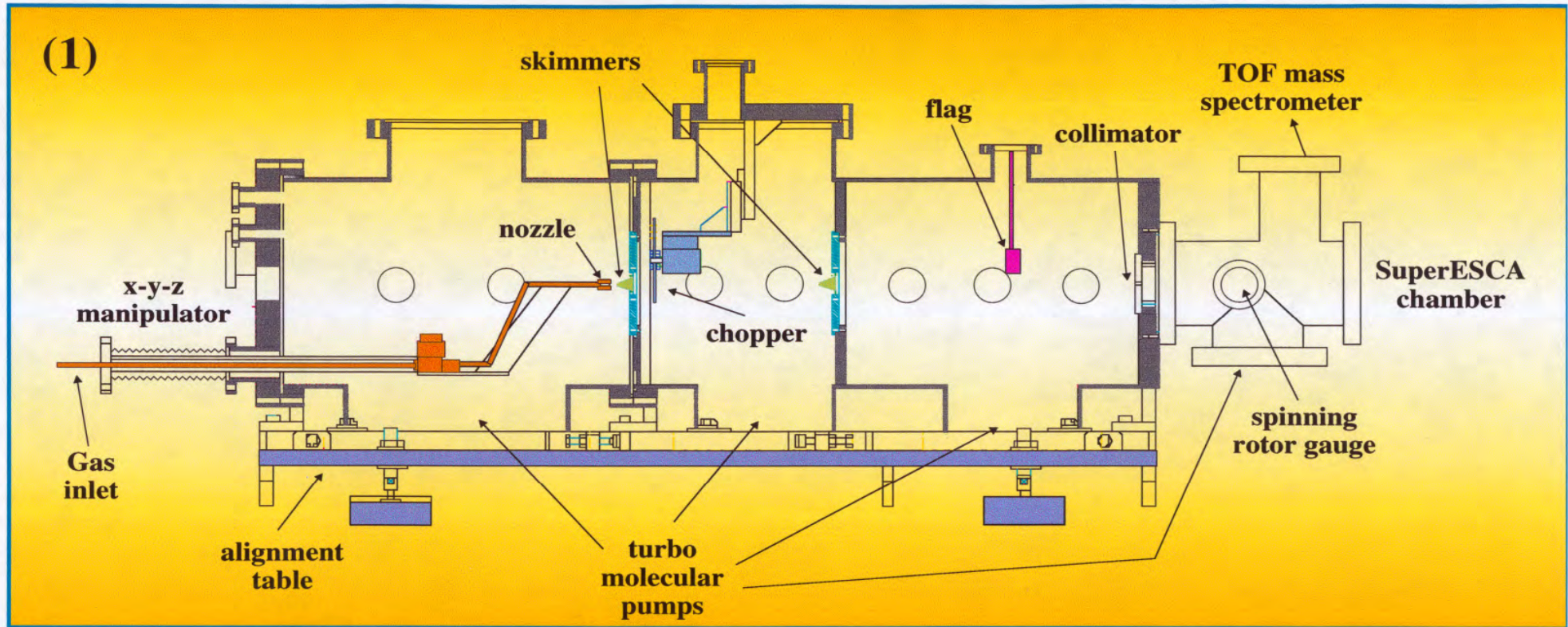


# Single shot spectrum ( $\sim 100$ ms):





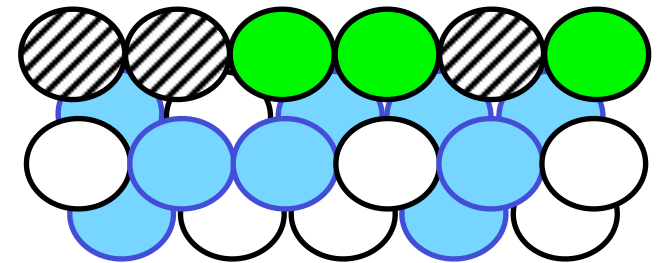
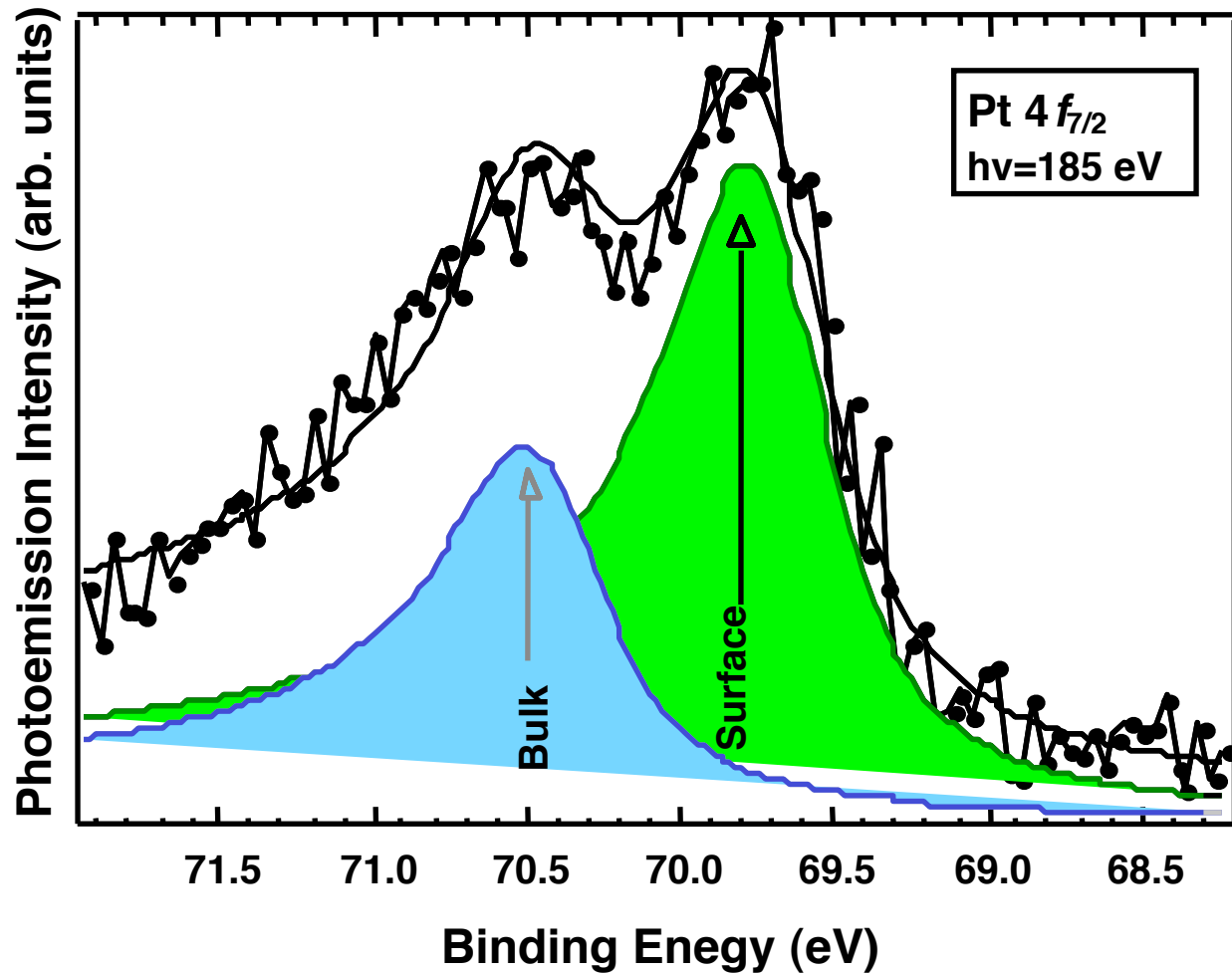
# The supersonic molecular beam

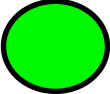


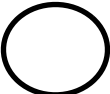


# Application of the supersonic molecular beam

Reaction between  $O_2$  and  $H_2$  on  $Pt_{50}Rh_{50}(100)$  via  
Surface core level shift

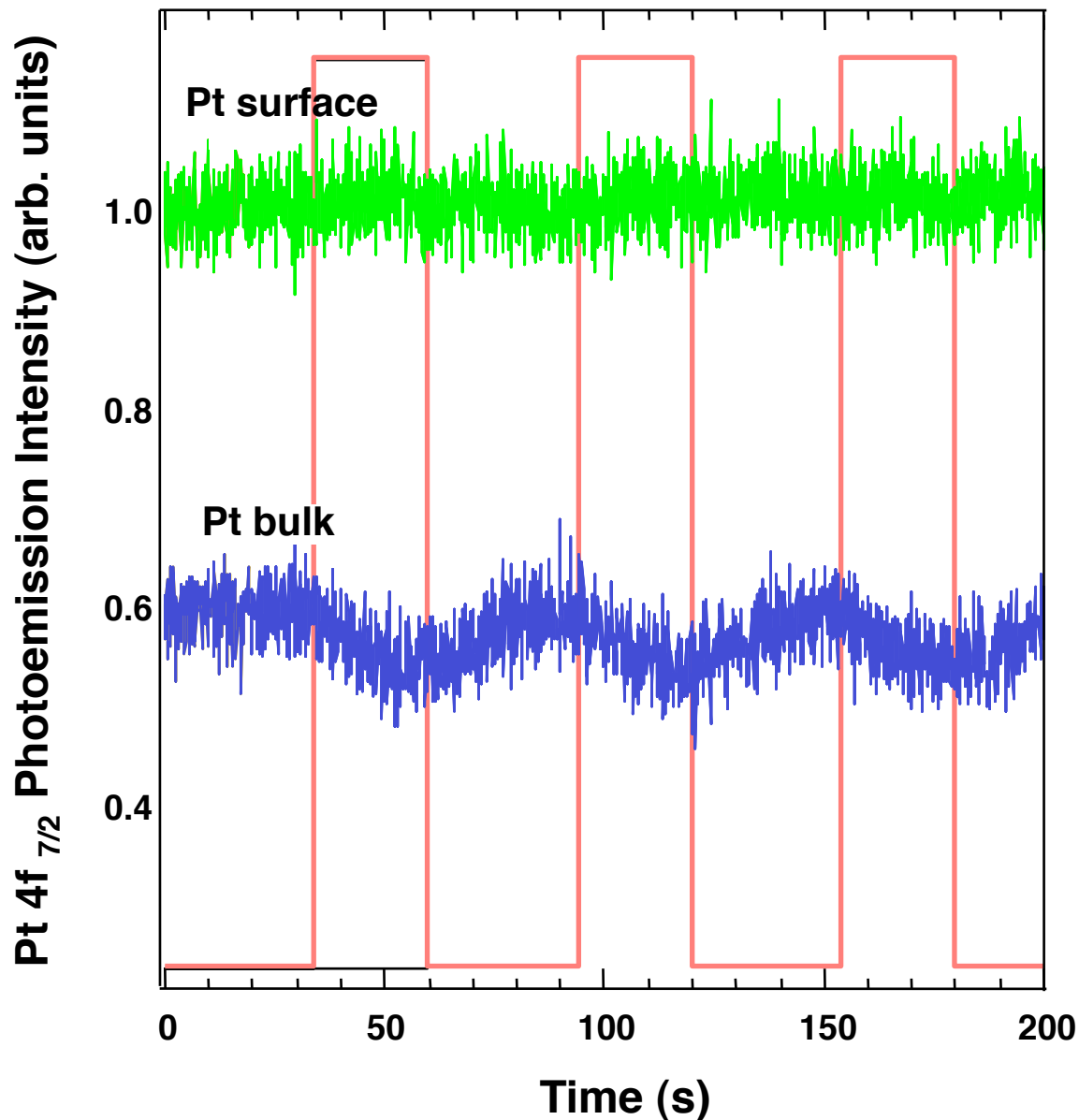
# The supersonic molecular beam



-  Pt surface
-  Pt bulk
-  Rh surface
-  Rh bulk

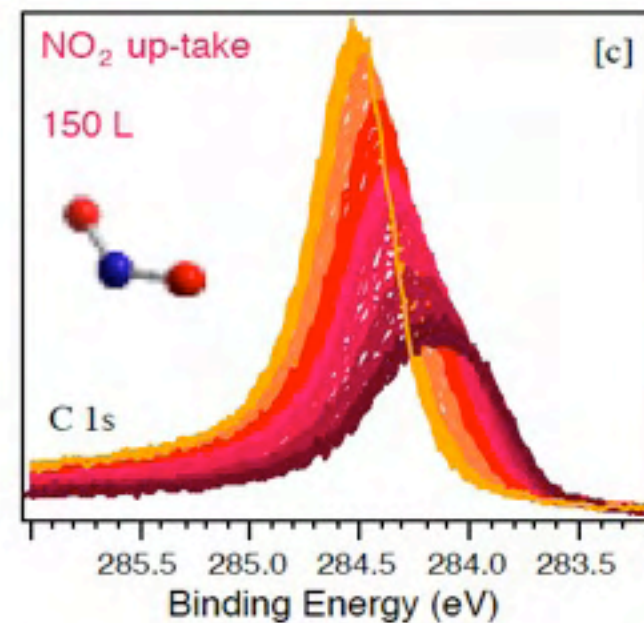
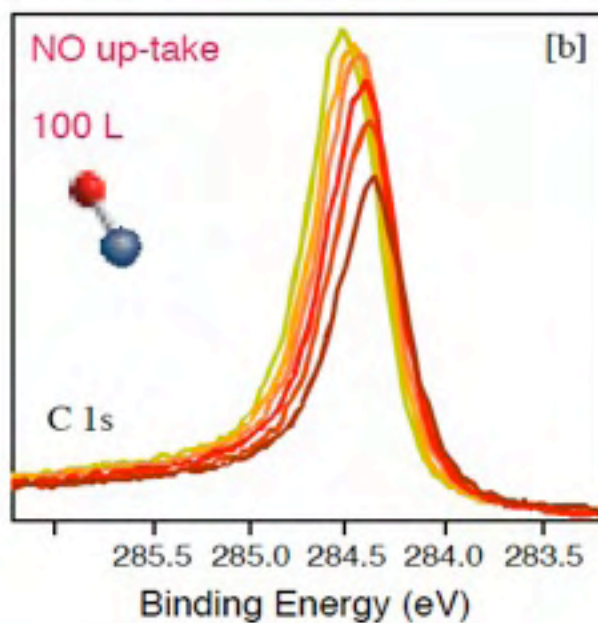
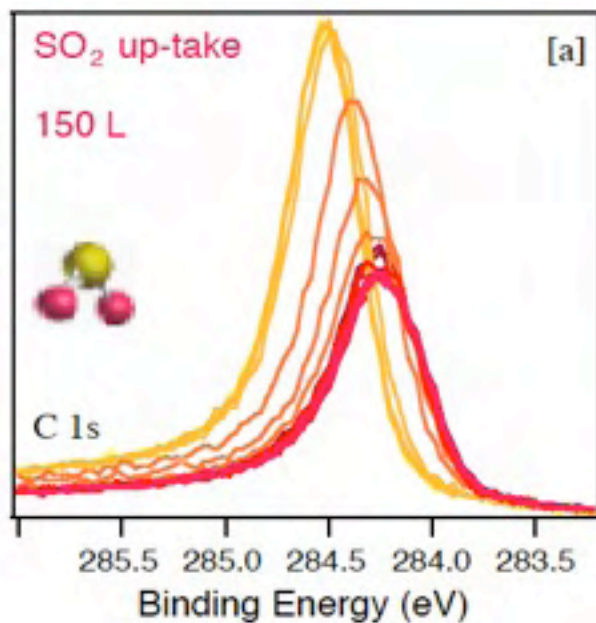
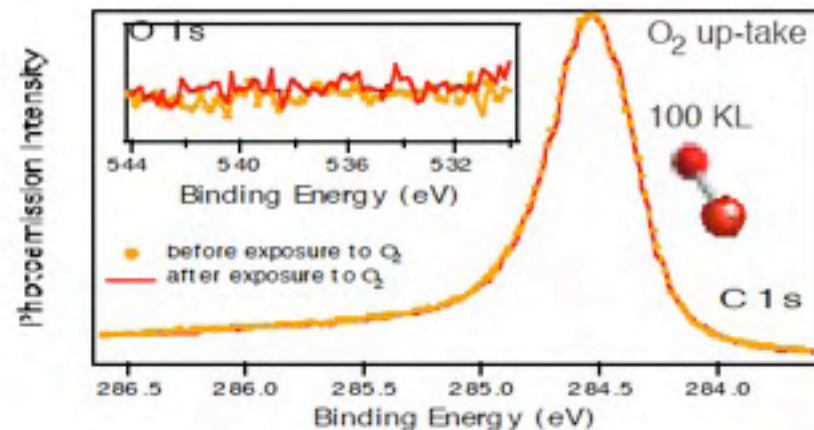
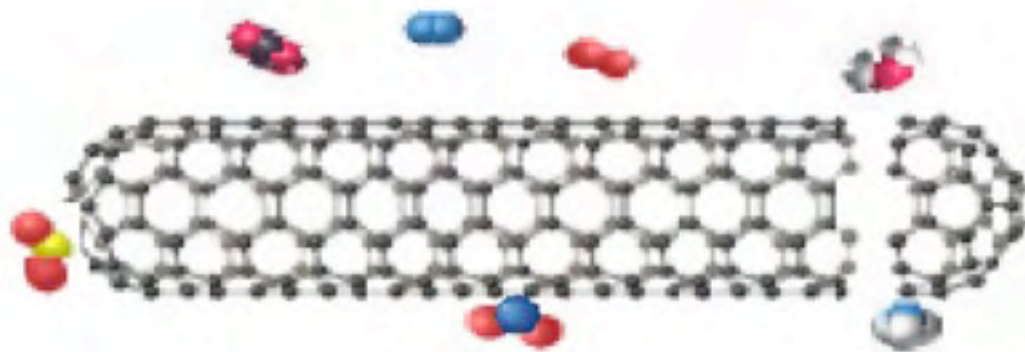
# The supersonic molecular beam

Oxygen sticks to Rh only and subsurface Pt is “attracted” from O on the surface





# Reactivity of carbon nanotubes



# Reactivity of carbon nanotubes

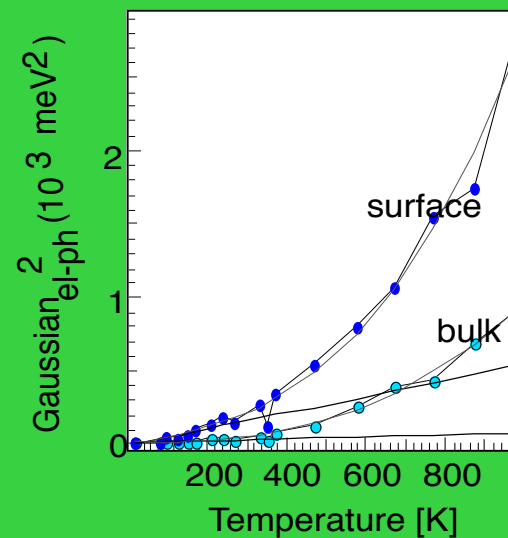
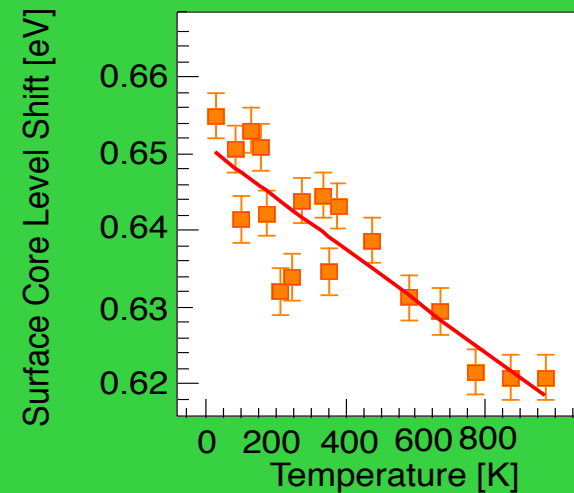
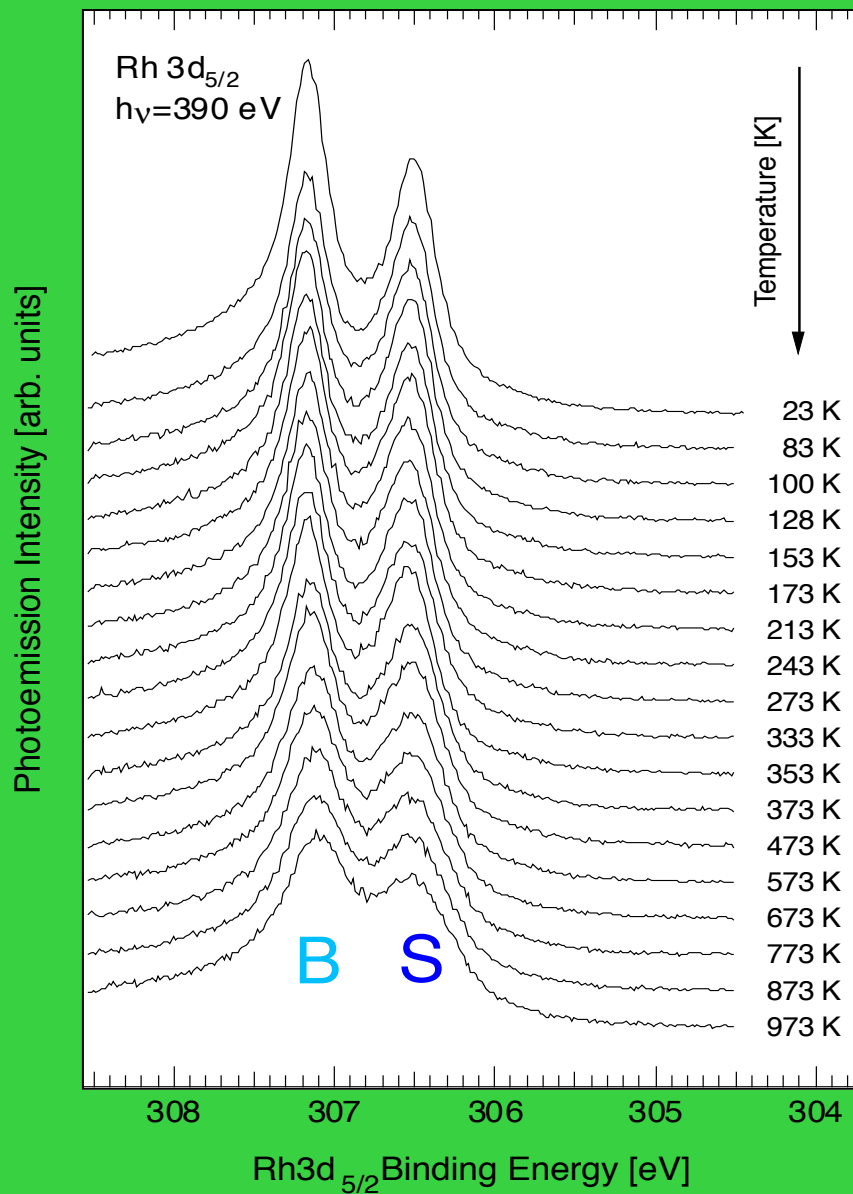
When contaminants are removed from SWCNTs they show little (or no) interaction of SWCNTs with  $O_2$ ,  $H_2O$  and  $N_2$  (contrary to what reported by P.G. Collins et al., Science **287**, 1801 (2000))

Strong reactivity of purified SWCNTs towards  $NO_x$  and  $SO_x$

# Temperature dependence of core levels

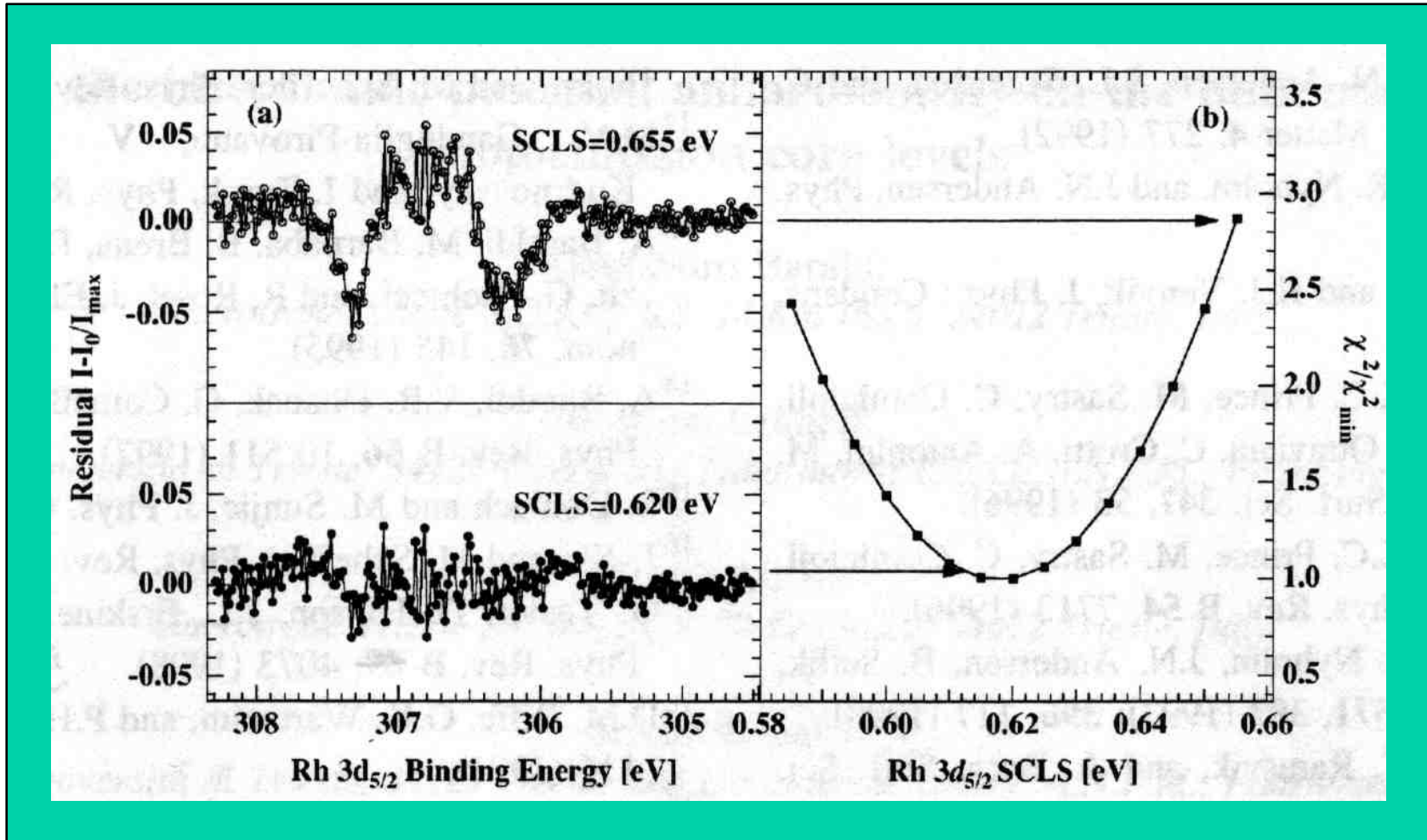
- Temperature dependent surface core level shift
  - surface thermal expansion
- T-dependent width of C 1s in C<sub>60</sub>
  - a measure of surface specific heat

# Temperature dependence of Rh(100) surface core level shift





# A real effect?



comparison of the residuals obtained by forcing the SCLS to its low-T value with a T-dependent SCLS

# Surface thermal expansion

- Calculations (Xie and Scheffler) show that  $\Delta d_{12}/d_0$  goes from -2.5% (at 0 K) to 0% (at 770 K)
- The calculated SCLS is 0.62 eV for  $\Delta d_{12}/d_0 \sim 0$  (Andersen *et al.*) in very good agreement with our measurements and *increasing* with *decreasing*  $\Delta d_{12}$

**Our measurements support an inward relaxation in agreement with theory but not with LEED which gives  $\Delta d_{12}/d_0 \sim +1\%$  at 300 K (Teeter *et al.*)**

# Surface calorimetry

If

a core level lifetime broadening is small

and

there is a gap in the vibrational excitation spectrum

then

surface calorimetry by XPS is possible **molecular solids such as C<sub>60</sub> are good candidates**

Molecular solids such as C60 are good candidates as core level lifetime broadening is small

and

there is a gap in the vibrational excitation spectrum

then

surface calorimetry by XPS is possible

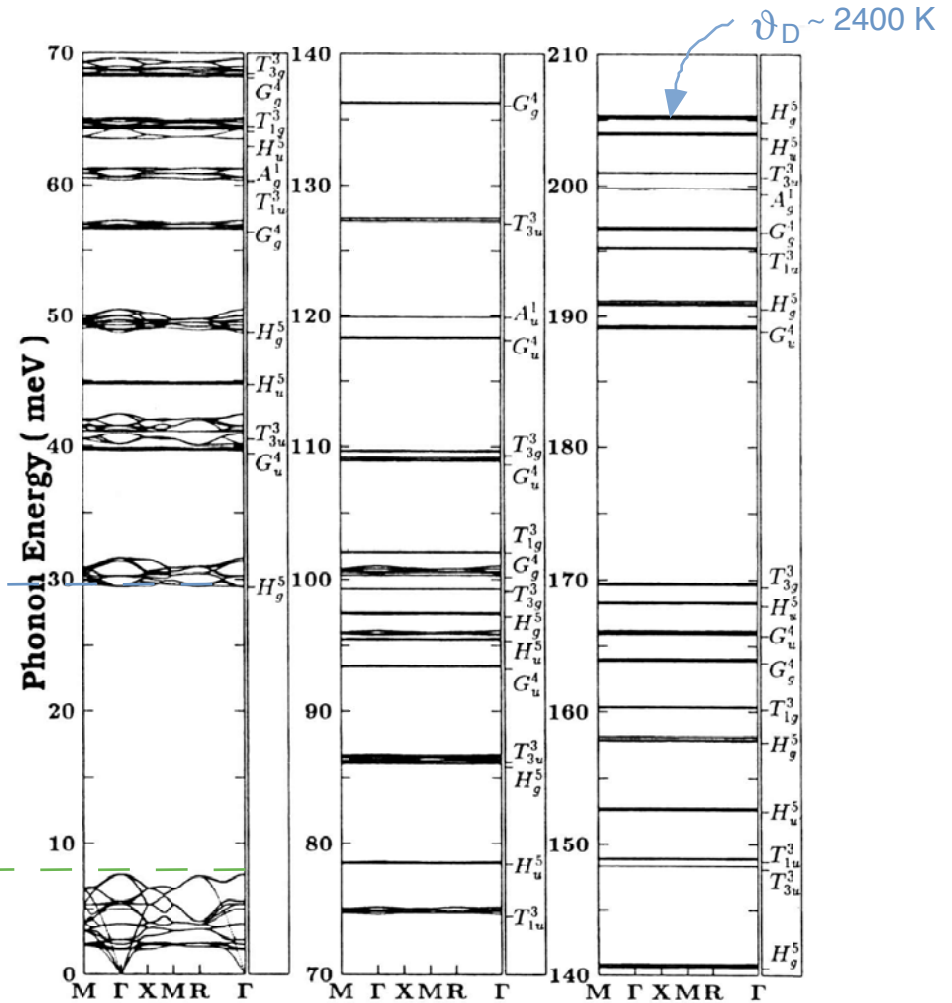
# The bulk phonon modes of solid C<sub>60</sub>

Two well separated energy regions:

- The contribution from the **low energy modes** to  $C_p$  is almost saturated above 40 K
- The **high energy modes** start to appreciably contribute to  $C_p$  above 100 K

On-ball Modes

Interball Modes  
 $\vartheta_D \sim 70$  K



# Photoemission experiments performed at:



SuperESCA beamline

$$h\nu = 380 \text{ eV}$$

$$\Delta E = 60 \text{ meV}$$

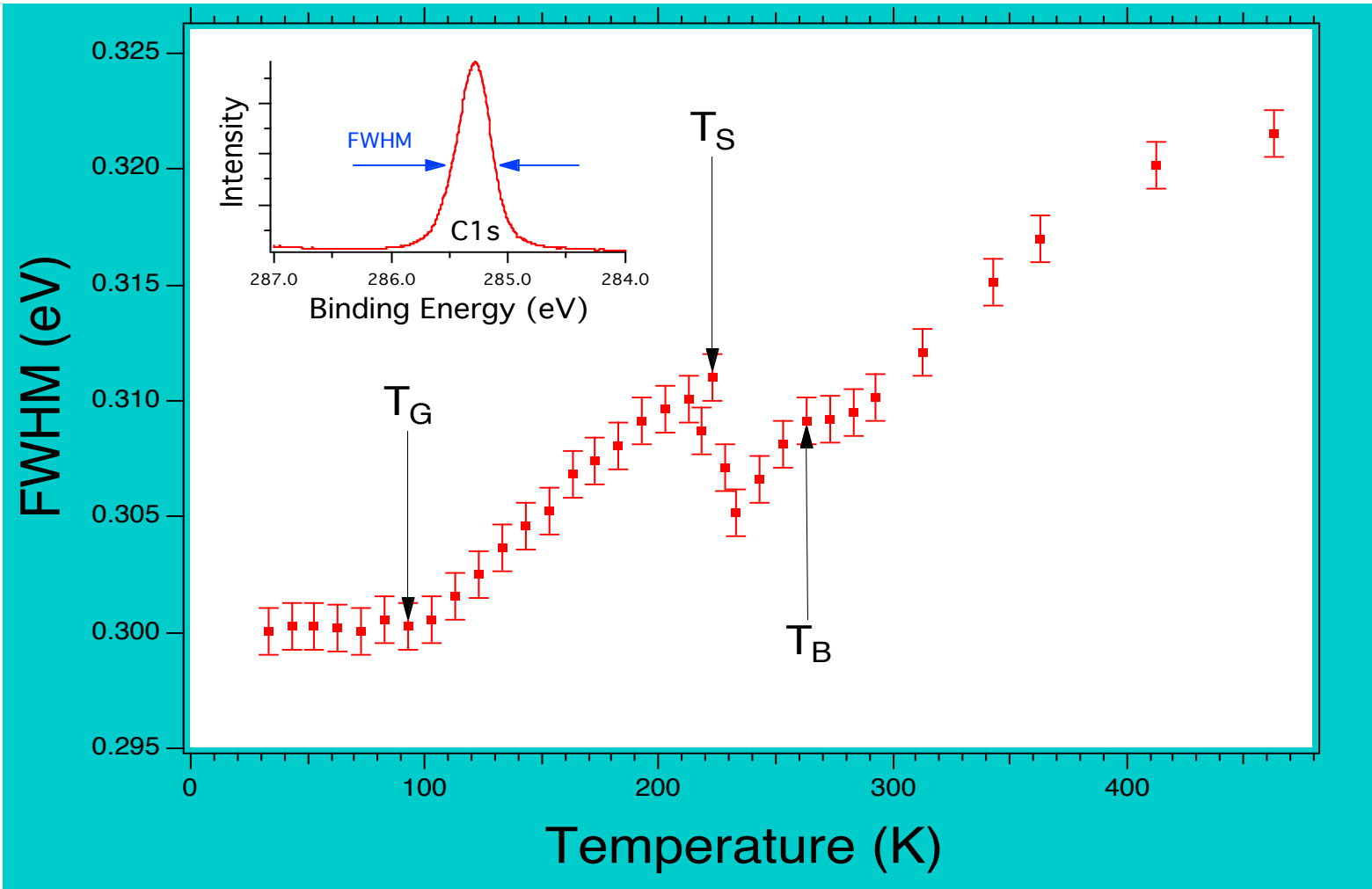
(overall)

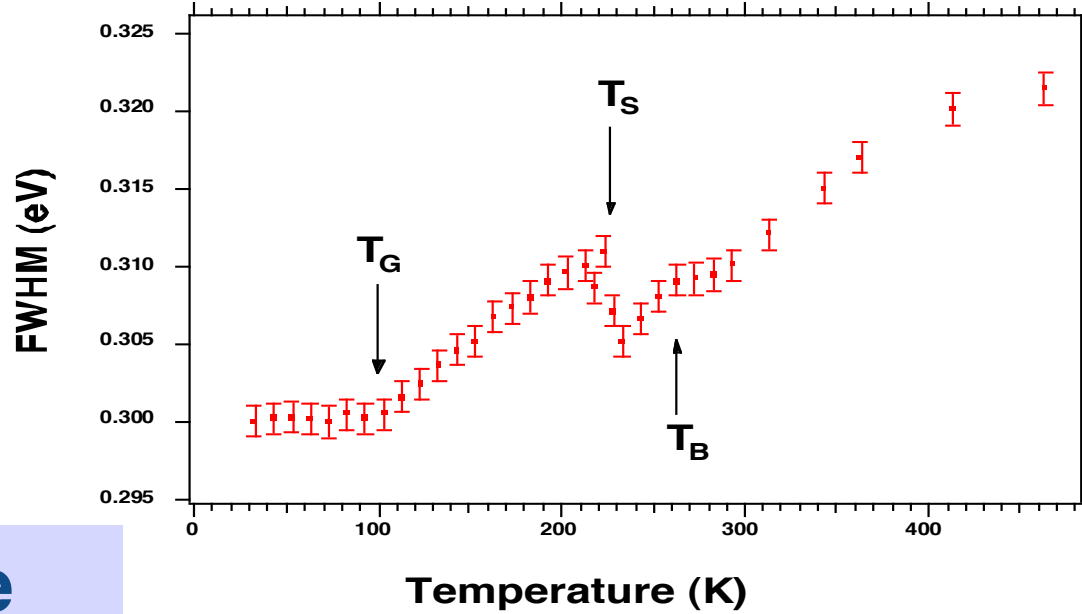
Double-pass hemispherical analyzer  
96-channels detector  
~ 20 seconds per spectrum  
high signal-to-noise ratio  
fine temperature control ( $\pm 0.1 \text{ K}$ )

Sample:

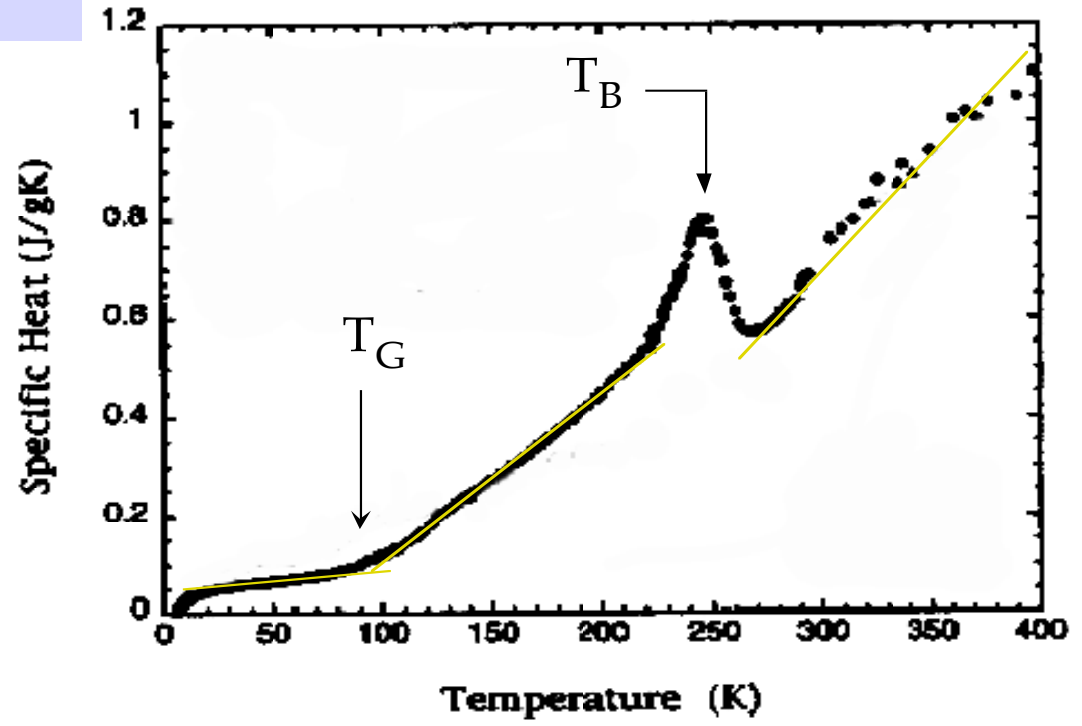
$C_{60}(111)$  thick film (20 ML) grown in situ on Ag(100)

# Temperature dependence of C1s level width





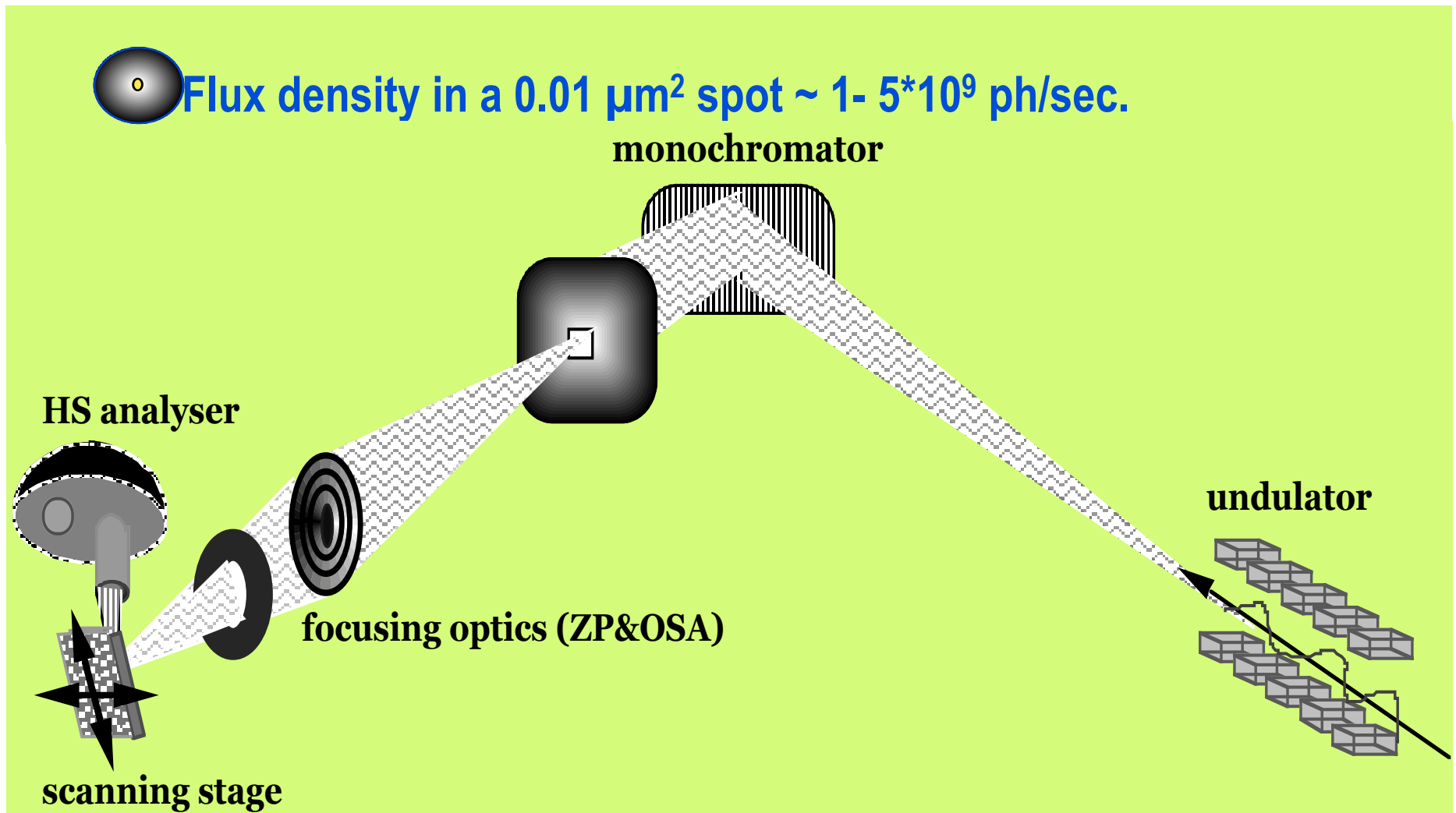
Close correspondence with Specific Heat





# Photoemission microscopy: spatial+chemical information

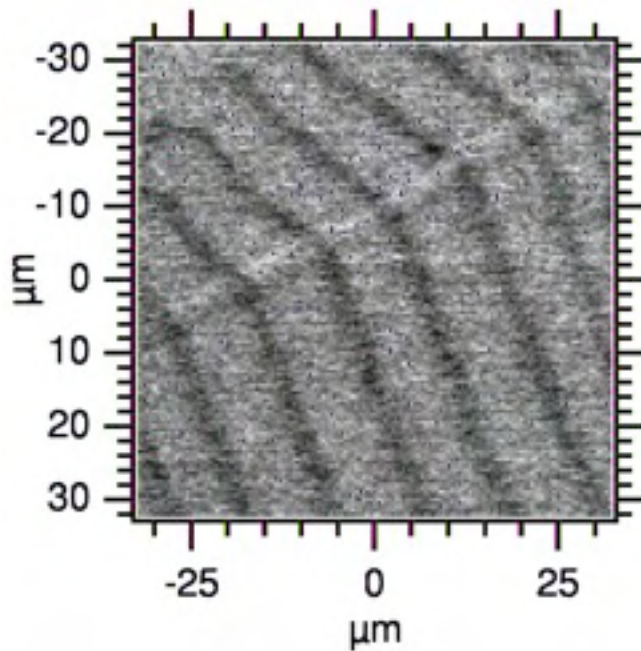
# ESCAmicroscopy Beamline and Scanning Photoelectron microscope layout



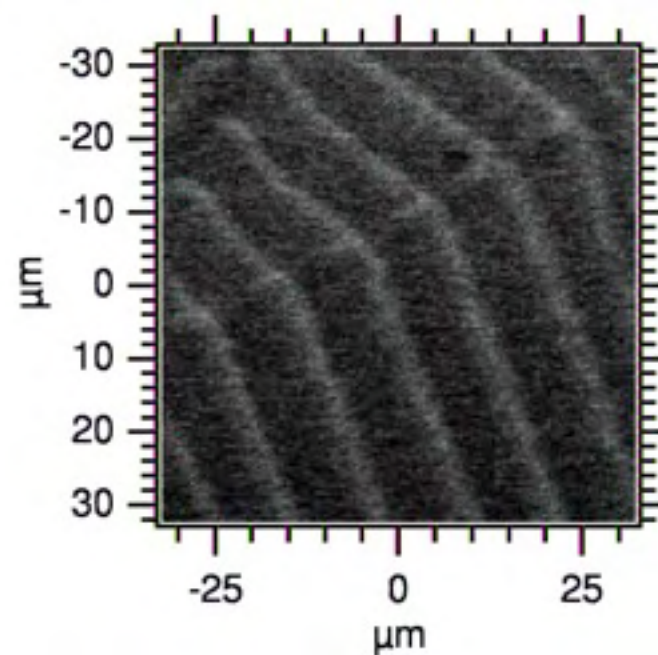
Elemental maps recorded with SPEM showing propagating pulse trains in the system Rh(110)/NO + H<sub>2</sub>.

Experimental conditions: T= 530 K, p<sub>NO</sub>=1.7x10<sup>-7</sup> mbar, p<sub>H<sub>2</sub></sub>=6.4x10<sup>-7</sup> mbar, photon energy 625.7 eV

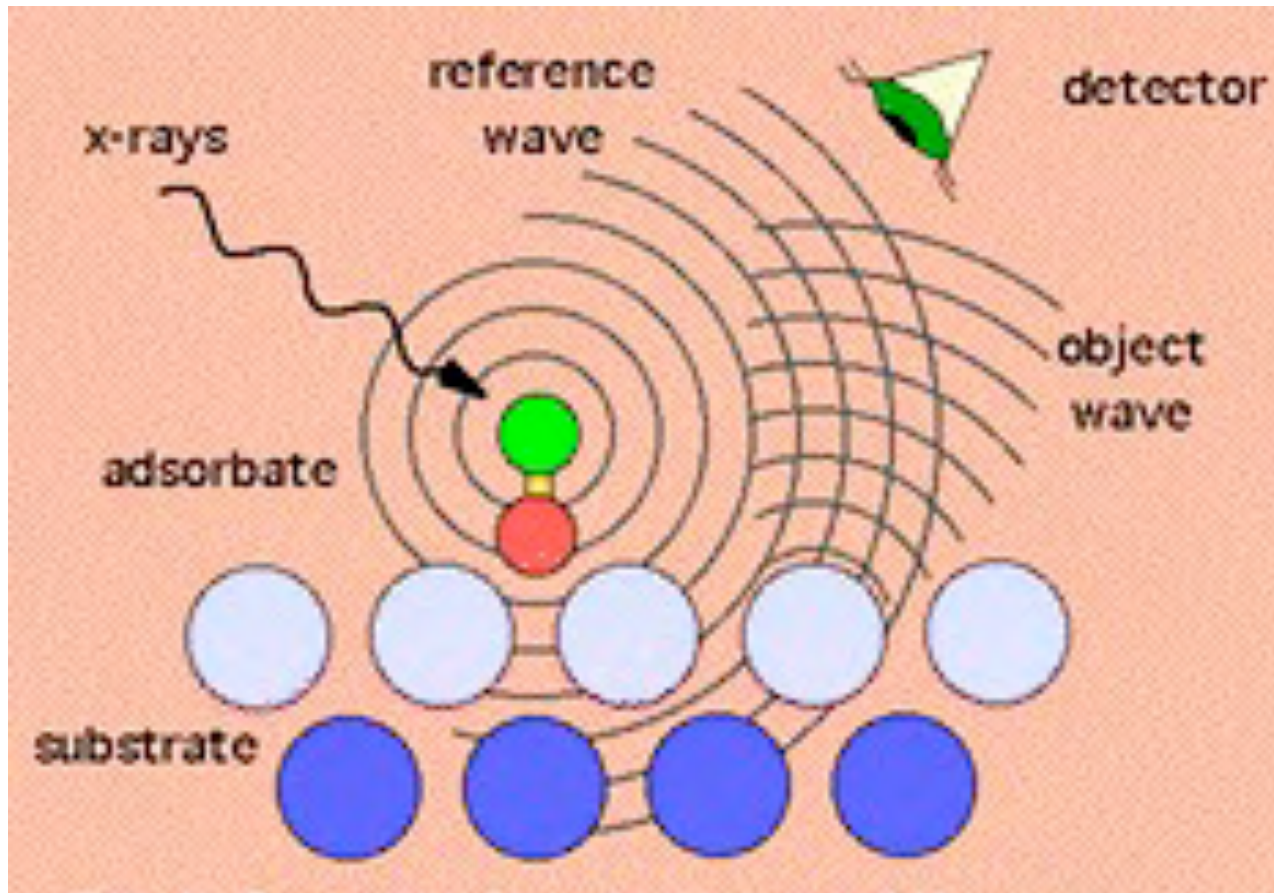
O 1s image



Rh 3d<sub>5/2</sub> image

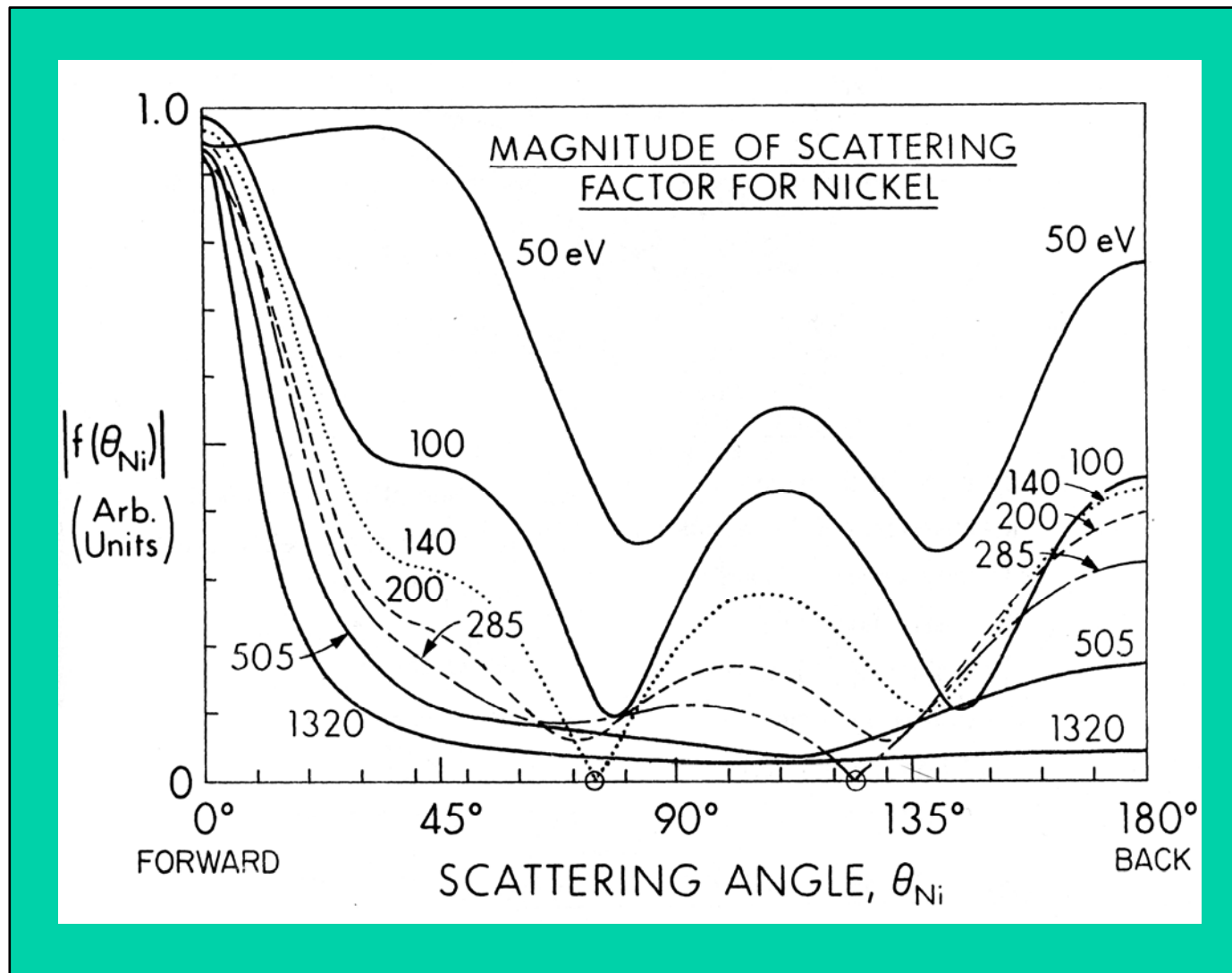


# The principle of photoelectron diffraction

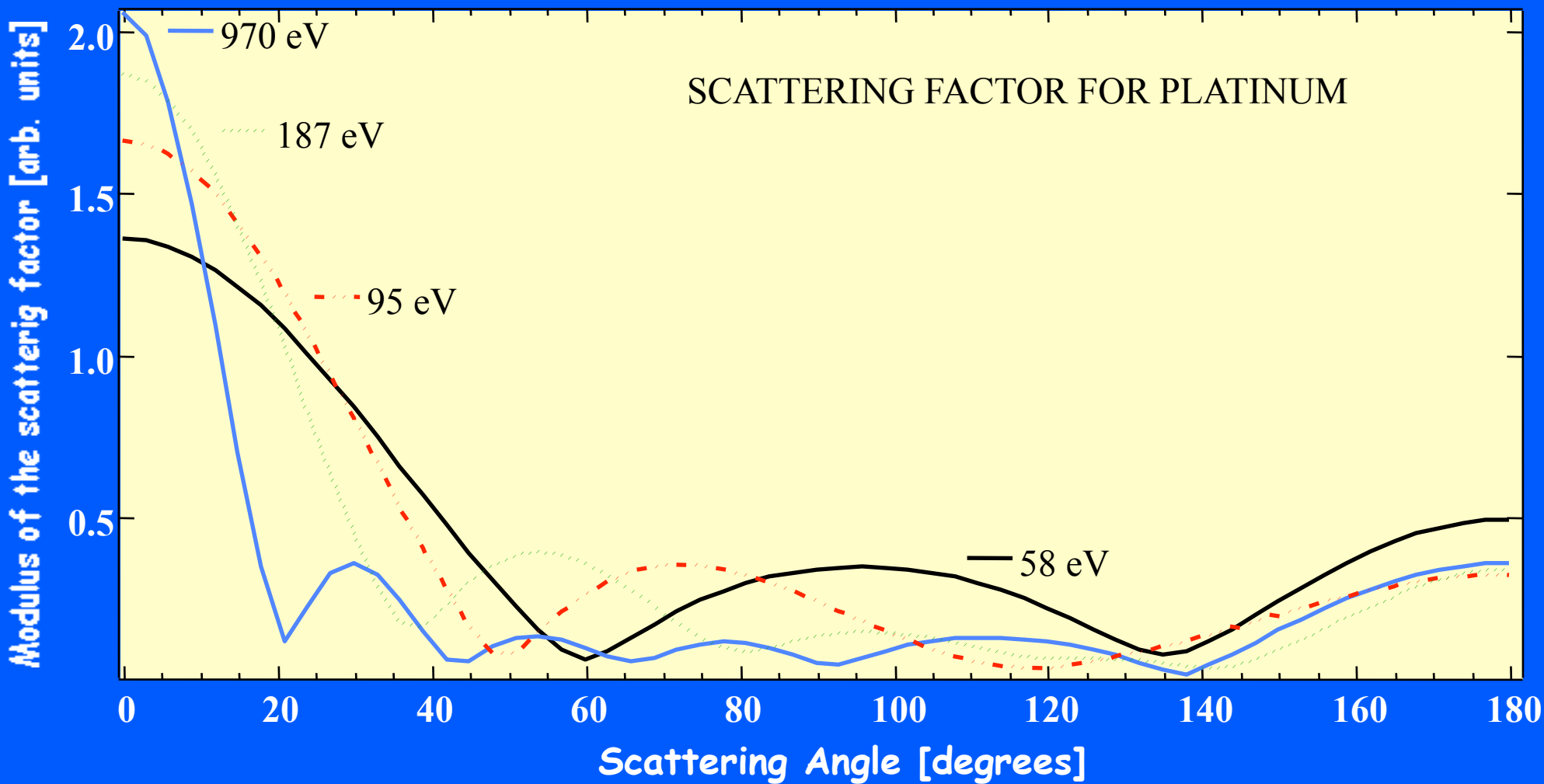


Modulations in the intensity of the photoemitted electron wave are measured. For a given arrangement of atoms, the intensity depends on the photon energy and on the emission angle

# Forward scattering is the dominant mechanism at high kinetic energy



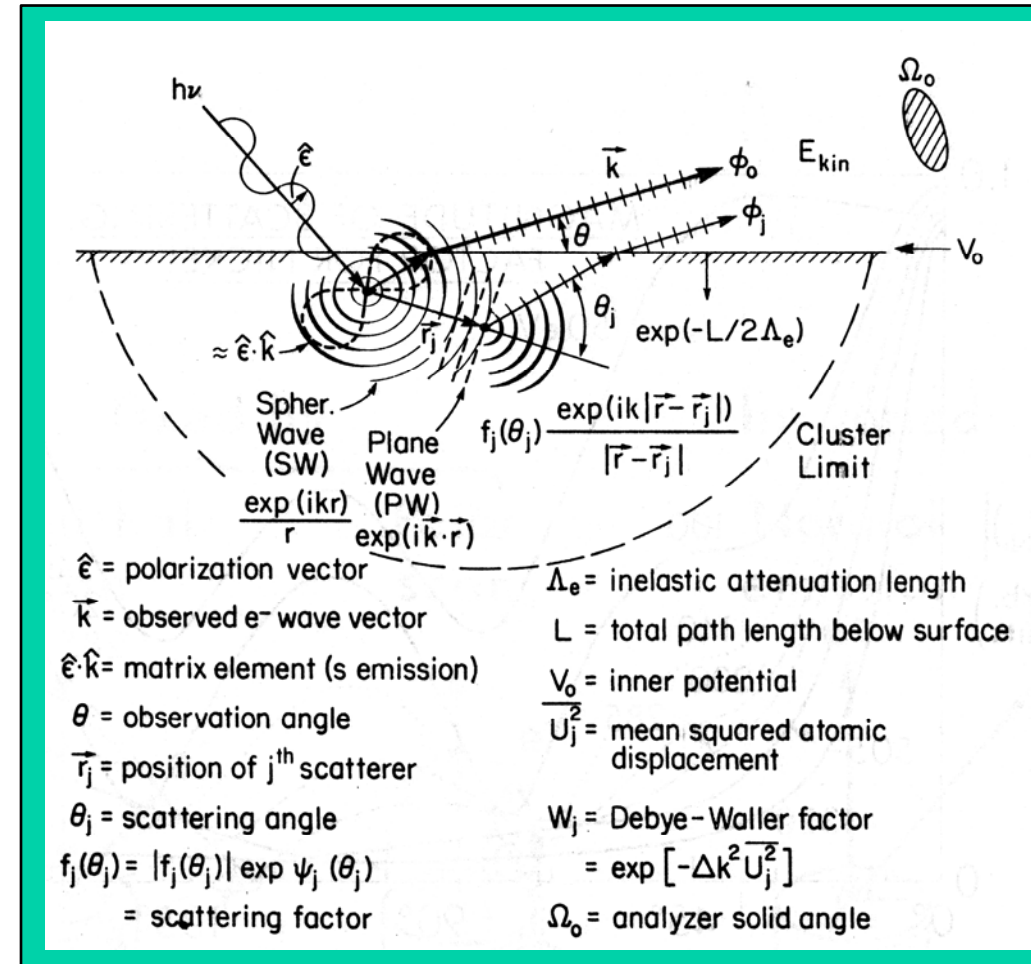
# Forward scattering and XPD



$$I(\vec{k}) \propto \left| \hat{\epsilon} \cdot \hat{k} e^{-\gamma L} + \sum_j \frac{\hat{\epsilon} \cdot \hat{r}_j}{r_j} |f_j(\theta_j)| W_j e^{-\gamma L_j} e^{i[kr_j(1-\cos\theta_j) + \psi_j(\theta_j)]} \right|^2 +$$

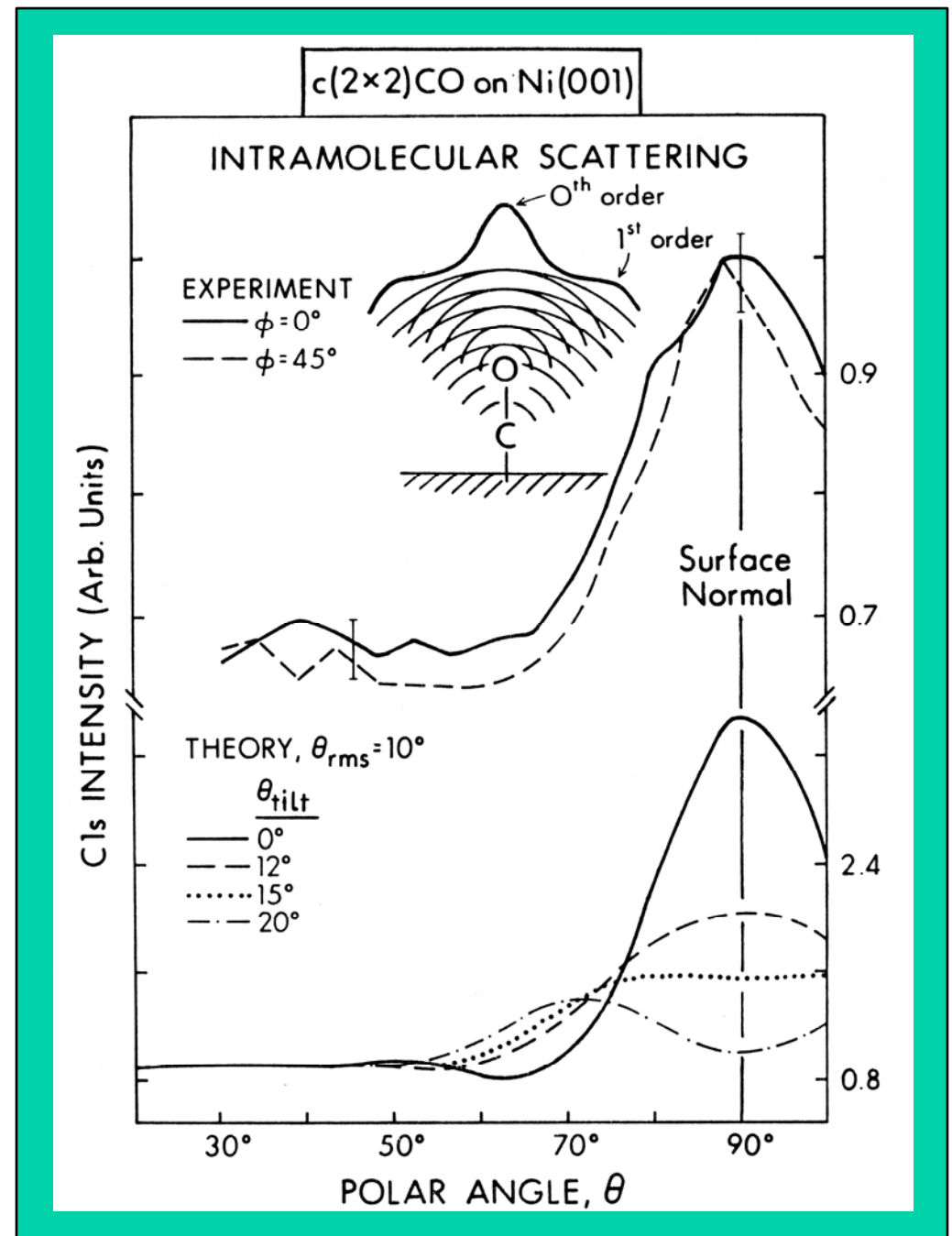
$$+ \sum_j (\hat{\epsilon} \cdot \hat{r}_j) \frac{|f_j(\theta_j)|^2}{r_j^2} (1 - W_j^2) e^{-2\gamma L_j}$$

# The single scattering cluster



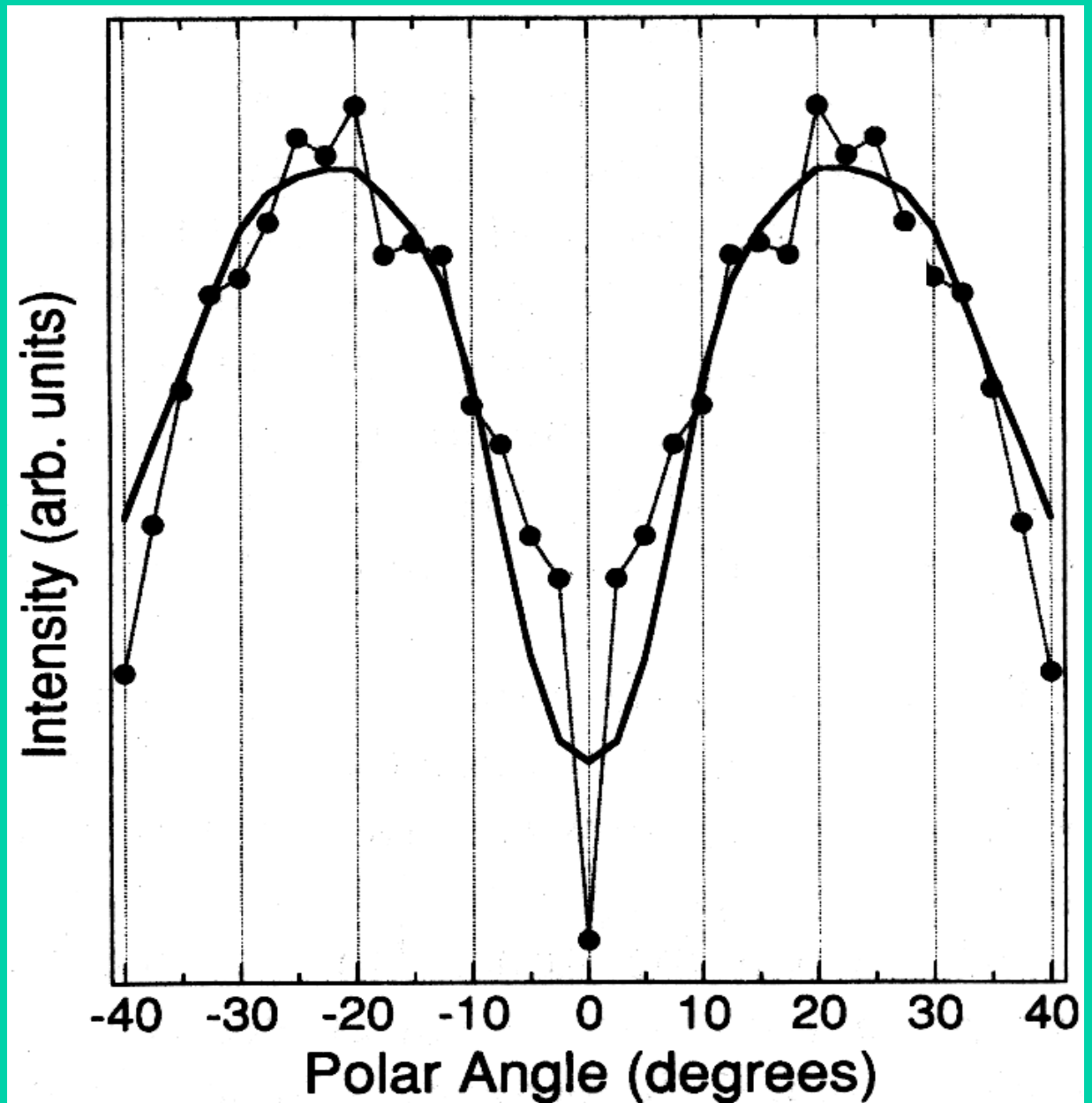


**CO/Ni(100): forward scattering produces a pronounced peak along the molecular axis (along the surface normal)**



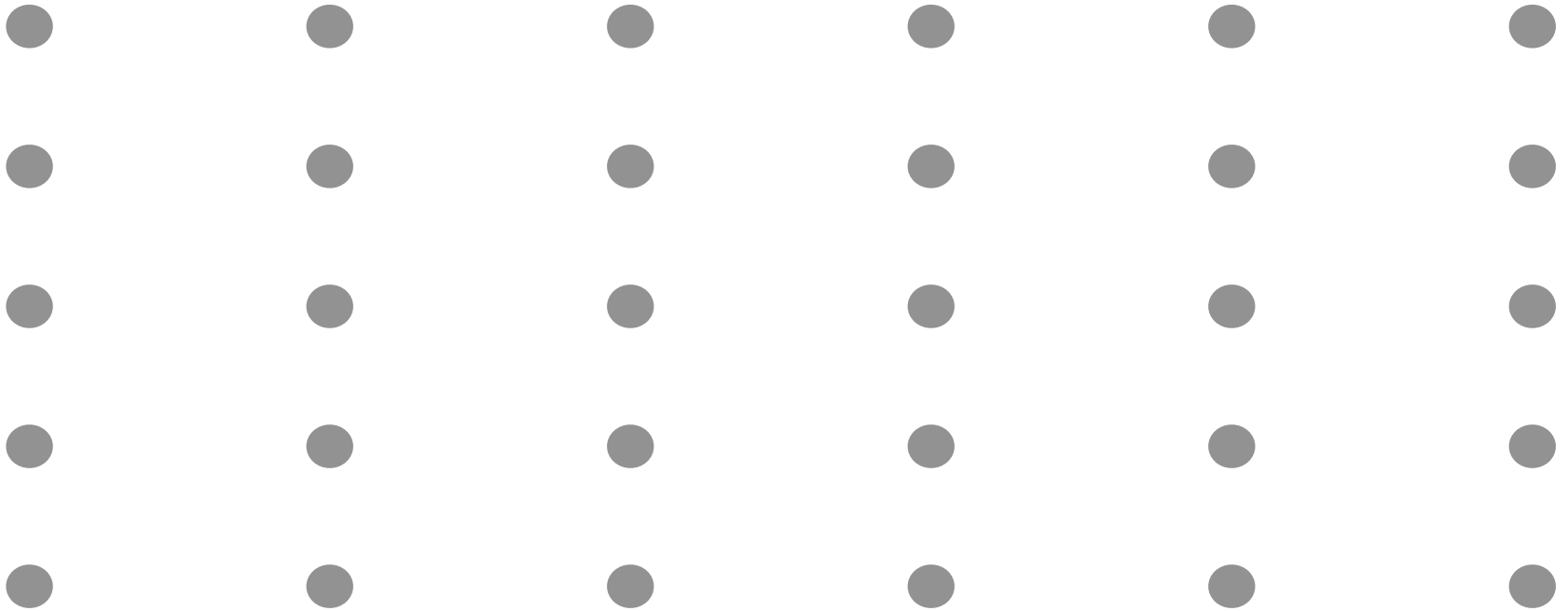


**CO/Pd(110): a  
compressed  
zig-zag  
structure**

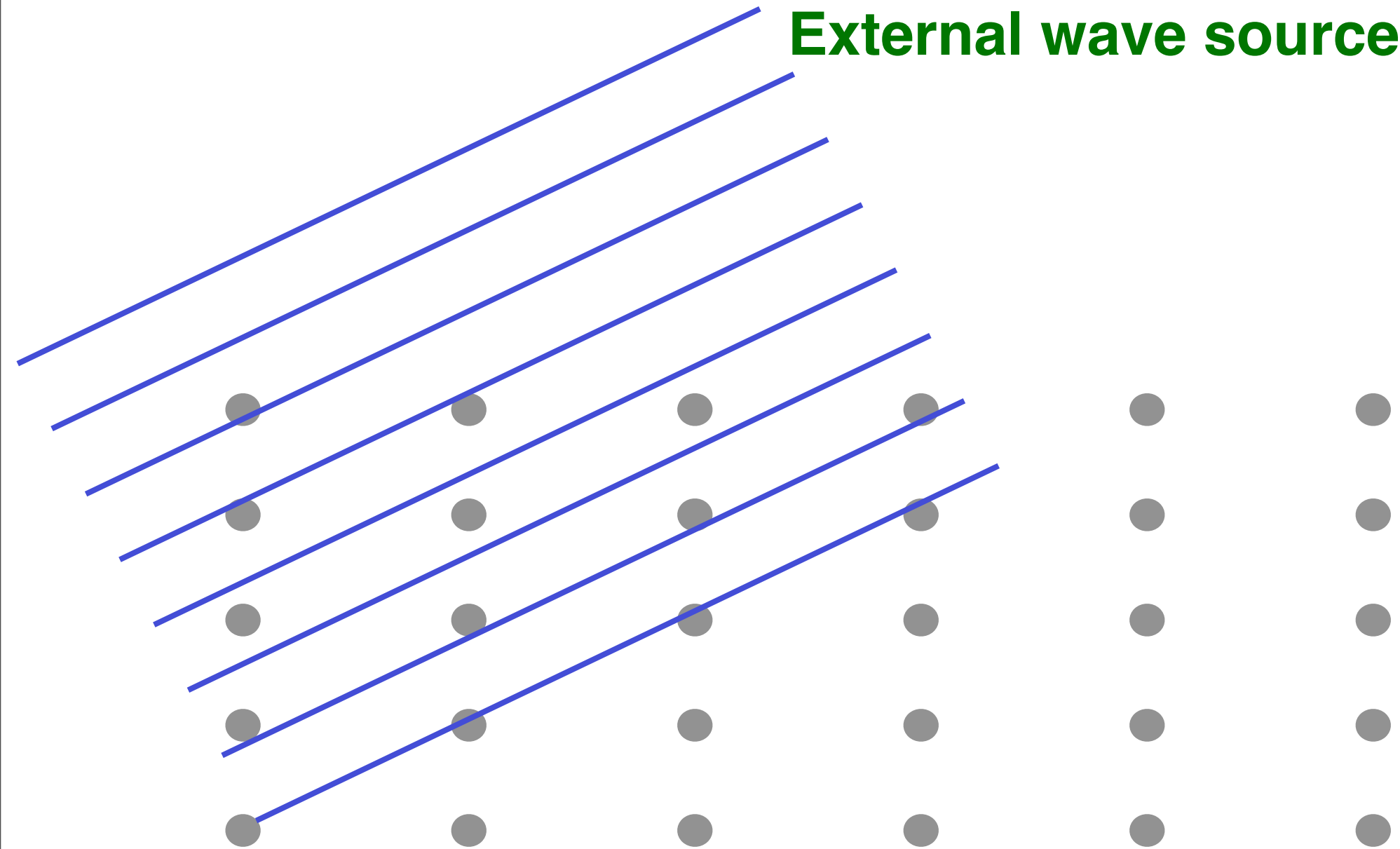


<b>Probe</b>	<b>E(<math>\lambda</math>)</b>	<b>Scatterers</b>
x-rays	$E = \frac{2\pi\hbar c}{\lambda}; \quad E(eV) = \frac{12400}{\lambda(\text{\AA})}$	electrons
electrons	$E = \frac{(2\pi\hbar)^2}{2m} \left(\frac{1}{\lambda}\right)^2; \quad E(eV) = \frac{150.4}{(\lambda(\text{\AA}))^2}$	electrons and nuclei
neutrons	$E = \frac{(2\pi\hbar)^2}{2M} \left(\frac{1}{\lambda}\right)^2; \quad E(eV) = \frac{8.19 \cdot 10^{-2}}{(\lambda(\text{\AA}))^2}$	nuclei
atoms (e.g. He)	$E = \frac{(2\pi\hbar)^2}{2MA} \left(\frac{1}{\lambda}\right)^2; \quad E(eV) = \frac{2.05 \cdot 10^{-2}}{(\lambda(\text{\AA}))^2}$	electrons

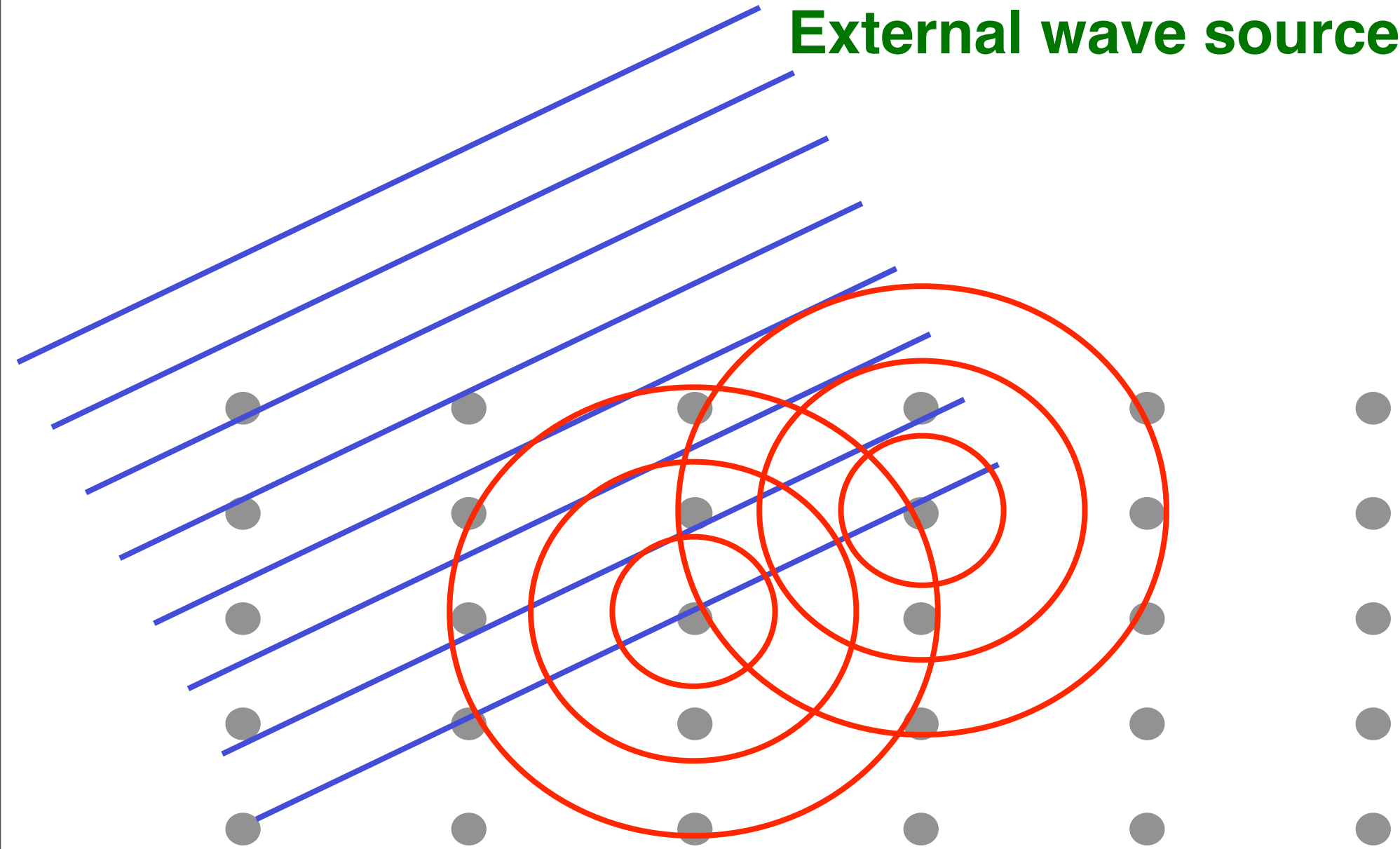
# External wave source



# External wave source



# External wave source



# Diffraction

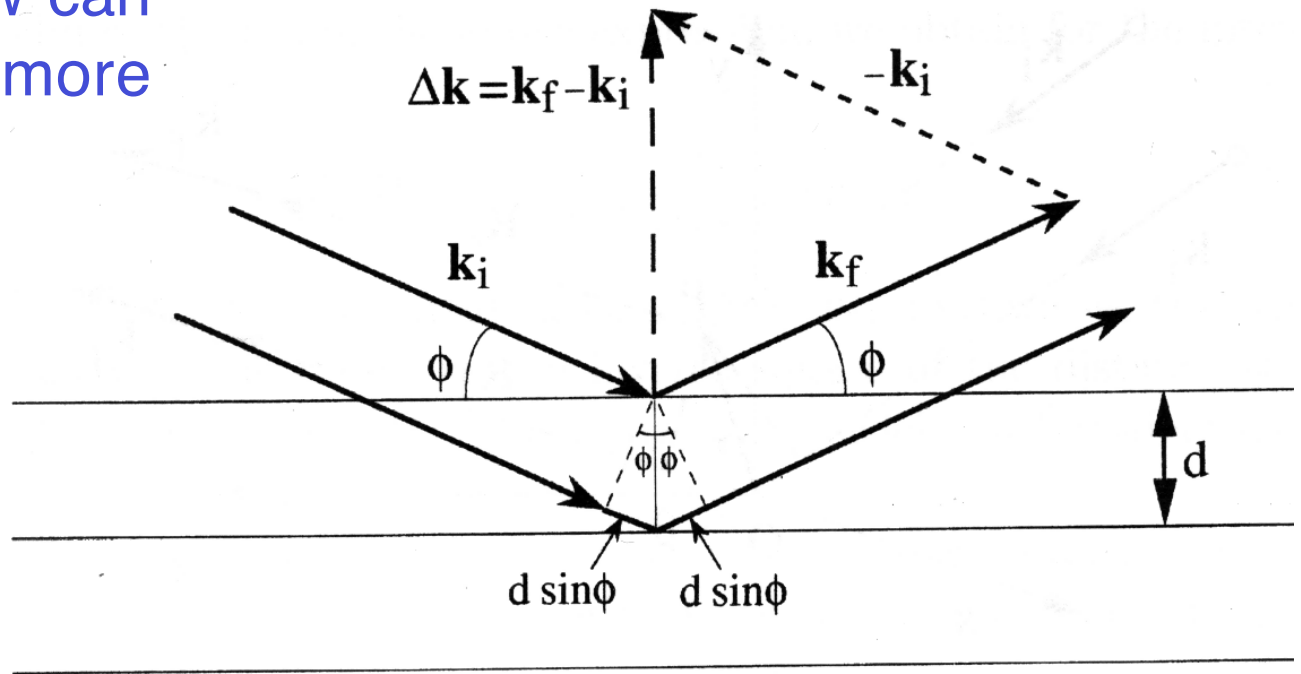
If one considers the wavevector  $\vec{k}$  of the plane wave

$$\vec{E}(\vec{r}, t) = \vec{E}_0 e^{i(\vec{k} \cdot \vec{r} - \omega t)}$$

with  $k=2\pi/\lambda$ , Bragg's law can be expressed in a more general vectorial form:

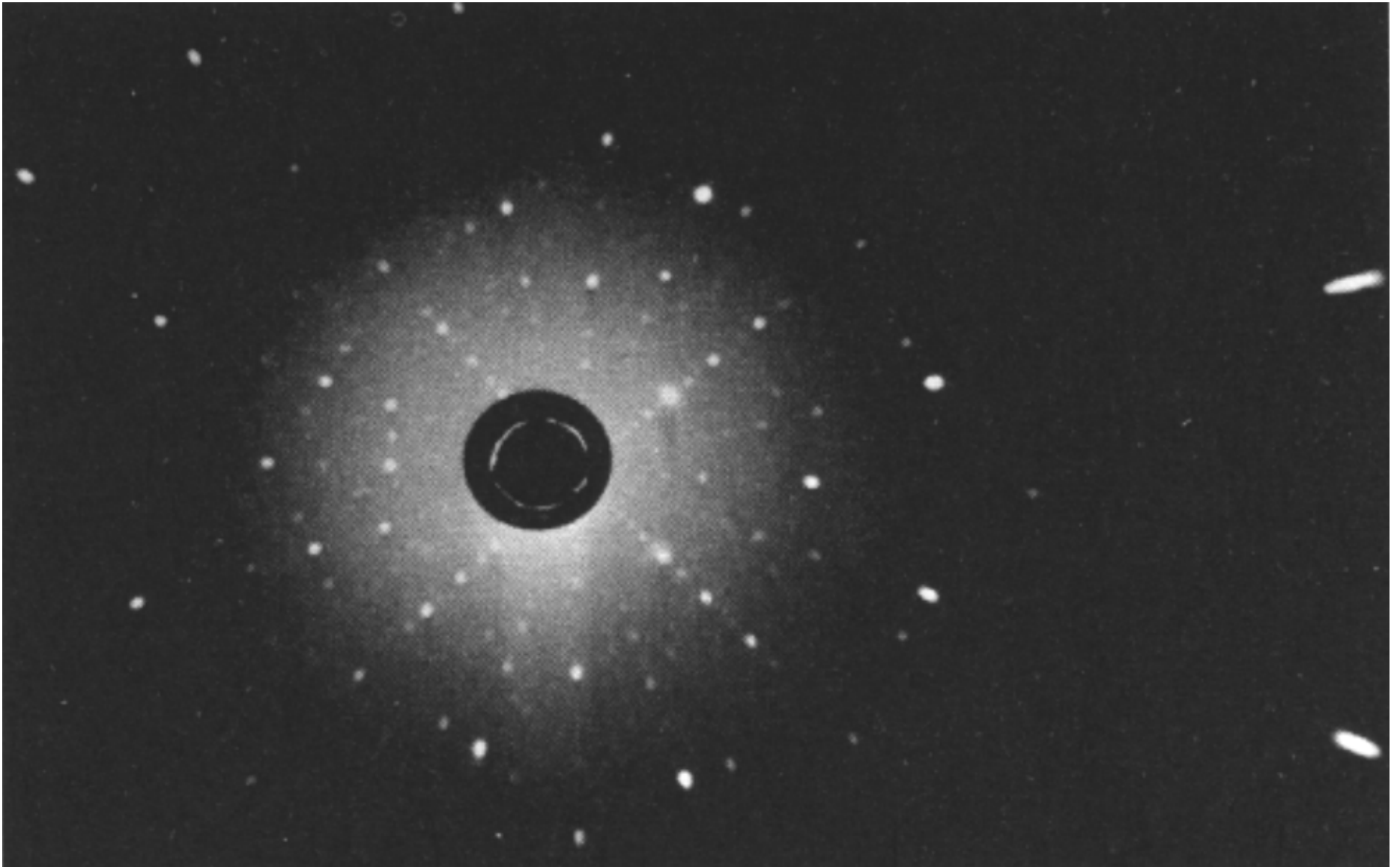
$$\Delta \vec{k} = \vec{G}$$

where  $\vec{G}$  is a reciprocal lattice vector

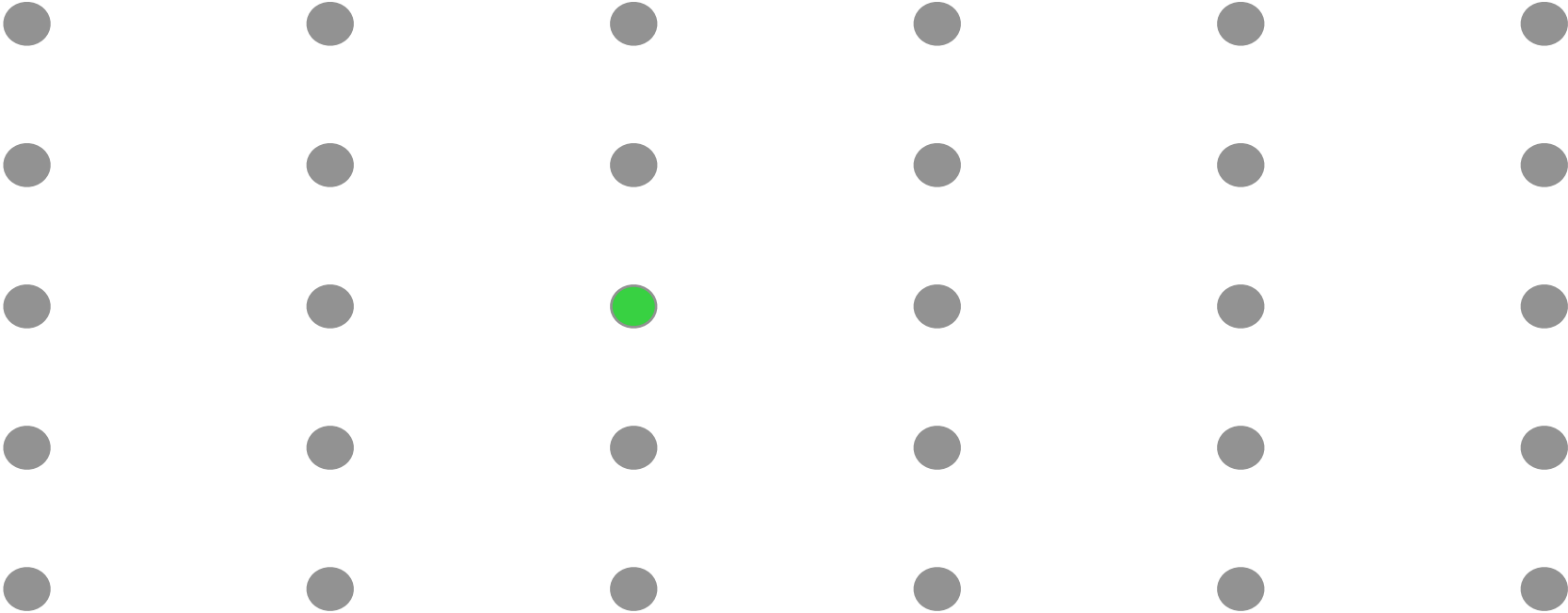


# Diffraction

A Laue pattern: Si(100)

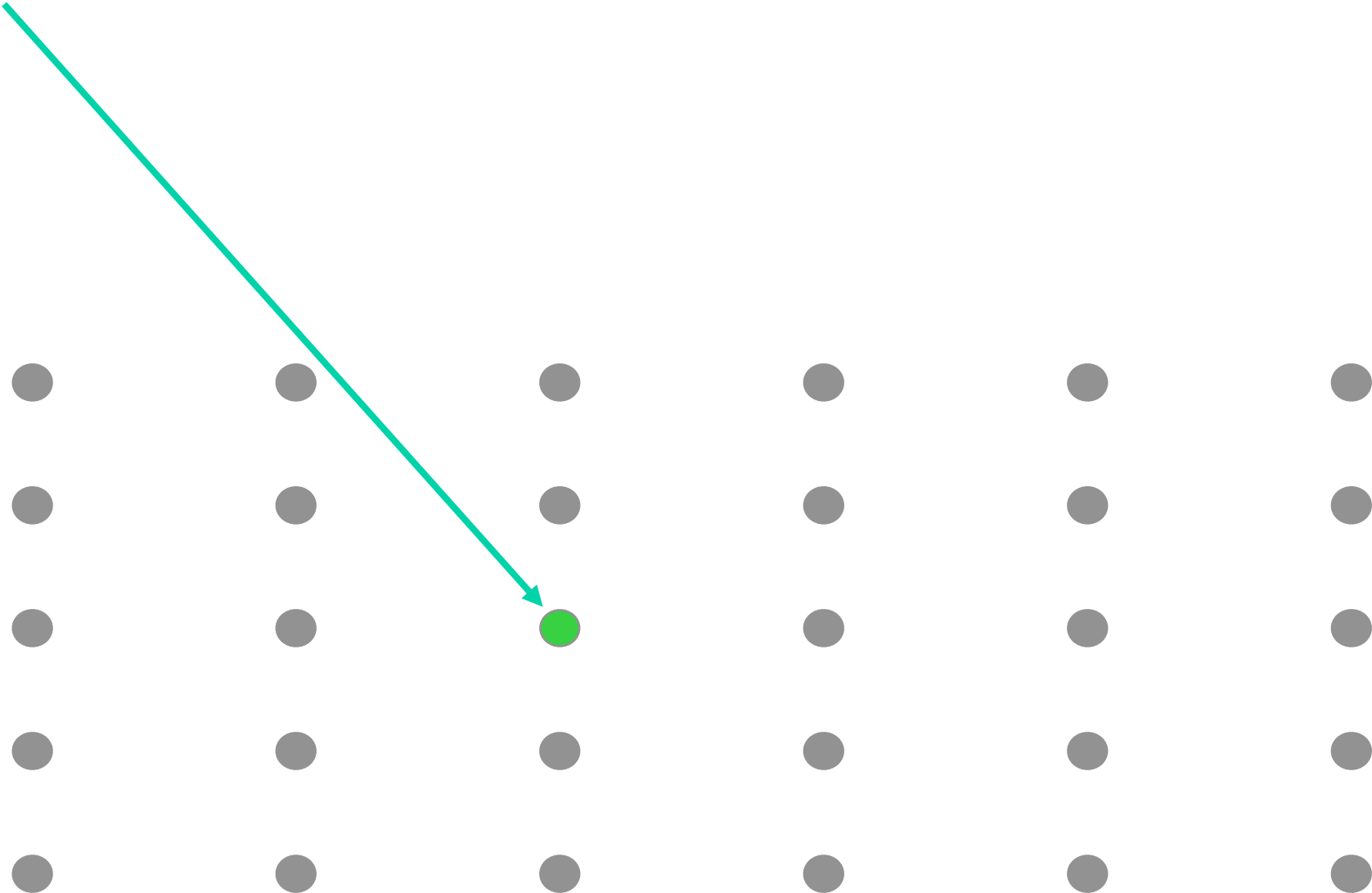


# Internal wave source

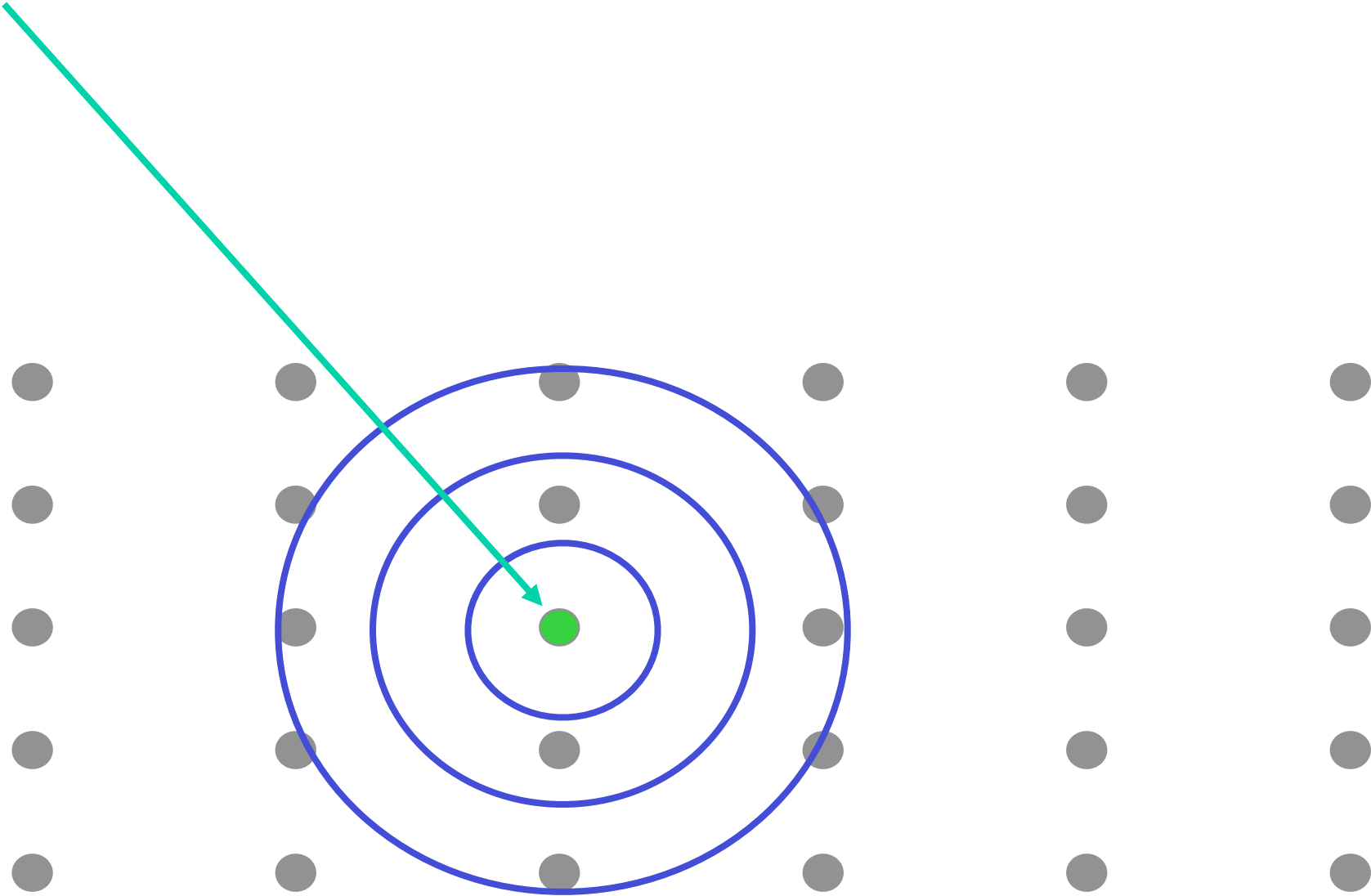




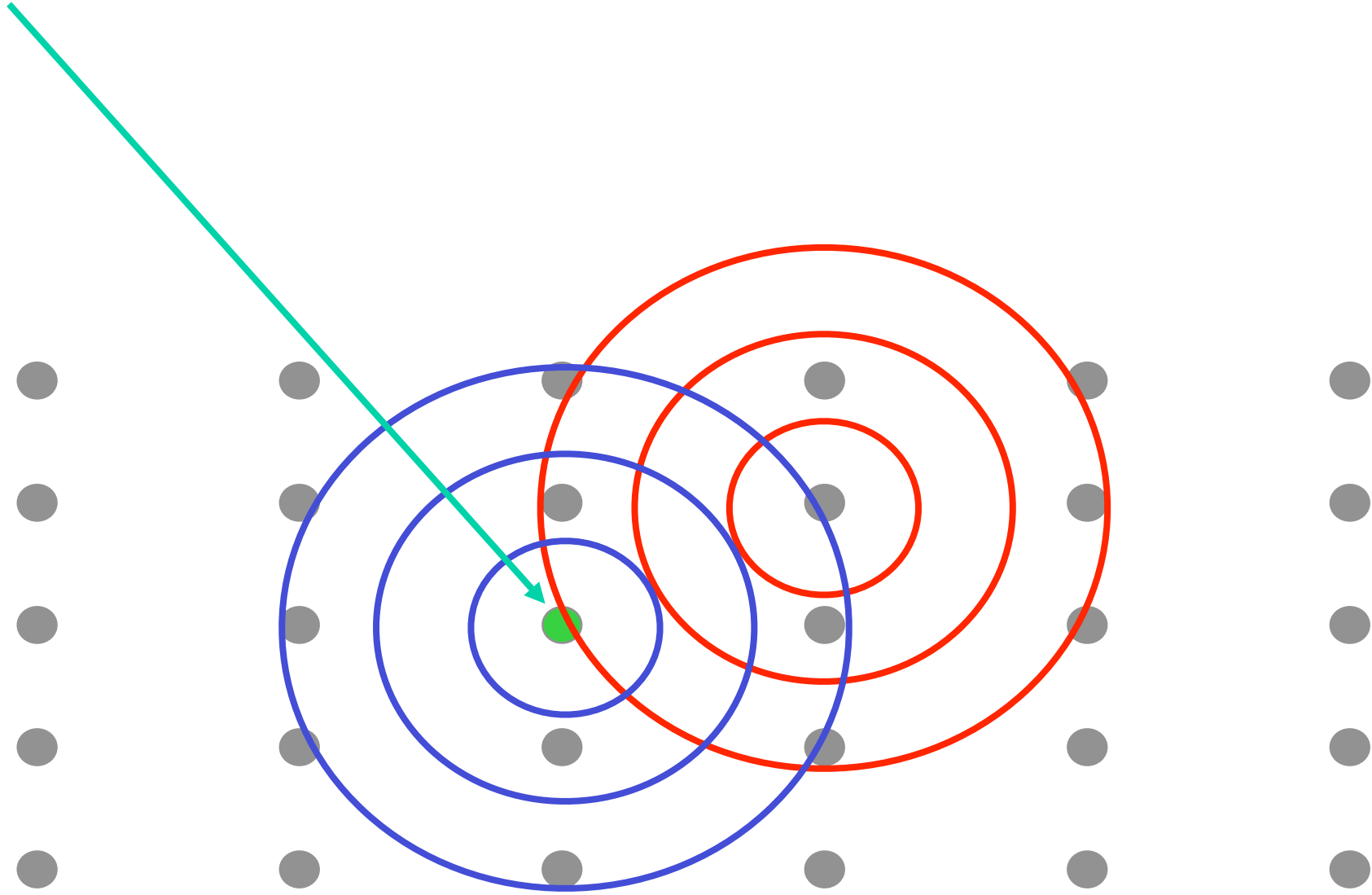
# Internal wave source



# Internal wave source



# Internal wave source

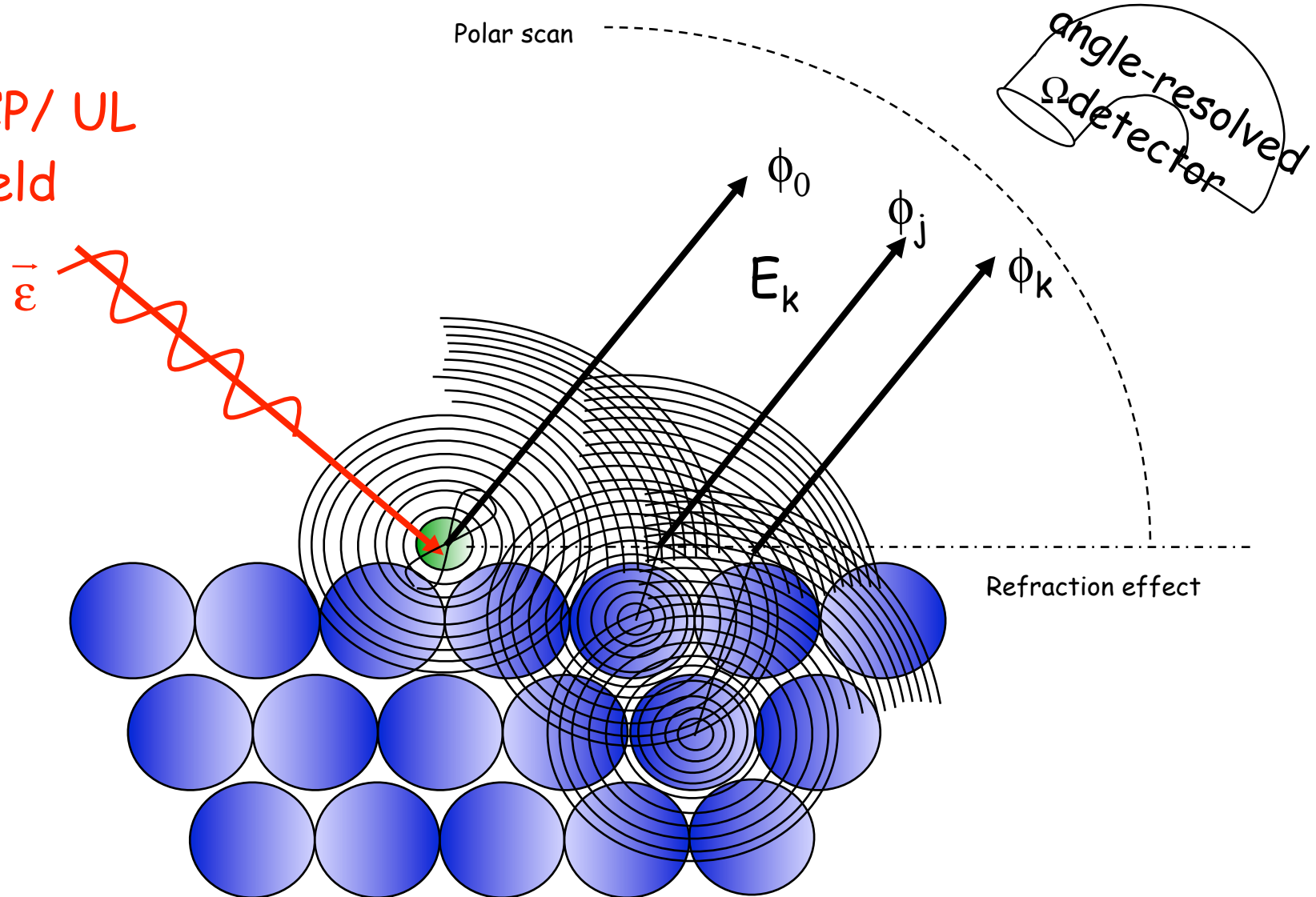


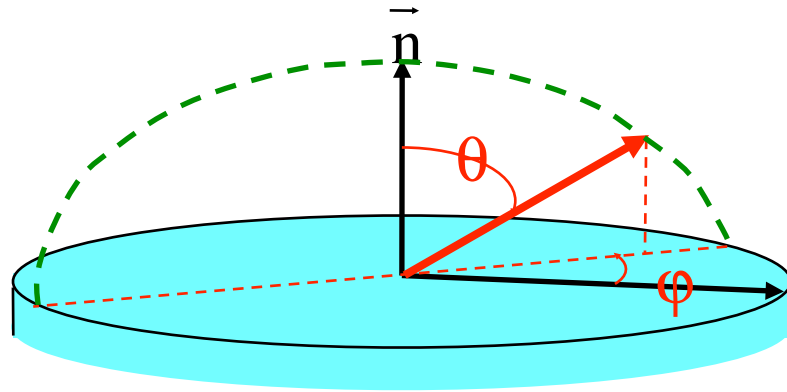
**External plane wave source:  
single crystal (long range order)**

**Internal spherical wave source:**

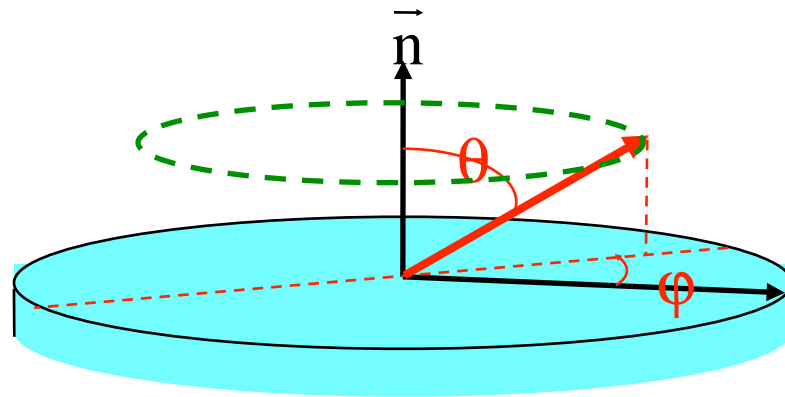
- 1) Measure what happens at the absorber  
(i.e. absorption) → short range order**
- 2) Measure outside the sample  
(i.e. photoemission) → short range  
order+same orientation at different sites**

LP/ RCP/ LCP/ UL  
radiation field



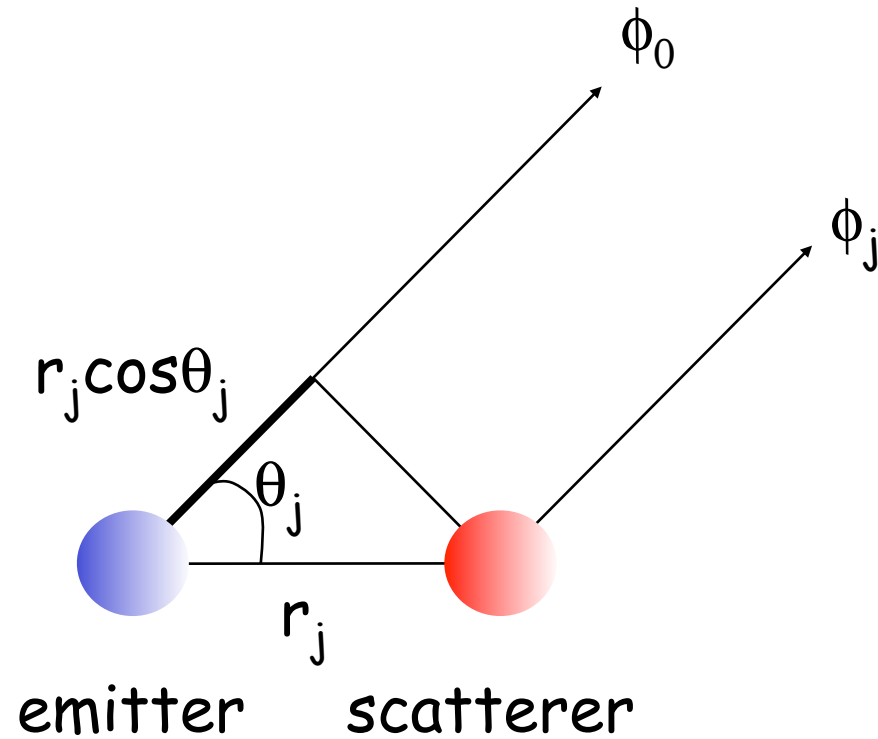


Polar scan

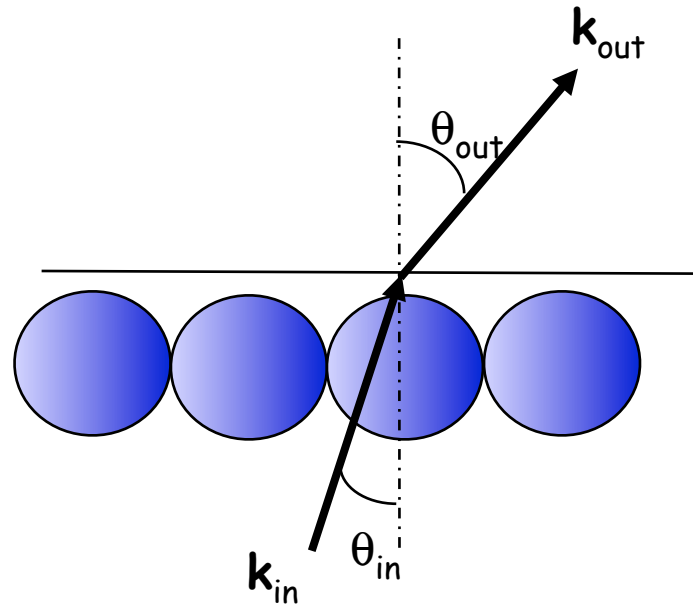


Azimuthal scan

# The basic scattering event:

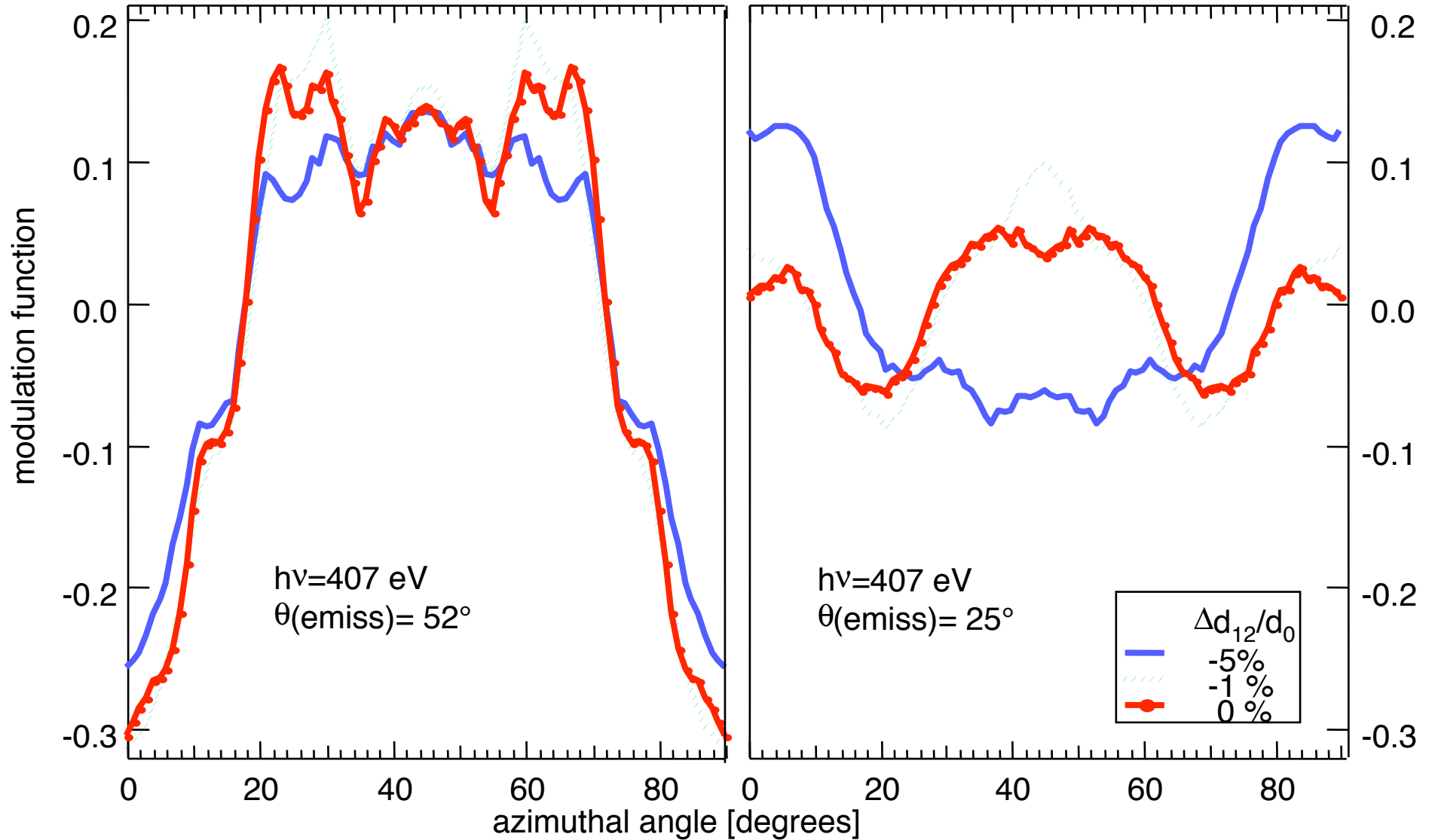


# Refraction at the surface

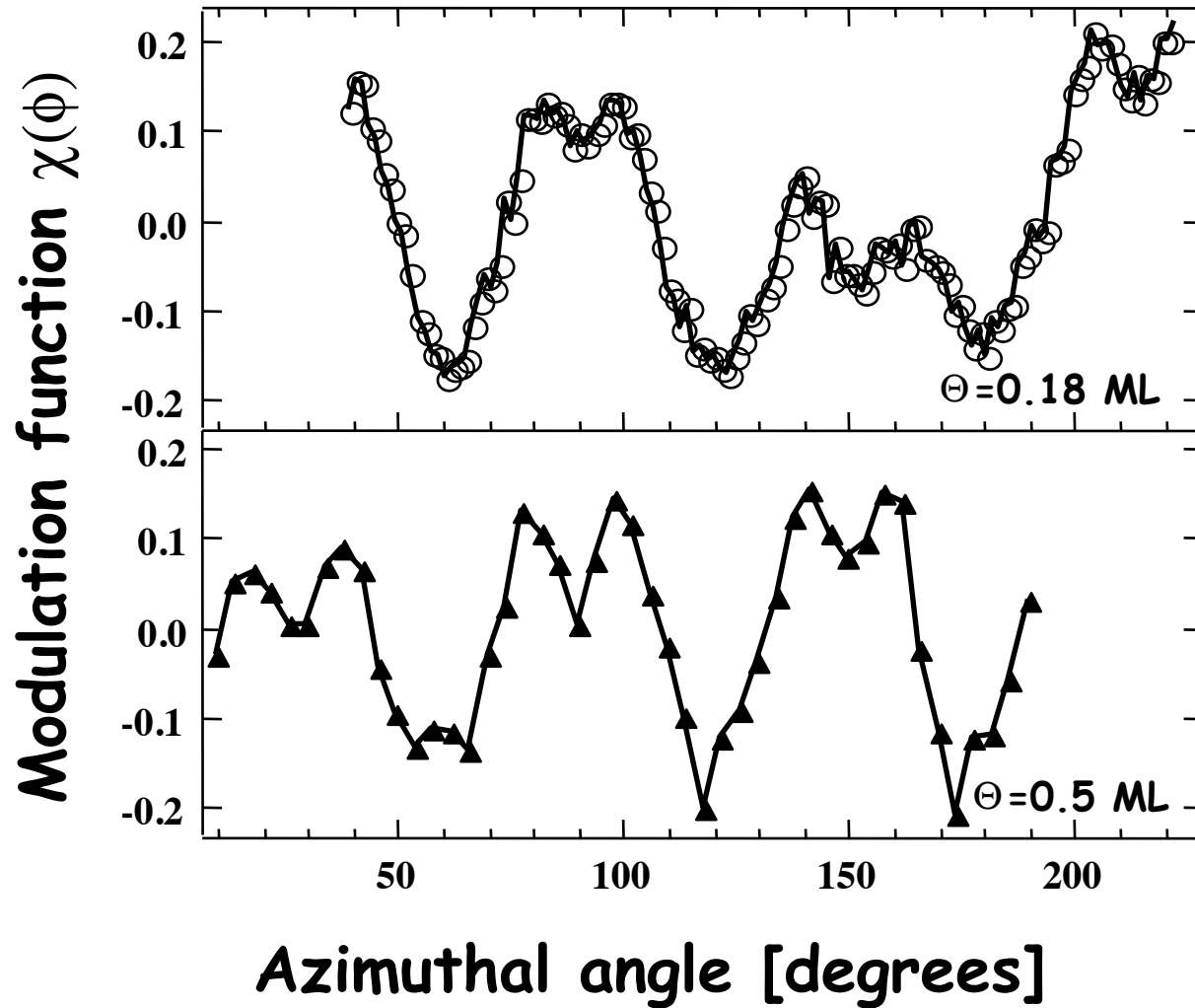


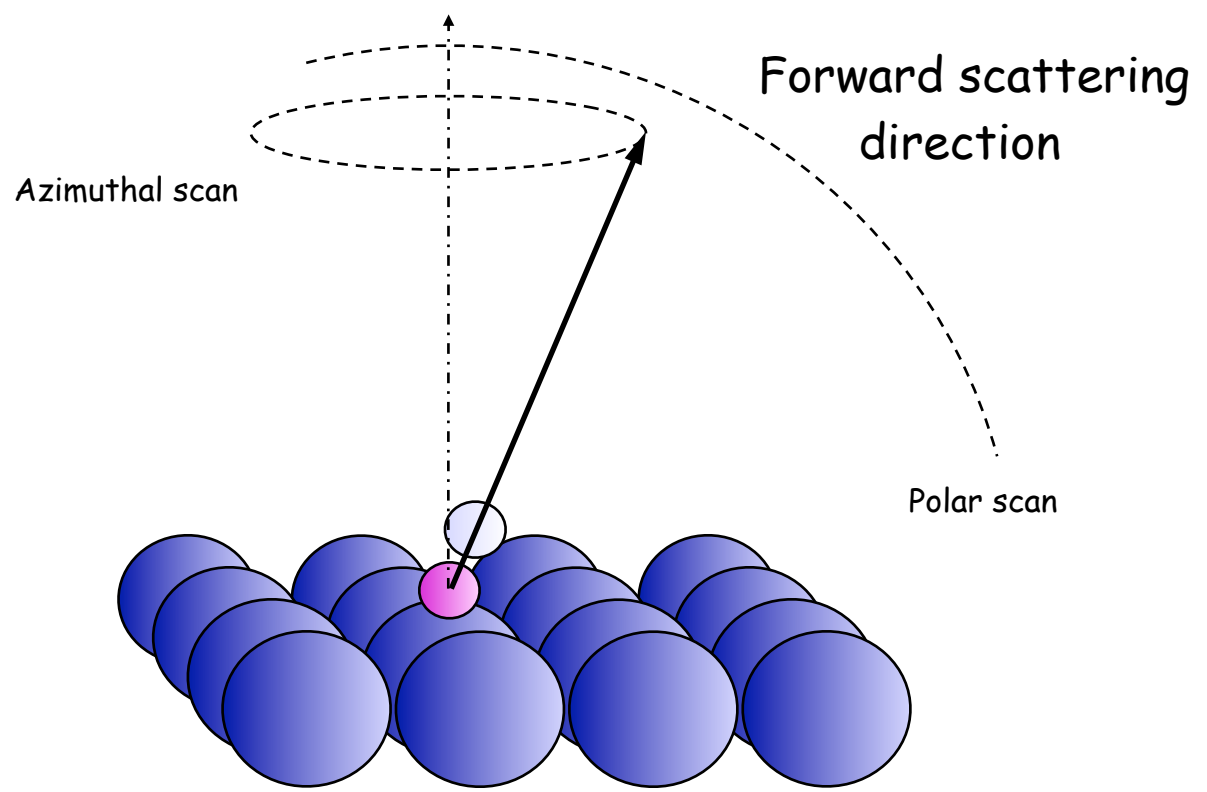


# Sensitivity to structural parameters in different measurement conditions: clean Rh(100)



# “Fingerprinting”: CO/Pt(111)



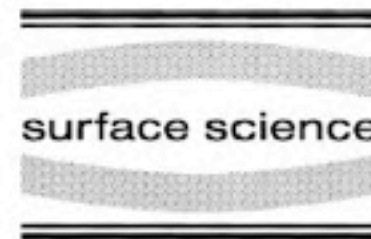


# **Chemical shift photoelectron diffraction**



ELSEVIER

Surface Science 408 (1998) 260–267



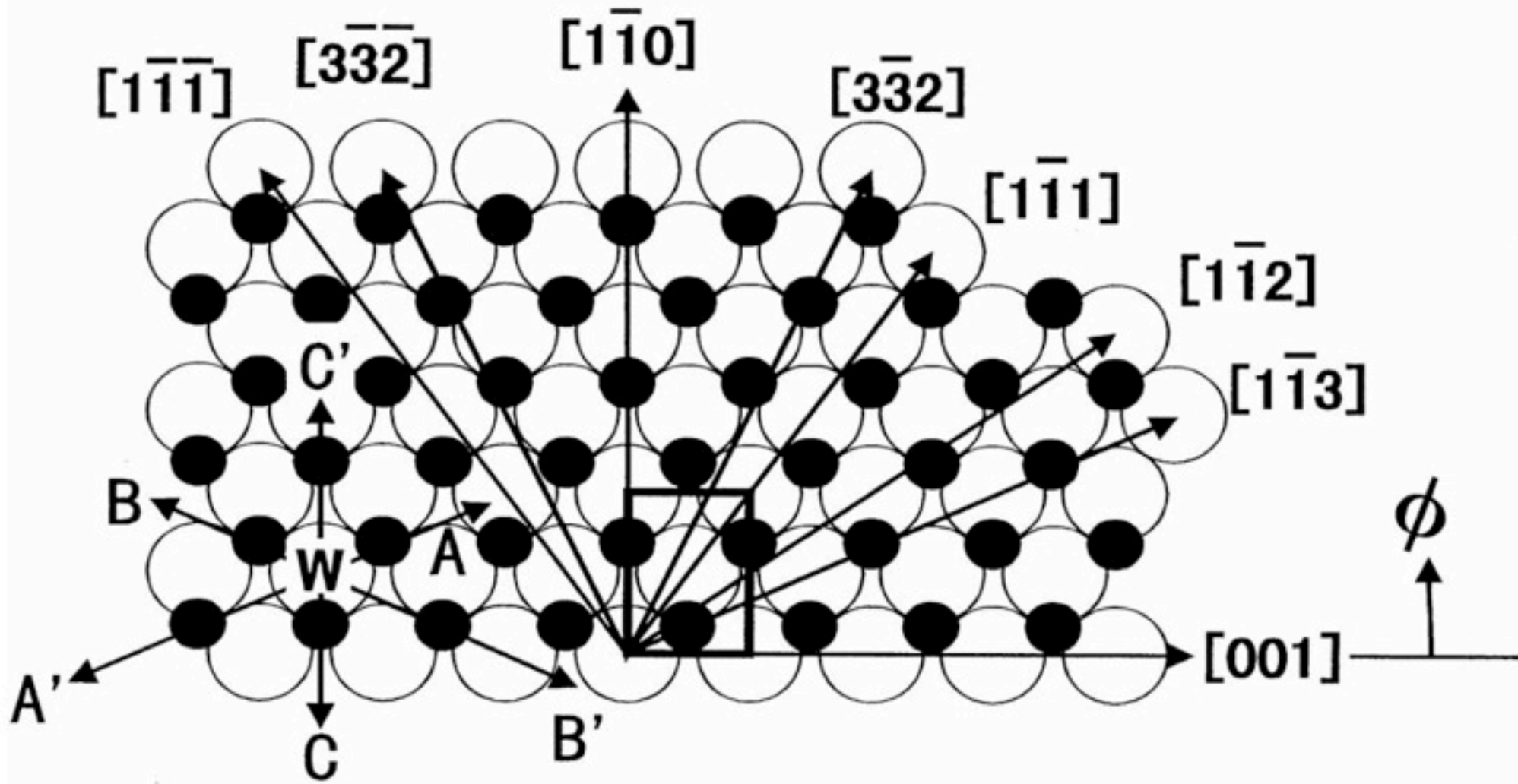
# Direct structure analysis of $W(110)-(1 \times 1)-O$ by full solid-angle X-ray photoelectron diffraction with chemical-state resolution

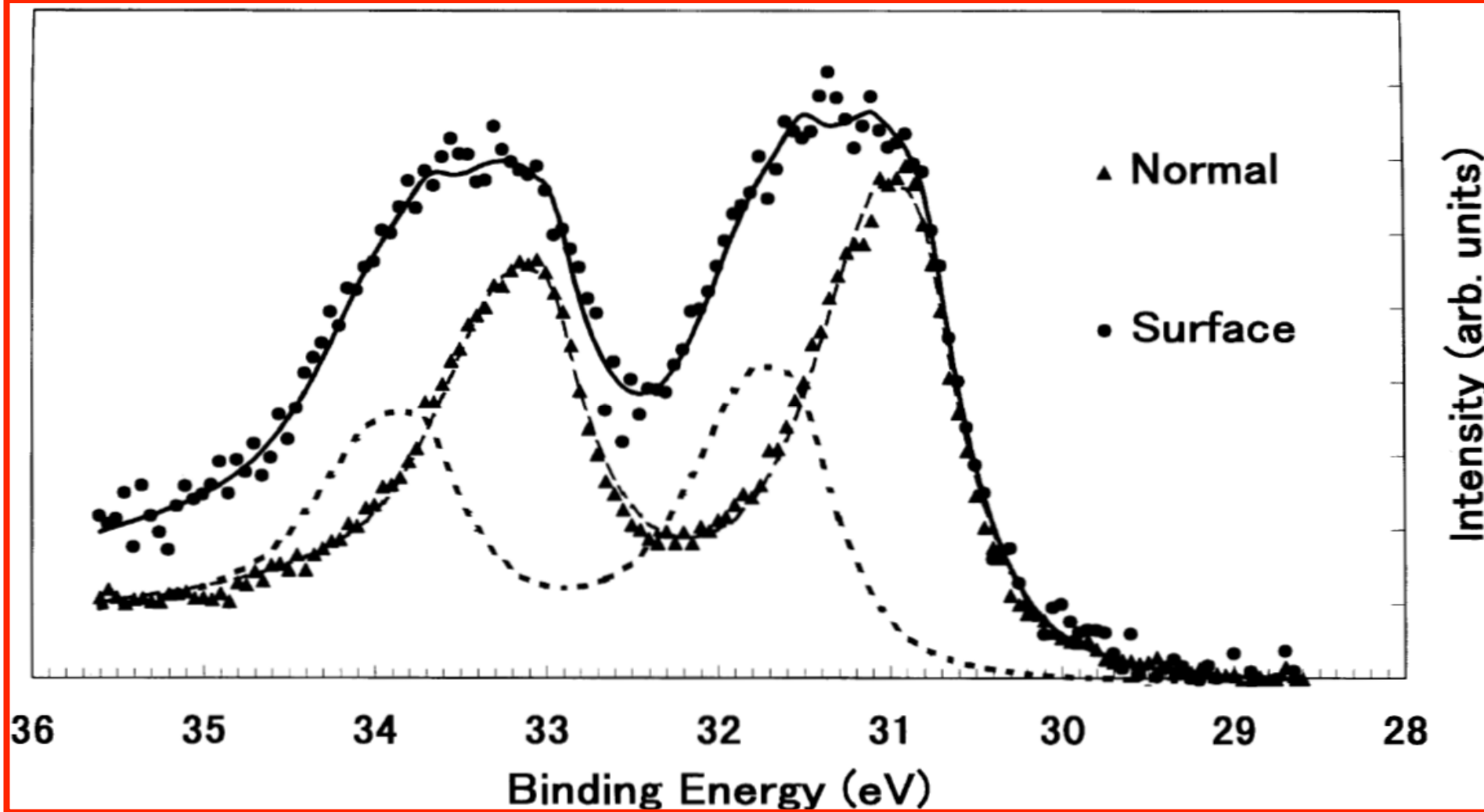
Hiroshi Daimon <sup>a,b,\*</sup>, Ramon Ynzunza <sup>a,c</sup>, Javier Palomares <sup>a,c</sup>, H. Takabi <sup>b</sup>,  
Charles S. Fadley <sup>a,c</sup>

<sup>a</sup> *Materials Sciences Division, Lawrence Berkeley National Laboratory, Berkeley, CA 94720, USA*

<sup>b</sup> *Faculty of Engineering Science, Osaka University, Toyonaka, Osaka 560, Japan*

<sup>c</sup> *Department of Physics, University of California–Davis, Davis, CA 95616, USA*





W4f XPS spectra from the W(110)-(1x1)-O surface as excited by Al  $K_{\alpha}$  radiation. The triangles represent a bulk-sensitive spectrum taken with emission normal to the surface. The circles represent data taken at a maximally surface-sensitive direction  $(\Theta, \phi) = (12^{\circ}, 26^{\circ})$ , where  $\Theta$  is the take-off angle with respect to the surface and  $\phi$  is measured with respect to [001]. The surface-sensitive spectrum is fitted well by the solid curve composed of two pairs of peaks having the same shape and separation. The dashed curve is that for normal emission and the dotted curve derived from this peak fitting we associate with electrons from the first-layer “oxide” W atoms which are directly bound to oxygen. The latter exhibit a core-level shift of 0.73 eV due to charge transfer from W to oxygen.

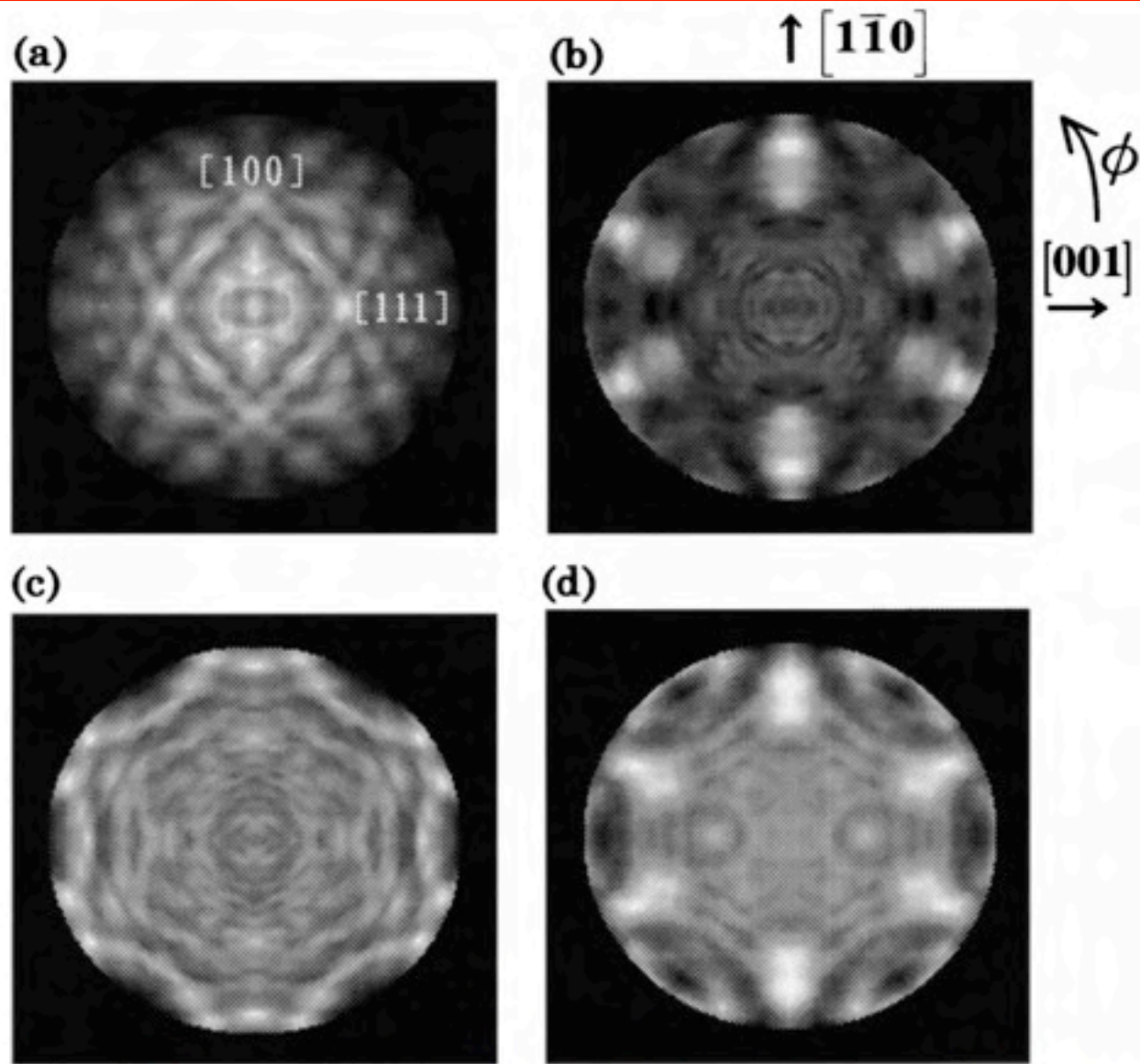
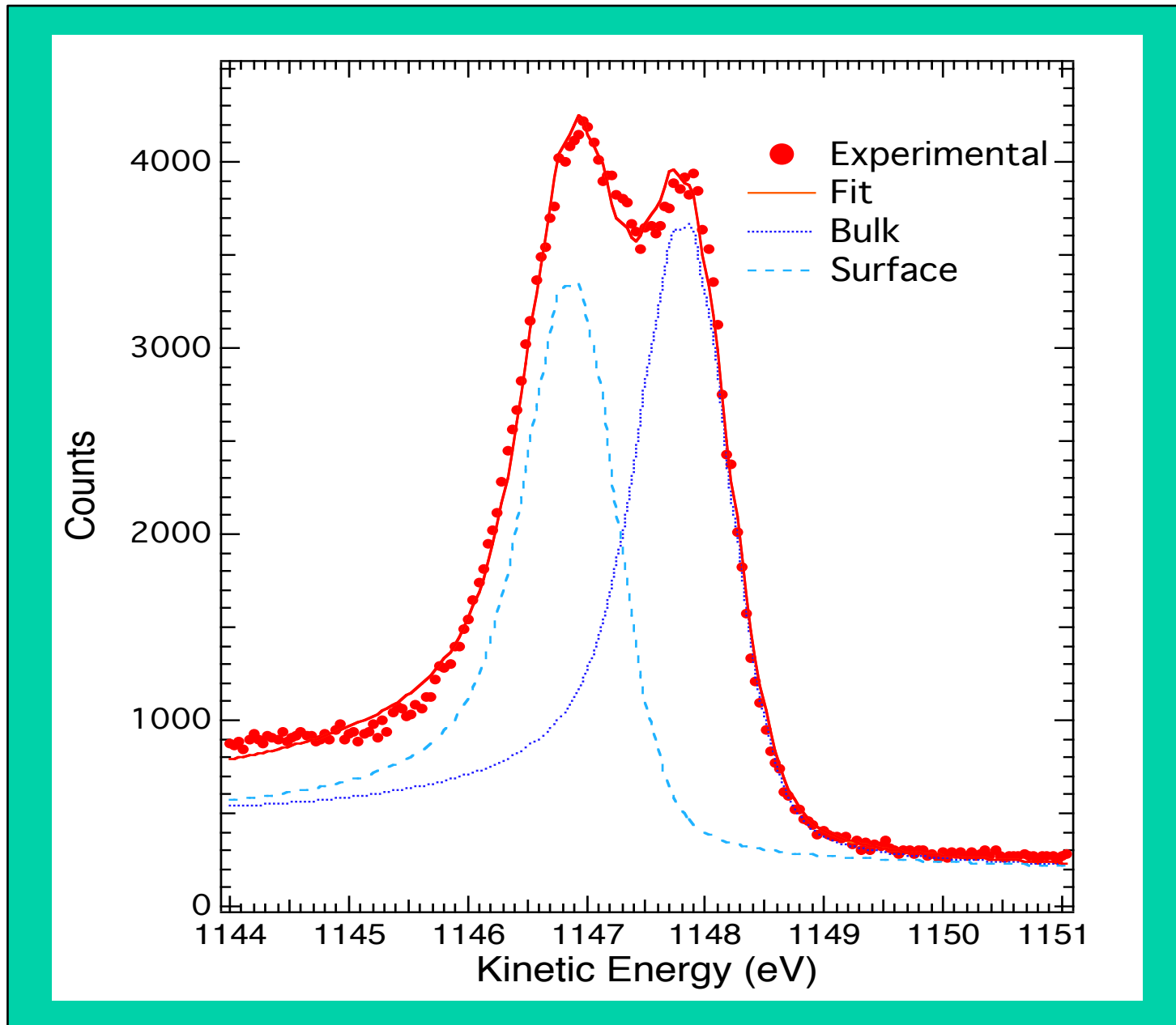


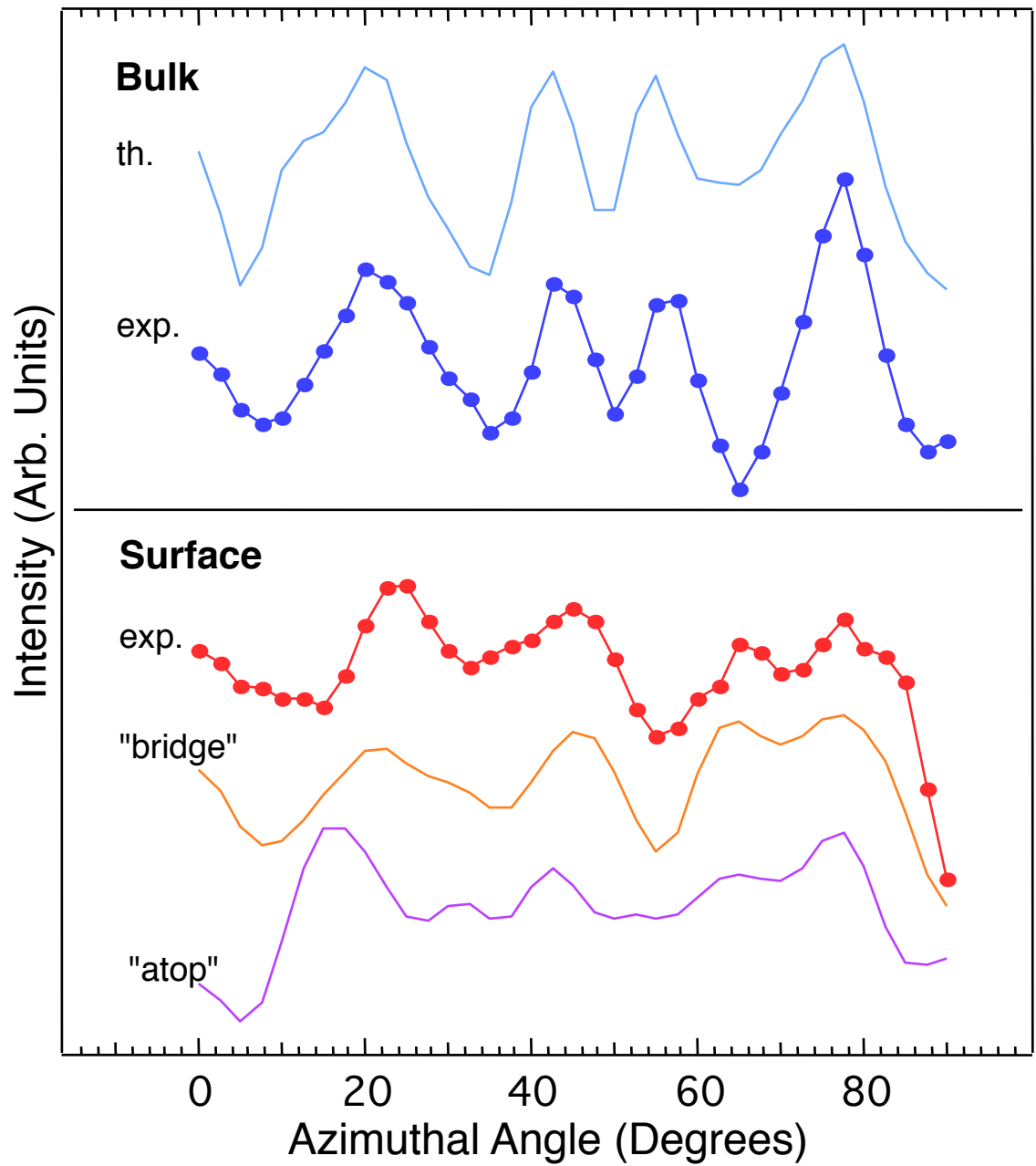
Fig. 3. Full solid-angle diffraction patterns of W 4f peaks for (a) bulk and (b) oxygen-coordinated "oxide". The center of each pattern corresponds to the surface normal ( $\Theta = 90^\circ$ ) and the periphery corresponds to  $\Theta = 9^\circ$ . The stereographic projection method was used to plot these data. The horizontal direction is  $[001]$  and the vertical direction is  $[1\bar{1}0]$ . These patterns have been averaged using mirror symmetry with respect to the  $[001]$  and  $[1\bar{1}0]$  directions. (c) Analogous full solid-angle diffraction pattern for the O 1s peak. (d) Theoretically simulated photoelectron diffraction pattern with the oxygen position of  $z = 0.84 \text{ \AA}$  and  $l = 1.52 \text{ \AA}$ .

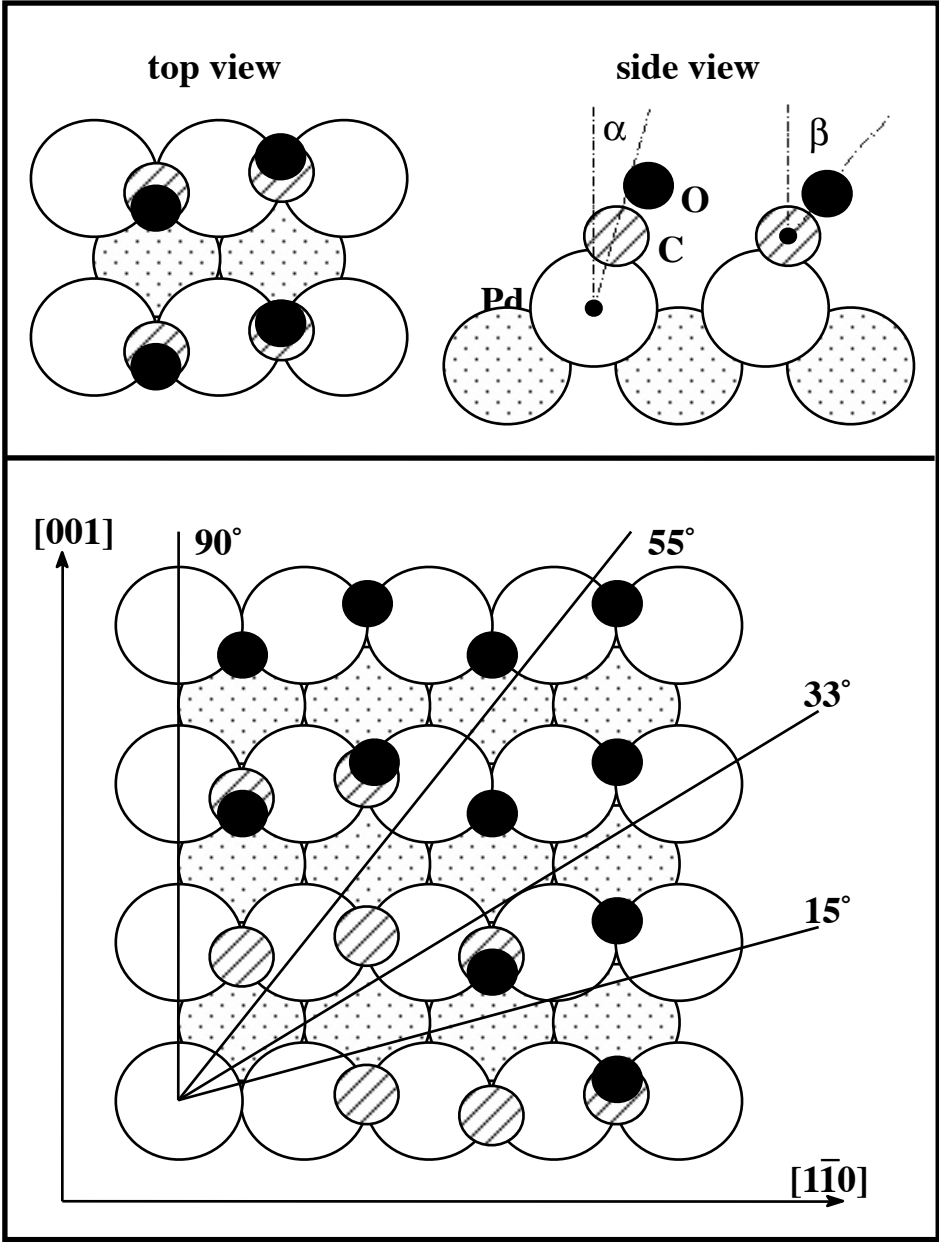


# SCLS induced by CO on Pd(110)

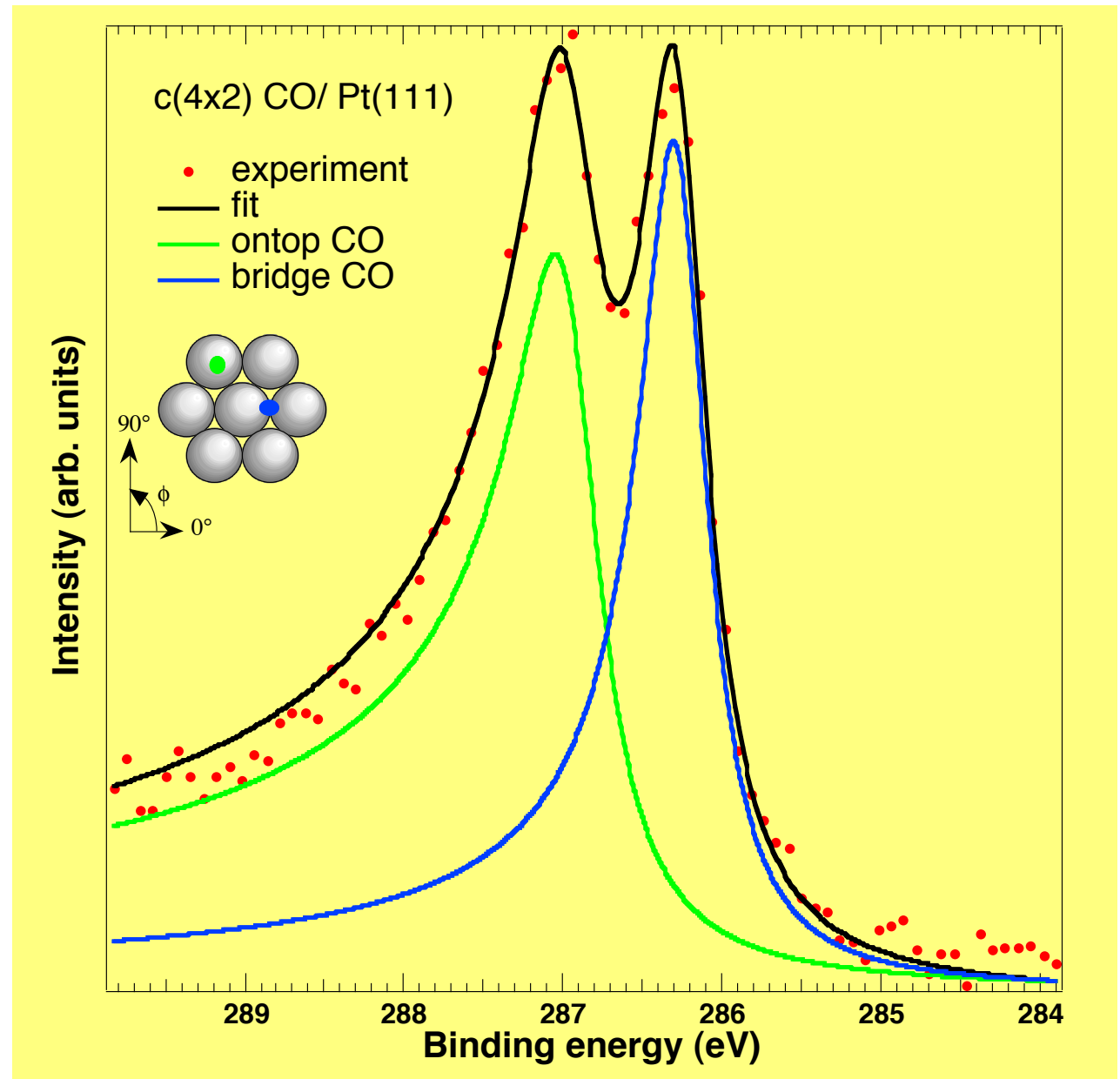
A. Locatelli *et al.*, Phys. Rev. Lett. 73, 90 (1994)



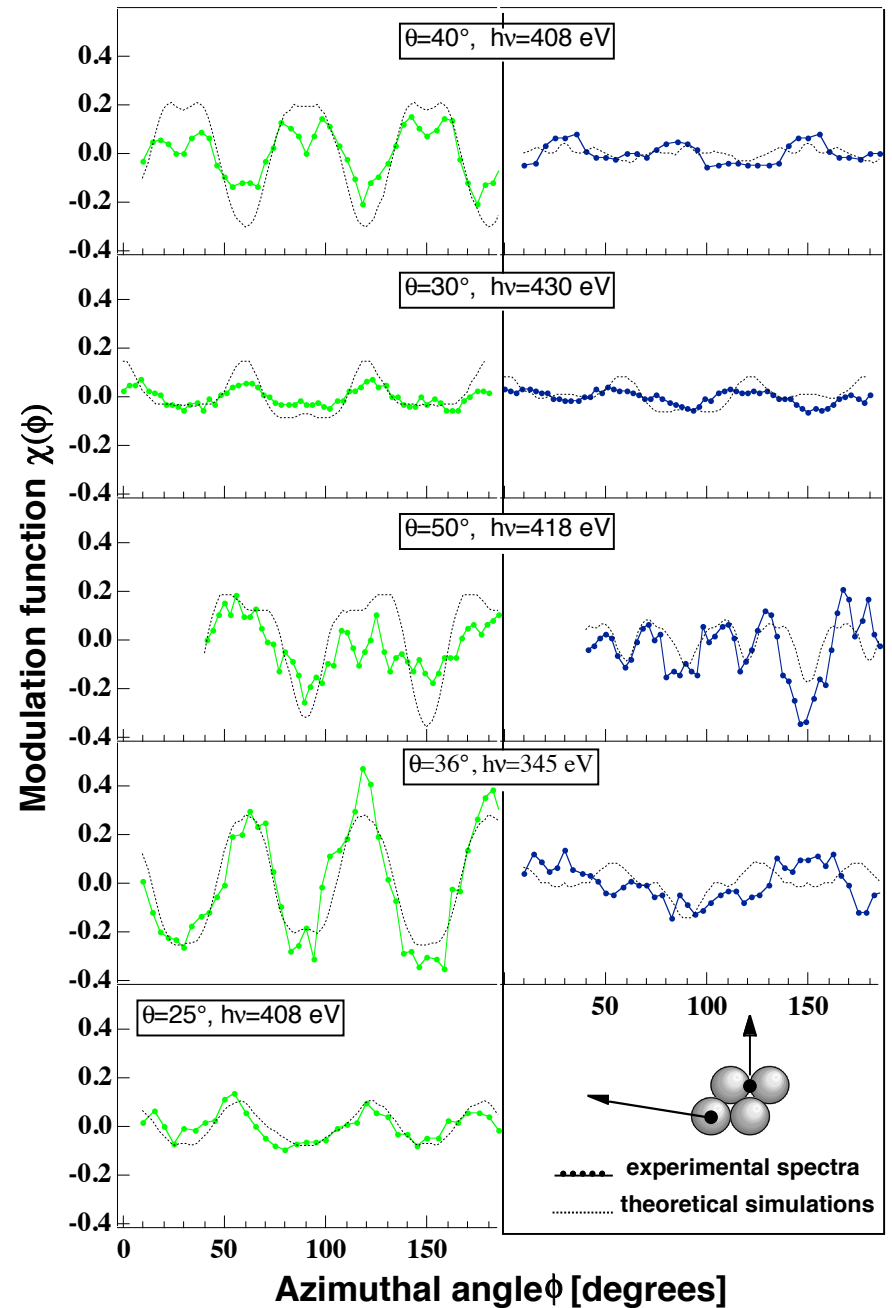




In the  $c(4 \times 2)$  structure of CO/Pt(111) the adsorbate occupies two adsorption sites: the photoelectron diffraction pattern is different for the two components and allows to measure the local geometry



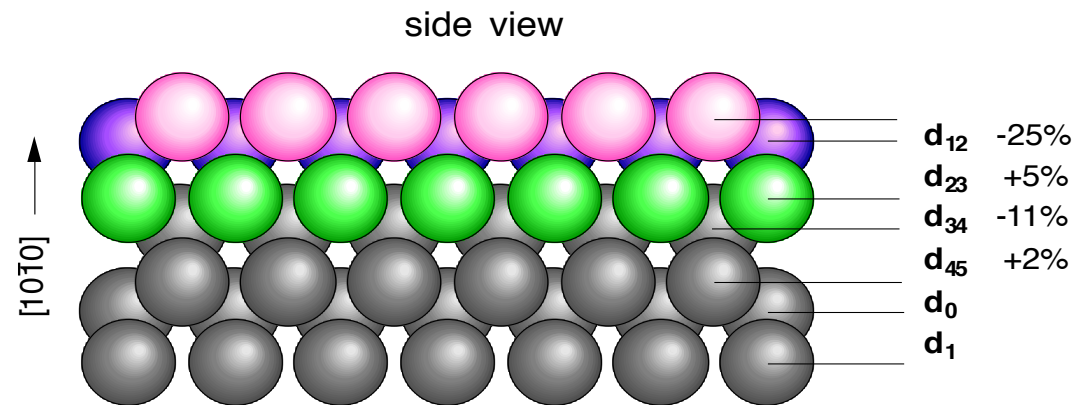
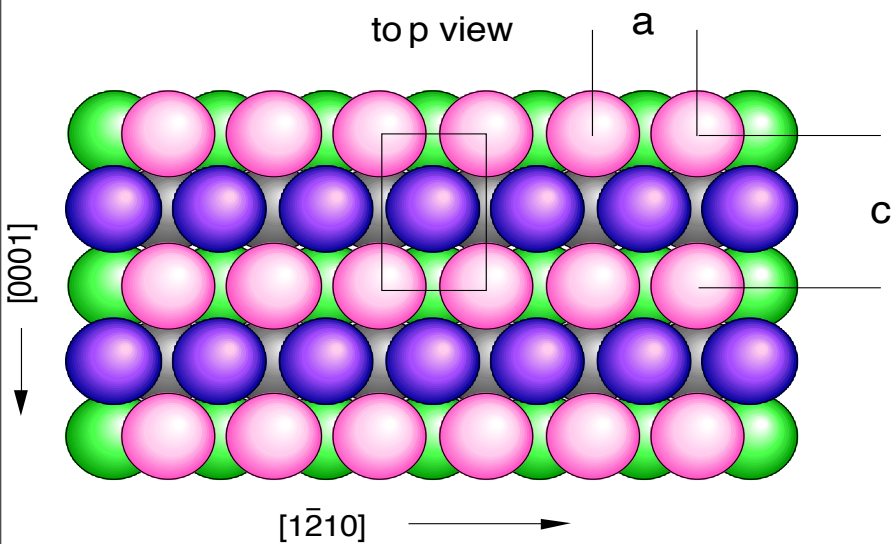
Multiple scattering  
calculations  
reproduce the  
experimental data,  
confirm the peak  
assignment and give  
the structural  
parameters



–

# Be (1010): a complex core

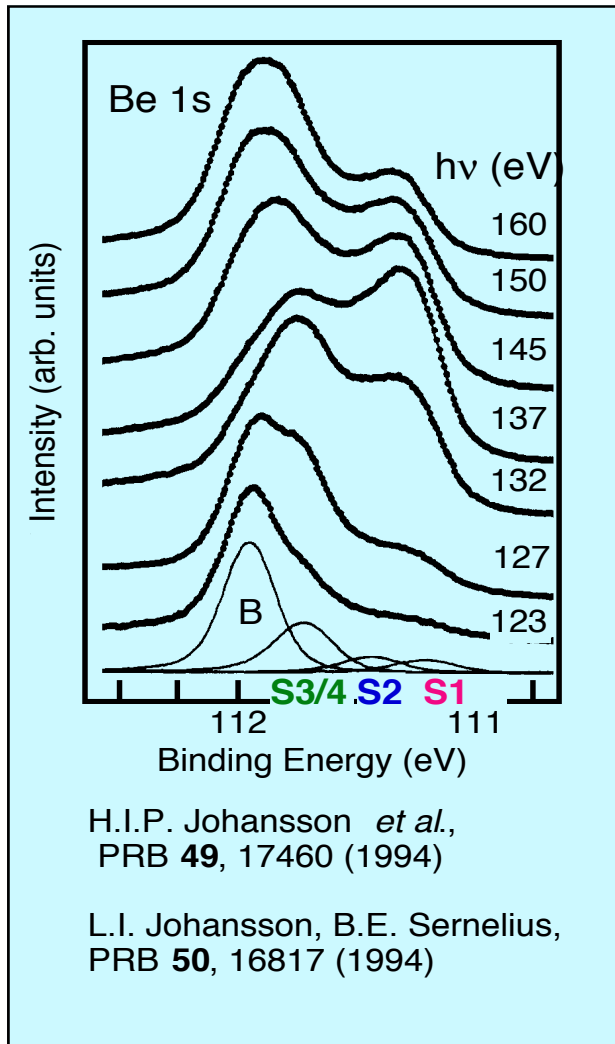
# Structure of the Be (10 $\bar{1}$ 0) surface



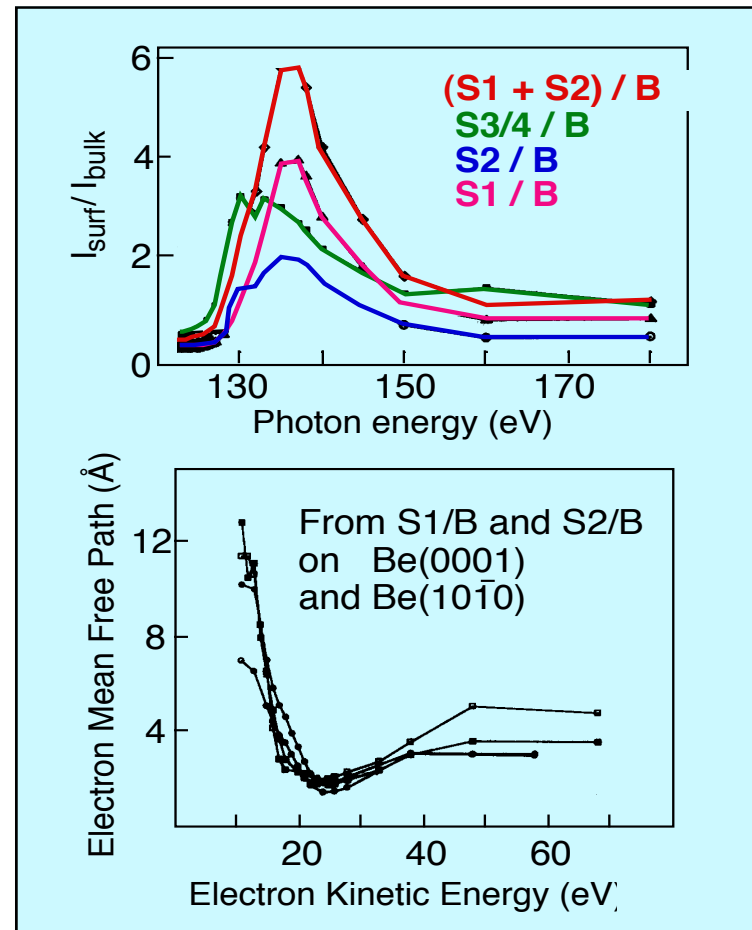
$$a = 2.28 \text{ \AA} \quad c = 3.58 \text{ \AA} \quad d_0 = 0.66 \text{ \AA} \quad d_1 = 1.32 \text{ \AA}$$

Hofmann et al., PRB **53**, 13715 (1996)

## energy dependence



## determination of the inelastic mean free path





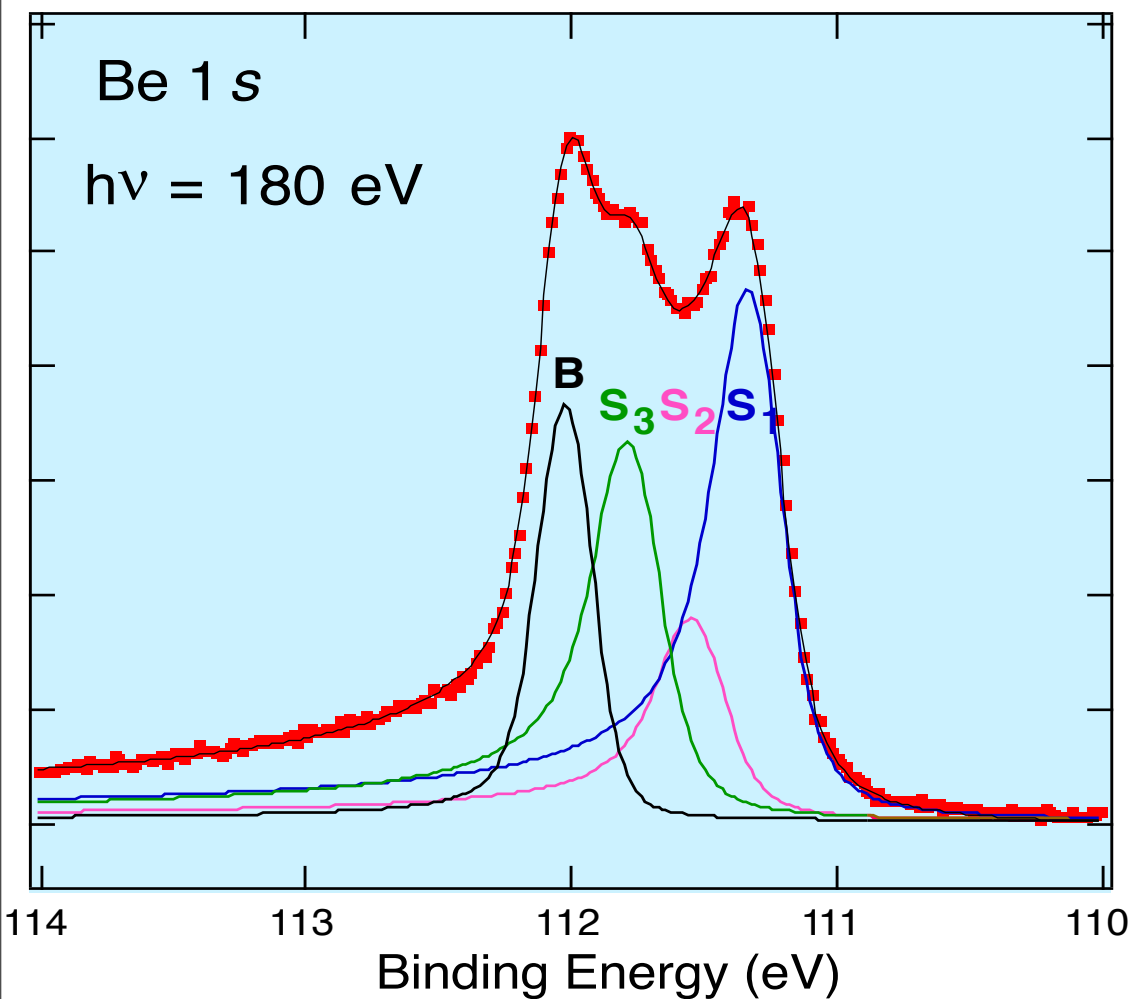
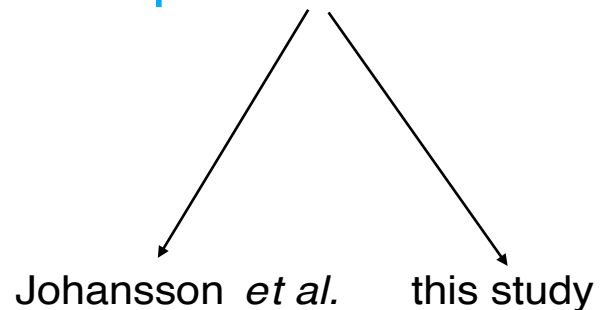
# The assignment of 1. And 2. layers is reversed between theory and experiment

	1. layer	2. layer	3. layer	4. layer	5. layer
full SCLS	<b>-0.42</b>	<b>-0.69</b>	-0.25	-0.19	-0.18
init. state					
electrost.	0.06	-0.54	-0.07	-0.11	0.01
XC	-0	1	-0.03	0	0
final state	-0.37	-0.12	-0.18	-0.08	-0.19
experiment	<b>-0.70</b>	<b>-0.50</b>	-0.22	-0.22	

R. Stumpf, to be published

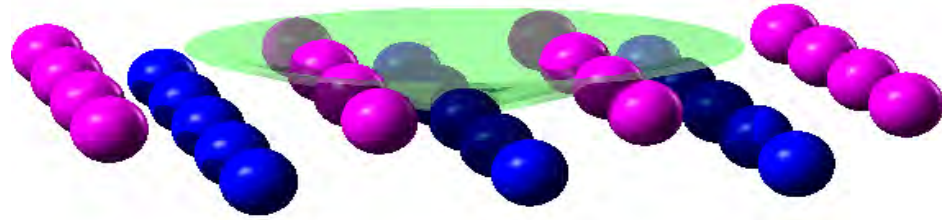


## Same fitting parameters



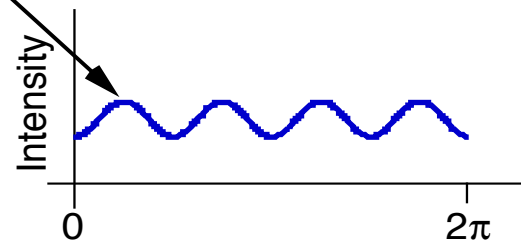
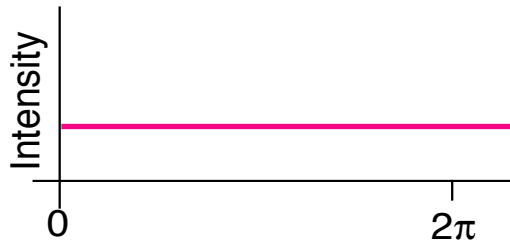
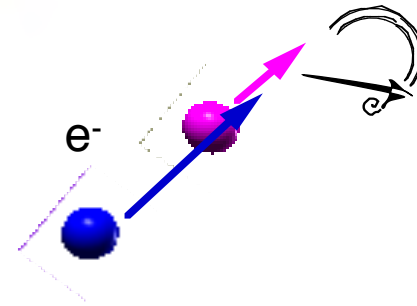
$S_3$ (eV)	0.22	0.24
$S_2$ (eV)	0.50	0.50
$S_1$ (eV)	0.70	0.71
$W_{Lor}$ bulk (eV)	0.09	0.09
Asym bulk	0.02	0.05
$W_{Gau}$ bulk (eV)	0.21	0.19
$W_{Lor}$ surf (eV)	0.09	0.10
Asym surf	0.06	0.08
$W_{Gau}$ surf (eV)	0.24	0.20

Azimuthal scan  $75^\circ$  away from the surface normal at high kinetic energy ( $> 400$  eV):

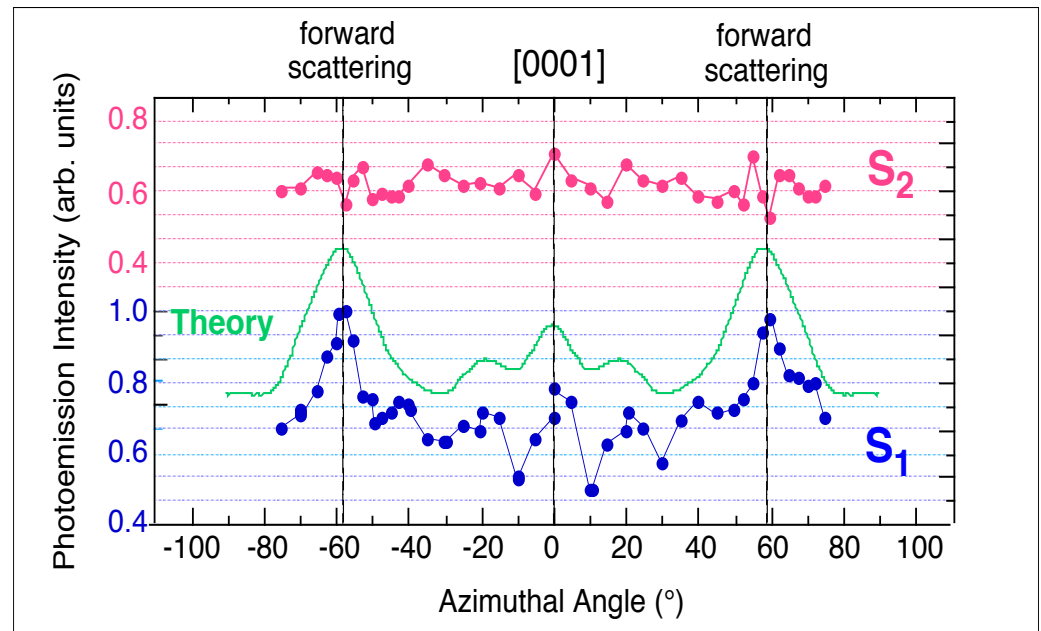
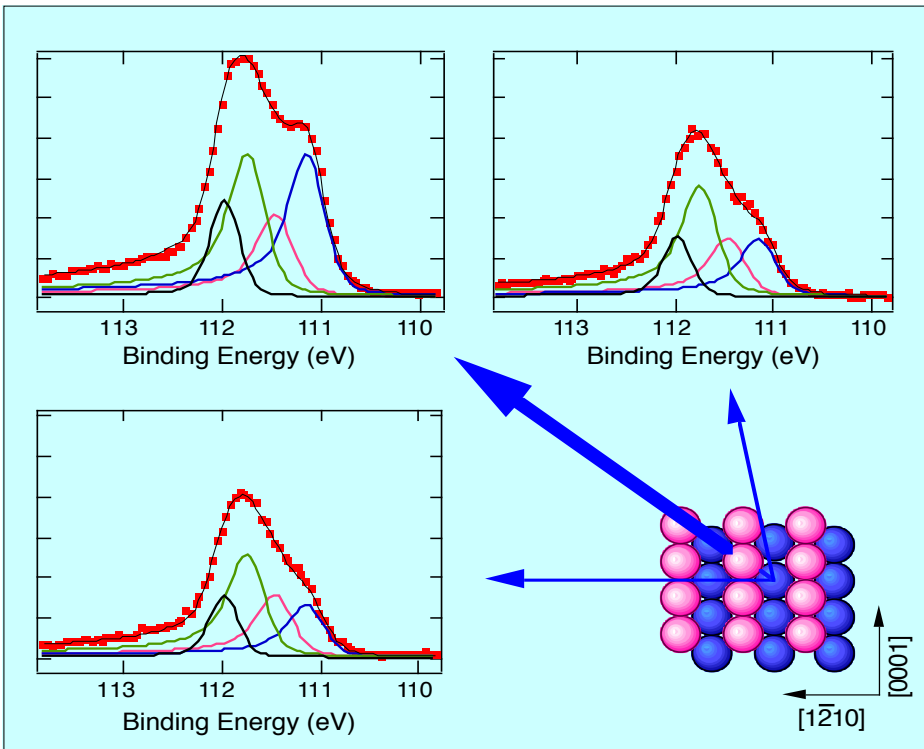


we expect (schematically):

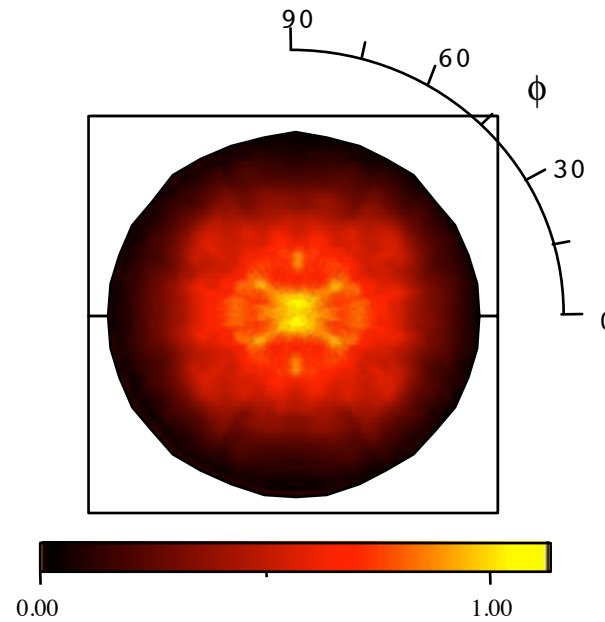
**forward scattering geometry:**



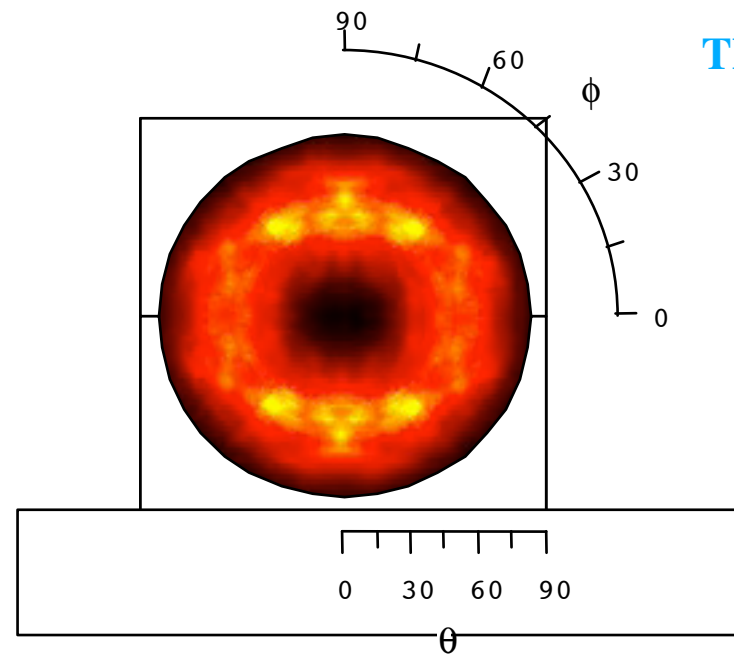
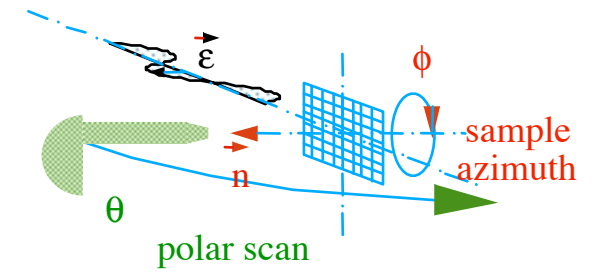
# Same assignment as theory



# Determination of surface relaxation by variable polarization photoelectron



TM - polarization



TE - polarization

